Class II Methanol Masers in Star Formation Regions

by

Simon Peter Ellingsen, B.Sc.(Hons.)

Submitted in fulfilment of the requirements
for the Degree of
Doctor of Philosophy

University of Tasmania
Hobart

January 1996

Declaration

This thesis contains no material which has been accepted for the award of any other higher degree or graduate diploma in any tertiary institution. To the best of my knowledge and belief, this thesis contains no material previously published or written by another person, except where due reference has been made in the text of the thesis.

Simon Peter Ellingsen

Authority of access

This thesis may be made available for loan and limited copying in accordance with the *Copyright Act 1968.*

Simon Peter Ellingsen

Thesis Summary

In 1991 maser emission from the 5_1-6_0 A^+ transition of CH_3OH at a frequency of 6.7 GHz was discovered by Menten (1991a). This transition is more common and stronger than the 12.2-GHz (2_0-3_{-1} E) transition discovered four years previously. This thesis contains the results of a detailed study of 6.7-GHz CH_3OH maser emission over a wide range of angular resolutions.

The University of Tasmania 26-m radio telescope has been used to perform a sensitive search for 6.7-GHz CH_3OH masers in a 28.5 square-degree region of the Galactic Plane. The search is complete, within a well defined velocity and flux density range. One hundred and eight 6.7-GHz CH_3OH masers were detected during the course of the survey, 57 of these being new detections. These new 6.7-GHz CH_3OH masers are generally weaker than those already known, but otherwise their spectral appearance is similar to those detected towards OH and 12.2-GHz CH_3OH masers. The sample of 6.7-GHz CH_3OH masers has been used to critically evaluate several *IRAS*-based search techniques and we find that all these techniques fail to detect a large fraction of the masers. Two targeted searches of the Large and Small Magellanic Clouds have been performed, resulting in the detection of three 6.7-GHz CH_3OH masers.

In addition, a search for 6.7-GHz CH_3OH megamasers was carried out toward 10 Extragalactic sources, nearly all of which are known OH or H_2O megamasers. No CH_3OH megamasers were detected with a peak flux comparable to the OH or H_2O megamasers in the galaxies searched.

Single dish spectra of 6.7- and 12.2-GHz CH_3OH masers are often complicated, with many spectral features spread over a velocity range of 10 km s^{-1} or more. High resolution observations of these maser sources show that each of the spectral features arise from a different region in the gas cloud. For OH and H_2O masers the high resolution spatial morphology typically shows little or no simple structure. Conversely, high resolution observations of 6.7- and 12.2-GHz CH_3OH masers (Norris *et al.*, 1988; Norris *et al.*, 1993) show that many have a simple curved, or linear morphology. The Australia Telescope Compact Array has been used to observe the radio continuum emission associated with three strong 6.7-GHz CH_3OH masers. It is shown that the position of the CH_3OH masers with respect to the continuum emission is consistent with the masers originating in a circumstellar disc.

Very Long Baseline Interferometry (VLBI) has been used to image strong class II CH_3OH maser emission associated with two star formation regions. The milli-arcsecond resolution images detected many new maser spots, but all of these

follow the general morphology revealed by lower resolution observations. Comparison of the 6.7- and 12.2-GHz images for the CH_3OH masers associated with NGC 6334F shows that five of the spots are coincident to within the positional errors of the observations ($\approx$ 4 milli-arcseconds).

VLBI observations were also used to measure the size of the 6.7- and 12.2-GHz CH_3OH maser spots. These show that the maser spots contain structure on two different scales, one of the order of tens of astronomical units, the other between a few and ten astronomical units. These findings are supported by the imaging data and the VLBI observations of Menten *et al.* (1988; 1992). The sizes of the 6.7- and 12.2-GHz spots toward the same sources are similar, which suggests that they are not broadened by interstellar scattering.

Acknowledgments

First and foremost I would like to thank three people, without whom this work would not have been possible. Dr. Ray Norris has been a constant source of advice and encouragement and his good humour and friendship have picked me up, and got me going again when things didn't go as planned. He has also patiently tutored me in the concepts and analysis of spectral line VLBI. Prof. Peter McCulloch has contributed enormously to the work described in this thesis. His efforts (in conjunction with Prof. Pip Hamilton) in establishing the Mt Pleasant observatory, and in building the autocorrelation spectrometer and cryogenically cooled receivers were the foundation upon which the 6.7-GHz CH_3OH maser survey rests. My partner Kristi Baker was the third vital person, her support and companionship have kept me focused and sane throughout the course of my studies.

I would like to thank Doctors John Whiteoak, Ray Norris, Jim Caswell and Bobbie Vaile for their assistance with the Parkes observations described in Chapter 3. John and Ray also assisted with the analysis and interpretation of the data, particularly of the search for CH_3OH masers in other galaxies. I would like to also thank Dr Jim Caswell for many useful discussions regarding the implementation of the Mt Pleasant survey and processing of connected element interferometry data.

I would like to thank the staff of the Mt Pleasant observatory, Messrs Gordon Gowland, Phil Jenkins and John Smith. They have assisted me above and beyond the call of duty, particularly by changing receivers during their own time and in the most inclement weather. Gordon also contributed greatly to the success of the CH_3OH survey with his ability to quickly determine and fix hardware problems when they arose, and his assistance (along with Phil) during many of the observing sessions.

Several other people have also been intimately involved with several stages of the Mt Pleasant maser survey. Messrs Tino Delbourgo and Phil Button played vital roles in the construction and development of the digital autocorrelation spectrometer and Dr. A A Deshpande assisted me greatly in writing the correlator observing software. Mr Mark von Bibra contributed greatly to the writing of the analysis software and the collection of data in the 330° – 335° Galactic longitude region.

The VLBI observations presented in Chapter 7 would not have been possible without the assistance of a large number of dedicated observers who supported the observations at various antennas. These were Dr E.King, Mr J.Lovell (Hobart), Dr J.Reynolds (Tidbinbilla), Dr T.Tzioumis, Mr S.Amy (Mopra), Dr R.Norris, Mr R.Ferris, Mr E.Troup (Parkes), Dr G.MacLeod (Hartebeesthoek), Dr R.Gough, Dr M.Wieringa and Ms R.Wark (Culgoora).

The National Radio Astronomical Observatory kindly provided the facilities I used to correlate the VLBI data presented in Chapter 7. I would like to thank Doctors Phil Diamond and Tony Beasley for instructing me in the use of the now defunct NRAO MK II correlator, and for their assistance with the correlation. The processing of the VLBI data would not have been possible without the work of Phil, who has written many of the specialized AIPS tasks and also guided me in how to use them. Tony and family were very generous in their hospitality during my two visits to Socorro, and provided me with many nights and weekends of company when a long way from home. I would also like to thank the director of the ATNF Dr. Ron Ekers who funded the airfares for my two trips to Socorro.

I would like to thank the staff of the Physics Department and fellow postgraduate students, Jim, Jenny, Chris, Mark and Edward for their support and the many memorable social occasions. I extend my thanks in particular to Jim, with whom I have had the pleasure of sharing an office for the past 4 and a half years. His ability to retain the most useless trivia and remain cheerful and calm even under extreme provocation continue to amaze me.

Finally I would like to thank my family for the kind and supporting environment in which I was raised. The interest in astronomy nurtured by my parents inspired me throughout my high school and undergraduate years.

I am grateful to the Australian Government for a Postgraduate Research Award, which provided me with the financial support necessary to undertake the work presented in this thesis.

Contents

List of Tables

List of Figures

Chapter 1

Introduction

1.1 A brief historical overview

The first maser emission from interstellar space was detected thirty years ago. Weaver *et al.* (1965) were searching for OH absorption, but instead detected strong emission (which they labelled "mysterium"), toward several Galactic HII regions. As this new type of source was observed with progressively higher angular resolution it became apparent that the observed emission could not have a thermal origin. Initially it was considered unlikely that a maser could arise by chance in interstellar space. However, the physical conditions in molecular gas clouds are such that population inversion in the rotational states of molecules can occur naturally.

H_2O maser emission at 22 GHz was discovered four years later, by Cheung *et al.* (1969). Water masers were observed to be stronger and exhibited greater temporal variability than OH masers. After the discovery of H_2O masers, no strong, common centimetre wavelength masers were discovered for nearly 20 years and the general belief was that no more would be. During this period many new molecular transitions from OH, NH_3, H_2CO, SiO, CH_3OH and other molecules were discovered toward star formation regions, some of these exhibited maser emission, but none were both common and strong. For this reason the majority of studies of masers in star formation regions concentrated on the ground state OH and H_2O maser emission.

Methanol (CH_3OH) was first detected in interstellar space by Ball *et al.* (1970) and the first CH_3OH masers were detected toward Orion-KL by Barrett *et al.* (1971), although strong evidence that they were masers was not presented until several years later (Barrett *et al.*, 1975). There then passed nearly a decade in which no further sites of CH_3OH maser emission were detected, and no new masing transitions were discovered. However in the 11 years since 1984 there have been 14 new masing transitions of CH_3OH discovered (see Table 2.1). Arguably the two most important of these are the 6.7-GHz 5_1-6_0 A^+ transition (Menten, 1991a) and the 12.2-GHz 2_0-3_{-1} E transition (Batrla *et al.*, 1987). The latter of these was discovered first, and searches for this new CH_3OH maser transition soon revealed it to be associated with star formation regions which showed OH maser emission (Norris *et al.*, 1987; Kemball *et al.*, 1988; Koo *et al.*, 1988). More importantly, it

typically had peak flux densities comparable to those of the associated OH masers.

6.7-GHz CH_3OH masers were discovered four years later, also associated with OH and 12.2-GHz CH_3OH masers (and hence massive star formation) (Menten, 1991a). Thus in the space of a few years the number of strong centimetre wavelength maser transitions associated with massive star formation regions doubled. While each of the CH_3OH maser discoveries was in itself important, it was quickly realised that the discovery of two strong transitions from the same molecule, toward the same regions was even more so. Initial observations showed the newly detected CH_3OH masers to have peak flux densities typically an order of magnitude greater than the associated OH masers. In addition, many of the 6.7-GHz CH_3OH masers had quite similar spectral morphology to their 12.2-GHz counterparts, suggesting that they originated from approximately the same areas of the star formation region.

These newly discovered CH_3OH masers clearly had great potential to provide many interesting developments in the study of massive star formation, and so the projects which constitute this thesis were conceived. The decision was made to concentrate on three major questions about the newly discovered masers :

1. Are all 6.7-GHz CH_3OH masers associated with massive star formation regions?

2. Where in massive star formation regions do the CH_3OH masers occur?

3. What, if any structure do the CH_3OH masers have at high spatial resolutions, and how big are the maser spots?

To answer the first of these questions it was decided to undertake a large scale search for 6.7-GHz CH_3OH masers. The location of the Mt Pleasant observatory means that the entire central region of the Galaxy is observable. The only previous large scale search for masers in the southern region of the Galactic Plane was for 1.665-GHz OH masers (Caswell *et al.*, 1980; Caswell and Haynes, 1983b; Caswell and Haynes, 1987) and had a limiting sensitivity of ≈ 1 Jy. As the 6.7-GHz CH_3OH masers were known to be approximately an order of magnitude stronger, a search for 6.7-GHz CH_3OH masers with similar sensitivity seemed likely to detect star formation regions with OH masers $\lesssim 1$ Jy, as well as any associated with other objects. In addition the results of a such a survey constitute a complete sample which allows the statistical properties of the spatial and flux density distribution of the masers to be determined.

Since the discovery of OH and H_2O masers, a lot of effort has been invested in determining where in the star formation regions the masers occur and their relationship to each other and the exciting star. The generally accepted view is that OH masers occur in, or near the interface between the HII region and the surrounding parent molecular cloud. While H_2O masers form in outflows from the newly formed star. The second major thrust of this thesis was to make high resolution images of the both the CH_3OH masers and the HII region with which they are associated, with the aim of trying to improve our models of star formation regions.

1.2 The rest frequencies of 6.7- and 12.2-GHz CH_3OH masers

The rest frequencies I have adopted throughout this work for the 5_1-6_0 A^+ and 2_0-3_{-1} E transitions of CH_3OH were 6.668518 and 12.178595 GHz respectively (Menten, 1991a; Gaines *et al.*, 1974). Recent work by Breckenridge and Kukolich (1995) has measured the rest frequencies for the two transitions to be 6.6685192 $\pm$ 0.0000004 GHz and 12.178597 $\pm$ 0.000002 GHz. Using the new rest frequency for the 5_1-6_0 A^+ transition would produce a shift in velocity of -0.05 km s^{-1} in the spectra. While the two values of the 2_0-3_{-1} E rest frequency are the same to within the measured uncertainty.

1.3 Outline of the Thesis

This project has involved work in the development of observing and analysis software for single dish spectral line observations, as well as the collection, processing and analysis of single dish, connected element interferometry and very long baseline interferometry data. The chapters of this thesis describe aspects of this work and present the results. A brief outline of the thesis is given below.

Chapter 2. The current state of knowledge regarding ultra-compact HII regions, with which many or all 6.7-GHz CH_3OH masers are associated is presented. This is followed by a brief review of OH and H_2O masers in star formation regions and the classification of CH_3OH masers, pumping schemes for CH_3OH masers and the formation of CH_3OH in interstellar space.

Chapter 3. Two searches for 6.7-GHz CH_3OH masers in the Magellanic Clouds and one towards other extragalactic sources are described. The results of the searches are presented and the implications for the abundance of complex molecules in the Magellanic Clouds and the existence of CH_3OH megamasers are discussed.

Chapter 4. The theoretical basis for the operation and analysis of data collected with a 1-bit digital autocorrelation spectrometer is outlined. The hardware and software used to control the Mt Pleasant autocorrelation spectrometer are described, as are the considerations which led to the choice of the observational parameters used in the 6.7-GHz CH_3OH maser survey and details of the observational procedure.

Chapter 5. Spectra of each of the 6.7-GHz CH_3OH masers detected in the Mt Pleasant survey are presented along with a summary of the observations of associated masers, infra-red or radio continuum emission is given. The efficiency of various *IRAS*-based maser search strategies is examined and the implications of the survey observations for the number of UCHII regions in the Galaxy is discussed.

Chapter 6. The relationship between the relative position of the UCHII region and the 6.7-GHz CH_3OH masers is discussed in the context of three different models for the origin of class II CH_3OH masers. High resolution observations of two UCHII regions associated with 6.7-GHz CH_3OH masers are presented and compared with the model predictions.

Chapter 7. Three very long baseline interferometry images of class II CH_3OH masers are presented. Images of the 6.7- and 12.2-GHz CH_3OH masers associated with the well known UCHII region NGC 6334F are compared. The results of an experiment to measure the size of the 6.7- and 12.2-GHz CH_3OH masers are presented and the implications discussed.

Chapter 8. The major results of the thesis are summarized and the important implications briefly discussed. Several suggestions for further work to examine questions raised by the results of this work are outlined.

Chapter 2

Masers and star formation regions

2.1 Introduction

Although the first interstellar masers were detected toward star formation regions (Weaver *et al.*, 1965), the connection was not immediately recognized. In the thirty years since that serendipitous discovery, observations of masers have become important tools in the study of massive star formation. These massive stars have a very important role to play in the star formation process. It is generally believed that their destruction in supernovae is a trigger for star formation in nearby molecular clouds, and that their ionizing flux destroys the parent molecular cloud, halting the formation of further stars. In this chapter I describe the current status of maser research, concentrating on CH_3OH masers and another sign post of massive star formation, HII regions.

2.2 Ultra-compact HII regions

Stars which have a spectral classification earlier than approximately B3 produce a large number of photons with sufficient energy to ionize neutral hydrogen. The production of ultraviolet photons begins when fusion commences in the core of the massive proto-star, which then becomes a zero age main-sequence (ZAMS) star. These photons rapidly ionize the material in the immediate vicinity of the star to form an ionization front (I-front). Initially the expansion of the ionized region is very rapid, but it slows as the radius of the I-front increases due to the rapidly increasing volume which must be kept ionized. This initial expansion is so rapid (of the order of a few years) that it is essentially unobservable. However, the ionizing process also heats the gas to a temperatures of around 10^4 K, while the surrounding molecular gas is at a temperature of less than $\approx$ 100 K. This produces a large pressure gradient and the HII region expands to try to obtain pressure equilibrium with the surrounding medium.

Using the simple model of HII regions outlined above, Wood and Churchwell (1989b) calculated that it would take approximately 3 x 10^6 years for the HII region to reach pressure equilibrium with the surrounding gas. This is approximately the same as the lifetime of O and B stars, but since many of these stars are visible then

this simple model of HII regions is clearly inaccurate in some way. Despite their importance in the star formation process the evolution of HII regions is not well understood. Observationally, HII regions are seen to dominate the emission from the Galactic Plane at radio and far infrared wavelengths. HII regions are observed to exist on a wide range of scales. The smallest and presumably the youngest are the compact and ultra-compact HII regions which are defined as having diameters of less than 1 and 0.15 pc respectively (Habing and Israel, 1979).

Soon after the discovery of OH masers it was found that many are associated with HII regions. Similarly many H_2O masers are also associated with HII regions, but it is the CH_3OH masers associated with HII regions that are the primary topic of this thesis. We are able to use the association of the CH_3OH masers with HII regions to study the global properties of the HII regions and the massive star formation they accompany. Further, the spatial distribution of the masers with respect to the HII region yields important information for models of masers in star formation regions and this is discussed in detail in section 6.1.

HII regions have been observed to have a very large range of sizes. Habing and Israel (1979) developed a classification scheme for HII regions based upon their linear size (d) and electron density (n_e). However, typically HII regions are classified by their emission measure ($EM = n_e^2 d$), which is greatest for the youngest and most compact HII regions and decreases as they evolve. Compact and ultra-compact HII regions are associated with very young massive stars, which have not had sufficient time to ionize a large amount of gas. Indeed, since masers are found nearby, there must be molecular gas in the region. Using the simple model of HII regions, they will be classified as compact or ultra-compact for only a few x 10^4 years. This implies that only a few hundred such objects will be present in the entire Galaxy. However, targeted searches, usually towards *IRAS* sources (Wood and Churchwell, 1989b; Garay *et al.*, 1993b; Kurtz *et al.*, 1994) observe a number consistent with a few thousand.

Clearly there is a mechanism operating to inhibit the expansion of HII regions, extending the period of time they spend in the ultra-compact and compact phases. Several models have been proposed, suggesting mechanisms which may be responsible for confining HII regions and these are described below.

2.2.1 The champagne flow model

The champagne flow, or blister, model of HII regions was conceived by Tenorio-Tagle (1979) and further developed in a series of papers by Bodenheimer, Tenorio-Tagle and Yorke (Bodenheimer *et al.*, 1979; Tenorio-Tagle *et al.*, 1979; Yorke *et al.*, 1982; Yorke *et al.*, 1983). They suggest, on the basis of observational evidence that massive stars form preferentially near the edges of molecular clouds. The initial expansion and evolution of the HII region proceeds as outlined in the simple model, but because of the position of the star near a cloud edge, the HII region quickly expands to the edge of the molecular cloud and breaks through into the lower density medium surrounding the cloud. This creates a pressure discontinuity at the break-through point (which is likened to the sudden release of the cork from a shaken champagne bottle), and much of the ionized gas from the HII region

is blown out into the inter-cloud region. The expansion of the ionized gas also creates a pressure confinement at the inner edge of the HII region which slows the rate of expansion.

The champagne model of HII regions predicts that the radio continuum emission from the regions should have a central core, with material flowing away from the core perpendicular to the molecular cloud edge. This roughly describes the appearance of the "cometary" UCHII regions observed by Wood & Churchwell (1989b), but an alternative interpretation of the cometary morphology is that they are caused by bow-shocks (see Section 2.2.3). The champagne model predicts that the peak of the radio brightness distribution should be at the centre of the core and that the escaping ionized gas should flare away as it flows into the intercloud regions However, Churchwell (1990) suggests that appearance of cometary HII regions is more consistent with the bow-shock model, as they are limb-brightened and the tails do not flare.

2.2.2 The infall model

This is an early model, which has now largely been discredited. The basic idea is that the expansion of the young HII regions is reduced by the continuing gravitational collapse of outer regions of the molecular cloud. This model was used to explain the well-studied HII region W3(OH), where Reid *et al.* (1980) observed that the OH masers, most of which are projected upon the HII region appear to be redshifted with respect to the observed radio recombination line velocity. While this appears to be good evidence that the OH masers are falling into the HII region, it has been demonstrated to be due to an optical depth effect in the measurement of the recombination line velocity (Berulis and Ershov, 1983). For lower frequency recombination lines the HII region is optically thick, so that only the emission from the front of the expanding HII region is observed and this is blue shifted with respect to the systematic velocity of the HII region. Recently published VLBI observations have demonstrated that the proper motion of the OH masers is consistent with either simple expansion or a cometary bow shock, but not infall (Bloemhof *et al.*, 1992). In addition, modelling of the infall shows it to be extremely unstable. Either it is insufficient to retard the expansion significantly, or it is too great and the HII region collapses.

2.2.3 The bow shock model

Many ($\sim$ 20%) UCHII regions are observed to have a cometary morphology (Wood and Churchwell, 1989b; Garay *et al.*, 1993b; Kurtz *et al.*, 1994). While the champagne flow model predicts this morphology (see Section 2.2.1), an alternative hypothesis has been proposed by Wood and Churchwell (1989b). They suggest that the cometary morphology is produced by a bow shock created by the relative motion of the massive star with respect to the parent molecular gas cloud. In this model, the HII region is supported by the stellar wind from the massive star, but the ram pressure caused by the motion of the HII region counteracts the natural expansion of the HII region. The bow shocks are able to form due to the low sound

speed within the molecular cloud, compared to the typical velocity dispersion of OB associations.

Theoretical modelling of the bow shocks has been performed by Van Buren *et al.* (1990) and this model was used to reproduce the observed radio brightness distribution of several cometary HII regions (Mac Low *et al.*, 1991). One of the predictions of this model is that that the observed proper motion of OH masers in the bow shock region should be tailward. There are two problems with the bow shock model. The first is that most observed HII regions do not have a cometary morphology, but if they have much longer lifetimes then they should constitute the majority. However, Mac Low *et al.* (1991) claim to be able to reproduce nearly all observed HII region morphologies by changing the orientation. The second problem, raised by Hollenbach *et al.* (1994), is that if the exciting star has a relative velocity with respect to the parent molecular cloud of $\approx$ 5–10 km s^{-1}, then it will reach the edge of the cloud in approximately 10^4 years. However, the star must remain within the molecular cloud for $\approx 10^5$ years, in order to account for the observed number of UCHII regions in the Galaxy.

2.2.4 The circumstellar disc photoionization model

Hollenbach *et al.* (1994) have proposed a model whereby the HII region expands as described in the simple model, but the photoionization of material from the circumstellar disc replenishes the expanding gas. The material in the disc is ionized mainly by recombination photons from the ionized gas above the disc, rather than directly from the star. Using this mechanism the dense gas close to the exciting star is continually replenished for the lifetime of the circumstellar stellar disc. Hollenbach *et al.* predict the initial mass of the circumstellar disc to be approximately 30% that of the star. Their models show that the destruction of the disc takes approximately 10^5 years, which is similar to the lifetime of an UCHII region as calculated from the number observed (Wood and Churchwell, 1989a).

According to the Hollenbach *et al.* model, the dense gas close to the exciting star will be optically thick at centimetre wavelengths and have a spectral index $\alpha = 0.6$ ($S_\nu = \nu^{0.6}$). This is the mean spectral index observed by Wood and Churchwell (1989b), but as noted by De Pree *et al.* (1995b), observed spectral indices cover a large range. Further, the photoionized disc model does not account for the large variety of UCHII region morphologies observed.

2.2.5 The warm, dense molecular gas hypothesis

De Pree *et al.* (1995b) have suggested that the simple model of HII regions (outlined above) is correct, but that the lifetime of the ultracompact phase has been underestimated because the molecular clouds in which the UCHII regions form are more warm and dense than has previously been assumed. Wood and Churchwell (1989b) assumed an ambient density of 10^5 cm^{-3} and kinetic temperature 25 K for the molecular cloud. However, De Pree *et al.* claim that recent observations [for example Hüttemeister *et al.* (1993) and Garay *et al.* (1993a)] show that typical molecular cloud densities and temperatures are approximately 10^7 cm^{-3} and

100 K respectively. The effect of higher estimates of the ambient density and temperature of the molecular gas is to reduce the pressure gradient and hence reduce the rate of expansion of the HII region, its final radius and the time taken for it to reach pressure equilibrium with the parent molecular cloud. The simplicity of this suggestion makes it appealing, but further study is required to determine whether the densities and temperatures observed for a small number of molecular clouds are the exception, or the rule.

2.2.6 The far infrared properties of UCHII regions

Far infrared (FIR) observations of HII regions were first performed in the early 1970's [for example Wynn-Williams *et al.* (1972))]. Unfortunately they typically have resolutions far worse than radio observations of the same regions, which makes it impossible to compare the emission from the two wavelength regions in detail. Interestingly, despite the variation in stars capable of forming HII regions, the spectra of HII regions in the radio-infrared are quite uniform (Chini *et al.*, 1986a; Wood and Churchwell, 1989b). It is generally accepted that all the energy emitted by the newly formed star as photons is absorbed by the surrounding dust and re-emitted at FIR wavelengths (see Churchwell, 1990 for a more detailed description), and it is this process which causes the observed similarity in the FIR spectrum of HII regions.

If the circumstellar dust reradiates the total photon energy of the star, then by measuring the FIR luminosity, the spectral class of the exciting star can be inferred. However, the poor resolution of FIR observations means that the FIR flux densities observed are most likely due to several objects and this will cause the luminosity of the star to be overestimated. An independent method of determining the spectral class of the exciting star is provided by radio observations of HII regions. The radio frequency flux density is proportional to the number of photons which have an energy greater than the Lyman limit, which in turn depends upon the spectral class of the exciting star. I have used this technique to estimate the spectral type of the stars in the NGC 6334F and G339.88-1.26 HII regions and a detailed description of the method used is given in Section 6.4.2. There are two major problems with this technique for estimating the class of the exciting star, the first is that the model atmospheres for OB stars are poorly determined compared to those for less massive stars (Churchwell, 1990). The second is that a significant fraction of the UV photons in the HII region are probably absorbed by dust, rather than ionizing neutral hydrogen as is assumed by the model. This means that the spectral class of the star as predicted from the radio continuum flux of the HII regions will be underestimated. Where both techniques have been applied to various HII regions, the spectral class predicted from the FIR luminosity is typically 2–4 subclasses hotter than that predicted by radio continuum observations (Wood and Churchwell, 1989b). Thus the true spectral class of the exciting star is probably in the range between the two estimates.

Since its publication in 1985, the IRAS Point-Source Catalogue has proved to be an extremely useful aid in the study of a wide range of objects, including UCHII regions. As stated above, the shape of the spectra of HII regions is very

uniform. This means that for HII regions the ratios between different wavelength bands (often call "colours") should also be very similar. Wood and Churchwell (1989a) examined the infrared colours for *IRAS* sources associated with a radio selected sample of UCHII regions. They found that they all satisfied the criteria $Log_{10}(S_{60}/S_{12}) \geq 1.30$ & $Log_{10}(S_{25}/S_{12}) \geq 0.57$, but that this region of the colour-colour diagram contained only a small percentage of all *IRAS* sources. These criteria have been widely used to target maser searches toward regions which have a high probability of being UCHII regions. The effectiveness of these maser search techniques is discussed in Sections 5.4.1.3 & 5.4.2. Hughes and MacLeod (1989) independently developed a very similar set of criteria using an optically selected sample of HII regions.

2.3 Masers associated with star formation

The early history of the discovery of masers has often been reviewed (see for example Anderson & Genzel 1993) and will not be repeated again here. It was initially hoped that masers alone would provide a detailed and comprehensive picture of massive star formation. However, it quickly became apparent that the pumping mechanisms for masers are extremely complex. Thirty years after their discovery, it is still not known whether OH masers in star formation regions are radiatively or collisionally pumped. Despite these problems, the study of multiple transitions from the same region (excited OH, submillimetre H_2O and class II CH_3OH) should be a powerful method of constraining, and refining possible pumping mechanisms. Future high resolution millimetre and far-infrared observations should provide much-needed information on the availability of pump photons in various wavelength ranges, and the state of knowledge of collisional cross-sections for potentially important interactions is also likely to improve with additional laboratory studies.

The gradual improvement in the understanding of masers in star formation regions has been assisted by parallel improvements in observational techniques and in the sensitivity of receivers and spectrometers. For example, high resolution observations of masers, and associated radio continuum emission, are now routine using instruments such as the ATCA and VLA. Instrumental improvements and specialized satellites have also lead to a more holistic approach to the study of star formation. Combining the results of high resolution observations of different maser species with molecular gas tracers such as CO and CS, radio continuum, radio recombination lines and far infrared continuum and spectral line observations, will aid realistic modelling of the whole region, rather than isolated systems such as the circumstellar disc or high velocity outflow.

2.3.1 OH masers in star formation regions

The first suggestion that OH masers were associated with HII regions was made by Zuckerman *et al.* (1965). This was confirmed by subsequent observations, but it was not until the high resolution observations of W3(OH) by Reid *et al.* (1980)

that it was demonstrated conclusively. Subsequent observations have shown that the masers appear to be preferentially located at the edges of HII regions (Baart and Cohen, 1985; Gaume and Mutel, 1987). The currently accepted interpretation of this is that the masers form in the shocked gas between the HII region and the surrounding molecular gas. Early observations of the OH masers associated with W3(OH) (see Section 2.2.2) were interpreted as suggesting they were falling into the HII region (Reid and Moran, 1981), and alternatively, that they were expanding with the HII region (Norris and Booth, 1981). The expansion model was eventually shown to be correct by the proper motion study of Bloemhof *et al.* (1992).

OH is the only paramagnetic masing molecule and this makes it very useful for studying the magnetic field in masing regions. Zeeman pairs of maser spots can be identified by high-resolution observations, and the difference in the Doppler shifted velocities allows the line of sight magnetic field to be calculated. The field strengths derived from such observations are typically in the range 1–10 mG, which suggests that magnetic fields play an important role in the star formation process. The splitting for the ground-state transitions of OH is ≈ 0.6 km s^{-1} for a 1 mG field, which can make identification of Zeeman pairs very difficult without the aid of high resolution interferometry. The splitting is less for some of the excited state transitions and identification of Zeeman pairs can often be made without the need for complementary high resolution observations (Caswell and Vaile, 1995).

2.3.2 H_2O masers in star formation regions

H_2O maser emission was first detected by Cheung *et al.* (1969), who detected emission toward Orion A and W49. The latter of these contains the most luminous maser emission in the Galaxy, with individual maser spots occasionally exhibiting isotropic luminosities of nearly 0.1 L$\odot$(Walker *et al.*, 1982). Like OH masers, the association of H_2O masers with HII regions is now well established, but unlike OH, the H_2O masers are typically offset from the HII region.

The spectral morphology of H_2O masers also differs significantly from that of OH and CH_3OH masers. H_2O masers typically have their strongest emission at velocities close to the systematic velocity of the star forming region, but in addition, the H_2O maser spectrum often exhibits weaker emission at velocities offset from the systematic velocity by 100 km s^{-1} or more. It was the existence of these high velocity features that lead to the now well accepted model, that H_2O masers form in the outflows from newly formed stars (Strel'nitskii and Syunayev, 1973). Interestingly, high-resolution observations show that the high velocity features occur in the same general area as the strong low velocity emission. The explanation for this somewhat surprising observation was provided by proper motion experiments, which show that the low velocity features have the largest proper motions [see section 10.3.1 of Elitzur (1992)]. This implies that the observed differences in velocity and strength of the various components in H_2O maser spectra are due primarily to orientation effects. A further implication is that the emission from H_2O masers must be beamed approximately perpendicular to the direction of motion of the masers, so that those masers with large line of sight velocities are preferentially

Table 2.1: All known CH_3OH maser transitions in the frequency range 1–150 GHz. The rest frequencies have been rounded to the nearest 100 kHz.

Rest Frequency	Transition	Class	Discovery Reference
6.7	5_1-6_0 A^+	II	Menten (1991a)
9.9	9_{-1}-8_{-2} E	I	Slysh *et al.* (1993)
12.2	2_0-3_{-1} E	II	Batrla *et al.* (1987)
19.9	2_1-3_0 E	II	Wilson *et al.* (1985)
23.1	9_2-10_1 A^+	II	Wilson *et al.* (1984)
24.9-25.5	J_2-J_1 E($J = 2 - 10$)	I	Barrett *et al.* (1971)
36.2	4_{-1}-3_0 E	I	Morimoto *et al.* (1985)
37.7	7_{-2}-8_{-1} E	II	Haschick *et al.* (1989)
38.3	6_2-5_3 A^+	II	Haschick *et al.* (1989)
38.5	6_2-5_3 A^-	II	Haschick *et al.* (1989)
44.1	7_0-6_1 A^+	I	Morimoto *et al.* (1985)
84.5	5_{-1}-4_0 E	I	Batrla and Menten (1988)
95.2	8_0-7_1 A^+	I	Nakano and Yoshida (1986)
107.0	3_1-4_0 A^+	II	Val'tts *et al.* (1995)
146.6	9_0-8_1 A^+	I	Menten (1991b)

weaker than those moving perpendicular to the line of sight (Genzel *et al.*, 1981).

2.4 CH_3OH masers in star formation regions

A brief history of early observations of interstellar CH_3OH emission is given in Section 1.1. CH_3OH has a molecular structure which is classified as an asymmetric rotor and exhibits hindered internal rotation along the carbon-oxygen bond. These two characteristics mean that the CH_3OH molecule has an extremely complex microwave spectrum. The very large number of microwave transitions is one of the major reasons why maser emission from the CH_3OH molecule has been difficult to detect, as until recently there have been no rules for determing which of the transitions are most likely to exhibit maser emission.

The first CH_3OH masers were serendipitously detected toward Orion A by Barrett *et al.* (1971) who were searching for emission from N_2O. Although thermal emission was detected from several millimetre transitions of CH_3OH, no new sites of CH_3OH maser emission or new CH_3OH masing transitions, were discovered for a further 23 years. In the period since 1984 14 new masing transitions of CH_3OH have been discovered at frequencies between 5 and 150 GHz, and these are summarized in Table 2.1 (other masing transitions have been detected at higher frequencies). A comprehensive review of the discovery and observational properties of CH_3OH masers up until 1991 has been written by Menten (1991b).

The discovery and subsequent searches for, and high-resolution observations of, the 6.7-GHz 5_1-6_0 A^+ and 12.2-GHz 2_0-3_{-1} E transitions of CH_3OH are reviewed in the introductions to Chapters 5, 6 & 7 and so that information will not be

repeated here.

2.4.1 The difference between class I and class II CH_3OH masers

The various masing transitions of CH_3OH have been divided observationally into two classes, known as I and II (Batrla *et al.*, 1987). Class I CH_3OH masers are observed to be offset from HII regions by between 0.1–1 pc. Each of the class I transitions from the same location have very similar spectra, typically consisting of a small number of narrow lines. The 44.1-GHz 7_0-6_1 A^+ transition is typically the strongest of the class I transitions. Absorption of class II transitions, particularly the 12.2-GHz transition, is often observed toward class I sources. The transitions of CH_3OH are labeled as J_k for E-type and J_K for A-type. E-type CH_3OH class I transitions have their upper level in the k = -1 ladder and their lower level in the $k = 0$, or occasionally the k = -2 ladder. A-type CH_3OH class I transitions have their upper level in the $K = 0$ ladder and their lower level in the $K = 1$ ladder.

Class II CH_3OH masers are observed to be associated with massive star formation regions, and often with OH and H_2O masers. The class II CH_3OH masers often have quite complex spectral morphology, with many components covering a wide velocity range. Although the class II CH_3OH masers observed in the same location typically cover the same velocity range, they are not as similar as the class I masers. The 6.7-GHz 5_1-6_0 A^+ transition is typically the strongest of the class II transitions.

There are clearly a large number of observable differences between class I and class II CH_3OH maser transitions. However, typically the difference has been summarized as "class II transitions are associated with HII regions and class I transitions are offset from them". A recent search for 44.1-GHz class I CH_3OH masers by Slysh *et al.* (1994) has cast some doubt on this simplistic definition of class I and class II sources. Slysh *et al.* detected 44.1-GHz CH_3OH maser emission toward 55 sources, many of which also show OH, H_2O or 6.7-GHz CH_3OH (class II) maser emission. However, the 44.1-GHz CH_3OH masers have a different velocity range to the 6.7-GHz masers and strong 44.1-GHz CH_3OH masers tend to be associated with weaker 6.7-GHz masers and vice versa. Slysh *et al.* suggest that class I and class II CH_3OH masers may arise from the same region, but that the action of one suppresses the other. This means that while relatively weak class I and class II transitions can co-exist in the same general region, strong class II emission will quench class I emission. For this reason, Slysh *et al.* suggest that the definition of class I and class II CH_3OH maser sources should be based on the type of transition alone.

The standard model of class I CH_3OH masers is that they are collisionally pumped in outflows, similar to the scheme for H_2O masers. High resolution observations of the 84.5- and 95.2-GHz CH_3OH masers associated with DR21(OH) (Batrla and Menten, 1988; Plambeck and Menten, 1990) show that they are separated by between 0.1–1 pc from HII regions. A linear separation of 1 pc corresponds to an angular separation of less than 10 arcsec, for a star formation region 2 kpc away. This is comparable to the positional accuracy of the observations of Slysh

et al. (1994). Therefore the 44.1-GHz CH_3OH masers detected by Slysh *et al.* may offset by 0.1–1 pc from the 6.7-GHz CH_3OH masers and the simplistic definition of class I and class II CH_3OH masers is still valid. Further evidence that class I and class II CH_3OH masers arise in separate regions comes from the modelling of Cragg *et al.* (1992). Their modelling found that that class I CH_3OH masers occur when the continuum temperature is less than the kinetic temperature of the gas, while the class II masers arise in the opposite conditions. High resolution observations of class I and class II sources toward the same star formation region are required to determine the precise nature of the relationship.

2.4.2 Pumping schemes

The basis of the pumping scheme for class I CH_3OH masers was developed by Lees (1973), who predicted that the 84.5-GHz 5_{-1}-4_0 E transition and 36.2-GHz 4_{-1}-3_0 E transition may exhibit maser emission. This scheme has been developed by several groups and the current version as outlined by Menten (1991b) is :

1. An E-type CH_3OH molecule which has been collisionally excited to a high energy state is likely to radiatively decay into the k=-1 ladder. This ladder has been labeled the backbone ladder).

2. The lower k = -1 levels become overpopulated with respect to those in adjacent ladders because of the $\Delta k = 0$ collisional selection rule, and radiative transitions out of the k = -1 ladder are slower than those down the ladder.

The pumping scheme for A-type CH_3OH is basically the same, but $K = 0$ is the backbone ladder. This simple pump scheme explains the observation that E-type CH_3OH masers have their upper level in the k = -1 ladder (with the exception of the $J_2 - J_1$ masers) and A-type have their upper level in the K = 0 ladder. It also explains why the 2_0-3_{-1} E and 5_1-6_0 A^+ class II transitions are sometimes observed in absorption toward class I sources as they have their lower level in the backbone ladder. The modelling of Cragg *et al.* (1992) suggests that class I CH_3OH masers will occur when the temperature of the continuum radiation is less than the kinetic temperature of the gas. They also found that the relative rates of radiative excitation and decay were the vital factors in determining which transitions became inverted, with collisional selection rules having little net effect. Their modelling produced maser emission from all class I CH_3OH masers known at the time and also for the 9.9-GHz transition discovered a year later by Slysh *et al.* (1993).

Unfortunately no simple model exists to explain the pumping of class II CH_3OH masers. Several schemes using far infrared or submillimetre radiative pumping have been suggested (Menten *et al.*, 1986; Cragg *et al.*, 1992; Peng and Whiteoak, 1993; Sobolev and Deguchi, 1994). The latter two of these models concentrate on only the 12.2-GHz CH_3OH masers. A common finding seems to be that the class II CH_3OH masers require the temperature of the background continuum radiation to be greater than the kinetic temperature of the masing gas. The various groups differ on whether consideration of the torsional levels above the

ground state are required. The model of Cragg *et al.* produced all the class II CH_3OH masers observed before 1992, but failed to predict maser emission from the recently discovered 107.0-GHz 3_1-4_0 A^+ transition (Val'tts *et al.*, 1995).

Radiative pumping schemes require a minimum of one pump photon for each maser photon produced. So the extremely high luminosity of the strongest 6.7-GHz CH_3OH masers may prove to be a problem for radiative pumping schemes. In order to determine if far infrared or submillimetre radiative pumping is feasible requires high-resolution observations of class II CH_3OH maser sources at these frequencies.

2.4.3 The formation of CH_3OH in molecular clouds

While the processes which produce the enhancement of OH at the edges of HII regions and H_2O in high velocity outflows are relatively well understood, the same is not true for the formation of CH_3OH in molecular clouds. One of the reasons for this is that it has not yet been determined where in the star formation regions the CH_3OH masers occur. Some observations support the hypothesis that the CH_3OH masers form in the circumstellar disc (Norris *et al.*, 1996), while others suggest that the CH_3OH masers form in the same regions as OH masers (Menten *et al.*, 1992; Caswell *et al.*, 1995d) (see Section 6.1 for a more detailed discussion).

The production of molecules in interstellar space is a complex field. Typically several different production and destruction pathways exist for each step required to form a given molecular species. In addition the rates for some of the reactions are unknown, or have not been calculated for the conditions applicable in molecular clouds. These two factors make detailed modelling of the chemistry of molecular clouds and star formation regions a formidable task. An excellent review of the current status of research into the production of CH_3OH in both molecular clouds and star formation regions is given by Herbst (1991) and I will mention only a few important points.

While the CH_3OH abundances observed in cold dark clouds can be accounted for by gas phase production mechanisms, the enhanced abundances observed in star formation regions cannot (Herbst, 1991; Charnley *et al.*, 1995). The alternative mechanism for the production of enhanced CH_3OH abundances is that it is desorbed from the surfaces of dust grains when the gas is heated by the gravitational collapse and formation of a proto-star. The addition of hydrogen atoms to molecules apparently proceeds easily on the surfaces of dust grains. However, the formation of CH_3OH by addition of H atoms to CO is impeded, though still possible at a slower rate (Tielens and Haden, 1982). An alternative grain surface production mechanism for CH_3OH is the addition of a methyl radical to a hydroxyl radical. The main problem with this is that heavy species such as these are much less mobile on the surface of the grains than hydrogen (Herbst, 1991). Thus while it is generally believed that enhanced abundances of CH_3OH observed in star formation regions are produced upon the surfaces of dust grains, the method by which this production occurs is not yet clear.

Chapter 3

Methanol masers in other Galaxies

3.1 Introduction

The first detection of a molecular transition in a galaxy other than our own was made by Weliachew (1971), who observed OH absorption toward M82 and NGC 253. Extragalactic maser emission was first detected two years later, also toward NGC 253 by Whiteoak & Gardner (1973). Since then maser emission from H_2O, CH and H_2CO has been detected toward extragalactic sources (Churchwell *et al.*, 1977; Whiteoak *et al.*, 1980; Baan *et al.*, 1986).

The first extragalactic OH and H_2O masers were detected in relatively nearby galaxies. Although in some cases they have luminosities which exceed those of any Galactic masers from the same transition, they appeared to be essentially very strong Galactic masers. Theoretical models dictate that maser emission must be beamed, but the degree of beaming is highly dependent on the particular model and its geometry. Because the degree of beaming has not been determined for any masers, their luminosities are typically quoted as isotropic luminosities (the luminosity it would have were it emitting the flux density we detect through 4π steradians). The typical isotropic luminosity for a Galactic OH maser is 10^{-3} L$\odot$ and the first extragalactic OH masers to be discovered had luminosities up to 100 times greater.

3.1.1 OH megamasers

Continuing investigation into extragalactic masers has shown that many belong to a different category of source, and are not just strong Galactic masers. The most startling discovery, which conclusively showed that extragalactic masers are a different class of sources was made by Baan *et al.* (1982). Baan *et al.* detected broad, strong OH maser emission toward the peculiar galaxy Arp 220. Initially this was thought to be a unique source, but subsequent searches towards other far infra-red (FIR) luminous, starburst galaxies have detected more than 50 similar sources. These sources are known as megamasers because they have isotropic luminosities more than 1 million times greater than typical Galactic OH masers.

The observational characteristics of OH megamasers have been summarised by Henkel *et al.* (1991). Some of the more important are that most of the galaxies are interacting, are highly luminous in the far infra-red, the line profiles are much broader than Galactic OH masers, and the 1667-GHz emission is usually stronger than the 1665-MHz emission.

3.1.1.1 Arp 220

Arp 220 is the prototypical OH megamaser galaxy and extremely luminous at far-infrared wavelengths. It has an irregular large scale morphology, a double nucleus, and is believed to be the result of a merger. There are two competing models for the cause of the extreme FIR luminosity of galaxies like Arp 220. The first is that they are the result of massive star formation, triggered by the merging of two galaxies (Solomon and Sage, 1988). The second, is that the merger has produced a proto-quasar. The nucleus of which is obscured by a dense molecular torus which reradiates shorter wavelengths in the far-infrared (Norris, 1985; Norris, 1988). The standard model for OH megamaser emission has been that it arises from a large region near the nucleus of the Galaxy. Recent observations have shown this not to be the case for Arp 220 (Lonsdale *et al.*, 1994). Very Long Baseline Interferometry (VLBI) observations reveal that the majority of the maser emission is confined to regions of 10 pc or less, rather than 100-1000 pc as had previously been thought. This finding supports the obscured quasar model for Arp 220 (Lonsdale *et al.*, 1994)

3.1.2 Superluminous H_2O masers

Many of the extragalactic H_2O masers which have been detected in nearby galaxies appear to be similar to W49, the strongest of the Galactic H_2O masers. However, there are 10 galaxies which exhibit a different type of H_2O maser emission : NGC 4945 (dos Santos and Lépine, 1979), Circinus (Gardner and Whiteoak, 1982), NGC 1068, NGC 4258 (Claussen *et al.*, 1984), NGC 3079 (Henkel *et al.*, 1984), Mrk 1, Mrk 1210, NGC 5506, NGC 1052 and NGC 2639 (Braatz *et al.*, 1994). While these masers also have luminosities approaching 1 million times that of a typical Galactic H_2O maser, their other characteristics are very different from OH megamasers and there are no sources in both categories. The emission from superluminous H_2O masers is narrow, highly variable and tightly confined to the nuclear region of the Galaxy (Claussen and Lo, 1986). Like the OH megamaser galaxies, these galaxies are all luminous in the far infrared and appear to have a very high rate of star formation. Searches for superluminous H_2O masers have in general been less successful than those for OH megamasers. One of the reasons has been the difficulty in determining which types of galaxies are more likely to exhibit superluminous H_2O maser emission. The most recent search by Braatz *et al.* (1994) has shown that superluminous H_2O masers are most likely to occur in active galaxies classified as Seyfert 2 or LINERs.

3.1.2.1 NGC 4258

Superluminous H_2O maser emission was first detected in the spiral galaxy NGC 4258 by Claussen *et al.* (1984). Subsequent observations by Claussen & Lo (1986) showed that the emission was both highly variable, and confined to a region of less than 1.3 pc toward the centre of the galaxy. The recent discovery by Nakai *et al.* (1993) of extremely high-velocity components in the H_2O maser emission from NGC 4258 has sparked a renewed interest in these sources. Nakai *et al.* detected maser emission offset from the systematic velocity of the galactic nucleus by nearly 1000 km s^{-1} (much greater than the observed rotation velocity). Offset components are detected both blue and redshifted from the central peak components which are centred approximately on the systematic velocity of the galaxy. Three theories have been put forward to explain the extremely high-velocity features :

1. They occur in jets being ejected from a black hole in the centre of the galaxy.
2. They lie in a near edge on accretion disk surrounding a massive black hole at the centre of the galaxy (Watson and Wallin, 1994).
3. They are due to stimulated Raman scattering of the central components (Deguchi, 1994).

The theory of stimulated Raman scattering is that in special conditions, maser radiation propagating through an electron plasma may interact with a plasma wave and redshift the radiation. It is more difficult, but possible, also to explain blueshifted radiation using this mechanism. A prediction of stimulated Raman scattering is that the scattered components should be linearly polarized, even if the incident radiation is not. Observations by Deguchi *et al.* (1995b) failed to detect linear polarisation in the extremely high-velocity components of NGC 4258, with a lower limit of 20%. While these observations do not directly rule out stimulated Raman scattering, they make it seem a less likely hypothesis.

Currently the favoured hypothesis for the extremely high-velocity components is that they occur in the accretion disc surrounding a massive black hole at the centre of NGC 4258. X-ray observations using the *ASCA* satellite show that NGC 4258 has an obscured, low luminosity active nucleus (Makishima *et al.*, 1994). The accretion disc hypothesis is strongly supported by recent VLBI observations, which show that the spatial and velocity distribution fit a Keplerian disc model very well (Greenhill *et al.*, 1995; Miyoshi *et al.*, 1995). The Keplerian system they model requires the presence of a mass of 3.6 x 10^7 M$\odot$ within a region of radius 0.13 pc or less. This implies a volume averaged mass density more than an order of magnitude greater than for any other black hole candidate. Maoz (1995) has argued that the observations of Miyoshi *et al.* effectively rule out a massive cluster of low-mass dark objects at the centre of NGC 4258. Future VLBI observations to measure the proper motion of the masers will enable further refinements of the accretion disc model. In addition to the information on the black hole candidate at the centre of NGC 4258 these observations may also provide information on the beaming of the superluminous H_2O masers and a purely geometric measurement

of the distance to NGC 4258. Miyoshi *et al.* have modelled the morphology of the H_2O masers as purely Keplerian motion. Smette & Kuijken (1995) calculate that there should be a detectable systematic offset from Keplerian motion due to gravitational redshift.

3.1.3 Extragalactic H_2CO and CH masers

Extragalactic maser emission from other molecules is much more rare than for either OH, or H_2O. Emission from the 6-cm transition of Ortho-formaldehyde has been detected towards two sources, NGC 253 and Arp 220 (Baan *et al.*, 1986; Baan *et al.*, 1990). In both cases the formaldehyde spectrum is very similar in appearance to that of the much stronger OH emission. Extragalactic CH maser emission seems to be associated with H_2O maser emission, rather than OH (Henkel *et al.*, 1991). Interestingly there are more known extragalactic than Galactic CH masers, illustrating again the different nature of the two types of sources.

Highly luminous extragalactic masers are currently thought to arise in the foreground portion of a dense circumnuclear cloud of molecular gas, amplifying the intense nucleus of the interacting galaxies in which they occur. OH and H_2CO megamasers have been assumed to be unsaturated, with a large fraction of the circumnuclear gas masing. The large volume of gas involved in the megamaser emission means that they should not be variable, despite being unsaturated and this is supported by observation (Baan, 1985). However, recent high resolution observations of the OH emission from Arp 220 shows that most of the emission originates from much smaller regions than had previously been thought (Lonsdale *et al.*, 1994).

Claussen & Lo (1986) have suggested that superluminous H_2O masers are saturated and occur in dense molecular pockets exposed to a nuclear outflow. This mechanism explains their compact size, the offset between the systematic and maser velocities, and the lack of correlation between FIR emission and the occurrence of H_2O masers (as only a small fraction of the circumnuclear gas is involved in the maser emission). Recent observations of NGC 4258 which appear to show that the H_2O masers lie in a circumnuclear disc surrounding a massive black hole (Miyoshi *et al.*, 1995), are roughly consistent with this picture. Further VLBI observations of superluminous water masers are required to determine whether the circumnuclear disc model applies to all, or whether NGC 4258 is an exceptional source.

3.1.4 Masers in the Magellanic Clouds

The Large and Small Magellanic Clouds, are the two galaxies closest to our own and their relative proximity makes them natural targets for maser searches. The rate at which masers occur can be used to compare the global rates of massive star formation in the Magellanic Clouds with the Milky Way. Although several searches have been made for OH and H_2O masers toward the Magellanic Clouds, all have been relatively unsuccessful. In total two OH masers have been detected in the Large Magellanic Cloud (LMC) (Caswell and Haynes, 1981; Haynes and

Caswell, 1981), one of which also shows emission in the excited 6.035-GHz transition (Caswell, 1995). Five H_2O masers have been detected in the LMC and two in the Small Magellanic Cloud (SMC) (Scalise Jr and Braz, 1982; Whiteoak *et al.*, 1983; Whiteoak and Gardner, 1986). Whiteoak & Gardner (1986) searched toward 80 HII regions, with a sensitivity limit equal to the average observed Galactic H_2O maser luminosity. They suggest that the low rate of detection may indicate a lower rate of massive star formation in the Magellanic Clouds.

3.2 Methanol masers in the Magellanic Clouds

Two searches for 6.7-GHz CH_3OH maser emission in the Magellanic Clouds have been made.

The first of these which I describe here in sections 3.2.1 & 3.2.2 and have published in Ellingsen *et al.* (1994b), used the Parkes radiotelescope to search for 6.7-GHz CH_3OH maser emission toward 35 HII regions in the LMC and 13 in the SMC.

The second search, is described below in sections 3.2.3 & 3.2.4 and will be published in a paper by Beasley *et al.* (1996). This search used the Australia Telescope Compact Array (ATCA) to search for 6.7-GHz CH_3OH maser emission toward 13 *IRAS* source in the SMC, 42 *IRAS* sources in the LMC and 12 LMC regions with thermal Hα emission.

3.2.1 Parkes Observations

The observations were made using a dual channel cooled HEMT 6.7-GHz receiver at the Parkes 64-m telescope during the periods 1992 February 25 to March 9, June 1–9 and September 24–30. The half-power beamwidth and receiver-system temperature were 3.3 arcmin and 50 K respectively. The search was performed during the first observing session, using a correlator configuration with a 2-MHz bandwidth and 1024 channels for each of two orthogonal circular polarizations. Two 15 minute observations were made towards each source, the second offset in frequency by 0.25 MHz. The final spectrum was produced off-line, by averaging the difference spectrum with itself, after a frequency shift of -0.25 MHz and inversion. The average rms noise level in the final spectrum was typically ≤ 0.05 Jy, although the sensitivity is less at the edges of the range due to the frequency switching. This yielded a total velocity coverage of approximately 100 km s^{-1} and a velocity resolution of 0.2 km s^{-1} after Hanning smoothing.

The SMC sources were selected from the catalogue of McGee, Brooks & Batchelor (1976) and are listed in Table 3.1. The LMC sources were selected from the catalogues of McGee *et al.* (1972) and Heinze (1956) and are listed in Table 3.2. The measured rms noise levels and observed velocity range for each source are listed in Tables 3.1 and 3.2. In addition to the targeted search, a 30 x 36 arcmin region centred at RA(B1950)=$05^h38^m05^s$, Dec(B1950)= $-69°18'00''$ (the molecular cloud/HII region South of the 30 Doradus nebula) was observed with a 3-arcmin grid. These observations had a typical rms noise level of 0.1 Jy.

Table 3.1: Observed HII regions in the Small Magellanic Cloud. Source names and positions are from McGee *et al.* (1976).

Source Name	Position (B1950)						Velocity search range	rms noise
	Right Ascension			Declination				
	(h	m	s)	(°	′	″)	(km s^{-1})	(Jy)
s7	00	44	48	-72	57	12	85–165	0.11
s9	00	45	30	-73	24	16	95–180	0.07
s10	00	46	23	-73	33	50	100–200	0.06
s15	00	48	36	-73	08	12	130–230	0.04
s16	00	49	18	-73	03	36	130–230	0.04
s17	00	57	37	-72	26	39	120–215	0.04
s18	01	01	00	-76	02	30	130–230	0.03
s19	01	01	48	-72	19	00	140–240	0.05
s20	01	02	23	-72	18	17	145–245	0.04
s21	01	03	36	-72	15	48	150–250	0.04
s23	01	06	24	-72	16	30	135–230	0.04
s26	01	12	49	-73	36	15	130–230	0.03
s27	01	28	19	-73	48	14	130–230	0.04

During the two latter observing sessions we re-observed the sources detected in the initial search to improve the signal-to-noise ratio of our spectra and to check for variability. For these sessions we used a correlator configuration with 2-MHz bandwidth and 2048 channels per polarization, yielding a velocity resolution of approximately 0.1 km s^{-1} after Hanning smoothing. The final spectra were produced by taking the quotient of a 30 minute on-source observation, with a common reference spectrum. The intensity scale was calibrated from observations of the sources Hydra A and PKS 1934-638, which were assumed to have peak flux densities of 9.8 and 4.1 Jy at a frequency of 6.7 GHz.

3.2.2 Parkes Results

This search detected 6.7-GHz CH_3OH maser emission toward two HII regions (MC18 & MC23) in the Large Magellanic Cloud. 6.7-GHz CH_3OH maser emission toward MC23 (N105a) had previously been detected by Sinclair *et al.* (1992). The spectrum (see Fig. 3.1) shows two main components at heliocentric velocities of 250.7 and 251.8 km s^{-1} (there may be a weaker component at 249.7 km s^{-1}). The two components have half-widths of 0.3 and 0.4 km s^{-1} respectively and approximately equal peak flux densities (0.17 Jy). Both OH and H_2O maser emission have been detected toward MC23, making it the only HII region in the Magellanic Clouds for which emission from each of these transitions and CH_3OH has been detected. OH maser emission at 1.665 and 1.667 GHz was detected at velocities of 253.5 and 253.9 km s^{-1} respectively (Haynes and Caswell, 1981). The 1.665-GHz emission is significantly stronger (0.76 Jy) and wider (half-width 0.84 km s^{-1}) than the 6.7-GHz CH_3OH maser emission. In general for Galactic

Table 3.2: Observed HII regions in the Large Magellanic Cloud. References : 1=McGee *et al.* (1972); 2=Heinze (1956)

Source Name		Position (B1950)						Velocity search range	rms noise
		Right Ascension			Declination				
(1)	(2)	(h	m	s)	(°	′	″)	(km s^{-1})	(Jy)
MC8	–	04	48	04	-69	20	30	210–310	0.04
MC10	N77	04	50	07	-69	16	30	210–310	0.05
MC12	N4a	04	51	56	-66	59	48	210–310	0.05
MC13	N79a	04	52	10	-69	27	00	210–310	0.04
MC16	N83b	04	54	35	-69	15	48	210–310	0.05
MC18	N11	04	56	41	-66	29	09	250–350	0.06
MC19	N91	04	57	33	-68	29	30	210–310	0.06
MC23	N105a	05	10	06	-68	57	00	210–310	0.03
MC24	N113	05	13	43	-69	25	56	213–287	0.04
MC27	–	05	16	04	-72	39	36	210–310	0.05
MC29	–	05	17	38	-72	39	48	210–310	0.04
MC30	N119	05	19	07	-69	16	24	210–310	0.04
MC33	N44d	05	23	11	-68	04	54	259–359	0.04
MC46	N51d	05	26	33	-67	30	48	210–310	0.04
MC50	N51a	05	27	56	-67	28	18	210–310	0.04
MC53	–	05	30	24	-72	47	06	210–310	0.04
MC54	N206a	05	32	05	-71	05	58	210–310	0.04
MC56	N148c	05	32	03	-68	31	54	210–310	0.04
MC57	N57	05	32	35	-67	43	48	210–310	0.04
MC58	N55	05	32	30	-66	28	48	210–310	0.05
MC61	N154	05	35	06	-69	50	16	210–310	0.04
MC64	N59a	05	35	31	-67	36	26	210–310	0.05
MC69	–	05	36	12	-69	14	30	210–310	0.03
MC71	N154a	05	36	29	-69	41	44	210–310	0.04
MC74	N157a	05	39	03	-67	07	07	230–300	0.05
MC75	N158c	05	39	25	-69	31	44	223–323	0.09
–	N159a	05	39	57	-69	48	50	213–287	0.03
MC76	N160a	05	40	08	-69	39	54	217–291	0.05
MC77	N159	05	40	22	-69	46	25	210–310	0.04
MC78	N158a	05	40	32	-69	21	18	210–310	0.05
MC79	–	05	42	32	-69	07	54	210–310	0.04
MC80	N214c	05	42	19	-71	21	05	210–310	0.04
MC82	N164	05	42	59	-69	04	15	210–310	0.04
MC84	N163	05	43	36	-69	46	49	210–310	0.05
MC91	N180a	05	49	21	-70	04	59	210–310	0.04

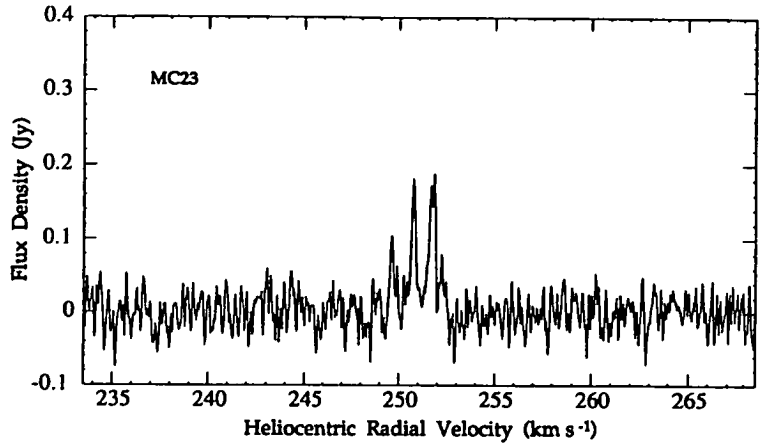

Figure 3.1: The spectrum of the 6.7-GHz CH_3OH maser MC23(N105a)

sources, 6.7-GHz CH_3OH masers have a peak flux density approximately an order of magnitude greater than the associated OH masers (Caswell *et al.*, 1995c). However, the distribution of CH_3OH:OH ratios is broad and Caswell *et al.* found that 25% of CH_3OH masers have peak flux densities less than the associated OH masers. This suggests that the CH_3OH:OH ratio observed for MC23 (0.22) is not particularly unusual in comparison with Galactic sources. H_2O maser emission toward MC23 is also stronger than the 6.7-GHz CH_3OH maser emission and covers a much greater velocity range (252–268 km s^{-1}) than either the OH or CH_3OH (Whiteoak *et al.*, 1983; Whiteoak and Gardner, 1986). High resolution observations of the 6.7-GHz radio continuum and CH_3OH masers have been made using the Australia Telescope Compact Array (ATCA) (Ellingsen *et al.*, 1994b). These observations show MC23 to be a large, complex HII region, the maser emission appears to be associated with one of the weaker continuum peaks.

6.7-GHz CH_3OH maser emission was also detected toward the HII region MC18 (N11) (see Fig. 3.2). For MC18 the CH_3OH maser emission has only a single peak, with a flux density of 0.3 Jy at a heliocentric velocity of 301 km s^{-1}. This is the first maser detected toward this HII region, searches for OH and H_2O masers failed to find emission with peak flux density greater than 0.02 and 0.5 Jy respectively (unpublished observations by J.L. Caswell ; Whiteoak *et al.* 1983). ATCA observations by Ellingsen *et al.* (1994b) find that the 6.7-GHz CH_3OH maser emission is slightly offset from the main continuum emission.

3.2.3 ATCA Observations

I have also been involved in a project headed by Tony Beasley of NRAO, to search for 6.7-GHz CH_3OH maser emission toward *IRAS* sources. The primary purpose of this project is to measure the proper motion of the Magellanic Clouds by phase referencing VLBI observations of background continuum sources to masers within the Magellanic Clouds. Proper motion studies of masers have previously been used to determine distances and dynamical models of several Galactic star formation regions and the nearby galaxy M33 (Greenhill *et al.*, 1990), and references therein.

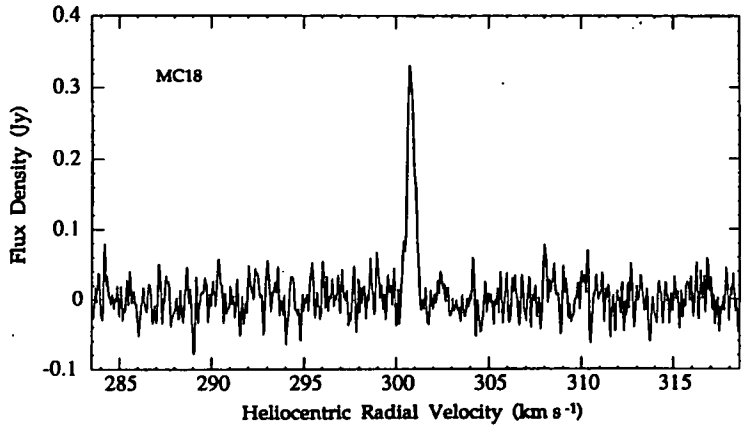

Figure 3.2: The spectrum of the 6.7-GHz CH_3OH maser MC18 (N11)

Phase referencing requires a relatively strong point source with an accurately measured position. The 6.7-GHz CH_3OH masers in MC18 and MC23 are both quite weak and phase referencing using them would be marginal. Because of this a second search for 6.7-GHz CH_3OH masers in the Magellanic Clouds was undertaken using the ATCA.

Wood & Churchwell (1989a) developed criteria for selecting sources which have a high probability of being compact or ultra-compact HII (UCHII) regions from the *IRAS* Point-Source Catalogue (PSC) (IRAS, 1985). These criteria are based on the logarithmic ratios of various *IRAS* wavebands and are discussed in detail in Section 5.4.1.1. As 6.7-GHz CH_3OH masers are typically associated with UCHII regions, the Wood & Churchwell criteria have been used successfully to select *IRAS* sources to search for maser emission (Schutte *et al.*, 1993; van der Walt *et al.*, 1995).

We searched the *IRAS* PSC for sources in the Magellanic Clouds region (270° $\leq l \leq$ 310° & -50° $\leq b \leq$ -27°) which meet the Wood & Churchwell criteria (see section 5.4.1.1). At 6 GHz the FWHM primary beam of the ATCA antennas is $\approx$ 5 arcmin, so any sources within 5 arcmin of each other were represented by a single entry and *IRAS* sources within 5 arcmin of a position observed during the Parkes search were excluded. This yielded 13 target sources in the SMC and 42 in the LMC (see Tables 3.3 & 3.4). In addition observations were also made toward 12 bright Hα knots, which exhibit thermal continuum emission. These were selected from the catalogue of Davies *et al.* (1976) (see Table 3.5).

The observations were made by Tony Beasley and myself during the period 1994 July 19–24. The ATCA was in the 6A configuration, which has a minimum baseline of 0.33 km and maximum baseline of 5.9 km. The correlator was configured to record both a 128-MHz bandwidth centred at 8.8 GHz, and a 4-MHz bandwidth centred at 6.662 GHz for LMC observations, and 6.665 GHz for SMC observations. This enabled us to search for 6.7-GHz CH_3OH masers, whilst simultaneously imaging the continuum emission associated with any detected masers. The 4-MHz band was split into 1024 channels yielding a velocity coverage of 180 km s^{-1} and a velocity resolution of $\approx$ 0.18 km s^{-1}. For the LMC

Table 3.3: Observed *IRAS* point-sources in the SMC. The noise level listed is the 1-σ error in the processed image (in Jy/beam).

IRAS PSC Name	Position (J2000) Right Ascension (h m s)			Declination (° ′ ″)			rms noise	*IRAS* PSC Flux Densities 12 (μm)	25 (μm)	60 (μm)	100 (μm)	*IRAS* colours Log_{10} of : S_{25}/S_{12}	S_{60}/S_{12}
00260-7315	00	28	10.774	-72	58	42.74	0.080	0.3	2.1	5.6	4.5	0.85	1.27
00430-7326	00	44	54.950	-73	10	21.14	0.081	0.4	3.0	9.7	20.4	0.88	1.38
00432-7332	00	45	04.615	-73	16	28.28	0.076	0.3	1.4	9.6	28.7	0.67	1.51
00435-7339	00	45	22.433	-73	22	46.53	0.081	0.3	1.6	17.6	33.6	0.73	1.77
00462-7331	00	48	05.264	-73	15	15.90	0.079	0.9	8.9	51.0	99.6	1.00	1.75
00466-7322	00	48	25.697	-73	05	49.21	0.084	0.3	1.6	24.5	61.5	0.73	1.91
00489-7302	00	50	44.350	-72	46	40.35	0.084	0.3	1.0	7.2	17.4	0.52	1.38
00569-7243	00	58	40.443	-72	27	32.48	0.084	0.3	2.6	6.2	11.3	0.94	1.32
01035-7215	01	05	06.689	-71	59	24.93	0.087	1.2	10.7	46.7	54.0	0.95	1.59
01077-7327	01	09	11.995	-73	11	42.12	0.086	0.5	3.0	18.8	21.9	0.78	1.58
01126-7332	01	14	04.358	-73	16	50.67	0.089	0.6	2.8	26.4	54.3	0.67	1.64
01133-7336	01	14	45.324	-73	20	42.62	0.084	0.2	2.1	24.6	54.3	1.02	2.09
01228-7324	01	24	07.287	-73	09	08.52	0.083	1.7	19.4	51.5	49.4	1.06	1.48

the observing frequency corresponded to a heliocentric velocity range centred on $\approx$ 300 km s^{-1} and for the SMC, $\approx$ 160 km s^{-1}.

Each program source was observed 4 or 5 times for a 7-minute period over the eleven hour observing session. A four minute observation of a calibration source was made once every twenty-five minutes. One of the two known sources (MC18 and MC23) was observed on each day, in order to check the integrity of the observations.

3.2.4 ATCA Results

The data were processed at NRAO by Tony Beasley using the Astronomical Image Processing System (AIPS) to perform the calibration and imaging. For each source a naturally weighted spectral line image cube was produced of the inner 800 channels. Each image was 6.8 x 6.8 arcmin in size. This means that for each source we searched a 6.8-square-arcmin region, centred on the *IRAS* position over a velocity range of 140 km s^{-1} centred on a heliocentric velocity of 300 km s^{-1} for the LMC and 160 km s^{-1} for the SMC. The typical rms noise in each image was 80–100 mJy. The noise distribution was examined for several cubes, and found to be nearly Gaussian, but with more high points than for purely Gaussian statistics. Each cube was then searched for pixels above 7-σ, or a pixel with flux density > 600 mJy. The typical velocity half-width of a 6.7-GHz CH_3OH maser is $\sim$ 0.47 km s^{-1} (Ellingsen *et al.*, 1996b), so the emission from surrounding velocity channels was then examined to see if they also contained emission at the same spatial position. We believe that this technique will detect all 6.7-GHz CH_3OH masers with a peak flux density $\geq$ 600 mJy.

The search detected three masers (see Table 3.6) : the two masers in MC18 and MC23, and an additional maser toward the *IRAS* source 05011-6815 (see Fig. 3.3). The 6.7-GHz CH_3OH maser associated with 05011-6815 has a peak flux density of 3.8 Jy, more than an order of magnitude stronger than either of the previously detected masers in the LMC. It is equivalent to a 720 Jy maser at a distance of 4 kpc (assuming a distance of 55 kpc for the LMC), which is a relatively strong

Table 3.4: Observed *IRAS* point-sources in the LMC. The noise level listed is the 1-σ error in the processed image, except for 05011-6815 where it is the peak flux detected in the ATCA observations (in Jy/beam).

IRAS PSC	Position (J2000)						rms	*IRAS* PSC Flux Densities				*IRAS* colours	
Name	Right Ascension			Declination			noise	12	25	60	100	Log_{10} of :	
	(h	m	s)	(°	′	″)		(μm)	(μm)	(μm)	(μm)	S_{25}/S_{12}	S_{60}/S_{12}
04491-6915	04	48	53.862	-69	09	55.49	0.098	0.5	2.2	14.2	98.5	0.64	1.45
04531-6808	04	53	02.243	-68	03	52.49	0.098	0.9	3.8	33.0	58.3	0.63	1.56
04540-6650	04	54	05.039	-66	45	54.54	0.090	0.4	1.8	11.1	24.3	0.65	1.44
04540-6721	04	54	03.604	-67	16	20.57	0.100	0.3	1.8	8.3	19.1	0.78	1.44
04544-6925	04	54	08.637	-69	20	24.52	0.096	0.3	1.2	11.3	39.7	0.60	1.58
04555-6829	04	55	26.427	-68	25	20.69	0.098	0.5	2.2	12.5	34.9	0.64	1.40
04556-6630	04	55	44.225	-66	25	46.41	0.095	0.3	1.1	20.3	87.2	0.56	1.83
04557-6639	04	55	50.062	-66	34	37.85	0.098	0.3	1.2	12.3	83.8	0.60	1.61
04573-6849	04	57	11.353	-68	44	41.15	0.098	0.8	3.6	43.1	94.3	0.65	1.73
04580-6626	04	58	11.260	-66	21	45.72	0.098	0.2	1.6	24.3	40.8	0.90	2.08
05011-6815	05	01	02.965	-68	10	46.30	2.913	0.3	1.0	5.9	15.5	0.52	1.29
05047-6644	05	04	46.253	-66	40	22.69	0.095	0.5	2.2	15.3	26.4	0.64	1.49
05049-7047	05	04	24.425	-70	43	50.39	0.088	0.5	2.1	22.6	50.3	0.62	1.66
05051-6807	05	05	00.360	-68	03	33.07	0.104	0.2	1.5	17.9	41.9	0.88	1.95
05051-7058	05	04	37.406	-70	54	31.38	0.088	1.6	11.4	62.0	85.2	0.85	1.59
05052-7011	05	04	51.281	-70	07	31.08	0.103	0.6	2.4	23.7	45.6	0.60	1.60
05053-6659	05	05	20.465	-66	55	06.18	0.099	0.5	5.4	29.0	38.0	1.03	1.76
05094-6833	05	09	14.270	-68	30	13.24	0.098	0.3	2.0	12.7	36.3	0.82	1.63
05139-6730	05	13	51.733	-67	27	18.73	0.087	1.6	8.5	42.4	72.0	0.73	1.42
05141-6938	05	13	44.509	-69	35	36.87	0.091	0.2	1.9	24.8	62.5	0.98	2.09
05148-6933	05	14	32.095	-69	29	50.24	0.087	0.3	1.4	18.0	43.3	0.67	1.78
05174-6936	05	17	04.726	-69	33	41.20	0.088	0.4	1.7	17.9	155.4	0.63	1.65
05175-6645	05	17	33.577	-66	42	48.42	0.088	0.5	5.2	25.0	49.0	1.02	1.70
05192-6824	05	19	04.325	-68	21	24.40	0.089	0.4	1.3	11.0	18.9	0.51	1.44
05202-6655	05	20	15.809	-66	52	56.11	0.087	0.3	2.2	20.0	39.1	0.87	1.82
05214-6532	05	21	33.433	-65	29	16.34	0.085	0.3	2.2	12.1	20.6	0.87	1.61
05219-6943	05	21	34.978	-69	40	19.65	0.082	1.8	7.1	67.1	173.8	0.60	1.57
05221-6800	05	22	01.351	-67	57	47.00	0.098	3.2	35.2	211.9	470.5	1.04	1.82
05222-6737	05	22	09.503	-67	34	57.48	0.100	0.2	0.7	6.2	11.9	0.54	1.49
05228-6643	05	22	50.484	-66	41	09.18	0.092	0.4	1.8	12.9	36.8	0.65	1.51
05240-6809	05	23	50.056	-68	07	10.88	0.095	0.3	1.6	5.3	142.5	0.73	1.25
05270-6851	05	26	48.727	-68	49	11.98	0.093	3.9	24.2	99.5	180.6	0.79	1.41
05330-6826	05	32	48.122	-68	24	04.84	0.089	0.5	3.1	28.2	66.9	0.79	1.75
05333-6948	05	32	53.396	-69	46	26.67	0.089	1.4	8.8	68.9	83.6	0.80	1.69
05339-6847	05	33	41.375	-68	45	57.81	0.085	1.7	8.0	64.2	102.5	0.67	1.58
05356-6604	05	35	44.656	-66	02	16.97	0.087	0.4	2.1	16.8	55.6	0.72	1.62
05389-7042	05	38	21.404	-70	41	06.80	0.116	1.3	5.0	43.3	82.8	0.59	1.52
05391-6926	05	38	46.175	-69	24	56.14	0.088	0.6	3.2	30.3	347.1	0.73	1.70
05400-7013	05	39	30.905	-70	12	20.67	0.099	0.4	2.1	16.4	44.2	0.72	1.61
05406-7111	05	39	54.738	-71	10	03.77	0.095	1.7	9.9	65.4	112.7	0.77	1.59
05438-6926	05	43	28.211	-69	24	53.64	0.101	0.3	1.2	11.8	56.8	0.60	1.59
05458-6947	05	45	25.857	-69	46	34.32	0.098	0.5	4.2	35.6	38.9	0.92	1.85

Table 3.5: Observed Sources from Davies *et al.* (1976) in the LMC. The noise level listed is the 1-σ error in the processed image

Source Name	Position (J2000) Right Ascension (h m s)	Declination (° ′ ″)	rms noise (Jy/beam)
DEM85	05 09 15.618	-69 45 45.74	0.085
DEM121	05 16 52.403	-67 19 51.63	0.088
DEM150	05 21 37.313	-67 46 35.22	0.087
DEM162	05 23 06.810	-66 22 34.28	0.087
DEM173	05 24 04.388	-69 40 15.41	0.087
DEM176b	05 24 09.218	-68 55 54.51	0.084
DEM183	05 25 27.670	-66 21 47.43	0.083
DEM186	05 25 17.371	-69 39 29.67	0.079
DEM190	05 26 01.607	-66 04 59.80	0.087
DEM242	05 34 47.761	-69 31 17.87	0.087
DEM273	05 40 11.312	-68 59 25.18	0.085
DEM320	05 48 02.365	-69 53 50.76	0.086

Table 3.6: 6.7-GHz CH_3OH masers detected in the Magellanic Clouds. The velocities in the table are heliocentric and the positions for MC18 and MC23 are from Ellingsen *et al.* (1994b)

Source Name	Position (B1950) Right Ascension (h m s)	Declination (° ′ ″)	Peak Flux Density (Jy)	Velocity of Peak (km s^{-1})	Velocity range (km s^{-1})
MC18 (N11)	04 56 40.87	-66 29 05.00	0.30	300.7	300–301
MC23 (N105a)	05 10 11.61	-68 57 19.00	0.17	250.7	249–252
05011-6815	05 01 09.84	-68 14 43.22	3.80	267.9	265–269

for a Galactic 6.7-GHz CH_3OH maser. There are no other masers known to be associated with this source. A search for 12.2-GHz CH_3OH maser emission using the University of Tasmania 26-m radiotelescope failed to detect any emission with peak flux density > 0.66 Jy (3-σ noise level).

3.2.5 Discussion

The two searches described above have detected 6.7-GHz CH_3OH maser emission toward only 3 of 115 sites. This represents a detection rate of 2.6%. For the Parkes search the 5-σ detection limit was typically 250 mJy, or less. If we assume that the distance to the LMC is 55 kpc, then this corresponds to a flux density of 47 Jy at a distance of 4 kpc (a typical distance for Galactic masers). So far Galactic searches (including the one described in Chapter 5) have detected 392 6.7-GHz CH_3OH masers (Menten, 1991a; MacLeod and Gaylard, 1992; MacLeod *et al.*, 1992; MacLeod *et al.*, 1993a; Schutte *et al.*, 1993; Caswell *et al.*, 1995c; van der Walt *et al.*, 1995; Ellingsen *et al.*, 1996b; Caswell, 1996), of these 109 ($\approx$ 28%) have a peak flux density greater than 47 Jy.

Searches for maser emission toward sources selected from the *IRAS* Point-Source Catalogue have become common in the last 5–8 years (see Section 5.4.1.1).

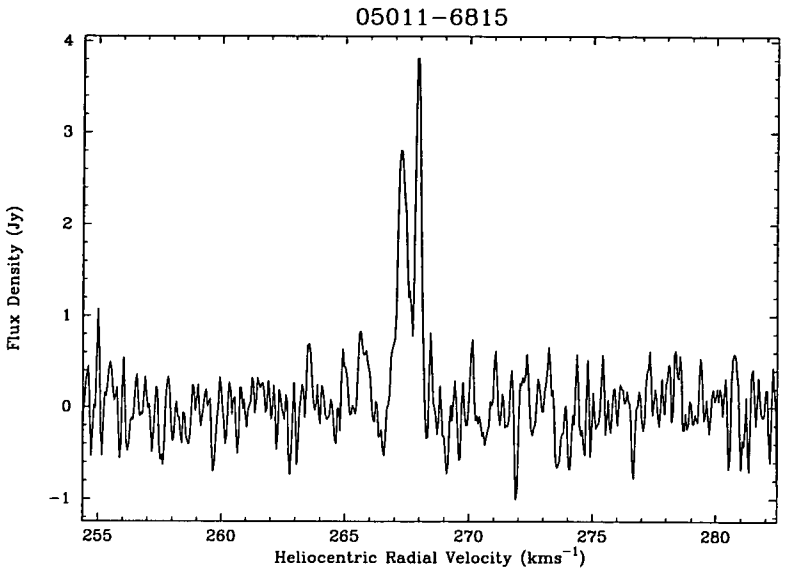

Figure 3.3: The spectrum of the 6.7-GHz CH_3OH maser 05011-6815 observed with the Mt Pleasant 26-m radiotelescope

These searches have generally been quite successful, detecting masers toward a sizable fraction of the *IRAS* sources observed. A total of 13 sources in the SMC and 62 in the LMC, meet the criteria $Log_{10}(S_{60}/S_{12}) \geq 1.30$ & $Log_{10}(S_{25}/S_{12}) \geq 0.57$ and have high quality flux density measurements at 25 and 60 μm (Wood and Churchwell, 1989a). All of these have been searched for 6.7-GHz CH_3OH maser emission (combining the Parkes and ATCA observations). If masers within 1 arcmin of an *IRAS* source are associated with it, those more than 2 arcmin away are not associated and those in between may be associated, then of the 3 detected 6.7-GHz CH_3OH masers in the Magellanic Clouds, one falls into each category. This represents a detection rate of between 1.6–3.2% for the LMC and between 1.3–2.7% for the Magellanic Clouds as a whole. In comparison, the detection rate for the Galactic Plane is between 17–20% (see section 5.4.2). However, to make a meaningful comparison, we must adjust the luminosity limit of the Galactic survey to make it comparable to the LMC search. If we assume that the Galactic masers detected in the Mt Pleasant survey (see Chapter 5) are typically at a distance of 4 kpc and that the distance to the LMC is 55 kpc, then a detection limit of 600 mJy for the Magellanic Clouds observations corresponds to 113 Jy for the Galactic observations. The rate of detection for a Galactic *IRAS* search using the Wood and Churchwell criteria becomes four 6.7-GHz CH_3OH masers from 151 *IRAS* sources. This is a detection rate of 2.6%, which is comparable to the rate observed for the Magellanic Clouds. Further, in some of the outer regions of the Galaxy, the *IRAS* based detection rate is comparable to that observed in the Magellanic Clouds, without taking into account any sensitivity differences in the two sets of observations (see Section 5.4.1).

These observations suggest that the Magellanic Clouds may be deficient in

CH_3OH maser emission relative to our Galaxy, which would agree with the results of searches for other maser species (Whiteoak and Gardner, 1986). A more sensitive *IRAS* search appears to be the easiest way to determine if this really is the case, as a comparison with similar Galactic searches can easily be made. If there is a deficiency in the number of CH_3OH masers in the Magellanic Clouds, two possible causes are; a lower rate of massive star formation, or a deficiency of complex molecules, which might result from a lower metallicity. Beasley *et al.* (1996) have used the results of the Parkes and ATCA surveys of the Magellanic Clouds to examine the effect of metallicity on the number of 6.7-GHz CH_3OH masers. They suggest that the detected number of 6.7 GHz CH_3OH masers in the Magellanic Clouds is consistent with a CH_3OH abundance 6-12 times less than the Galactic abundance. This is consistent with the metallicity implied by observed Magellanic Cloud abundances for similar molecules, such as CO and H_2CO (Cohen *et al.*, 1988b; Whiteoak and Gardner, 1976)

Observations of 6.7-GHz CH_3OH masers in our Galaxy have shown that the median ratio of the peak flux densities of the CH_3OH and OH masers is 5.9 (Caswell *et al.*, 1995c). However, they also find that for 25% of sources the OH emission is stronger than the corresponding CH_3OH emission. There are three sites in the LMC where either 6.7-GHz CH_3OH maser emission or OH emission has been detected, and a search has been made for the other species (MC18, MC23 and MC76). For two of these three sources (MC23 & MC76) the OH emission is stronger than the 6.7-GHz CH_3OH. If we assume that the CH_3OH:OH flux density ratio is the same as observed for Galactic masers, then there is a 14% chance that the OH peak flux density will exceed the CH_3OH peak flux density in 2 out of three sources. Thus the observed peak flux density ratios for 6.7-GHz CH_3OH:OH are consistent with those found for Galactic star-forming regions.

3.3 Methanol masers in other external galaxies

In our Galaxy, 6.7-GHz CH_3OH masers are found frequently in star formation regions, and are closely associated with OH and H_2O masers. Existing surveys (Menten, 1991a; MacLeod and Gaylard, 1992; MacLeod *et al.*, 1992; MacLeod *et al.*, 1993a; Caswell *et al.*, 1995c) indicate that nearly all known OH masers are accompanied by 6.7–GHz CH_3OH activity. Since the same conditions appear to produce both OH and CH_3OH masers within the Galaxy, we might expect the OH maser and megamaser emission in other galaxies to be accompanied by detectable CH_3OH maser emission, possibly even CH_3OH megamaser emission. Furthermore, in Galactic sources, the 6.7-GHz CH_3OH maser emission is typically much stronger than the corresponding OH emission, and so we might even expect extragalactic CH_3OH maser emission to be much stronger than the OH emission. The ratio of the peak flux densities of 6.7–GHz CH_3OH and OH masers spans several orders of magnitude, but is typically of the order of ten. A preliminary search for 12.2-GHz CH_3OH masers was made by Norris *et al.* (1987), but no systematic searches of extragalactic sources had been published, before the searched described here, which has been published by Ellingsen *et al.* (1994a). I was assisted in the

Table 3.7: The selected sample of galaxies. References : 1=Whiteoak & Gardner (1986); 2=Staveley-Smith *et al.* (1992); 3=Baan *et al.* (1982); 4=Bottinelli *et al.* (1987); 5=Whiteoak & Gardner (1973); 6=Norris *et al.* (Norris *et al.*, 1989); 7=Lépine & dos Santos (1977); 8=dos Santos & Lépine (1979); 9=Claussen *et al.* (1984).

Source Name	Position (B1950) RA (h m s)	Declination (° ′ ″)	Velocity range (km s^{-1})	rms noise (Jy)	OH Peak Flux (Jy)	H_2O Peak Flux (Jy)	Ref.
NGC 253	00 45 06	-25 34 00	-900–1400	0.01	0.120	5	2,5,7
NGC 1068	02 40 07	-00 13 30	300–2500	0.03	–	0.7	9
NGC 1487	04 04 05	-42 30 42	-300–1900	0.008	–	–	
NGC 1566	04 18 53	-55 03 24	400–2600	0.01	< 0.04	–	6
10039-3338	10 03 55	-33 38 43	9000–11200	0.02	0.315	–	2
11506-3851	11 50 40	-38 51 10	2000–4200	0.01	0.105	–	2
NGC 4418	12 24 23	-00 36 14	1100–3400	0.02	0.004	–	4
NGC 4945	13 02 32	-49 12 02	-600–1700	0.02	-0.800	9–16	1,2,5,8
Circinus	14 09 18	-65 06 19	-600–1700	0.02	–	3–12	1
Arp 220	15 32 47	23 40 10	4300–6500	0.01	0.280	–	3

observing and analysis of the data presented in this section by Doctors John Whiteoak and Ray Norris.

3.3.1 Observations

Ten galaxies were surveyed for the 5_1-6_0 A^+ CH_3OH transition (see Table 3.7) ; six are known OH maser or megamaser sources (Whiteoak and Gardner, 1973; Norris *et al.*, 1989; Kazès *et al.*, 1990) and two are known superluminous H_2O masers (Whiteoak and Gardner, 1986). Thus the sample is strongly biased towards galaxies which show ultraluminous maser emission in other transitions.

The observations were made between 1992 February 25 and March 9 using the dual–channel cooled HEMT 6.7/12.2–GHz receiver at the Parkes 64–m telescope which, at 6.7 GHz, has a beamwidth of 3.3 arcmin. The equivalent system temperature for the observations was $\sim$ 60 K. An autocorrelator provided two 512–channel spectra in orthogonal linear polarizations, each spread over 64 MHz. Thus the observations covered a velocity extent of $\sim$ 2800 km s^{-1} and had a velocity resolution (after Hanning smoothing) of 7.8 km s^{-1}. Spectra were obtained by making two 10–min observations on–source and two reference observations, one offset by +15 min and the other by -15 min of right ascension. These were then used to produce two quotient spectra each with different references, yielding a total on–source time of 20 min. The resulting spectra for the two polarizations were then averaged and Hanning smoothed. The resulting rms noise level of a 10–min observation was typically 0.04 Jy. To achieve the desired sensitivity, multiple observations were made of each source. The total integration time for most sources was 20–40 min, but sometimes exceeded 1 h; the resulting 3-σ detection level was typically $\leq$ 0.06 Jy. However, due to the coarse spectral resolution of these observations, the sensitivity to narrow Galactic type 6.7-GHz CH_3OH maser emission is approximately 5 times worse.

Flux density calibration was carried out using observations of the sources PKS 0407-658, Hydra A and PKS 1934-638, which were assumed to have flux densities of 2.19, 9.84 and 4.09 Jy respectively.

3.3.2 Results and Discussion

No 6.7-GHz CH_3OH maser emission, or absorption was detected in any of the ten galaxies observed. The detection threshold of 60 mJy is significantly lower than that necessary to detect all but one of the OH and H_2O masers which exist in these sources. Given that the Galactic CH_3OH masers are typically much stronger than Galactic OH masers, this detection limit places a severe constraint on any CH_3OH maser emission, and demonstrates that the OH megamaser emission and superluminous H_2O maser emission are not accompanied by corresponding CH_3OH megamaser emission.

If we assume that in our sample there are no 6.7–GHz CH_3OH sources with peak flux greater than 3 times the quoted rms noise level, then we have four sources with CH_3OH:OH flux ratios less than 0.3. Among Galactic masers, approximately 23% have CH_3OH:OH flux ratios less than 0.3, (Caswell *et al.*, 1995c) thus if we assume the same CH_3OH:OH flux ratio distribution for extragalactic sources then the probability that any four will all have flux ratios less than 0.3, is 0.28%. Hence it appears extremely unlikely that the extragalactic CH_3OH:OH flux ratio distribution is the same as that observed for Galactic masers.

The differences between Galactic and extragalactic masers sources might be attributed to one of the following causes.

(i) CH_3OH megamasers do not exist, because the physical conditions required to produce them do not exist.

(ii) Extragalactic CH_3OH masers or megamasers do exist, but require different physical conditions from those which produce ultraluminous OH and H_2O maser emission.

(iii) The pumping mechanism or efficiency of CH_3OH masers is such that peak flux density of extragalactic CH_3OH masers is below the detection limit of these observations.

Megamaser emission requires a number of basic ingredients, such as a sufficient column density of molecules along the line of sight, a means of pumping the masers, and perhaps a background continuum source to provide the input to the maser. Galactic masers appear to require precise physical conditions such as a particular optical depth to the pump radiation. However, megamasers are relatively insensitive to the precise conditions, because the maser activity in these sources is distributed throughout a large region, and a wide range of physical conditions are available if the basic ingredients are present. Recent observations have shown that the majority of the emission arises from only a small portion of the gas in the nuclear region of the galaxy (Lonsdale *et al.*, 1994). However, some of the emission does originate on larger scales, so the basic argument is still valid.

Thus our first hypothesis, that CH_3OH megamasers do not exist because the physical conditions required to produce them do not exist, implies that some physical condition is required for CH_3OH maser emission, but that this condition is found only in special circumstances. An example might be if Galactic CH_3OH masers occur only in concentrations of high density within circumstellar discs

(Norris *et al.*, 1993; Norris *et al.*, 1996). It is possible that the mechanisms which produce increased CH_3OH density in Galactic star formation regions (Herbst, 1991) cannot operate on a sufficiently large scale, or the radiation field in these regions causes depletion by disassociation of the CH_3OH molecules.

Our second hypothesis, that CH_3OH megamasers do exist, but require different physical conditions from those of OH megamasers, would be appropriate if, for example, the CH_3OH masers were radiatively pumped but the OH megamasers collisionally pumped. However, detailed differences, such as optical-depth effects, would not be sufficient to prevent megamaser emission.

The final hypothesis, that the extragalactic methanol masers are below the detection limit of our observations, implies that either the peak flux density of CH_3OH masers cannot greatly exceed that of the strongest Galactic CH_3OH masers, or the conditions which produce ultraluminous Galactic type OH and H_2O masers are not suitable for producing ultraluminous CH_3OH masers. We cannot attribute the non-detection of extragalactic masers to a deficiency of CH_3OH, as it has been detected towards several galaxies at millimetre wavelengths (Henkel *et al.*, 1987). One of the galaxies which we also observed (NGC 253), was found to have methanol abundances similar to those found in our Galaxy. NGC 253 is also the closest of the observed galaxies, but to detect any masers in our observations, an intrinsic peak flux density at least an order of magnitude greater than the strongest of the Galactic CH_3OH masers would have been required.

All of these cases place a severe constraint on models of CH_3OH maser emission. To determine whether extragalactic CH_3OH masers are common requires a more sensitive and more comprehensive survey.

We conclude that the absence of CH_3OH maser or megamasers implies that either the physical conditions required to produce ultraluminous CH_3OH maser emission are incompatible with those required to produce OH or H_2O emission, or that the ingredients necessary to produce masing in CH_3OH are not present on a large enough scale to produce megamaser emission.

Chapter 4

Spectral line observations using the Mt Pleasant radiotelescope

4.1 Introduction

The Physics Department at the University of Tasmania operates two radiotelescopes at the Mt Pleasant Observatory, approximately 20 km from the city of Hobart. The smaller of the two antennas has a 14-m diameter and a wire mesh surface and is exclusively dedicated to timing observations of the Vela pulsar. The larger one is an ex-NASA 26-m diameter prime-focus antenna with a solid aluminum surface. Prior to 1985 it was located at Orroral valley outside Canberra and used in NASA's deep space network. The antenna has an X-Y mount, aligned East-West. This telescope was used for the collection of the data presented in Chapter 5.

In this chapter I describe in detail the hardware and software system used to collect the data for the 6.7-GHz CH_3OH maser survey. I also discuss how the observational parameters used in the survey were chosen, and the implications of those decisions for the completeness of the survey. Finally I describe in detail how the survey observations were made, and the procedure used to obtain an accurate source position and a high quality spectrum. The scientific motivation for the survey is presented in Chapter 5, together with a discussion of the results.

4.2 The digital autocorrelation spectrometer

4.2.1 Theory

The wavelength of the radiation observed with a radio telescope means that glass prisms, diffraction gratings or similar methods typically used in optical spectroscopy to produce a spectrum of the incident radiation, do not work. There are several ways of obtaining spectral information from the signal output of a radio receiver, these are in principal the same as techniques used at optical wavelengths and provide the same information. The first to be developed, and conceptually the easiest to understand is the filter bank, which consists of a series of filters covering

different frequency ranges each followed by an independent detector. There are several problems with filter banks ; one is that each channel in the filter bank has independent electronics and this can make relative calibration of the channels difficult ; another is that the spectral resolution cannot easily be changed.

Fortunately there is a way of obtaining spectral information from the time varying signal output from the receiver. This relies on the Wiener-Khinchin theorem (Equation 4.1) which states that the Fourier transform of the temporal autocorrelation is equal to the power spectrum of the incident radiation. This type of spectrometer was first developed by Weinreb (1963) and is called an autocorrelation spectrometer. In order to obtain a power spectrum all we must do is autocorrelate the signal output from our receiver. The sampling theorem states that in order to obtain all the information present in a signal we must sample at twice the rate of the fastest variation. Thus if we are trying to obtain a spectrum of bandwidth B Hz, we must sample the input signal at a rate of $2B$ Hz. This means that for a bandwidth of the order of 10 MHz then we must have a sampling interval of 50 ns or less. Although autocorrelation spectrometers can easily be implemented in software, the sampling speed required for even moderate bandwidths makes it much more practical to use custom built hardware to measure the autocorrelation function.

$$S(\nu) = \int_{-\infty}^{\infty} R(\tau) e^{-2\pi i \nu \tau} d\tau \tag{4.1}$$

For a time varying signal, an autocorrelation is the correlation coefficient of the signal with itself delayed by some interval, and the autocorrelation function is simply the variation of this correlation coefficient as a function of delay. In theory the autocorrelation function extends from delays of $-\infty$ to delays of $+\infty$, but of course in practice we are only able to measure the autocorrelation function for a finite number of delay intervals (or lags). There is a second practical problem with the scheme outlined above ; the electronics required to make an analogue autocorrelation spectrometer are very complex. The solution to this problem is to build the autocorrelation spectrometer using digital electronics. A finite number of delay lags and digital electronics are used in all autocorrelation spectrometers and both have important consequences for the data processing.

Observing a finite number of delay channels is equivalent to observing an infinite number and applying a top hat function. Effectively the top hat function windows the delay lags of the autocorrelation function which are measured. The Fourier transform of a top hat function is a sinc function ($\frac{sin(x)}{x}$), which has the unfortunate property of having very high sidelobes (22% of the peak). Thus if a strong, narrow spectral feature (such as a maser) is being observed sidelobes (commonly called "ringing") will be produced in nearby spectral channels. Since this ringing is caused by the sharp edges of the top hat function, it can be reduced by tapering the top hat function to something smoother. Tapering in the delay domain has the effect of reducing the effective spectral resolution in the frequency domain as adjacent channels are no longer independent. The spectral resolution after tapering and the reduction in ringing depend upon the function used, but there is always a compromise between the reduction in ringing and the decrease

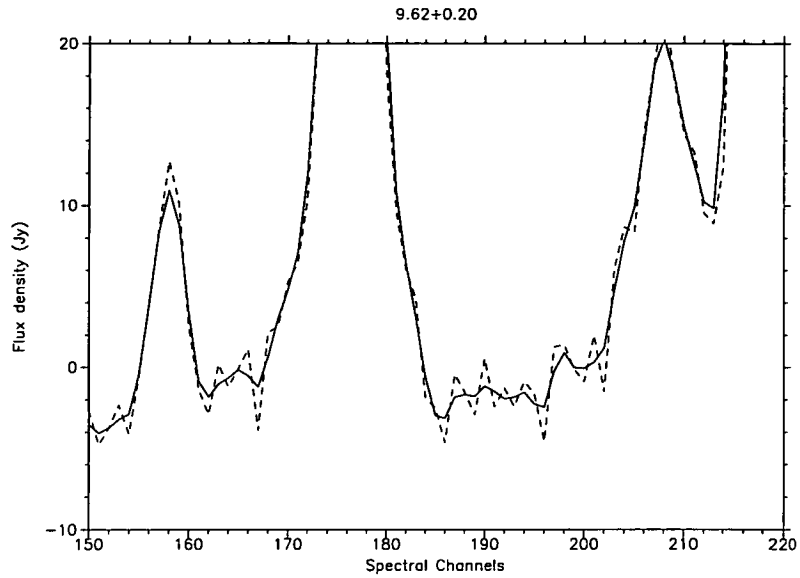

Figure 4.1: An observation of the strong 6.7-GHz CH_3OH maser G9.62+0.20 plotted with Hanning smoothing applied (solid line) and without Hanning smoothing (dashed line). Note the reduction in the ringing in the channels with no emission.

in spectral resolution. The most commonly used method of tapering the delay lag window is Hanning weighting, (Equation 4.2) which has sidelobes no greater than 2.6% of the peak and reduces the spectral resolution by 40%. Figure 4.1 shows the same spectrum with and without Hanning smoothing. The Hanning smoothing clearly reduces the ringing in the channels between the maser emission.

$$W_{Hanning}(\tau) = \begin{cases} Cos^2(\frac{\pi\tau}{2\tau_m}) & \text{for } |\tau| \leq \tau_m \text{ (maximum delay)} \\ 0 & \text{otherwise} \end{cases} \tag{4.2}$$

Until recently most autocorrelation spectrometers have been implemented using 1-bit digital electronics. The design of a 1-bit digital autocorrelation spectrometer is relatively simple [see for example section 7.6.2 of Rohlfs (1986)] and the components required are cheap and easy to acquire. In order to use 1-bit electronics, we must take the analogue input signal and sample it so that we only pass the sign of the signal to the autocorrelation spectrometer. Intuitively it would seem that the normalized autocorrelation function produced from the spectrometer ($R_{1-bit}(\tau)$) would bear little resemblance to what we are trying to measure ($R_{analogue}(\tau)$). However, there is a simple relationship, called the van Vleck relation, which allows us to obtain $R_{analogue}(\tau)$ from $R_{1-bit}(\tau)$.

$$R_{analogue}(\tau) = R_{anaolgue}(0) sin[\frac{\pi}{2} R_{1-bit}(\tau)] \tag{4.3}$$

Reducing the input signal to simply a sign throws away some of the information contained in the received signal and causes a reduction in sensitivity. 1-bit sampling reduces the sensitivity of the spectrometer to 64% ($\frac{2}{\pi}$) of that obtainable using an analogue autocorrelation spectrometer. 2-bit digital autocorrelation

spectrometers are significantly more complicated and expensive to build, but only have an efficiency of 87% (a 36% improvement over 1-bit electronics). One further disadvantage to 1-bit digitization is that all power information is lost from the signal, so additional independent measurements must be made to calibrate the flux density scale.

4.2.2 Hardware

The current spectrometer at the Mt Pleasant Radioastronomy Observatory is a 1-bit digital autocorrelation spectrometer (Fig. 4.2). The correlator is configurable in two basic modes, these accept either one polarization and 1024 spectral channels, or two polarizations each with 512 spectral channels. There are three distinct sections of correlator hardware, labelled 1–3 in Fig. 4.2. The first section is a frequency translator which is used to convert the IF signal from the receiver to frequency range used within the correlator. The second section filters the signal to one of 6 possible bandwidths (40, 20, 10, 2.5, 0.625 or 0.15625 MHz) and attenuates the signal to the level required for input into the autocorrelation spectrometer. It also contains several detectors and A-D converters (analogue-to-digital converters) which are used to measure the noise power of the signal and hence the system equivalent flux density. The third section is the autocorrelation spectrometer itself, consisting of 32 circuit boards, each of which contain the electronics for 32 spectral channels.

4.2.3 Software

The autocorrelation spectrometer and related hardware is controlled by an Olivetti 386 PC. At the commencement of my PhD the autocorrelation spectrometer hardware was nearly complete but much work was still required on the software. With the assistance of Dr A Deshpande and Messrs P. Button and T. Delbourgo I have written much of the software required to control the autocorrelation spectrometer. Most of the software is written in FORTRAN-77, with the exception of the routines which interact directly with the hardware. The hardware interface routines were originally written in 16-bit x86 assembly code and I have modified them to 32-bit x86 assembly code. There are six separate hardware components under computer control :

1. The frequency synthesizer is set so that the signal being input into the correlator is mixed to the right frequency. The frequency synthesizer (a Rohde and Schwarz SMX) is designed to be controlled via a GPIB interface (General Purpose Interface Bus). Nearly all the functions of the synthesizer can be accessed using this interface, but the only functions I use are to set the frequency and power level of the output signal.

2. The selection of filters which control the bandwidth of the observations.

3. The attenuators which control the level of the signal input into the autocorrelation spectrometer and the A-D converters. These attenuators are used

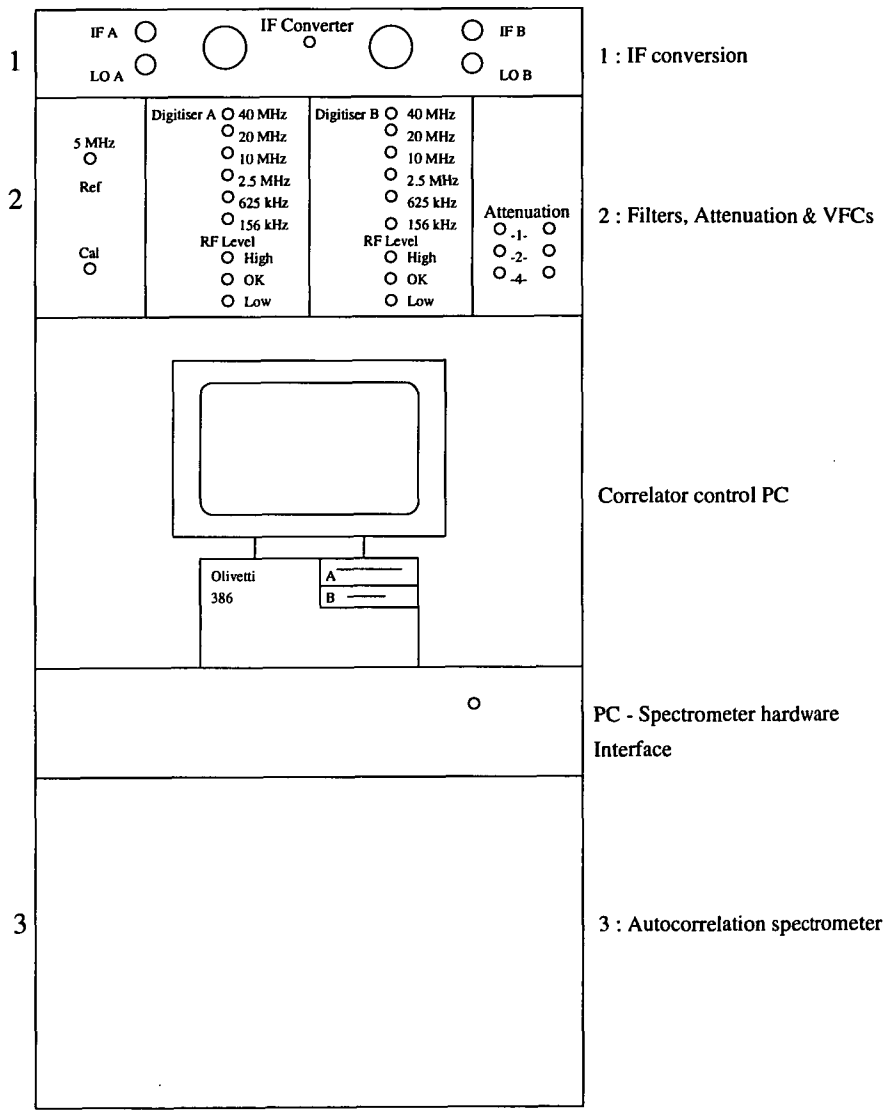

Figure 4.2: A schematic diagram of the Mt Pleasant Observatory 1-bit digital autocorrelation spectrometer

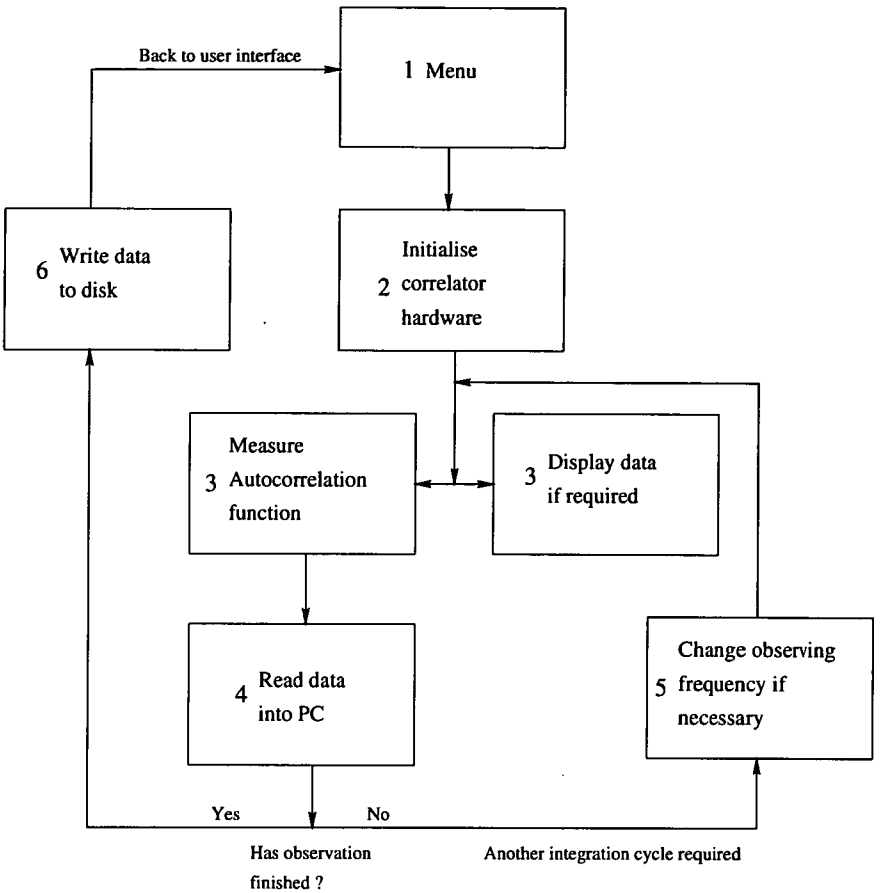

Figure 4.3: A flow chart showing the basic observing strategy for the Mt Pleasant digital autocorrelation spectrometer

to give a fine adjustment of the level of the input signal. The attenuator banks can be set to 8 separate levels, from 0-7 dB. When the attenuators are set to a given level they return a status flag indicating whether the signal level into the correlator is too high, too low, or OK.

4. The A-D converters which are used to measure the system equivalent flux density.

5. The receiver calibration noise diode which is also used in measuring the system equivalent flux density.

6. The autocorrelation spectrometer which measures the autocorrelation function of the input 1-bit signal stream.

4.2.3.1 The observing software

The software which controls the autocorrelation spectrometer hardware is only a relatively small fraction of the total software required to make spectral line observations. A flow-chart of the basic observing procedure is shown in Fig. 4.3 and each of the sections are discussed in order below

1. The observing program is controlled via a simple menu-driven interface. Using the menu, the observer can select the required hardware configuration, control the flux density calibration and the online display, and supply information on the velocity, position and rest frequency at which to observe.

2. Once the observer gives the command to commence the observation, the correlator hardware is configured as requested. This includes setting the frequency synthesizer so that the specified spectral line is observed at the requested velocity.

3. Typically, the observation is split into a series of equal duration intervals. The total observation is then made up of a series of shorter observations. There are several reasons for observing this way. One is that the observing frequency must be regularly updated to correct for the rotation of the Earth (see section 4.2.3.2). Another is so that the data can be displayed and updated during the observation. If the data from each integration is saved separately, then this scheme also allows post-observation editing of the data to exclude integrations with sporadic interference. At present external interference at 6.7 GHz is very rare, so all the data is averaged together before writing to disk, to save storage space.

   Since the measurement of the autocorrelation function is performed under interrupt, the PC is able to calculate the observing frequency, Fourier transform and display the data from the previous integration cycle while the observation is in progress. This means that there is no time penalty incurred for displaying the data, provided that the integration cycle time is greater than the time taken for this processing.

4. At the completion of each integration cycle the PC reads the data from the autocorrelation spectrometer. If more integration cycles are required, then it continues to step 5, otherwise the data is written to disk (step 6)

5. The observing frequency which has been calculated in step 3 is compared to that used for the previous cycle and if necessary the setting of the frequency synthesizer is updated. The combination of this step and the previous one has a time overhead of ≈ 1 s and because of this it is best not to make the integration cycle too short. Once the observing frequency is set the next observing cycle is commenced (return to step 3)

6. At the completion of the observation the data is written to the PC disk-drive in FITS (Flexible Image Transport System) format. As this format is machine independent we are able to transfer and reduce the data on a variety of different computer architectures.

   Finally, the observing software returns to the menu interface (step 1), ready to start another observation.

4.2.3.2 Doppler correction

The frequency at which we observe a spectral feature associated with a celestial source is constantly changing due to the rotation of the Earth. This is because as the Earth rotates the radial component of velocity of the observatory with respect to the source changes, and if this is not taken into account then it will broaden any spectral features. This problem becomes worse as the observing frequency increases and as the width of the spectral channels decreases.

The question naturally arises, how often must we change the observing frequency in order to avoid smearing the spectral features? This depends upon two factors : the spectral resolution of the observations and the frequency resolution of the local oscillator. The observing frequency should be updated when it has changed by a small, but significant fraction of the spectral resolution. I use a nominal value of 10%.

Most frequency synthesizers can be set to a resolution of 1 Hz or better. However, the frequency of the output signal will often differ slightly in frequency from that requested. The resolution of the frequency settings which the synthesizer is able to produce exactly is typically much more coarse than the apparent frequency resolution. For example for the frequency synthesizer used to control the autocorrelation spectrometer observing frequency at the Mt Pleasant observatory (a Rohde and Schwarz SMX) the resolution of the exact frequencies it can produce is of the order of 10 Hz, but the apparent frequency resolution is 1 Hz. In order to avoid possible complications the observing software has been designed to always set the frequency synthesizer to a frequency which it can reproduce exactly. This way the exact frequency at which the observation was made is known, and if post-observation corrections are required they can easily be calculated.

I have done some crude simulations at the highest observing frequencies (22 GHz) and finest spectral resolutions (150 Hz per spectral channel) available at the Mt Pleasant observatory and these show that the observing frequency should be updated approximately every 30 s. Thus for the 6.7-GHz CH_3OH maser survey which is at a lower observing frequency, and uses a coarser spectral resolution (see section 4.3), updating the observing frequency every 30 s is more than sufficient to ensure that emission from narrow features is not smeared across multiple spectral channels.

4.3 Observational parameters of the 6.7-GHz CH_3OH maser survey

4.3.1 Introduction

The method of observation is of primary importance for any large astronomical survey. Statistical estimation of global properties and distributions usually requires a "complete" sample, i.e. the sample must contain all members within a well defined set of parameters. For example the luminosity distribution for 6.7-GHz CH_3OH masers cannot be determined from an *IRAS*-selected search, as not all 6.7-GHz CH_3OH masers are associated with *IRAS* sources (see section 5.4.1).

It is also important to survey a representative region. Very sensitive observations of small areas may be biased by isolated deviations from the global distribution. In general, for large surveys the major constraining factor is the amount of telescope time available. This leads to a conflict between the area covered by the survey and the sensitivity of the survey.

4.3.2 Where to survey?

Fortunately masers are Galactic objects, and this reduces the decision of where to survey to choices of different regions of the Galaxy, rather than the entire sky. Previous searches for 6.7-GHz CH_3OH masers toward OH and 12.2-GHz CH_3OH masers have shown that they are associated with the formation of massive stars. These have a distribution which falls off more rapidly with Galactic latitude than for older Galactic objects, such as late-type stars or pulsars. For this reason, most 6.7-GHz CH_3OH masers should be at very low Galactic latitudes and I have restricted the survey to $|b| \lesssim 0.^{\circ}5$. If I were to survey the entire Galactic Plane in this latitude range it would still only represent 0.8% of the sky.

The spiral arms of our Galaxy are the most active regions of star formation, and so it was decided to target the survey toward these areas. The greatest concentration of star-formation regions along a line of site arises tangentially to inner spiral arms. This occurs approximately 30° either side of the Galactic Centre and two of the regions which I have surveyed are centred on $l \approx 30^{\circ}$ and $l \approx 330^{\circ}$.

4.3.3 The observing grid

To be able to derive global and statistical information from a survey it must be complete within a well defined region of parameter space. In my case this requires a uniform sensitivity limit across the survey region and a fully sampled spatial grid. By the sampling theorem, if we are observing with a 7-arcmin telescope beamwidth (FWHM) then we must use an observing grid where the separation of any given point from all adjacent points is no more than half the telescope beamwidth (i.e. 3.5 arcmin). The most efficient gridding which satisfies that criterion is an equilateral triangular grid with sides which have a length equal to half the telescope beamwidth. An equilateral triangular grid, with a separation of 3.5 arcmin between points, implies $\approx$ 350 grid points per square-degree.

Even though this is a fully sampled spatial grid, the sensitivity across the grid is not uniform. Typically the 6.7-GHz CH_3OH masers will not lie at the centre of the beam. In the worst case, the maser could be equidistant ($\approx$ 2 arcmin) from three grid points. Assuming a circular Gaussian beam, the peak flux density detected in each of the grid points from such a maser would be only 79% of the true peak flux density. In most cases the maser will lie somewhere in between the best and worst possible positions with respect to the survey grid and should be detected on average at 94.5% of its true peak flux density.

4.3.4 The receiver

The 6.7-GHz CH_3OH maser survey used a cryogenically cooled receiver with low noise HEMT (high electron mobility transistor) amplifiers. It accepts two orthogonal circular polarizations and has a typical system equivalent flux density (SEFD) of 650 Jy ($\approx$ 65 K). The measured SEFD varies according to the weather and approximate elevation of the telescope but seldom varies more than 10% from 650 Jy.

4.3.5 Correlator configuration

The rms noise in each spectral channel for a Hanning smoothed spectrum observed using a 1-bit digital autocorrelation spectrometer is given by a modified form of the radiometer equation (see Equation 4.4). The system equivalent flux density of the receiver ($SEFD$) and the number of polarization products it is able to measure (N_{pol}) are parameters over which the observer usually has little control. Thus the sensitivity of the observations made using a given receiver-correlator package depend upon the integration time of the observations (τ) and the correlator configuration (the observing bandwidth Δf and the number of spectral channels across that band $N_{channels}$). Examination of equation 4.4 shows that in order to minimize the rms noise in each spectral channel (ΔS), we must minimize the number of spectral channels and maximize the bandwidth and integration time.

$$\Delta S = \frac{\frac{\pi}{2} SEFD \sqrt{N_{channels}}}{\sqrt{2 \Delta f \tau N_{pol}}} \tag{4.4}$$

By maximizing the observing bandwidth, we also increase the velocity coverage of the observations. This is desirable for a maser survey, since along any line of sight in the Galactic Plane, the Doppler shift of the spectral line due to the Galactic rotation along that line will vary with the distance from the Sun. In addition, some star-forming regions will have peculiar velocities (velocities which differ significantly from the Galactic rotation curve). Thus in order to detect all masers with a peak flux density greater than the survey sensitivity limit, the observing bandwidth must be large enough to cover all line-of-sight Galactic velocities. Minimizing the number of spectral channels reduces the velocity resolution of the observations. As individual maser features are typically very narrow (see below) their observed amplitude will be reduced if the spectral resolution is too coarse. This effectively decreases the sensitivity of the observations, as although the noise in an individual spectral channel may be very small, to be detectable, the maser must have a peak flux density well in excess of 5-σ (σ = rms noise level), or any other nominal noise-limit.

To maximize the sensitivity of a spectral line survey, the width of the spectral channels must be well matched to the observed line widths of the target objects. In the spectral domain, Hanning smoothing is equivalent to the running average shown in Equation 4.5. This means that any spectral feature which has a half-width of less than 3 spectral channels will be reduced in peak amplitude by Hanning smoothing.

Chapter 5

The Mt Pleasant 6.7-GHz methanol maser survey

5.1 Introduction

Soon after the discovery of OH masers (Weaver *et al.*, 1965) it was suggested that many were associated with HII regions and hence massive star formation (Zuckerman *et al.*, 1965). Since that discovery, searches for masers have typically been targeted toward regions which show indications of massive star formation, such as optical HII regions or more recently sources satisfying *IRAS* colour criteria. Typically these searches have been relatively successful, finding many new masers. However, by their nature targeted searches are unable to answer important questions regarding the statistical properties of the masers, and also are unlikely to detect masers associated with other classes of object. This is illustrated by the fact that OH masers associated with late-type stars were not discovered until 3 years after the discovery of OH masers associated with HII regions (Wilson and Barrett, 1968). Also, a search for masers is likely to discover new star formation regions, in the words of Anderson and Genzel (1993)

"The maser community might have used these correlations to find sites of star formation by performing maser surveys. In fact, however, this has never been done and the current style is to search for masers in objects drawn from some other kind of survey, e.g., the *IRAS* catalogue. In this sense, the community may have missed an opportunity to point the way in the study of star formation"

Despite these compelling arguments, relatively few large, blind searches for masers have ever been performed (Caswell *et al.*, 1980; Caswell and Haynes, 1983b; Caswell and Haynes, 1987).

In the four years since the discovery of maser emission from the 5_1-6_0 A^+ transition of CH_3OH, several searches for 6.7-GHz CH_3OH maser emission have been made towards sites of OH and 12.2-GHz CH_3OH masers (Menten, 1991a; MacLeod and Gaylard, 1992; MacLeod *et al.*, 1992; Gaylard and MacLeod, 1993; Caswell *et al.*, 1995c). Other searches have been targeted toward *IRAS* sources believed to be ultra-compact HII regions on the basis of their far-infrared colours (Schutte *et al.*, 1993; van der Walt *et al.*, 1995). In nearly all cases, the 6.7-GHz

CH_3OH masers are stronger than their 12.2-GHz and OH counterparts. Thus, the first search method is likely to find few weak 6.7-GHz masers. The *IRAS* satellite had a beamwidth of 2 arcmin at 100 μm, so that in the extremely crowded and confused regions close to the Galactic Plane many ultra-compact HII (UCHII) regions may not have been detected. Thus, the second search method is likely to miss a significant number of CH_3OH masers associated with UCHII regions. In addition, all these searches have been implicitly targeted toward HII regions, thus we currently have no knowledge of whether 6.7-GHz CH_3OH masers are associated with any other type of object.

In this chapter I present the results of an untargeted search of several regions of the Galactic Plane. Some of this work has also been published by Ellingsen *et al.* (1996b). The 6.7-GHz transition of CH_3OH is very good for detecting new sites of massive star formation because :

- It is the second strongest maser transition known, after the 22-GHz transition of H_2O.
- It occurs at a far lower frequency than does the H_2O maser transition, so the telescope beam will be larger, enabling a more rapid search of a large portion of the Galactic Plane.
- The 6.7-GHz CH_3OH masers are less variable than either H_2O or 12.2-GHz CH_3OH masers (Caswell *et al.*, 1995a), so that there is less chance that a source will drop below the detectability threshold in the interval between the initial survey and final observations.

Since the release of the *IRAS* Point-Source Catalog (1985), many searches for masers have been made by observing towards *IRAS* sources which satisfy various criteria, [e.g. Braz and Sivagnanam (1987); Cohen *et al.* (1988a); MacLeod *et al.* (1993b); Masheder *et al.* (1993); Palla *et al.* (1991); Schutte *et al.* (1993); van der Walt *et al.* (1995)]. The *IRAS* satellite made observations in four wavelength bands at 12, 25, 60 and 100 μm. Each flux density measurement has an associated quality flag, indicating whether the observation is of high or moderate quality, or only an upper limit. The most frequently used criteria for selecting UCHII regions from the *IRAS* catalog were developed by Wood and Churchwell (1989a). They found that *IRAS* sources which satisfied $Log_{10}(S_{60}/S_{12}) \geq 1.30$ & $Log_{10}(S_{25}/S_{12}) \geq 0.57$ were more likely to be UCHII regions than those in other regions of the colour–colour diagram (see section 5.4.1.1). Currently, searches using *IRAS* selection criteria seem to be amongst the most reliable methods of finding UCHII regions. Furthermore, if all 6.7-GHz CH_3OH masers are associated with UCHII regions, they may allow a more accurate determination of the number of UCHII regions in the Galaxy.

5.2 Observations

A detailed description of the equipment and observing techniques is given in Chapter 4 and I will only give a brief summary here. The observations were made

Table 5.1: The regions and velocity ranges searched so far by the Mt Pleasant 6.7-GHz CH_3OH maser survey.

Galactic longitude (l^{II})	Galactic latitude (b^{II})	Central velocity (km s^{-1})	Velocity range (km s^{-1})
25° – 35°	-0°.53–0°.53	100	43.8 –156.2
282°–286°	-1°.03–0°.03	0	-56.2 – 56.2
291°–295°	-1°.03–0°.03	0	-56.2 – 56.2
295°–296°	-1°.03–0°.03	20	-36.2 – 76.2
325°–330°	-0°.53–0°.53	-50	-106.2– 6.2
330°–335°	-0°.53–0°.53	-30	-86.2 – 26.2
335°–338°	-0°.53–0°.53	-50	-106.2– 6.2

between 1993 April and 1995 July using the University of Tasmania's 26-m antenna at the Mt Pleasant Observatory. This antenna has rms pointing errors of 0.7 arcmin and a 7-arcmin telescope beam (FWHM) at 6.7 GHz. A dual-channel, cryogenically cooled HEMT receiver, with two orthogonal circular polarizations, was used for all observations. A 1-bit digital autocorrelation spectrometer, with 512 channels per polarization covering 2.5 MHz, was used for the survey observations. This configuration gives a velocity coverage of 112.5 km s^{-1} and a velocity resolution after Hanning smoothing of 0.44 km s^{-1} at 6668.518 MHz, the rest frequency of the 5_1-6_0 A^+ transition of CH_3OH. The velocity range observed for each region was determined by examining the velocities of OH masers detected in the same region. A summary of the spatial and velocity ranges which have been surveyed is given in Table 5.1. Hydra A and Virgo A were used as flux density calibrators, with assumed peak flux densities of 10.4 and 54.1 Jy in a 7-arcmin beam. The survey observations were made in an equilateral triangular grid pattern, with each grid point separated by 3.5 arcmin (half the FWHM of the telescope beamwidth at the observing frequency) from all adjacent points. In total, the survey consisted of observations at approximately 10000 sky positions. The on-source integration time at each grid point was 10 min. The system equivalent flux density was typically < 650 Jy, yielding an rms noise level of 330 mJy in each spectral channel after Hanning smoothing and averaging the two polarizations. As the survey observations were made in a wide variety of conditions, the sensitivity limit is not uniform across the entire region. I minimized variations in the sensitivity limit of the individual spectra by limiting the range of elevations over which I observed, and re-observing poor-quality spectra. The width of the maser features with respect to the correlator spectral channels and the separation of points in the observing grid pattern also played an important role in determining the sensitivity of the survey and these are discussed in detail in Section 4.3. With an rms level of 330 mJy, my effective 5-σ detection limit lies in the range 2.4 (best) to 3.0 Jy (worst), with a mean of 2.6 Jy.

Most of the masers were detected in several beam positions in the initial survey. The relative intensities were then used to obtain an approximate position for the source. I then determined a more accurate position by observing a grid of 5 points

centred on the approximate position (1 at the approximate position and 4 in a square surrounding it). Some of the sources have positions determined from the Parkes telescope, or Australia Telescope Compact Array (ATCA) observations, and the rms difference between these and my positions is $\leq$ 0.6 arcmin. Finally, I made high signal-to-noise ratio observations of all detected sources. On-source integration times ranged from 10 to 90 min, resulting in spectra with signal-to-noise ratios of at least 15:1. All but the weakest sources (326.40+0.51, 327.61-0.11, 332.33-0.44 and 337.07-0.46) were re-observed using a correlator configuration of two 512-channel spectra, each spanning 0.625 MHz, resulting in a velocity resolution after Hanning smoothing of 0.11 km s^{-1}. The four sources listed above were re-observed using the same correlator configuration as for the main part of the survey. Most sources were observed at the positions which I determined, although for several close groups of sources the Parkes and ATCA positions were used because of the difficulty in determining exact separations with my larger beam. The position at which each source was observed is listed in Table 5.2.

5.3 Results

These observations resulted in the detection of 108 individual 6.7-GHz CH_3OH masers. Of these 57 are new detections (summarized in Table 5.2). Spectra from all sources are shown in Fig. 5.1. Some of the new detections have also been independently discovered by van der Walt *et al.* (1995) and, or, Caswell (1996) and this is indicated in column 8 of Table 5.2. Of the 108 sources, 92 lie in the spatial and velocity range which the survey sampled completely. The remaining 16 sources were detected either because they had a sufficiently high flux density that they were detected even though they lay outside the survey region, or because they were detected by accident while refining source positions or taking off-source reference spectra. As these positioning observations were centred at the detected velocity, they occasionally resulted in the serendipitous discovery of sources offset in either position or velocity from the parameter space sampled by the survey. Of these 16 sources detected which lie outside the fully sampled parameter space of the survey, 7 were new discoveries and 9 were already known. Most of the sources in the region l = 330°– 335° which lie outside the complete sample do so because their velocities are more negative than -86.2 km s^{-1} (the lower velocity limit for spectra centred at a velocity of -30 km s^{-1}). This region was the first searched and so the central velocity for subsequent searches of adjacent regions was set to -50 km s^{-1}.

Figs. 5.2– 5.11 show the positions of all the detected 6.7-GHz CH_3OH masers, superimposed upon 5-GHz radio continuum images of the Galactic Plane (Haynes *et al.*, 1978). In many cases the maser emission is closely associated with local maxima in the continuum emission. Sometimes the position of the maser is slightly offset from the local maximum, probably at the location of an ultra-compact core embedded in a cloud of more diffuse gas. Several centres of maser emission are often contained within one HII region, indicating several separated sites of star formation within the one larger molecular cloud. Regions with generally low level

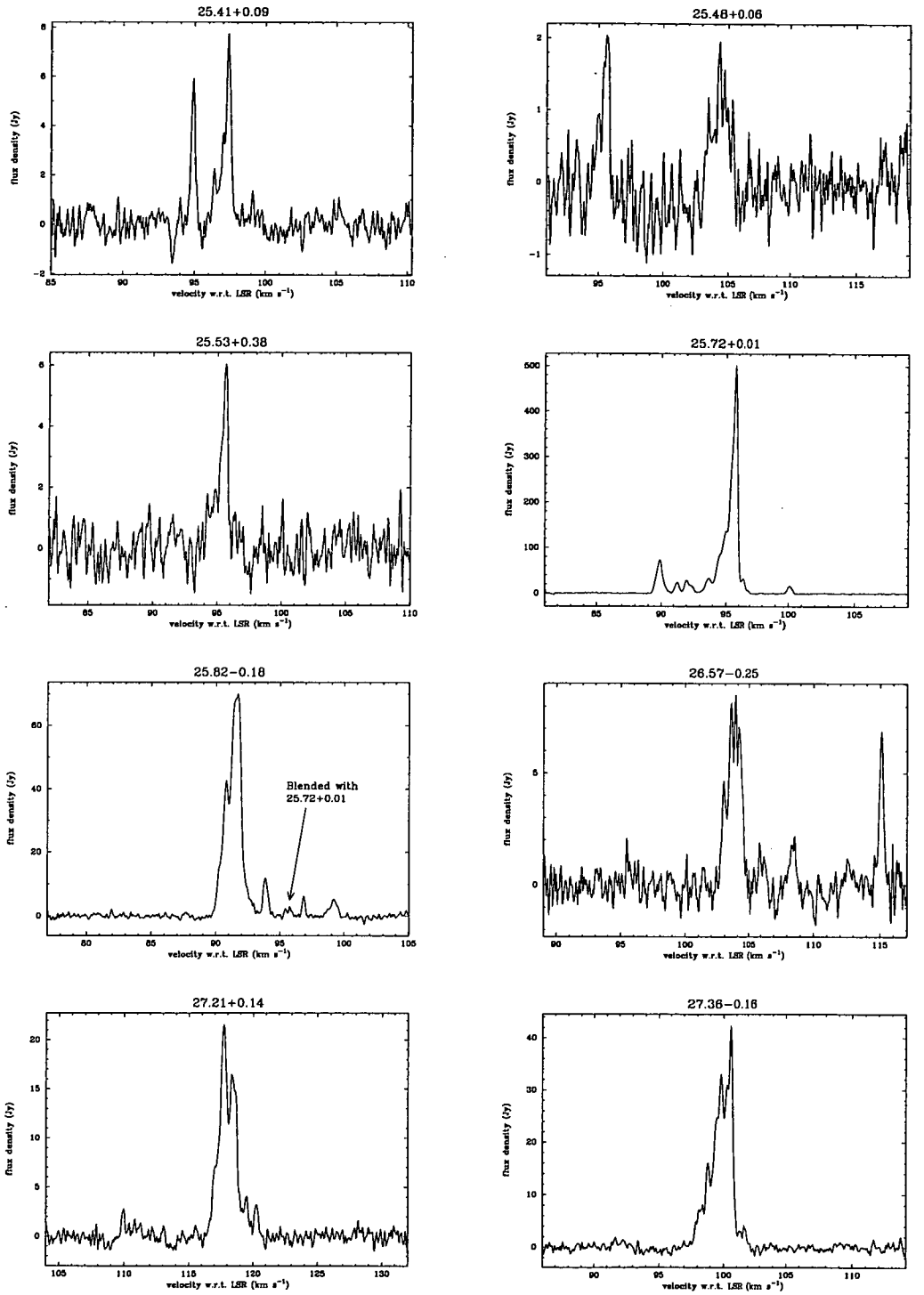

Figure 5.1: Spectra of 6.7-GHz CH_3OH masers detected in the Mt Pleasant survey of the regions l = 282°– 286°, 291°– 296°; b = -1.°03 – 0.°03 and l = 25°– 30°, 325°– 338°; b = -0.°53 – 0.°53.

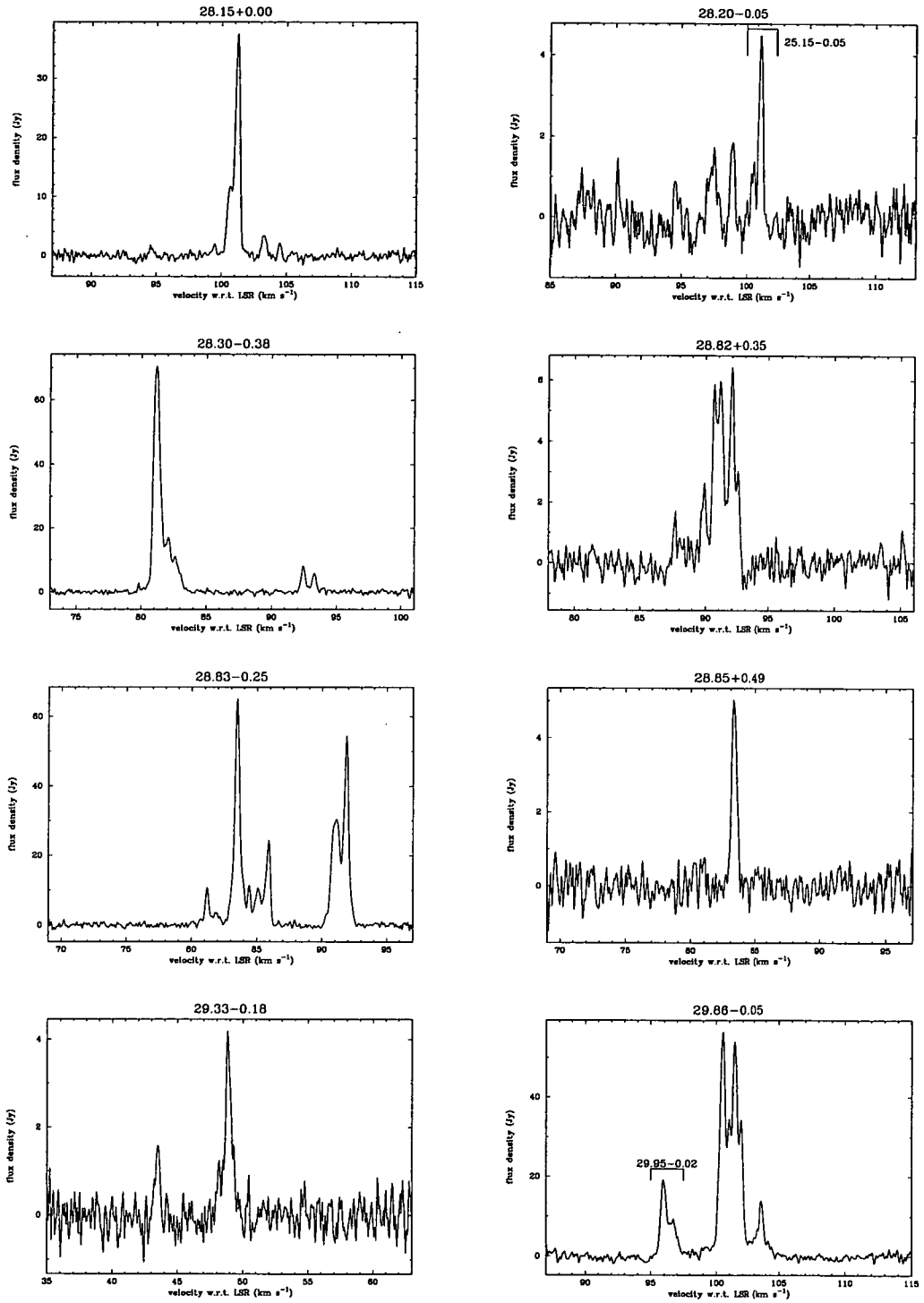

Figure 5.1: *continued...*

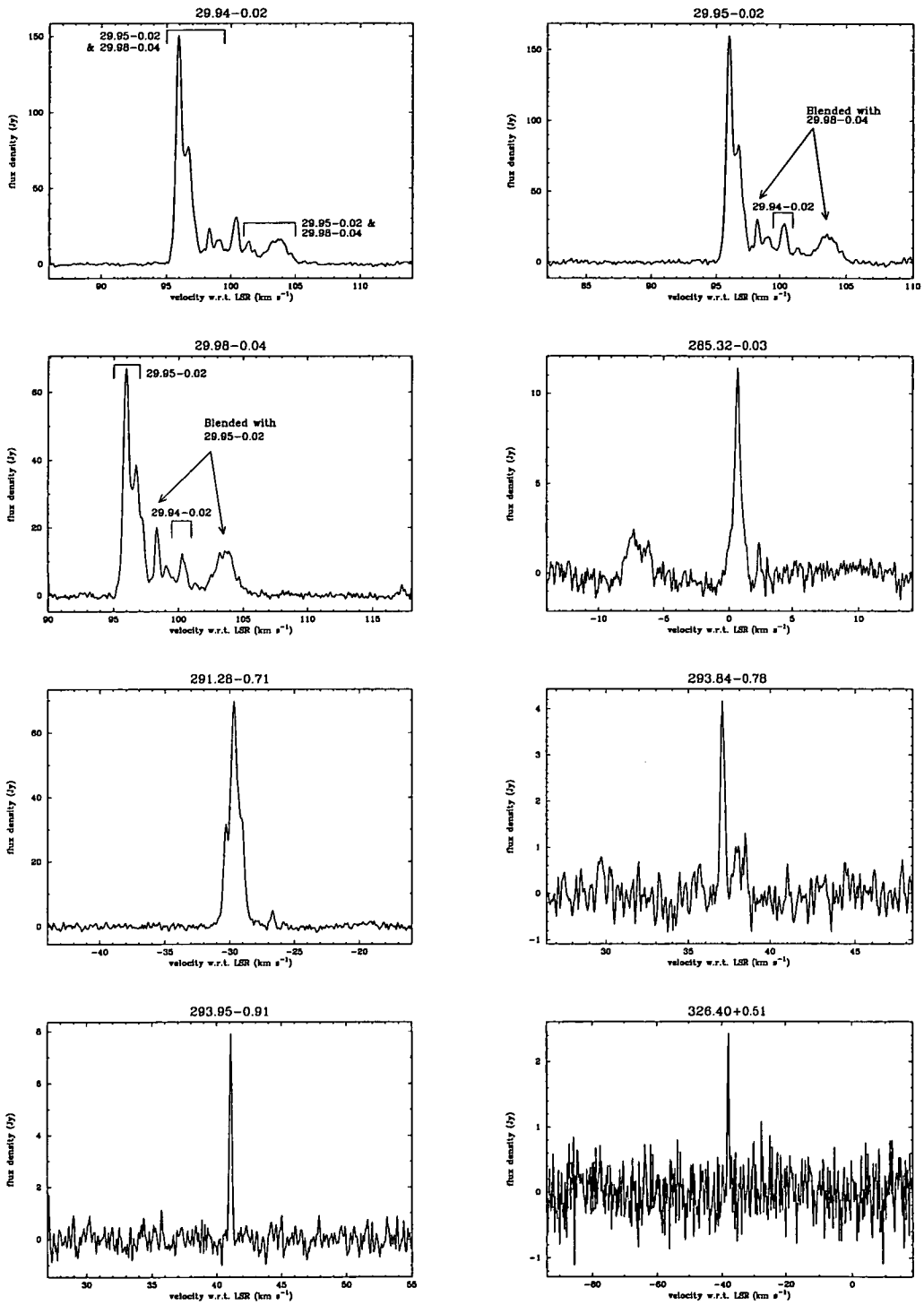

Figure 5.1: *continued...*

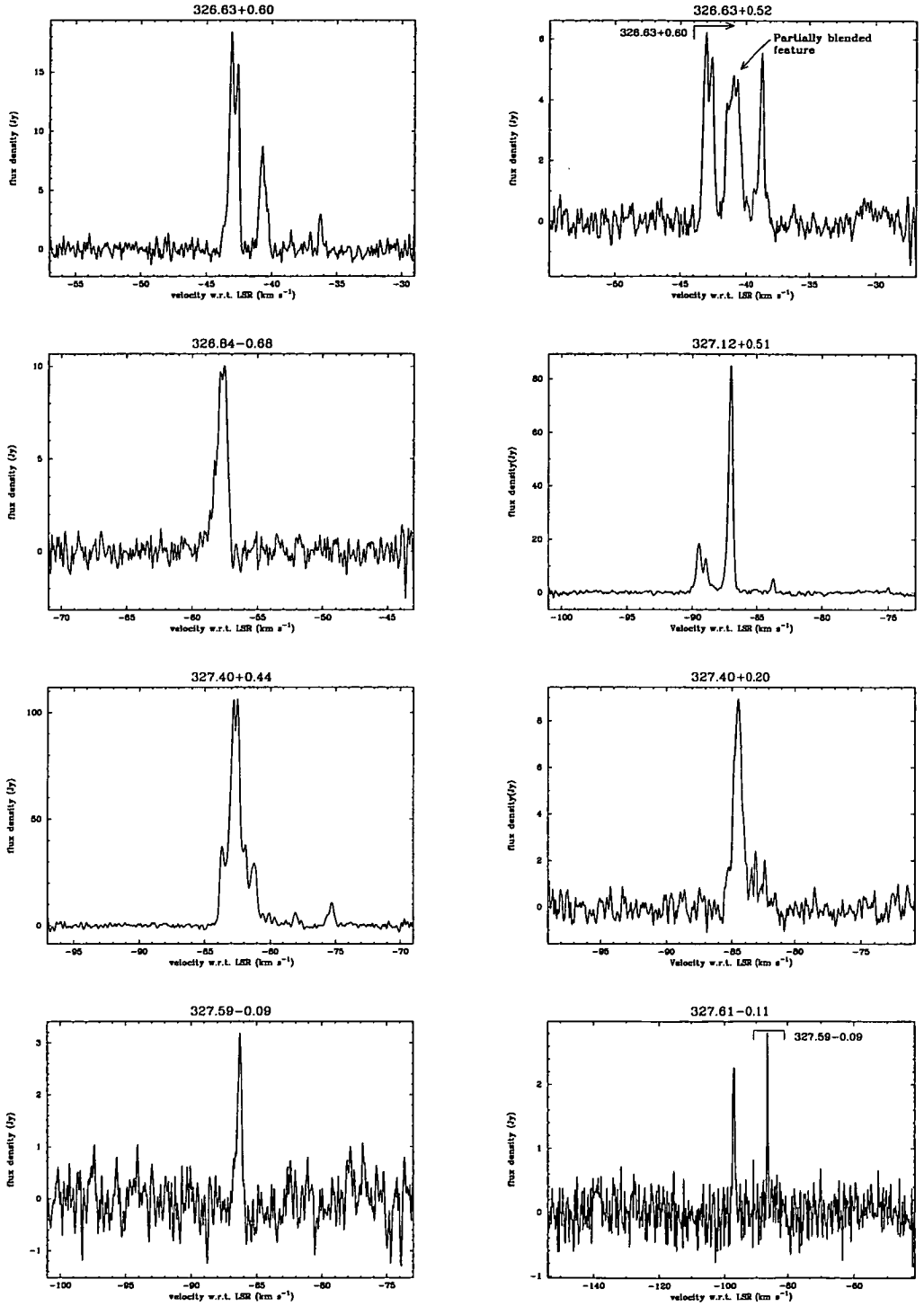

Figure 5.1: *continued...*

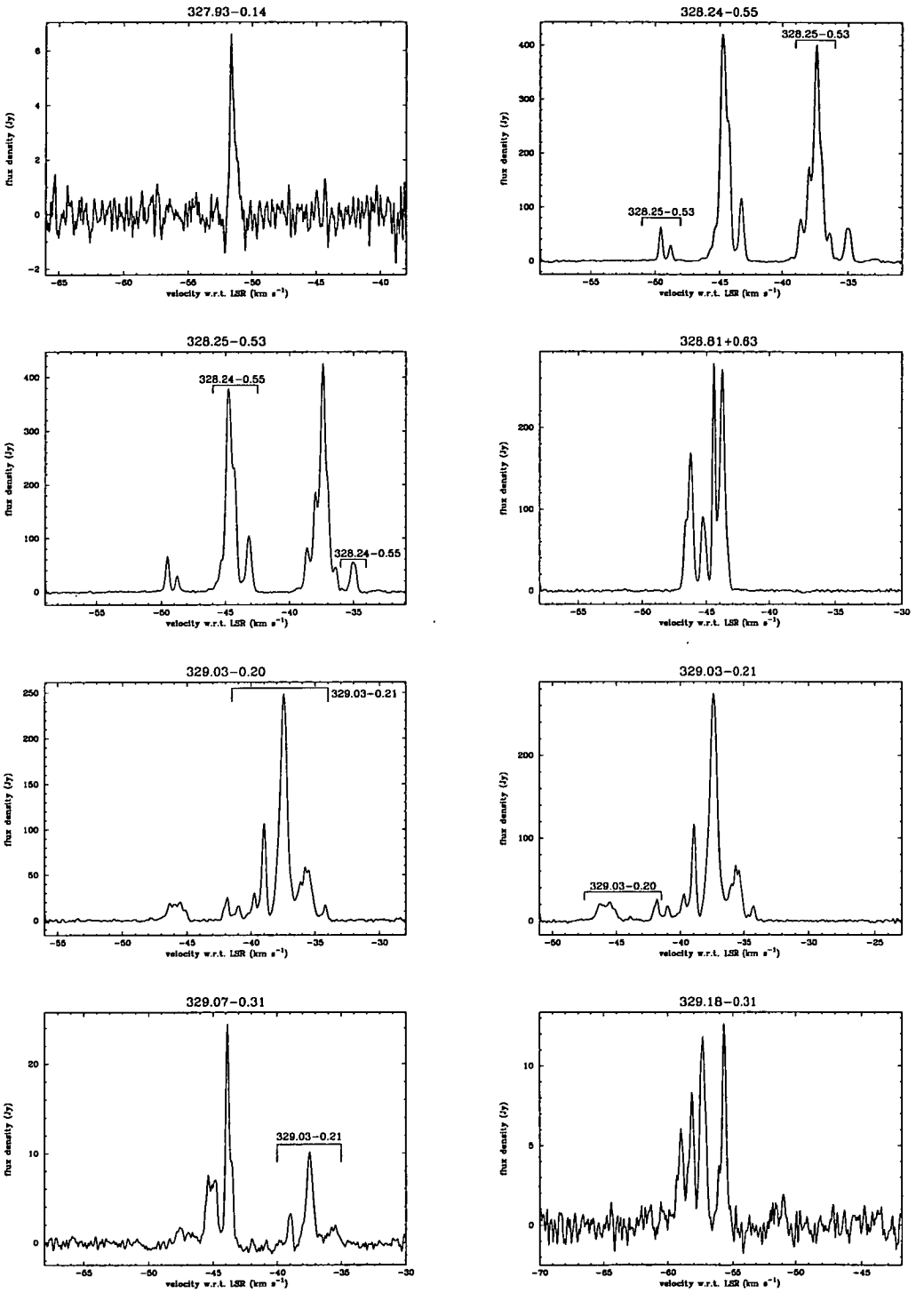

Figure 5.1: *continued...*

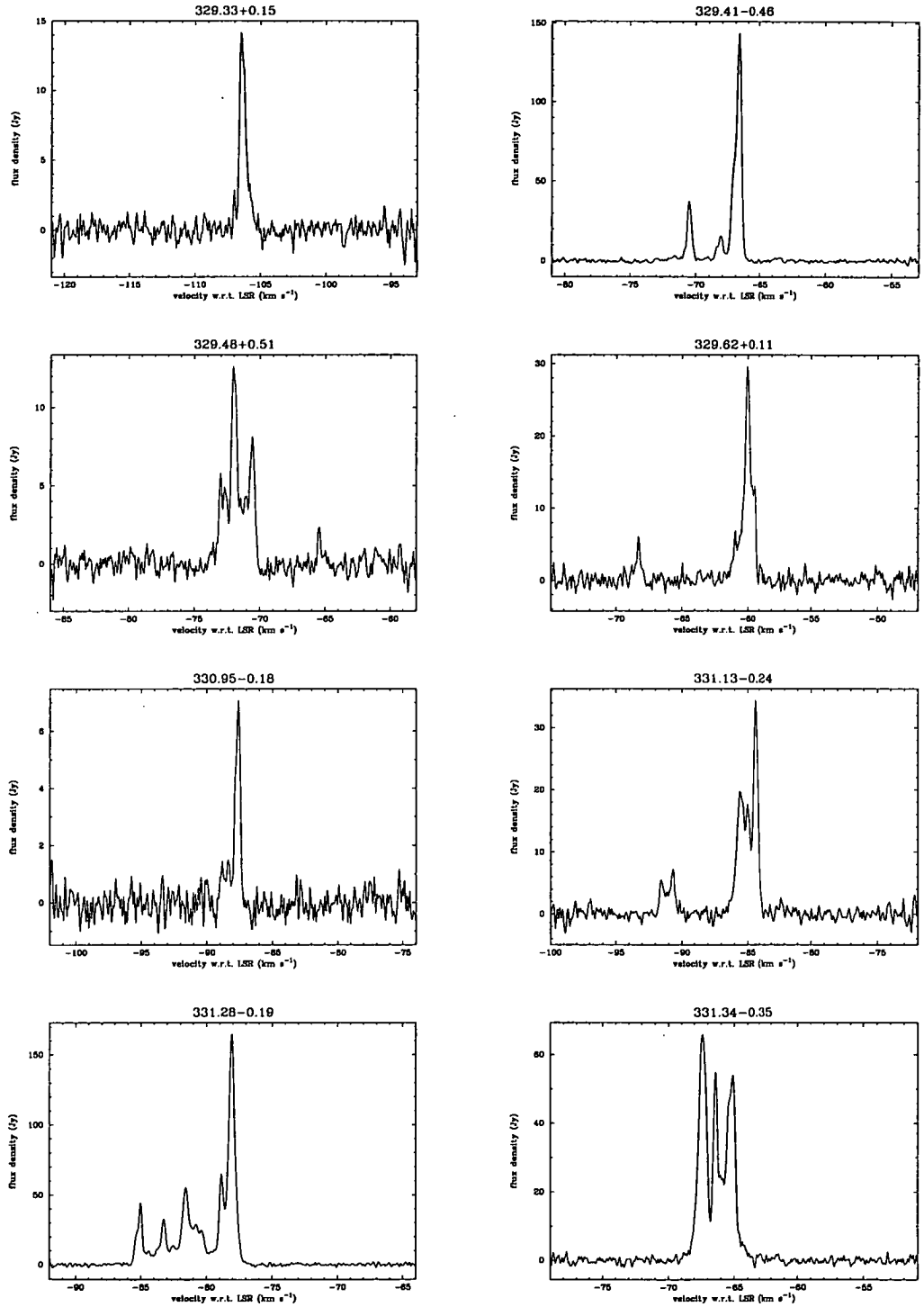

Figure 5.1: *continued...*

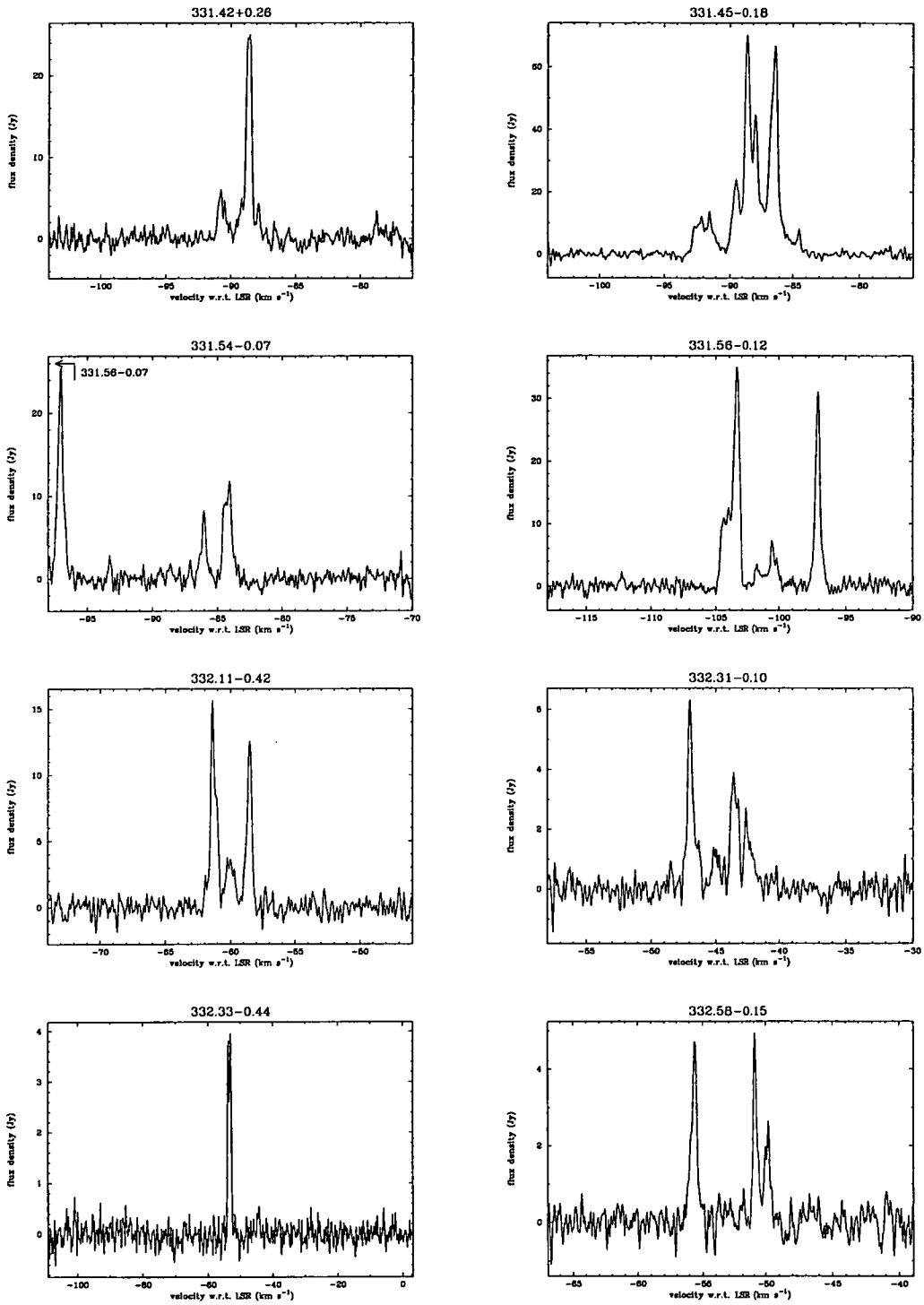

Figure 5.1: *continued...*

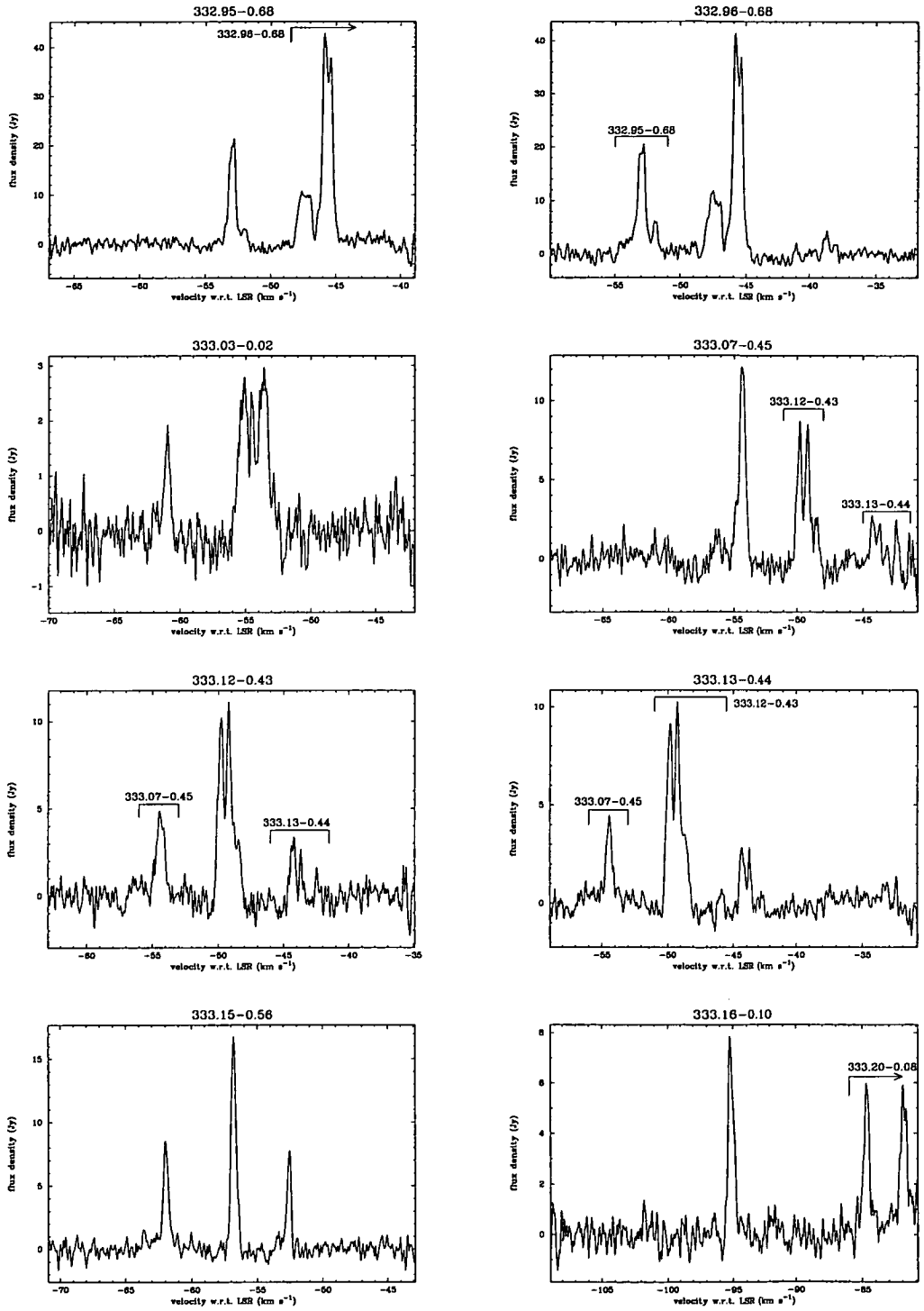

Figure 5.1: *continued...*

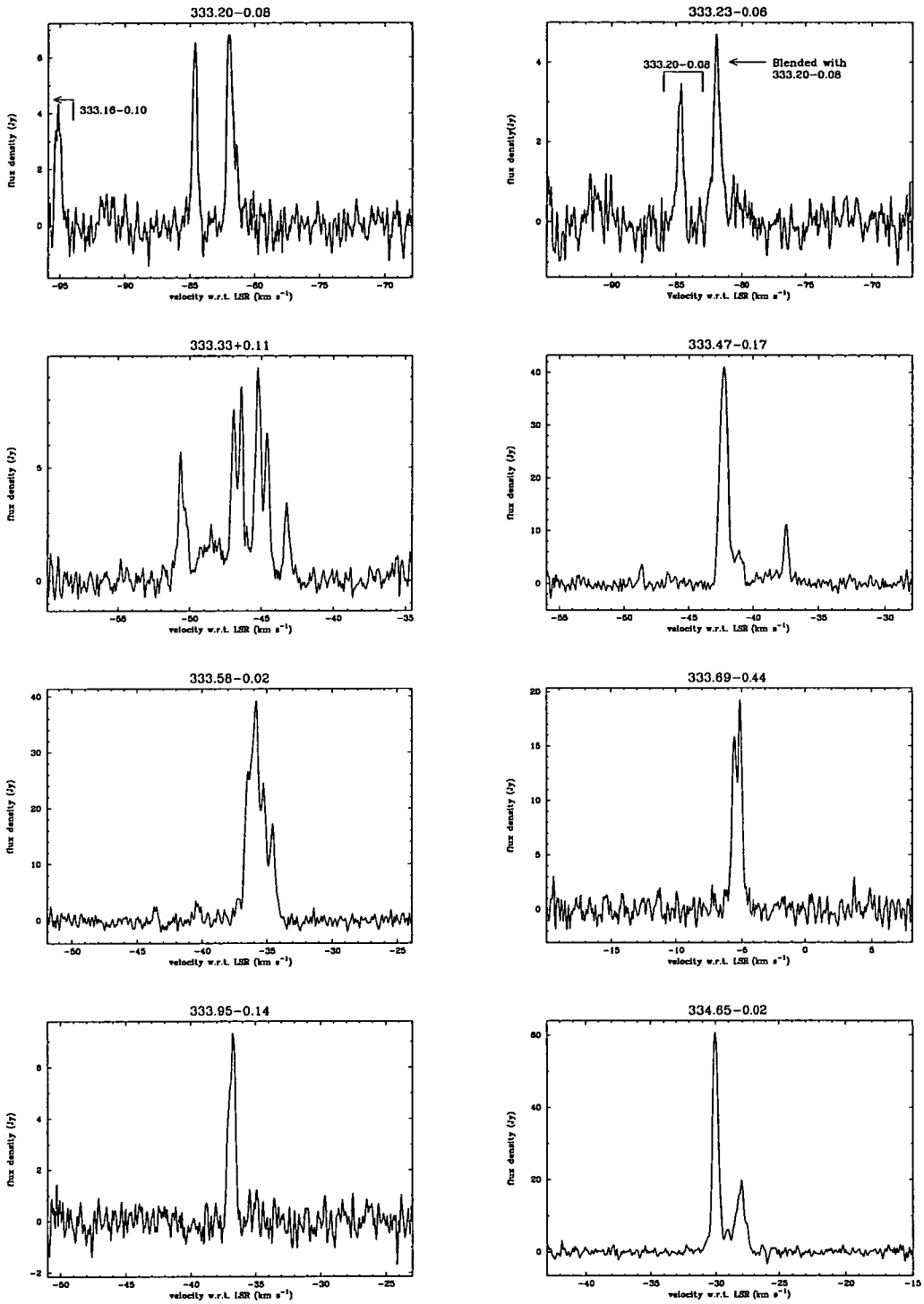

Figure 5.1: *continued...*

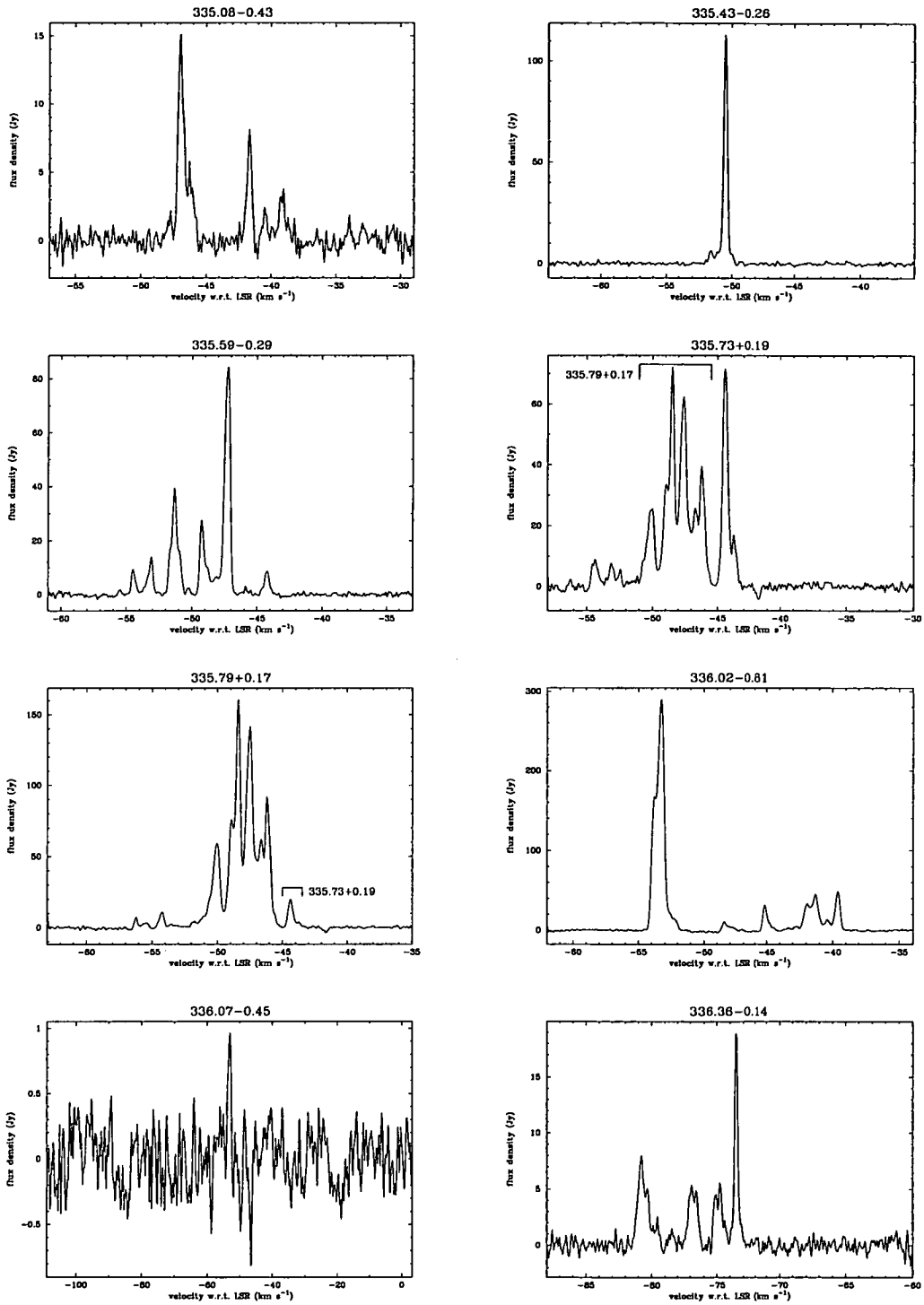

Figure 5.1: *continued...*

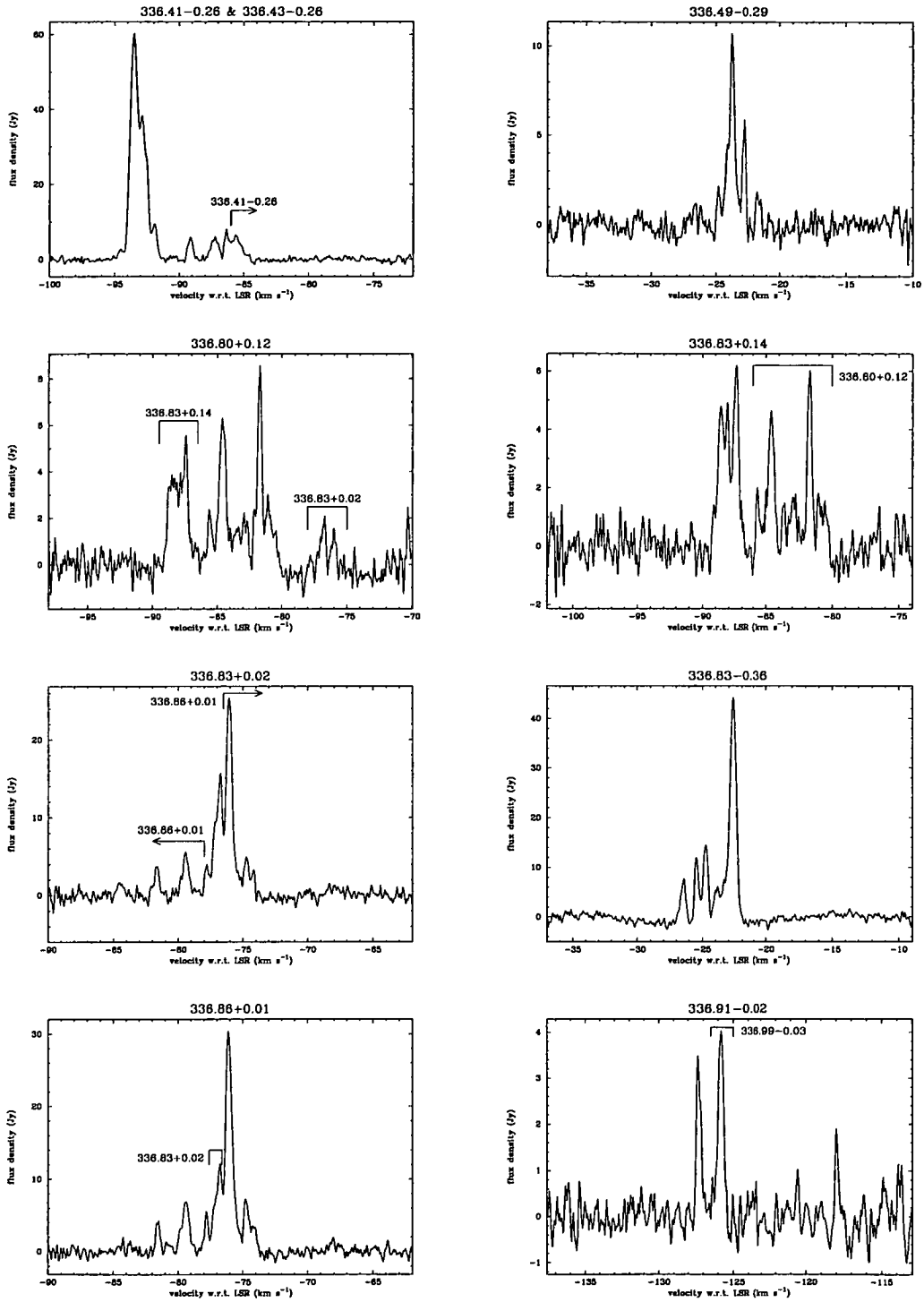

Figure 5.1: *continued...*

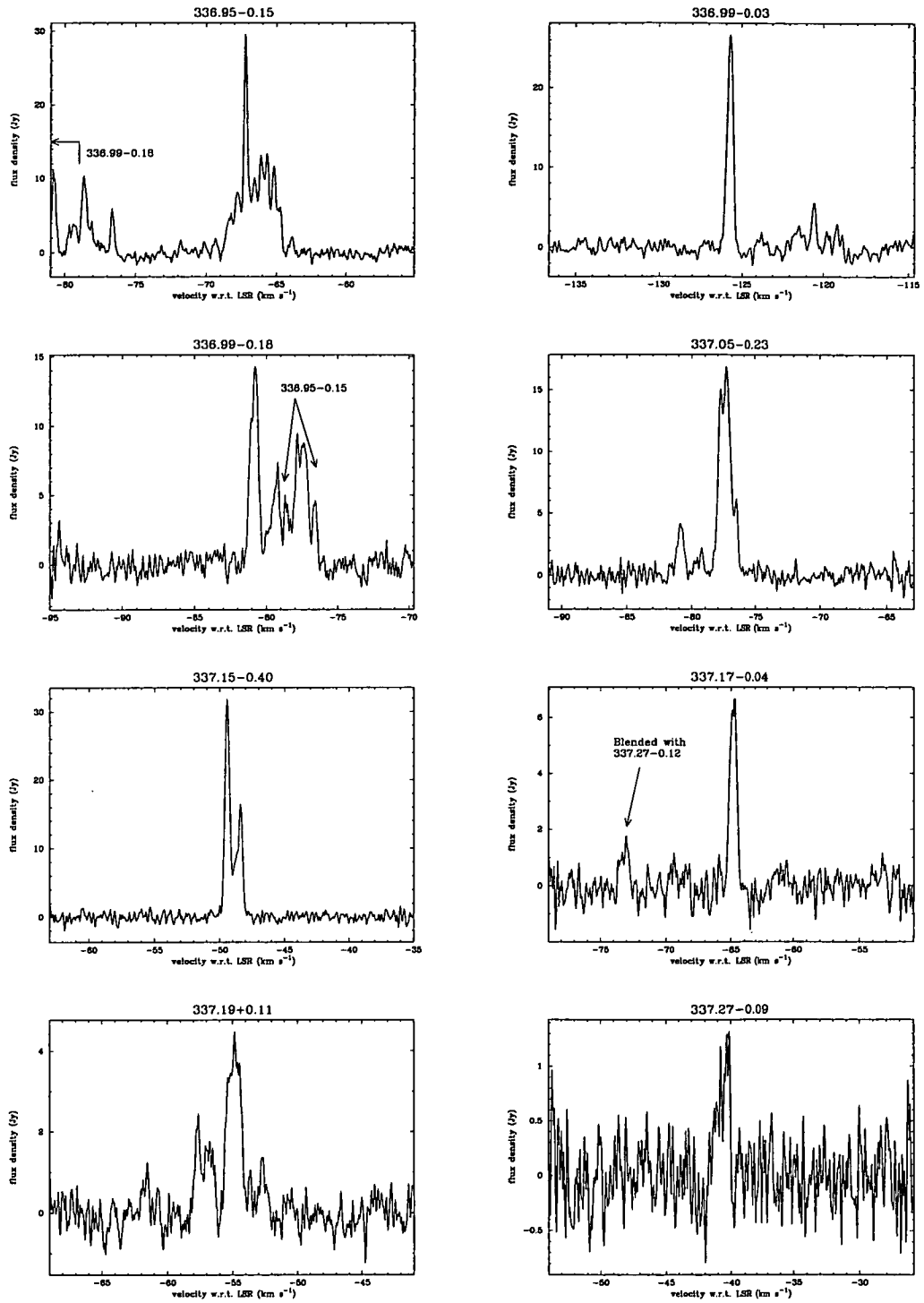

Figure 5.1: *continued...*

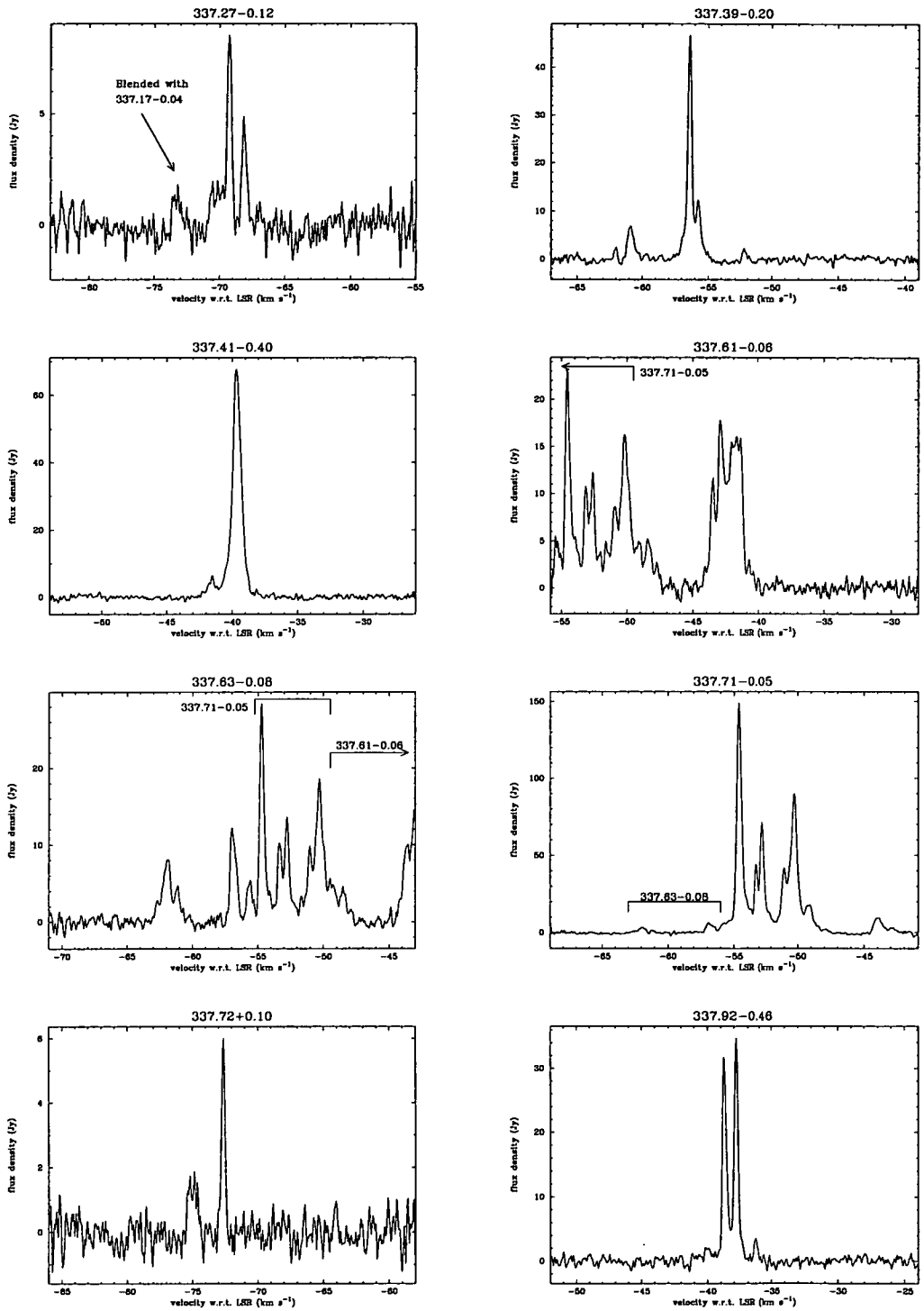

Figure 5.1: *continued...*

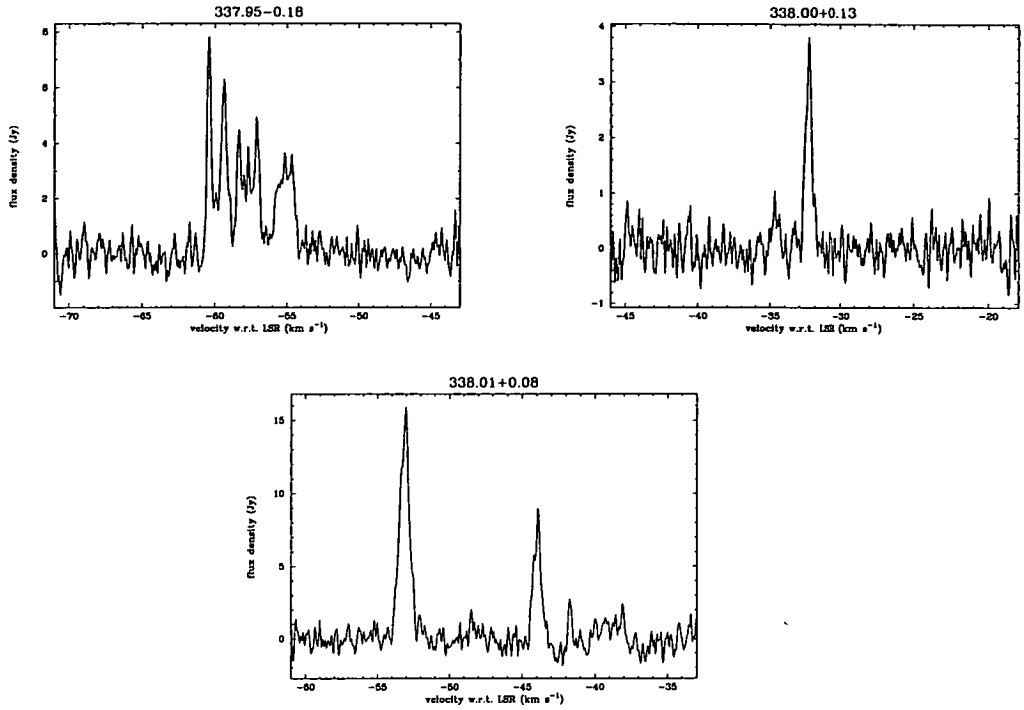

Figure 5.1: *continued...*

continuum emission (e.g. 325° $\lesssim l \lesssim$ 326° and 329.°6 $\lesssim l \lesssim$ 331.°0), often have no detected 6.7-GHz CH_3OH masers. However, a lack of strong continuum emission does not preclude masers, as the regions 329° $\lesssim l \lesssim$ 329.°5 and 293° $\lesssim l \lesssim$ 295° demonstrate. That the large scale radio continuum emission does not always correlate well with the location of the 6.7-GHz CH_3OH masers is not surprising. The large scale radio continuum emission traces the older more developed massive star formation regions. In some cases massive star formation is continuing in that region, but in others it is not and thus the 6.7-GHz CH_3OH masers are found associated with some continuum peaks and not others. Where the masers occur in regions with little or no radio continuum it may indicate that this is the first epoch of massive star formation in those regions. Alternatively, it may indicate that these 6.7-GHz CH_3OH masers are not associated with massive star formation. So while not all of the continuum features within the survey region have 6.7-GHz CH_3OH masers associated with them, approximately half do, and high-latitude searches towards regions of enhanced continuum emission may prove to be an effective searching method. A comparison with the *IRAS* Point-Source Catalog (1985), reveals that only 49 of the 108 sources detected have positions within 1 arcmin of an *IRAS* source, and in many cases the nearest *IRAS* source is more than 2 arcmin away.

5.3.1 Comments on individual sources

25.41+0.09: This is one of three weak newly detected sources in this region. It

Table 5.2: 6.7-GHz CH_3OH masers detected in the Mt Pleasant survey. References : *=new source (note, some were independently discovered by 12 or 31); 1=Batchelor *et al.* (1980); 2=Caswell, *et al.* (1980); 3=Caswell *et al.* (1983); 4=Caswell and Haynes (1983a); 5=Caswell *et al.* (1989); 6=Caswell *et al.* (1993); 7=Caswell *et al.* (1995c); 8=Caswell *et al.* (1995a); 9=Caswell *et al.* (1995b); 10=Caswell *et al.* (1995d); 11=Caswell and Vaile (1995); 12=Caswell (1996); 13=Cesaroni *et al.* (1988); 14=Gardner and Whiteoak (1984); 15=Gaylard and MacLeod Ga1993; 16=Koo *et al.* (1988); 17=Kurtz *et al.* (1994); 18=MacLeod *et al.* (1992); 19=MacLeod and Gaylard (1992); 20=MacLeod *et al.* (1993a); 21=McCutcheon *et al.* (1988); 22=Menten (1991a); 23=Norris *et al.* (1987); 24=Norris *et al.* (1988); 25=Norris *et al.* (1993); 26=Norris *et al.* (1996); 27=Schutte *et al.* (1993); 28=Peng and Whiteoak (1992); 29=Slysh *et al.* (1994); 30=Smits (1994); 31=van der Walt *et al.* (1995); 32=Wood and Churchwell (1989b)

Methanol maser (l,b)	Right Ascension (J2000)	Dec. (J2000)	Peak Flux (Jy)	Peak Vel. wrt LSR (km s^{-1})	Velocity Range (km s^{-1})	Integrated Flux (Jykm s^{-1})	references
25.41+0.09	18:37:18.8	-06:39:06	8	97.4	94,98	7.4	*,31
25.48+0.06	18:37:34.7	-06:35:57	2	95.5	95,106	3.0	*
25.53+0.38	18:36:32.6	-06:24:26	6	95.6	89,96	4.7	*
25.72+0.01	18:38:10.4	-06:24:41	502	95.7	89,101	488.6	*,32
25.82−0.18	18:39:03.0	-06:24:40	70	91.7	90,100	103.5	27
26.57−0.25	18:40:40.6	-05:46:23	9	103.8	102,115	10.4	*,31
27.21+0.14	18:40:29.3	-05:01:25	22	117.7	110,121	30.8	*
27.36−0.16	18:41:51.1	-05:02:07	42	100.5	98,102	60.7	3,4,7,9,22
28.15+0.00	18:42:45.7	-04:15:09	37	101.2	100,105	21.9	7,9
28.20−0.05	18:42:58.0	-04:14:01	2	98.9	94,99	0.9	3,4,7,11,17,22,29
28.30−0.38	18:44:20.1	-04:17:58	71	81.1	80,94	66.9	17,27
28.82+0.35	18:42:40.3	-03:29:42	6	91.1	87,93	9.8	*
28.83−0.25	18:44:51.8	-03:45:31	65	83.5	81,93	110.1	3,4,6,7,9,13,22,29
28.85+0.49	18:42:14.4	-03:24:30	5	83.2	83,84	2.3	*
29.33−0.18	18:45:29.2	-03:17:12	4	48.8	43,50	3.0	*
29.86−0.05	18:46:02.9	-02:45:04	57	100.5	100,105	87.9	6,7,8,9
29.94−0.02	18:46:02.5	-02:40:08	31	100.4	100,101	20.5	7,13,14,32
29.95−0.02	18:46:03.6	-02:39:24	160	95.9	95,105	230.4	6,7,9,13,14,16,22,32
29.98−0.04	18:46:11.7	-02:39:04	23	97.2	97,105	42.2	7,9,14,32
285.32−0.03	10:31:57.6	-58:03:18	11	0.6	-8,3	8.0	*,7,31
291.28−0.71	11:12:00.1	-61:20:29	70	-29.7	-31,-26	74.9	1,5,6,7,8,9,14,18,23,28,29
293.84−0.78	11:32:07.4	-62:14:47	4	36.9	36,39	1.9	*
293.95−0.91	11:32:40.7	-62:23:57	8	41.4	,	1.8	*
326.40+0.51	15:43:40.7	-54:19:28	2	-38.1	,	1.4	*
326.63+0.60	15:44:33.3	-54:06:23	17	-43.1	-44,-40	17.9	1,27
326.63+0.52	15:44:52.1	-54:10:30	5	-41.0	-42,-29	8.9	*,28
326.84−0.68	15:51:11.1	-54:59:01	10	-57.6	-59,-57	9.7	*
327.12+0.51	15:47:33.6	-53:52:35	80	-87.1	-90,-83	48.6	1,2,7,9,19
327.40+0.44	15:49:14.0	-53:45:36	106	-82.6	-84,-75	153.0	1,2,6,7,9,18,23
327.40+0.20	15:50:21.4	-53:56:25	9	-84.6	-86,-82	9.0	*
327.59−0.09	15:52:34.0	-54:03:12	3	-86.3	,	1.7	*
327.61−0.11	15:52:47.3	-54:03:15	2	-97.5	,	1.8	*
327.93−0.14	15:54:34.8	-53:52:18	7	-51.7	-52,-51	3.0	*
328.24−0.55	15:57:58.5	-53:59:23	421	-44.9	-46,-34	437.6	2,6,7,9,10,11,14,18,23,25,26,28
328.25−0.53	15:57:59.9	-53:58:01	425	-37.4	-50,-36	428.0	2,6,7,9,10,14,18,23,25,26,28
328.81+0.63	15:55:51.2	-52:42:36	278	-44.5	-47,-43	352.9	2,6,7,9,10,11,18,23,25,30
329.03−0.20	16:00:22.1	-53:12:57	25	-41.9	-47,-41	38.2	2,6,7,9,10,18,23
329.03−0.21	16:00:36.0	-53:12:17	275	-37.5	-41,-34	359.9	2,6,7,9,10,18,23
329.07−0.31	16:01:12.7	-53:15:58	24	-43.9	-48,-43	17.4	*,10
329.18−0.31	16:01:36.3	-53:11:49	13	-55.7	-60,-51	18.6	1,2,7,9,19
329.33+0.15	16:00:29.3	-52:44:39	14	-106.5	-107,-105	8.3	*
329.41−0.46	16:03:36.5	-53:08:58	144	-66.8	-71,-66	105.9	1,2,7,9,11,19,20
329.48+0.51	15:59:39.9	-52:22:45	13	-72.1	-73,-65	17.1	27
329.62+0.11	16:02:07.3	-52:35:13	30	-60.1	-69,-59	26.5	*,31
330.95−0.18	16:09:53.3	-51:55:38	7	-87.6	-89,-87	4.1	1,2,7,11,14,15,28
331.13−0.24	16:11:00.7	-51:51:18	34	-84.4	-92,-84	43.3	1,2,7,19
331.28−0.19	16:11:22.3	-51:42:26	165	-78.1	-86,-78	250.2	2,6,7,9,10,12,18,23,24,25,26
331.34−0.35	16:12:23.3	-51:46:11	66	-67.4	-68,-64	124.9	2,7,19
331.42+0.26	16:10:10.3	-51:16:18	25	-88.6	-91,-88	19.9	*
331.45−0.18	16:12:14.6	-51:34:39	70	-88.5	-93,-84	157.9	*,12,31

Table 5.2: *continued...*

Methanol maser (l,b)	Right Ascension (J2000)	Dec. (J2000)	Peak Flux (Jy)	Peak Vel. wrt LSR (km s^{-1})	Velocity Range (km s^{-1})	Integrated Flux (Jykm s^{-1})	references
331.54−0.07	16:12:10.9	-51:25:24	12	-84.1	-87,-83	12.4	1,2,7,11,12,19,28
331.56−0.12	16:12:28.7	-51:27:04	35	-103.4	-105,-94	46.0	7,9,12
332.11−0.42	16:16:19.3	-51:17:50	16	-61.4	-62,-58	16.8	*
332.31−0.10	16:15:50.5	-50:55:26	6	-47.0	-47,-42	8.3	*
332.33−0.44	16:17:29.3	-51:09:24	4	-53.1	,	4.5	*
332.58−0.15	16:17:19.2	-50:46:33	5	-51.0	-56,-49	5.6	*,12
332.95−0.68	16:21:19.9	-50:53:40	21	-52.9	-54,-52	14.9	*
332.96−0.68	16:21:23.2	-50:53:02	41	-45.9	-48,-38	49.2	*
333.03−0.02	16:18:47.3	-50:21:56	3	-53.6	-61,-53	6.3	*,12
333.07−0.45	16:20:53.7	-50:37:32	12	-54.5	-55,-53	7.7	7,9,28
333.12−0.43	16:20:59.5	-50:35:47	11	-49.3	-50,-48	11.6	1,2,7,12,19,28
333.13−0.44	16:21:02.7	-50:35:54	3	-44.4	-45,-42	1.9	7,12,14,28
333.15−0.56	16:21:39.1	-50:40:06	17	-56.8	-63,-52	14.9	*
333.16−0.10	16:19:41.7	-50:19:53	8	-95.3	-95,-91	3.7	7,9,12
333.20−0.08	16:19:46.3	-50:17:20	7	-82.0	-85,-81	5.0	7
333.23−0.06	16:19:51.1	-50:15:18	7	-84.7	-85,-81	6.7	1,2,7
333.33+0.11	16:19:31.7	-50:04:03	9	-43.7	-50,-41	24.7	*,12
333.47−0.17	16:21:18.1	-50:09:47	41	-42.4	-49,-37	39.2	2,7,10,12,19
333.58−0.02	16:21:13.7	-49:58:49	39	-35.9	-37,-34	58.0	*,12
333.69−0.44	16:23:32.6	-50:12:05	19	-5.2	-6,-4	13.2	*
333.95−0.14	16:23:19.5	-49:48:14	7	-36.8	-37,-36	4.3	*,12
334.65−0.02	16:25:51.1	-49:13:07	61	-30.1	-31,-27	53.5	*,12
335.08−0.43	16:29:28.9	-49:11:36	15	-47.0	-48,-39	16.5	*
335.43−0.26	16:30:12.2	-48:49:15	113	-50.5	-52,-49	42.5	*
335.59−0.29	16:30:59.1	-48:43:40	84	-47.3	-55,-44	101.4	2,7,10,12,19,29
335.73+0.19	16:29:24.5	-48:17:06	72	-44.5	-55,-43	53.6	7,9,10,12,27
335.79+0.17	16:29:47.4	-48:15:15	161	-48.4	-57,-45	333.8	1,2,6,7,8,9,10,12,18,21,23,29
336.02−0.81	16:35:04.7	-48:46:19	290	-53.3	-54,-39	329.8	*,31
336.07−0.45	16:33:40.6	-48:29:26	1	-53.1	,	0.9	*
336.36−0.14	16:33:27.2	-48:04:18	19	-73.6	-82,-73	21.3	2,7,9,11,12,19,29
336.41−0.26	16:34:13.5	-48:06:24	7	-85.7	-86,-85	5.3	7,29
336.43−0.26	16:34:20.3	-48:05:33	60	-93.5	-95,-86	80.8	6,7,9,25,26
336.49−0.29	16:34:40.2	-48:04:17	11	-23.9	-25,-21	8.5	*
336.80+0.12	16:34:09.2	-47:33:59	9	-81.7	-86,-81	12.0	*
336.83+0.14	16:34:08.8	-47:31:38	6	-87.5	-89,-87	7.5	*
336.83+0.02	16:34:38.3	-47:36:32	16	-76.8	-77.5,-76.	9.8	2,7,9,11,12,14,19,28,29
336.83−0.36	16:36:22.2	-47:51:48	46	-22.7	-27,-22	50.8	*,31
336.86+0.01	16:34:53.7	-47:36:01	30	-76.1	-82,-67	41.5	7,9,12,14,28,29
336.91−0.02	16:35:12.6	-47:34:24	4	-127.4	-128,-117	1.6	*
336.95−0.15	16:35:56.1	-47:38:13	30	-67.3	-69,-65	37.0	*,12
336.99−0.03	16:35:33.1	-47:30:58	27	-125.8	-126,-119	13.2	1,2,7,8,12,19,29
336.99−0.18	16:36:14.9	-47:37:31	14	-80.9	-82,-76	27.2	*,12
337.05−0.23	16:36:41.8	-47:36:44	17	-77.4	-82,-76	21.5	*
337.15−0.40	16:37:50.6	-47:39:12	32	-49.5	-50,-48	23.9	*
337.17−0.04	16:36:18.0	-47:24:01	7	-64.8	-66,-64	3.9	*,12
337.19+0.11	16:35:45.4	-47:16:40	5	-54.9	-62,-52	8.3	*
337.27−0.09	16:36:55.4	-47:21:18	1	-40.1	-42,-40	0.9	*
337.27−0.12	16:37:02.4	-47:22:45	9	-69.3	-74,-68	7.7	*,12
337.39−0.20	16:37:54.6	-47:20:25	47	-56.4	-62,-52	29.0	*
337.41−0.40	16:38:50.9	-47:28:02	68	-39.7	-42,-38	62.9	1,2,7,9,11,19,29
337.61−0.06	16:38:09.3	-47:04:43	18	-43.1	-49,-41	37.3	1,2,6,7,9,11,12,18,23,29
337.63−0.08	16:38:19.3	-47:04:57	12	-57.0	-63,-55	19.0	7,9,12,29
337.71−0.05	16:38:30.8	-47:01:37	149	-54.7	-55,-43	229.4	1,2,6,7,9,10,11,12,14,18,23,29
337.72+0.10	16:37:52.2	-46:53:49	6	-72.6	-76,-72	3.0	*,12
337.92−0.46	16:41:05.7	-47:07:54	35	-37.9	-39,-36	27.7	1,2,7,8,9,14,19,28,29
337.95−0.18	16:40:00.0	-46:54:27	8	-60.4	-61,-54	16.8	*,12
338.00+0.13	16:38:49.8	-46:39:16	4	-32.4	-35,-32	1.7	2,7
338.08+0.01	16:39:46.3	-46:41:23	16	-53.1	-54,-37	18.4	2,6,7,9,11,19,29

overlaps the velocity range of the stronger of the two components of 25.48+0.06, but there appears to be little blending, although it is difficult to judge due to the low flux densities of both sources. 25.41+0.09 appears to be associated with the *IRAS* source 18345-0641, which has colours that suggest that it is probably an UCHII region (see section 5.4.1.1) and was independently discovered toward 18345-0641 by van der Walt *et al.* (1995) (hereafter referred to as WGM). WGM detected this source to have a peak flux density of 35 Jy at a velocity of $\approx$ 97.5 km s^{-1}. I detected no emission at this velocity with an upper limit of 1.5 Jy, but examination of the survey data collected during September 1993 shows that this feature was present then, though it is not possible to get an accurate estimate of its flux density.

25.48+0.06: This newly detected maser exhibits emission over two velocity ranges separated by nearly 10 km s^{-1}. This may indicate that it is in fact two sources with a small separation. However, it will require higher resolution observations to determine this, as the component at $\approx$ 94 km s^{-1} is confused with 25.41+0.09 in position fitting observations. There is no associated *IRAS* source, the nearest being 18349-0638 (1.4 arcmin away) which has colours that suggest that it is unlikely to be an UCHII region.

25.53+0.38: This newly detected 6.7-GHz CH_3OH maser is at the same velocity as the strongest component of 25.48+0.06. However, the separation between the two sources is such that there should be no blending of emission within the 7-arcmin beam. There are no *IRAS* sources within 4 arcmin of the maser and the closest source (18340-0629) has colours that suggest that it is unlikely to be an UCHII region.

25.72+0.01: This is the strongest maser detected in the survey and has a peak flux density more than four times greater than any of the other newly detected sources. It is one of the twenty strongest 6.7-GHz CH_3OH masers in the Galaxy and it is surprising that no other maser transitions have previously been detected from this region. The closest *IRAS* source 18353-0628 has colours which suggest that it is likely to be an UCHII region and is separated by 1.5 arcmin from the maser position. It has an upper limit for the 60-μm flux density measurement and so was not searched by either Schutte *et al.* (1993) (hereafter referred to as SWGM) or WGM. Wood and Churchwell (1989b) detected a spherical UCHII region associated with the *IRAS* source. Again this is well offset from the maser position and so probably not associated.

25.82-0.18: This source was discovered by SWGM associated with the *IRAS* source 18361-0627, which I measure to be nearly 3-arcmin from the 6.7-GHz CH_3OH maser position. I detected a peak flux density of 70 Jy, while SWGM list the peak flux density as being 54 Jy. However, the spectrum they display has a peak flux density of $\approx$ 80 Jy making it difficult to judge if the source has varied over the course of the last 3 years. Comparison of their spectrum with mine shows the relative amplitude of the strongest components to be similar. The higher signal to noise of my spectrum also shows that the emission covers a larger velocity range than measured by SWGM. Despite being well separated from 25.72+0.01, there is some blending of the emission at $\approx$ 96 km s^{-1}.

26.57-0.25: This newly detected 6.7-GHz CH_3OH maser was also independently discovered by WGM toward the *IRAS* source 18379-0546. However, I measure the closest *IRAS* source to be 18380-0548, which is separated by 1.5-arcmin from the maser position and has colours which suggest that it is unlikely to by an UCHII region (18379-0546 is separated by 3.1 arcmin from the maser position). My spectrum shows a component at 115 km s^{-1} which is not seen in the WGM spectrum. It was present in my original survey observations from December 1993, but was < 3 Jy in April 1995 a month before the final observation shown in Fig 5.1. The large separation of velocity, and high degree of variability compared to other components of 26.57-0.25 suggests that it may be an offset source.

27.21+0.14: This newly detected source has its strongest emission at 118 km s^{-1}, but appears to have weaker associated emission extending down to 110 km s^{-1}. The closest *IRAS* source is more than 3 arcmin from the maser position and has colours which suggest that it is probably not an UCHII region.

27.36-0.16: This source is associated with an weak (1.1 Jy) OH maser, which has its peak velocity at 87 km s^{-1} (Caswell and Haynes, 1983a). This is significantly different from the velocity at which the 6.7-GHz CH_3OH peak flux density occurs ($\approx$ 100 km s^{-1}), although the spectrum of Caswell *et al.* (1995c) shows weak emission at the same velocity as the OH peak. Caswell and Haynes (1983a) measured a velocity of 98 km s^{-1} for the associated HII region and Caswell *et al.* state that OH absorption extends to this region. This suggests that the OH maser and some of the weaker 6.7-GHz CH_3OH emission may be associated with an outflow.

No H_2O maser emission was detected associated with this source, with an upper limit of 2.5 Jy (Caswell *et al.*, 1983), but Caswell *et al.* (1995b) have detected 12.2-GHz CH_3OH maser emission, of comparable peak flux density to the 6.7-GHz emission, but covering a much smaller velocity range. Caswell *et al.* (1995c) list this source as slightly variable and comparison of their spectrum with mine shows that the 100.5 km s^{-1} component which was the second strongest in June 1992, has nearly doubled in strength over the last three years, while the features at lower velocities appear to have remained relatively constant over the same period. This source was discovered by Menten (1991a), who quotes a peak flux density of 12 Jy, but as the observation was made with a 0.44 km s^{-1} spectral resolution it probably does not indicate a large variation. There is an *IRAS* source (18391-0504) separated by less than 0.5 arcmin from the maser position, but it has colours which suggest that it is unlikely to be an UCHII region.

28.15+0.00: This source was discovered by Caswell *et al.* (1995c) and there is no discernible difference between their spectrum and mine. A 12.2-GHz counterpart was detected by Caswell *et al.* (1995b) and is notable for being very similar in spectral morphology to the 6.7-GHz CH_3OH maser.

28.20-0.05: This source is associated with a much stronger OH maser (Caswell and Haynes, 1983a) and even the 6.035-GHz excited OH is of comparable strength (Caswell and Vaile, 1995). Comparison of my spectrum with that of Caswell *et al.* (1995c) shows that the peak component in their spectrum has decreased by a factor of $\approx$ 3 in the 30 month period between the two observations. Searches for H_2O maser and 44.1-GHz CH_3OH masers have not detected any emission

(Caswell *et al.*, 1983; Slysh *et al.*, 1994). I measure the 6.7-GHz CH_3OH maser to be coincident with the *IRAS* source 18403-0417, towards which Kurtz, Churchwell and Wood (1994) detected a spherical UCHII region.

28.30-0.38: This source was discovered by SWGM toward the *IRAS* source 18416-0420. Comparison of their spectrum with mine shows some small variations in the relative fluxes of the features in the velocity range 80–83 km s^{-1}. I also detected two additional components not shown in their spectrum, offset in velocity by $\approx$ 10 km s^{-1} from the main emission, but apparently at the same position. A search for radio continuum emission toward the *IRAS* source by Kurtz *et al.* (1994) detected a bipolar UCHII region.

28.82+0.35: This new 6.7-GHz CH_3OH maser has an unusually large number of components considering its low peak flux density. There are no *IRAS* sources within 5-arcmin of the maser position.

28.83-0.25: OH, H_2O and 12.2-GHz CH_3OH maser emission have also been detected toward this source with a similar velocity range (Caswell and Haynes, 1983a; Cesaroni *et al.*, 1988; Caswell *et al.*, 1995b), but all are much weaker than the 6.7-GHz CH_3OH maser emission. Menten (1991a) lists this source as having a peak flux density of 85 Jy, Caswell *et al.* (1995c) measured 73 Jy and I detected 65 Jy. Despite this apparent slow decline in the peak flux density, overall my spectrum looks very similar to that of Caswell *et al.*. The 6.7-GHz CH_3OH maser appears to be associated with the *IRAS* source 18421-0348 toward which Wood and Churchwell (1989b) did not detect any radio continuum emission stronger than $\approx$ 3 mJy $beam^{-1}$. The nearby 6.7-GHz CH_3OH maser at 28.84-0.23 was below the detection threshold of this survey.

28.85+0.49: This new detection is another for which there is no *IRAS* source within a 5-arcmin radius.

29.33-0.18: This new 6.7-GHz CH_3OH maser is separated by slightly more than 1-arcmin from the nearest *IRAS* source (18427-0320), which has colours that suggest that it is not an UCHII region.

29.86-0.05: This source is listed as slightly variable by Caswell *et al.* (1995a) and my observations also support this conclusion. Comparison of my spectrum with those of Caswell *et al.* (1995c; 1995a) show that the peak component in their spectrum has decreased in flux density by between 20–30% and is now only the second strongest component. There are no *IRAS* sources within 5-arcmin of the 6.7-GHz CH_3OH maser position.

29.94-0.02, 29.95-0.02 & 29.98-0.04: There are more than 3 separate sites of 6.7-GHz CH_3OH maser emission in this region, as has already been noted by Caswell *et al.* (1995c). With the 7-arcmin beam of the 26-m telescope it is difficult even to separate the 3 regions listed by Caswell *et al.*, particularly as 29.95-0.02 and 29.98-0.04 overlap at several different velocities. Comparison of my spectrum with that of Caswell *et al.* shows a decrease of the strongest component by $\approx$ 25%, while the second strongest peak has remained constant. 12.2-GHz CH_3OH maser emission has been detected associated with the latter two sources (Caswell *et al.*, 1995b). The closest *IRAS* source to all three sites of maser emission is 18434-0242, the smallest separation is for 29.95-0.02. Wood & Churchwell (1989b) observed a cometary HII region at the *IRAS* position and 29.95-0.02 may well be associated

with it.

285.32-0.03: This source was also independently discovered by WGM associated with the *IRAS* source 10303-3746, although I measure the 6.7-GHz CH_3OH maser to be 2.5 arcmin from the *IRAS* source. Comparison of my spectrum with theirs shows additional emission centred on $\approx$ -7 km s^{-1} which is below the noise level of their observation. It appears that this source was also detected by Gaylard and MacLeod (1993). Who mistakenly believed it to be associated with the OH and H_2O maser site 285.26-0.05 (Caswell *et al.*, 1995c)

291.28-0.71: The first detection of a maser toward this source was by Goss *et al.* (1977) who detected H_2O maser emission. Subsequent observations (Caswell *et al.*, 1989) showed that there are three sites of H_2O maser emission, but no OH emission has ever been detected. Caswell *et al.* (1995c) determined that the 6.7-GHz CH_3OH maser emission is associated with the weakest of the H_2O masers, the other two appear to be high velocity outflows from this site. In addition the 12.2-GHz CH_3OH maser is highly variable and the 6.7-GHz CH_3OH maser is also variable, but to a lesser extent (Caswell *et al.*, 1995a). Caswell *et al.* found that the feature at -29.7 km s^{-1} was strongest in June 1992 with a peak flux density of 119 Jy, which had decreased to 88 Jy by September 1993. From my observations it appears that the decline has continued and I measure a flux density of 70 Jy for the same component.

291.58-0.43: This 6.7-GHz CH_3OH maser was independently discovered by Caswell *et al.* (1995c) and Gaylard and MacLeod (1993) and is associated with an OH maser and a strong H_2O maser (Manchester *et al.*, 1970; Caswell *et al.*, 1989). Caswell *et al.* measured the 6.7-GHz CH_3OH maser to have a peak flux density of 3.5 Jy, but I did not detect this source as part of my survey. Reexamination of the survey data shows a 1.8 Jy feature at the expected velocity in April 1994, in the survey observation closest to the maser position. This is not an accurate flux density as the observation was offset in position and made with coarse spectral resolution, but the feature was well above the peak-to-peak noise in the spectrum. On the basis of this first observation a second observation was made at the same position in March 1995, but no significant emission was detected. I made a sensitive observation at the position of the 6.7-GHz CH_3OH maser and measured it to have a peak flux density of $\approx$ 2.4 Jy, which is below the detection limit of this survey. Thus it appears that this source has decreased in strength during the course of the survey. There are several sources detected by the survey which have peak flux densities slightly above the sensitivity limit, and others (detected in other searches) which have peak flux densities just below the sensitivity limit which were not detected. These results give me confidence that the estimated sensitivity level of the survey is accurate.

293.84-0.78 & 293.95-0.91: These two new detections are close together both spatially and in velocity, but their ranges appear not to overlap. For both masers the nearest *IRAS* source has colours which suggest that it is probably an UCHII region. However 293.84-0.78 is separated by more than 2 arcmin from 11298-6155 while 293.95-0.91 is separated by 1 arcmin from 11304-6206. Interestingly these two masers lie in a region with virtually no large scale radio continuum emission and no masers are detected in the surrounding stronger continuum emission (see

Fig. 5.7)

326.40+0.51: This source is one of the weakest detected in the survey and is the only source for which I was unable to improve the positional accuracy from the initial survey observations. There is no associated *IRAS* source, the nearest being 15395-5411 which is more than 3 arcmin away and has colours which suggest that it is unlikely to be an UCHII region.

326.63+0.60: This maser was discovered by SWGM, who reported it to have a peak flux density of 70 Jy. I measured a peak flux density of 18 Jy, implying a variation of more than a factor of 4 over a period of 15 months. A comparison of my spectrum with that of SWGM shows that the ratio of the various features has changed surprisingly little, considering the magnitude of the absolute variations. However, I detect a 2-Jy peak at -36 km s^{-1} which is beneath the noise level in their spectrum. SWGM detected this maser by searching toward the *IRAS* source 15408-5356, but I measure the maser emission to be separated from the IRAS source by 1.5 arcmin.

Molecular emission towards this region was first detected by Kaufmann *et al.* (1976), who discovered H_2O maser emission at a velocity of -41 km s^{-1}. Broad 12.2-GHz CH_3OH absorption, 14.5-GHz H_2CO absorption, recombination line emission and 44.1-GHz CH_3OH maser emission, have also been detected at nearby positions, all with velocities between -38 and -45 km s^{-1} (Gardner and Whiteoak, 1984; Peng and Whiteoak, 1992; Slysh *et al.*, 1994). Although I cannot be certain that all these sources are positionally coincident, their velocities suggest that they are, and the unusual combination of emission and absorption sources, a highly variable 6.7-GHz maser, and no detected OH maser implies that this would be an interesting source for further high-resolution study.

326.63+0.52: This maser is separated by nearly 5 arcmin from 326.63+0.60. However, there is an overlap in the velocity ranges, and the peak component is partially blended with the weaker component of 326.63+0.60. Again there is no nearby *IRAS* source, though the nearest source 15412-5359, (separated by 2.2 arcmin from the maser emission) is identified as an HII region, or dark cloud.

327.12+0.51: This source is typical of stronger class II CH_3OH masers, with associated OH and H_2O masers covering a similar velocity range (Caswell *et al.*, 1980; Batchelor *et al.*, 1980). Caswell *et al.* (1995c) detected no variability over the period of their observations. Our observations show that the source has remained relatively constant in the intervening period, with perhaps a slight decrease in the component at -83.5 km s^{-1}.

327.40+0.44: This source was first detected at the position of a known 12.2-GHz CH_3OH maser by MacLeod *et al.* (1992). There is an anticorrelation between the the strongest and weaker features of the 6.7- and 12.2-GHz CH_3OH emission and those of the associated OH and H_2O masers (Caswell *et al.*, 1993; Caswell *et al.*, 1980; Batchelor *et al.*, 1980). The 6.7-GHz emission covers a greater velocity range than any of the other transitions, which suggests that the H_2O and OH masers are part of a blue-shifted outflow.

327.40+0.20: A new detection, this source appears to be associated with the *IRAS* source 15464-5348, which lies in region III of the colour–colour diagram as defined by SWGM, but fails their 60- and 100-μm flux density criteria. It was

subsequently searched by WGM, but they failed to detected any maser emission.

327.59-0.09 & 327.61-0.11: These two new sources are separated by 2 arcmin. Each has only a single component and neither has an *IRAS* counterpart.

327.93-0.14: This new detection has a single asymmetric feature which is probably a blend of two or more components. The closest *IRAS* source (15507-5345), is separated by 1.6 arcmin from the maser emission and has colours atypical of an UCHII region.

328.24-0.55 & 328.25-0.53: These two masers are in one of the best studied regions of molecular emission in the Southern Hemisphere, exhibiting maser emission from the 6.7-, 12.2- and 44.1-GHz transitions of CH_3OH as well as OH (Caswell *et al.*, 1993; Slysh *et al.*, 1994; Caswell *et al.*, 1980). High-resolution images of the 6.7-GHz emission made with the ATCA by Norris *et al.* (1993) show that the spatial morphology of the maser spots is approximately linear at both centres of emission. The 44.1-GHz emission is centred on a velocity of -41 km s^{-1} (Slysh *et al.*, 1994). However, at this velocity there is no emission from the other CH_3OH transitions and the 12.2-GHz absorption is strongest (Caswell *et al.*, 1995b). This is consistent with current theories of class I CH_3OH maser emission which suggest that they are partially collisionally pumped (Cragg *et al.*, 1992), possibly by high-velocity outflows interacting with the parent molecular cloud (Menten, 1993). These sources are listed as slightly variable at 6.7 GHz by Caswell *et al.* (1995c), and the peak flux I measure for 328.24-0.55 appears to be slightly larger than that observed by Caswell *et al.*

328.81+0.63: This source is also strong and well studied, showing maser emission from the 6.7-, 12.2- and 44.1-GHz transitions of CH_3OH and the 1.665- and 6.035-GHz transitions of OH (Caswell *et al.*, 1993; Slysh *et al.*, 1994; Caswell *et al.*, 1980; Smits, 1994). It is a good example of the radial velocity anticorrelation between class I and class II CH_3OH masers, noted by Slysh *et al.*, with the 6.7-GHz emission covering the range -47 to -43 km s^{-1} and the 44.1-GHz emission covering the range -43 to -40 km s^{-1}. The peak of the OH emission is at a similar velocity to that of the class II CH_3OH but the total velocity range is larger, encompassing the ranges of both the class I and II CH_3OH masers. 328.81+0.63 is another source for which high-resolution studies show the spatial distribution of the 6.7-GHz maser spots to be highly linear (Norris *et al.*, 1993). Most of the maser species associated with this source are relatively strong, making it an excellent candidate for studying the relationship between the different molecular transitions, and star formation in general. Comparison of my spectrum with that of Caswell *et al.* (1995c), shows a decrease in the peak flux of approximately 25% over the last two years.

329.03-0.20 & 329.03-0.21: Maser emission from a wide range of transitions (12.2- and 44.1-GHz CH_3OH and OH) is associated with these two sources, though primarily with 329.03-0.21, which is the stronger at 6.7 GHz (Norris *et al.*, 1987; Slysh *et al.*, 1994; Caswell *et al.*, 1980). The closest *IRAS* source to both centres of maser emission is 15566-5304, which is not likely to be an UCHII region, as it has a 12-μm flux density which is greater than the 25-μm flux density. However, it is possible that this is due to a poor estimate of the 12-μm which is only an upper limit. ATCA observations by S. P. Ellingsen *et al.* (in preparation) failed

to detect any continuum emission associated with either of the masing regions.

329.07-0.31: This source is close to 329.03-0.20 and 329.03-0.21, and a sidelobe response from the latter can been seen quite clearly in the spectrum. Although the velocity ranges of 329.03-0.20 and 329.07-0.31 overlap, 329.03 appears to be sufficiently distant that it does not contribute significantly to the observed flux density of 329.07-0.31. The maser appears to be associated with the *IRAS* source 15573-5307, which falls in region I of SWGM's *IRAS* colour-colour diagram. However, the 60- and 100-μm fluxes fail their criteria. A search toward 15573-5307 by WGM failed to detect a 6.7-GHz CH_3OH maser associated with this source, perhaps indicating that it is highly variable.

329.18-0.31: This is another well-known maser source, with associated 12.2-GHz CH_3OH, OH and H_2O maser emission (Caswell *et al.*, 1993; Caswell *et al.*, 1980; Batchelor *et al.*, 1980). It exhibits much weaker CH_3OH maser emission in both class II transitions than most other sources in this category.

329.33+0.15: This new detection appears to be associated with the *IRAS* source 15567-5236, with the 6.7-GHz CH_3OH maser situated 0.6 arcmin from the *IRAS* source. This source is listed as a non-detection by SWGM, which implies that in mid-1993 it had a flux density of < 5 Jy. I observed a peak flux density of 14 Jy, which implies a lower limit on the increase of nearly 3 in less than a year.

329.41-0.46: This object shows OH and H_2O maser emission, and both absorption and weak emission from 12.2-GHz CH_3OH (Caswell *et al.*, 1980; Batchelor *et al.*, 1980; Caswell *et al.*, 1995b). The strongest absorption is redshifted with respect to the peak emission in all transitions, although there is some OH emission in this region which may represent an outflow.

329.48+0.51: This 6.7-GHz CH_3OH maser was discovered by SWGM toward the *IRAS* source 15557-5215, which I measure to be 1.2 arcmin from the maser position. It has a somewhat unusual spectral morphology, with at least six maser spots within a 3 km s^{-1} velocity range and one further feature blueshifted by 5 km s^{-1} from the other emission. The offset feature is not a separate source, as far as I can determine from my single-dish observations.

330.95-0.18: This source is unusual in that the OH and H_2O maser emission is much more complex and covers a far greater velocity range than that of the 6.7-GHz CH_3OH (Caswell *et al.*, 1980; Batchelor *et al.*, 1980). It is also one of the few sources for which the OH maser emission is stronger than the 6.7-GHz CH_3OH. Studying this source in detail and comparing it with other more typical sources may yield important insights into the physical conditions required to pump both OH and CH_3OH masers.

331.13-0.24: This is one of the most variable 6.7-GHz CH_3OH masers, with some features changing by more than an order of magnitude over a period of a few months (Caswell *et al.*, 1995a). Comparison of my spectrum with those published in the literature shows that large-scale variations are continuing (MacLeod and Gaylard, 1992; Caswell *et al.*, 1995c; Caswell *et al.*, 1995a). The H_2O maser emission is quite weak and spans a larger velocity range than the CH_3OH, while the OH emission has its peak in between the two centres of CH_3OH emission (Batchelor *et al.*, 1980; Caswell *et al.*, 1980). The 44.1-GHz CH_3OH maser also has several discrete regions of emission, the peak corresponding to the the weaker of

the two regions in my 6.7-GHz spectra and the secondary approximately coincident with the peak of the OH emission (Slysh *et al.*, 1994).

331.28-0.19: This source is one of the better studied CH_3OH maser sources, with high-resolution 6.7- and 12.2-GHz images showing a positional coincidence of some of the aligned spectral features to better than 20 milliarcsec (Norris *et al.*, 1988; Norris *et al.*, 1993). Caswell *et al.* (1995c) list this source as slightly variable, and a comparison of my spectrum with that of Caswell *et al.* shows that the strongest component appears to have decreased by 20% over the last two years. This source also exhibits strong maser emission in the 12.2-GHz transition of CH_3OH. As the peak components at 6.7 and 12.2 GHz exhibit both a spectral and positional coincidence, a comparison of the variability at the two frequencies may yield important information on the pumping mechanism for the class II CH_3OH masers.

331.34-0.35: Caswell *et al.* (1995a) found that the stronger 6.7-GHz CH_3OH masers are typically less variable than the weaker maser sources. However, 331.34-0.35 appears to be an exception. A comparison of my spectrum with that of Caswell *et al.* (1995c) shows that the feature at -65 km s^{-1} has decreased by about a factor of 2, while at the same time the feature at -68 km s^{-1} has increased by a factor of 2 and the feature at -67 km s^{-1} has remained relatively unchanged. Unusually, the class I 44.1-GHz CH_3OH maser emission lies in the same velocity range as the class II 6.7-GHz emission (Slysh *et al.*, 1994).

331.42+0.26: This new detection lies at the edge of a large region of complex continuum emission (see Fig. 5.9). The nearest *IRAS* source 16062-5108 is 1 arcmin away and has colours atypical of an HII region.

331.45-0.18: This is one of the stronger 6.7-GHz CH_3OH masers discovered by this survey and has a complex spectral morphology. It lies in the region of the Galactic Plane which Caswell *et al.* (1980) searched for OH maser emission, implying that there was no OH maser with peak flux density > 1 Jy. Unless OH emission is present but was missed in the earlier surveys, this source lies at an extreme of the 6.7-GHz CH_3OH:OH flux ratio distribution. This source lies 0.6 arcmin from an *IRAS* source (16084-5127) which has colours placing it in region III of SWGM's *IRAS* colour–colour diagram, but fails their 100-μm flux density criterion. WGM searched for 6.7-GHz CH_3OH maser emission toward 16084-5127, but surprisingly failed to detect anything.

331.54-0.07 & 331.56-0.12: The first of these sources was discovered by Caswell *et al.* (1995c) and is near 331.56-0.12, which can be seen at the edge of my spectrum. There is OH and H_2O maser emission in the general direction of these two sources, though exactly which features are associated with each of the CH_3OH sources has not yet been clearly determined (Caswell *et al.*, 1995c). The OH emission has a velocity range from approximately -85 to -94 km s^{-1} and the H_2O emission has a velocity range from approximately -75 to -105 km s^{-1} with a blueshifted outflow at a velocity of approximately -140 km s^{-1} (Caswell *et al.*, 1980; Batchelor *et al.*, 1980). 331.56-0.12 also has a 12.2-GHz CH_3OH maser associated with it which has a similar spectral morphology to the 6.7-GHz maser (Caswell *et al.*, 1995b).

332.11-0.42: This is the first of several new 6.7-GHz CH_3OH masers discovered

between Galactic latitudes 332° and 333°. This source has a good positional coincidence with the *IRAS* source 16124-5110, which has colours atypical of an UCHII region.

332.31-0.10: This new detection is close to the *IRAS* source 16119-5048. This source meets the colour and flux-limit criteria for region III of SWGM's *IRAS* colour–colour diagram, but it has an upper limit for the 100-μm flux density and so was not searched by them. It was searched by WGM, but they list it as a non-detection.

332.33-0.44: This maser lies at the edge of a peak in the continuum emission (see Fig. 5.10), but does not appear to have an *IRAS* counterpart. The nearest *IRAS* source (16357-5100) is 1.3 arcmin away and has colours which suggest that it is probably not an UCHII region.

332.58-0.15: This source also lies at the edge of a continuum peak, but has no *IRAS* counterpart, the nearest *IRAS* source 16136-5038 being 2 arcmin away.

332.95-0.68 & 332.96-0.68: Discovered serendipitously while taking a reference spectrum for another observation, these sources are separated by only 48 arcsec, but have non-overlapping velocity ranges. 332.95-0.68 appears to be associated with the *IRAS* source 16175-5046, and 332.96-0.68 with 16175-5045, both of which lie in region III of SWGM's *IRAS* colour–colour diagram. However, each has upper limits for several of the *IRAS* flux density bands and so neither *IRAS* source was searched by them.

333.03-0.02: This is a weak 6.7-GHz CH_3OH maser which lies near the edge of a continuum peak (see Fig. 5.10), and has no *IRAS* counterpart. It differs from most sources of this strength in that it has at least four components.

333.07-0.45, 333.12-0.43 & 333.13-0.44: Although positionally adjacent, these sources are widely separated in velocity. There is 12.2- and 44.1-GHz CH_3OH maser emission as well as OH and H_2O maser emission from this general region (Caswell *et al.*, 1995b; Slysh *et al.*, 1994; Caswell *et al.*, 1980; Batchelor *et al.*, 1980). Caswell *et al.* (1995b) detected weak 12.2-GHz emission associated with 333.07-0.54 and Caswell *et al.* (1995c), determined that the OH emission is associated with 333.12-0.43, making this another case where the OH emission is stronger that of the 6.7-GHz CH_3OH emission and also covers a wider velocity range. The 44.1-GHz CH_3OH and H_2O maser emission cover the velocity ranges of both 333.12-0.43 and 333.13-0.44, and may not be closely associated with either source.

333.15-0.56: This new detection shows a somewhat unusual spectral morphology, with three distinct single peaks. Its position is close to a peak in the continuum emission (see Fig. 5.10), but has no associated *IRAS* source.

333.16-0.10, 333.20-0.08 & 333.23-0.06: These sources are close together and the latter two are severely blended in the 7-arcmin beam of the Hobart telescope. Caswell *et al.* (1995c) list all of the components of 333.23-0.06 as being variable and they measure a flux density of 3.8 Jy for the -80.5 km s^{-1} peak, whereas in my spectrum it has a flux density of < 1 Jy. The strongest peak in 333.23-0.06 is at a velocity of -81.9 km s^{-1} but it is blended with emission from 333.20-0.08, and the true flux density of this component is probably less than half that listed in Table 5.2. Once again there is emission from 12.2- and 44.1-GHz CH_3OH, OH

and H_2O (Caswell *et al.*, 1995b; Slysh *et al.*, 1994; Caswell *et al.*, 1980; Batchelor *et al.*, 1980). Caswell *et al.* (1995c) determined that the OH emission is most closely associated with 333.23-0.06 and this also appears to be the case for the H_2O and 44.1-GHz CH_3OH maser emission. This is somewhat surprising as it is the weakest of this group of sources at 6.7 GHz.

333.33+0.11: An unusually large number of components distinguishes this source from most others with low peak flux density. I made several observations of this source while trying to determine its position and found its flux density to vary significantly over a period of a week. It appears to be associated with the *IRAS* source 16157-4957, which lies in region I of SWGM's colour–colour diagram, but does not satisfy their 60-μm flux density criterion.

333.47-0.17: This maser has a weak OH counterpart, with emission and absorption spanning the range of most of the 6.7-GHz CH_3OH emission (Caswell *et al.*, 1980). Comparison of my spectrum with that of Caswell *et al.* (1995c) shows that the flux density of the peak component in this source has nearly halved in intensity (from 70 to 41 Jy) over a period of 18 months, but the rest of the features have remained relatively constant. This source appears to be associated with the *IRAS* source 16175-5002, which is 0.4 arcmin away and has colours which place it in region III of SWGM's colour–colour diagram.

333.58-0.02: This is one of the stronger new sources, showing several strong peaks within a small velocity range. There are also several weak features blueshifted from the peak emission by a few km s^{-1}. This source has no *IRAS* counterpart.

333.69-0.44: This source is associated with a peak in the continuum emission (see Fig. 5.10) and with the *IRAS* source 16196-5005. The *IRAS* source lies in region III of SWGM's colour–colour diagram, but has upper limits for all but the 25-μm flux density measurements and so was not included in their search, or that of WGM. This source has a velocity quite close to the local standard of rest and the *IRAS* counterpart is identified as an HII region or dark cloud.

333.95-0.14: This new 6.7-GHz CH_3OH maser appears to be associated with the *IRAS* source 16194-4941, which lies well outside the region of the colour–colour diagram which SWGM searched. Like the previous source, the *IRAS* counterpart is identified as an HII region, or a dark cloud.

334.65-0.02: This strong new detection appears to be associated with the *IRAS* source 16220-4906, which has colours that suggest that it is unlikely to be an UCHII region.

335.08-0.43: This source lies at the edge of a large area of low-level continuum emission (see Fig. 5.10). It does not appear to be associated with an *IRAS* source, the closest being 16256-4905.

335.43-0.26: This new detection has an unusual spectral morphology as it covers quite a small velocity range and the peak component is more than 10 times stronger than any of the other components. The nearest *IRAS* source (16264-4841) is separated from the maser position by more than 1.5 arcmin and has colours which suggest that it is unlikely to be an UCHII region.

335.59-0.29: This source, which was discovered by MacLeod & Gaylard (1992) has a large velocity range. However, high resolution observations with the ATCA by Caswell *et al.* (1995d) and Caswell (1996) have found the emission to arise from

three separate sources. Caswell *et al.* (1995c), list this source as slightly variable and my spectrum is significantly different to theirs. The strongest component at -47 km s^{-1} has decreased from 110 to 84 Jy, the component at -55 km s^{-1} has decreased from $\approx$ 40 to 10 Jy, but the component at -49 km s^{-1} has slightly increased and the component at -51 km s^{-1} has remained constant. OH and strong 44.1-GHz CH_3OH maser emission has been detected associated with the 6.7-GHz CH_3OH maser emission, but no 12.2-GHz CH_3OH or H_2O masers (Caswell *et al.*, 1980; Slysh *et al.*, 1994).

335.73+0.19 & 335.79+0.17: These two strong 6.7-GHz CH_3OH masers have been well studied at high resolution and 335.79+0.17 in particular exhibits emission from a wide range of molecules and transitions. Only 6.7- and 12.2-GHz CH_3OH maser emission have been detected associated with 335.73+0.19 (Caswell *et al.*, 1995c; Caswell *et al.*, 1995b). However, 6.7-, 12.2- and 44.1-GHz CH_3OH, as well as OH and H_2O maser emission have been detected associated with 335.79+0.17, which is a well known star formation region (Batchelor *et al.*, 1980; Caswell *et al.*, 1980; MacLeod *et al.*, 1992; Norris *et al.*, 1987; Slysh *et al.*, 1994).

Several interferometric observations have been made of both sources, including the VLBI observations described in Chapter 7. Caswell *et al.* (1995d; 1996) and Phillips *et al.* (1996) have all used the ATCA to observe the 6.7-GHz CH_3OH maser emission from both sources. Phillips *et al.* found the spatial distribution of the 6.7-GHz emission to have a similar spatial morphology to the 12.2-GHz VLBI images (Fig 7.15), but did not detected any radio continuum emission stronger than 0.3 mJy $beam^{-1}$ at 8.6 GHz.

335.79+0.17 is listed as variable at both 6.7 and 12.2-GHz by Caswell *et al.* (1995a). Comparison of my spectrum with theirs shows that the component at -49 km s^{-1} which they observed to decrease from 154 to 102 Jy between June 1992 and September 1993 has continued to decline and I now detected it to have a flux density of $\approx$ 75 Jy. In contrast the -50 km s^{-1} component has a similar flux density to that last observed by Caswell *et al.* of $\approx$ 60 Jy.

336.02-0.81: This new 6.7-GHz CH_3OH maser was serendipitously detected in a reference observation for another source. It appears to be associated with the *IRAS* source 16313-4840, which has colours typical of an UCHII region. This source was independently discovered by WGM toward the 16313-4840. Comparison of their spectrum with mine shows that the flux density of the strongest component has reduced by more than 25% in the 2 years separating the observations.

336.07-0.45: This new 6.7-GHz CH_3OH maser has decreased in peak flux from its initial detection and is the weakest maser discovered in the survey. The closest *IRAS* source (16301-4823) is separated by 2 arcmin from the maser position and has colours which suggest that it is unlikely to be an UCHII region.

336.36-0.14: Comparison of my spectrum with that of Caswell *et al.* (1995c) shows little variation in the spectral morphology between 1992 and 1995. This source is accompanied by weak 12.2-GHz CH_3OH, 1.665-GHz and 6.035-GHz OH masers (Caswell *et al.*, 1980; Caswell *et al.*, 1995b; Caswell and Vaile, 1995). The maser position is less than 1 arcmin from the *IRAS* source 16297-4757 which has colours that suggest that it is probably an UCHII region.

336.41-0.26 & 336.43-0.26: These two 6.7-GHz CH_3OH masers were difficult to separate in my observations and so I have displayed them in a common spectrum. The observation was made at the position of 336.41-0.26, so the amplitude of 336.43-0.26 is slightly reduced. Caswell *et al.* list 336.43-0.26 as being slightly variable. Comparison of my spectrum with those of Norris *et al.* (1993) and Caswell *et al.* show that the flux density of the strongest component has increased from slightly more than 30 Jy in January 1992 to 46 Jy by June of the same year and I measure it to be 60 Jy. Interestingly no OH or H_2O maser emission has been detected towards either of these sites, but other CH_3OH transitions have, at 44.1-GHz toward 336.41-0.26 and 12.2-GHz toward 336.43-0.26 (Caswell *et al.*, 1993; Slysh *et al.*, 1994).

The 6.7-GHz CH_3OH maser was discovered by Norris *et al.* using the ATCA and they observed the spatial morphology of the maser spots to be approximately linear and have a monotonic velocity gradient. Modelling the masers as lying in an edge on circumstellar disc, Norris *et al.* (1996) derive a mass of 110 $M\odot$ for the exciting star. The closest *IRAS* source to both sites is 16306-4758, which has colours that suggest that it is likely to be an UCHII region.

336.49-0.29: This newly detected 6.7-GHz CH_3OH maser is spatially relatively close to the previous two sources, but their velocity ranges are very different. The nearest *IRAS* source to the maser position (1.4 arcmin separation) is 16310-4756, which has colours typical of an UCHII region, but has an upper limit for the 60- and 100-μm flux density measurements and so was not searched by either SWGM or WGM.

336.80+0.12 & 336.83+0.14: These two new 6.7-GHz CH_3OH masers are close together both spatially and in velocity, but their ranges do not overlap at all. For both sources the nearest *IRAS* source is separated by more than 3 arcmin from the measured maser position.

336.83+0.02 & 336.86+0.01: The velocity range of the former of these two sources lies approximately in the centre of the latter. Despite being weaker and having a smaller velocity range, the stronger 12.2-GHz CH_3OH and 1.665- and 6.035-GHz OH masers are all associated with 336.83+0.02 (Caswell *et al.*, 1980; Caswell *et al.*, 1995b; Caswell and Vaile, 1995). The nearest *IRAS* source is separated by 3.9 and 1.3 arcmin respectively from the maser positions, but has colours which suggest that it is probably an UCHII region.

336.83-0.36: This newly detected 6.7-GHz CH_3OH maser was independently discovered by WGM toward the *IRAS* source 16327-4746, which I measure to be separated from the maser position by 1 arcmin. Comparison of my spectrum with that of WGM shows that the source has remained relatively steady over the last 3 years.

336.91-0.02: This new 6.7-GHz CH_3OH maser was discovered when determining the position of 336.99-0.03. The component at -118 km s^{-1} was not observed during the position fitting observations and I have not yet been able to determine if it is associated with 336.91-0.02, or another new source.

336.95-0.15 & 336.99-0.18: These two new 6.7-GHz CH_3OH masers were also independently discovered in ATCA observations by Caswell (1996). The flux densities he determined agree well with mine, as do the spectra. However with his

higher resolution observations he found that the the velocity ranges of the two sources overlap in the range -79 to -76 km s^{-1}. For both masers the nearest *IRAS* source (16320-4734 and 16325-4731 respectively) have colours which suggest that they are probably UCHII regions. 16325-4731 is separated from the maser position by less than 1 arcmin, but has an upper limit for the 60-μm flux density and so was not searched by WGM.

336.99-0.03: This highly variable 6.7-GHz CH_3OH maser was detected while determining the position of 336.86+0.01. Caswell *et al.* (1995a) observed the strongest component to vary by more than a factor of 3 over a 15 month period. These variations have continued, I measured a peak flux density of 27 Jy, compared to 11 Jy observed by Caswell *et al.* in September 1993.

337.05-0.23: This newly detected 6.7-GHz CH_3OH maser is separated by less than 1 arcmin from the nearest *IRAS* source (16329-4730), which has colours that suggest that it is not an UCHII region.

337.15-0.40 This newly detected 6.7-GHz CH_3OH maser appears to be associated with the *IRAS* source 16340-4732, which has colours that suggest that it is probably an UCHII region.

337.17-0.04 & 337.27-0.12: Despite being spatially separated by quite a long way, the velocity ranges of these two new sources overlap at -73 km s^{-1}. They were independently discovered by Caswell (1996) and though the spectral morphology I observe agrees well with his, the peak flux density I detected is in both cases less. I measure 337.17-0.04 to be separated by less than 1 arcmin from the nearest *IRAS* source 16326-4718, which has colours that suggest that it is probably an UCHII region. WGM searched for 6.7-GHz CH_3OH maser emission toward this *IRAS* source, but did not detect emission above their 3-σ flux density limit of 5 Jy, which suggests that this source may be slightly variable.

337.19+0.11 & 337.27-0.09: There are no *IRAS* sources within 3.5 arcmin of the positions of either of these newly detected, weak 6.7-GHz CH_3OH masers.

337.39-0.20: This newly detected 6.7-GHz CH_3OH maser appears to be associated with the *IRAS* source 16341-4722. This *IRAS* source has colours which suggest that it is probably an UCHII region, but the flux density measurements at both 25 and 60 μm are upper limits and so the source did not meet the selection criteria of either the SWGM or WGM searches.

337.41-0.40: This source exhibits maser emission from a large range of molecules and transitions. The 6.7- and 12.2-GHz CH_3OH maser emission is has quite a small velocity range which roughly coincides with the stronger of two separate velocity ranges in the 1.665- and 1.667-GHz OH emission (Caswell *et al.*, 1980; Caswell *et al.*, 1995b). The 6.035-GHz excited OH emission roughly straddles the CH_3OH range (Caswell and Vaile, 1995) and the 44.1-GHz CH_3OH lies in the velocity range between the two main-line OH ranges (Slysh *et al.*, 1994). I measure the 6.7-GHz CH_3OH maser emission to be approximately coincident with the *IRAS* source 16351-4722 which has colours that suggest that it is probably an UCHII region.

337.61-0.06 & 336.63-0.08: The majority of the maser transitions which have been detected toward these two sources are associated with 337.61-0.06 (Batchelor *et al.*, 1980; Caswell *et al.*, 1980; Caswell *et al.*, 1995b; Caswell and Vaile, 1995).

I am unable to observe the components of 337.61-0.06 in the velocity range -50 to -55 km s^{-1}, due to the proximity of 337.71-0.05. Caswell *et al.* (1995c) listed 336.61-0.06 to be non-variable, but in the 30 months since their observations the strongest component at -42 km s^{-1} has decreased by 25% and is now the second strongest component. 16344-4658 is the closest *IRAS* source to both maser positions and has colours that suggests that it is likely to be an UCHII region.

337.71-0.05: Like most other sites of strong 6.7-GHz CH_3OH maser emission, masers of many other transitions have also been detected (Batchelor *et al.*, 1980; Caswell *et al.*, 1980; Caswell and Vaile, 1995; Norris *et al.*, 1987). This source has been observed to be unusually stable at both 6.7- and 12.2-GHz (Caswell *et al.*, 1995c; Caswell *et al.*, 1995b) and there are no discernible differences between my 6.7-GHz spectrum and that of Caswell *et al.*, suggesting that no variations have occurred in the 2 years between the two observations.

337.72+0.10: This newly detected source was independently discovered in the ATCA survey of Caswell (1996). The nearest *IRAS* source is separated from the maser position by 1.7 arcmin, but has colours which suggest that it is probably an UCHII region. The reliability of the *IRAS* colours for this source are dubious though as all but the 12-μm flux density measurement are upper limits.

337.92-0.46: The main-line OH emission toward this source covers a much larger velocity range (Caswell *et al.*, 1980) and the 6.7-GHz CH_3OH maser emission coincides with the deepest OH absorption. The 44.1-GHz CH_3OH maser emission lies roughly in the centre of the OH emission range (Slysh *et al.*, 1994). Caswell *et al.* (1995a) observed the 6.7-GHz CH_3OH component at -37.9 km s^{-1} to be decreasing at the same time as the -38.8 component was increasing. Comparing my observations with theirs, the -37.9 component is at roughly the same level as their last observation in September 1993, but the -38.8 km s^{-1} has decreased by $\approx$ 25% in the same period.

337.95-0.18: This new 6.7-GHz CH_3OH maser was independently discovered in the ATCA survey of Caswell (1996). My spectrum appears to be essentially identical to his, though with a higher signal to noise ratio it is clear that this source has many components within a relatively small velocity range. The closest *IRAS* source to the maser position is 16363-4650 (2.4 arcmin separation), which has colours that suggest that it is unlikely to be an UCHII region.

338.00+0.13: This 6.7-GHz CH_3OH maser is somewhat unusual as it is associate with 1.612-, 1.665- and 1.667-GHz OH maser emission (Caswell *et al.*, 1980), but no emission from other transitions. Caswell *et al.* (1995c) list the source as being non-variable and there are no discernible differences between my spectrum and their's.

338.08+0.01: 1.665-GHz main-line and 6.035-GHz excited OH, 12.2-GHz CH_3OH maser emission are detected associated with this site, in addition to 6.7-GHz CH_3OH (Caswell *et al.*, 1980; Caswell *et al.*, 1993; Caswell and Vaile, 1995). Caswell *et al.* (1995c) list this source as being slightly variable and comparison of my spectrum with their's shows that the component at -44 km s^{-1} has decreased by $\approx$ 30% over the course of the last 2 years.

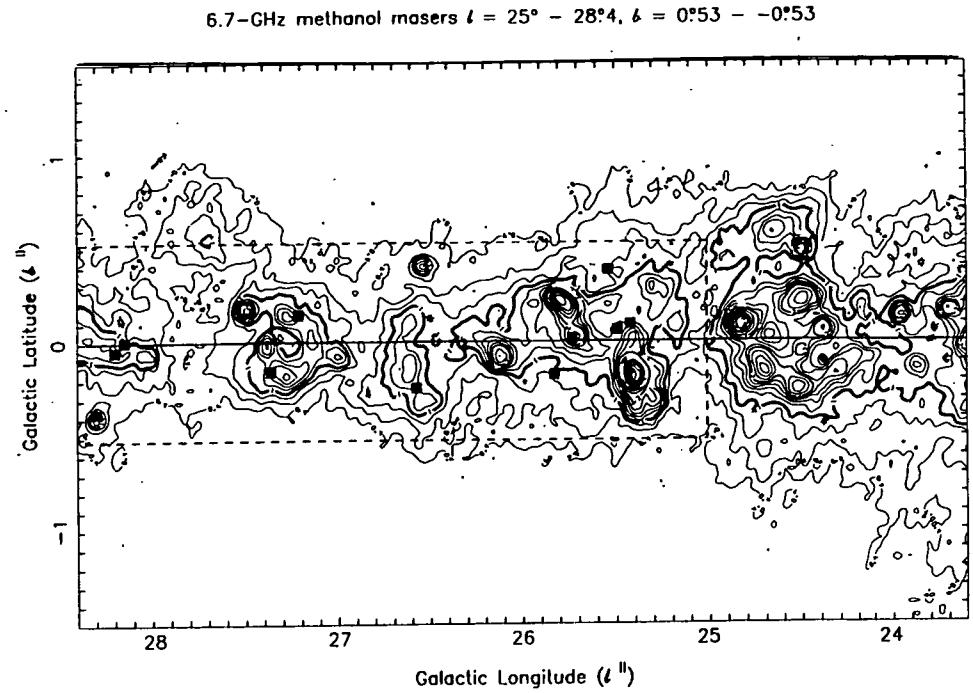

Figure 5.2: 5-GHz continuum emission l = 23°.6 – 28°.4, b = -1°.5 – 1°.5 (Haynes *et al.*, 1978). The positions of the 6.7-GHz CH_3OH masers are marked with filled squares and the dashed line marks the region covered by the Mt Pleasant survey.

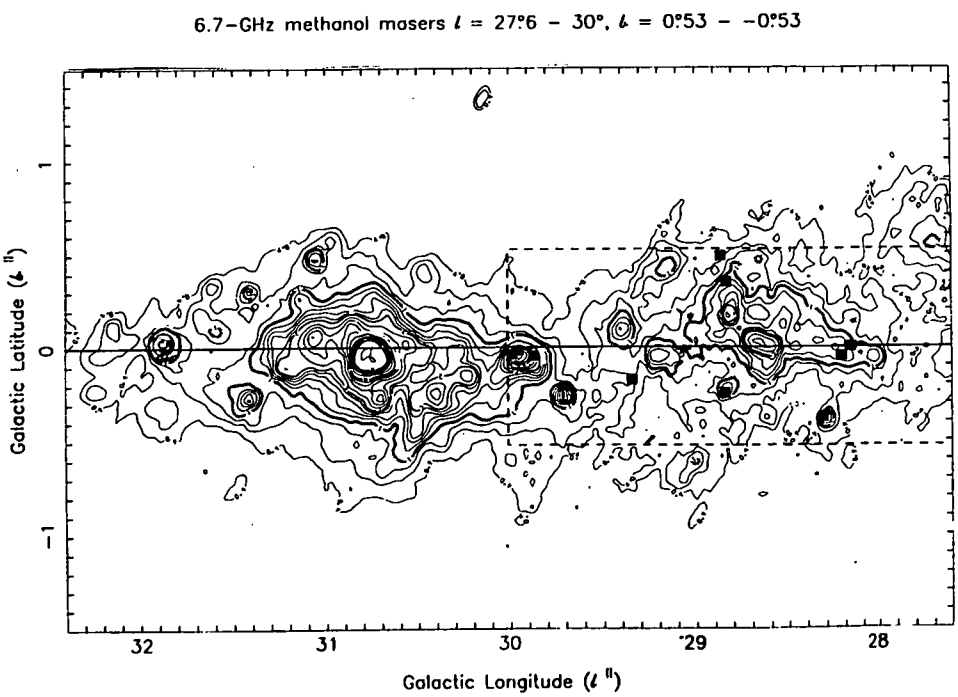

Figure 5.3: 5-GHz continuum emission l = 27°.6 – 32°.4, b = -1°.5 – 1°.5 (Haynes *et al.*, 1978). The positions of the 6.7-GHz CH_3OH masers are marked with filled squares and the dashed line marks the region covered by the Mt Pleasant survey.

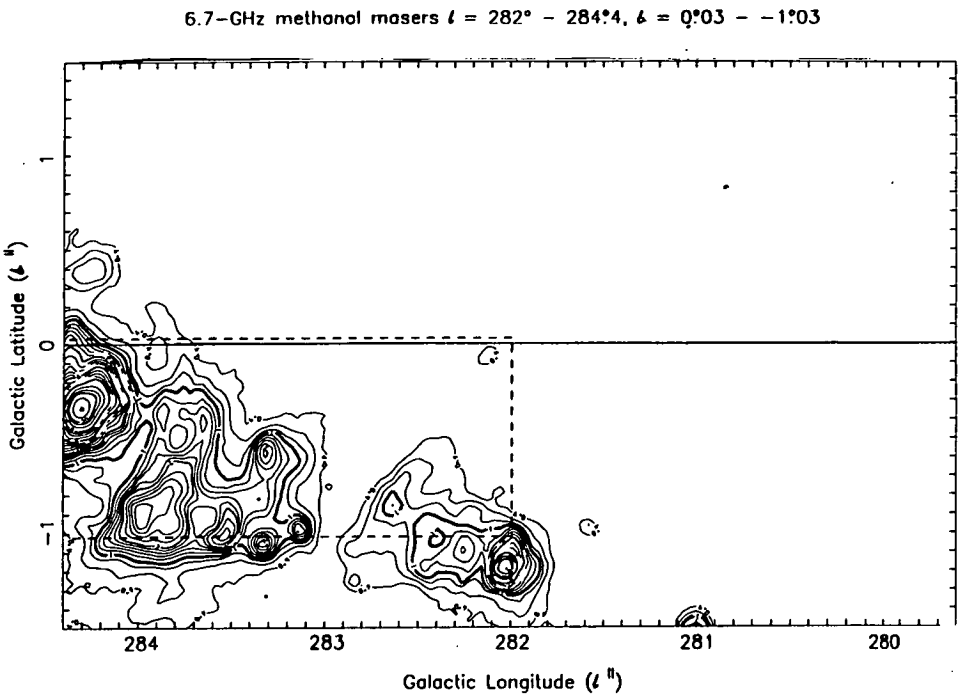

Figure 5.4: 5-GHz continuum emission l = 279°.6 – 284°.4, b = -1°.5 – 1°.5 (Haynes *et al.*, 1978). The positions of the 6.7-GHz CH_3OH masers are marked with filled squares and the dashed line marks the region covered by the Mt Pleasant survey.

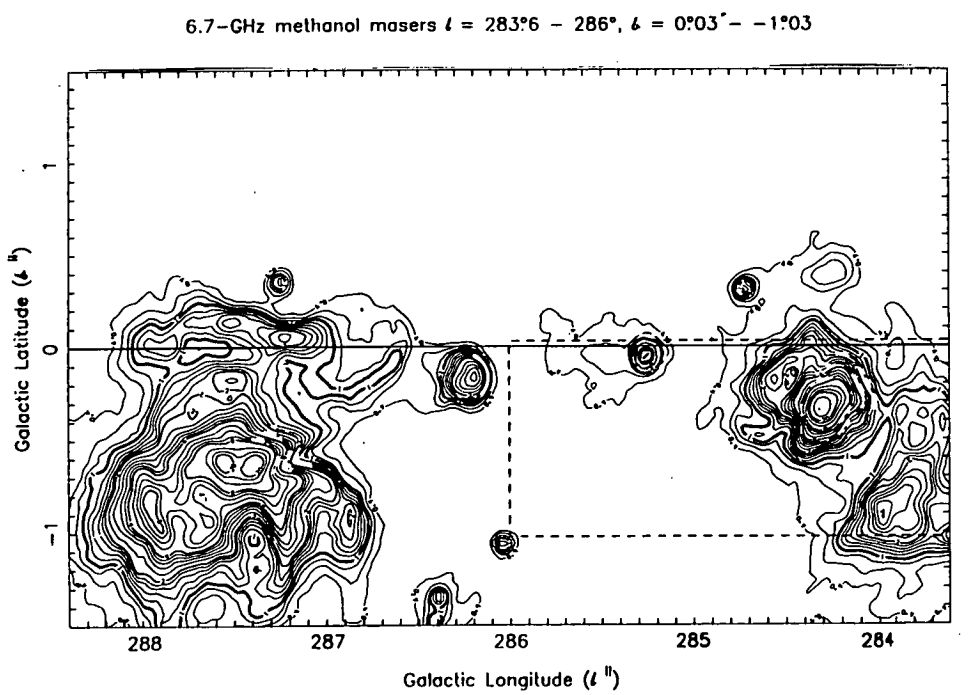

Figure 5.5: 5-GHz continuum emission l = 283°.6 – 288°.4, b = -1°.5 – 1°.5 (Haynes *et al.*, 1978). The positions of the 6.7-GHz CH_3OH masers are marked with filled squares and the dashed line marks the region covered by the Mt Pleasant survey.

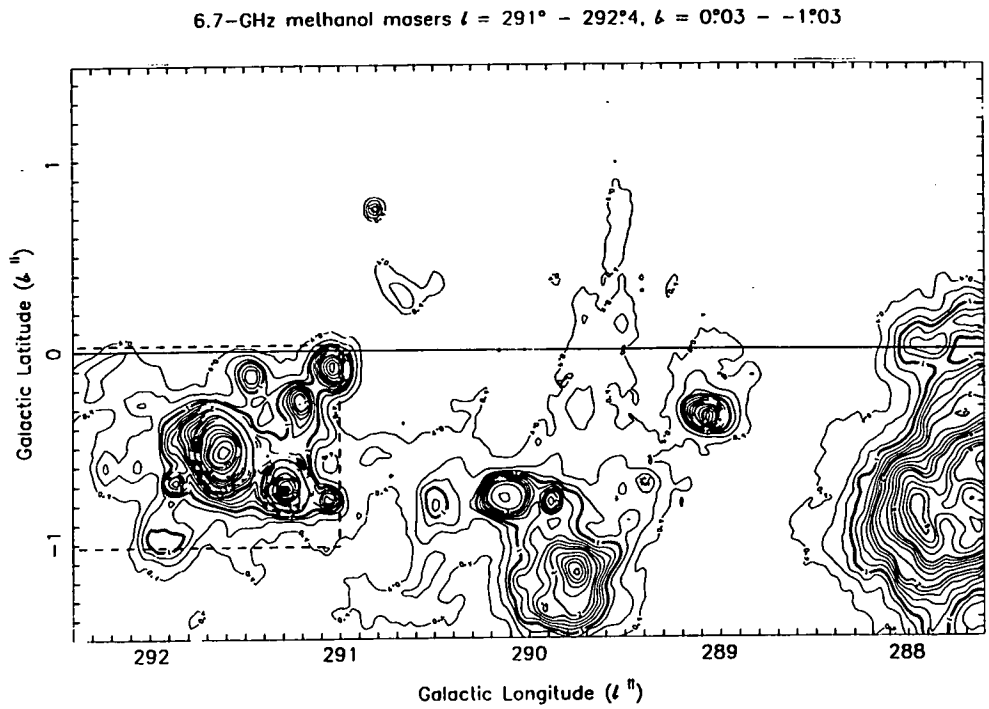

Figure 5.6: 5-GHz continuum emission l = 287°.6 – 292°.4, b = -1°.5 – 1°.5 (Haynes *et al.*, 1978). The positions of the 6.7-GHz CH_3OH masers are marked with filled squares and the dashed line marks the region covered by the Mt Pleasant survey.

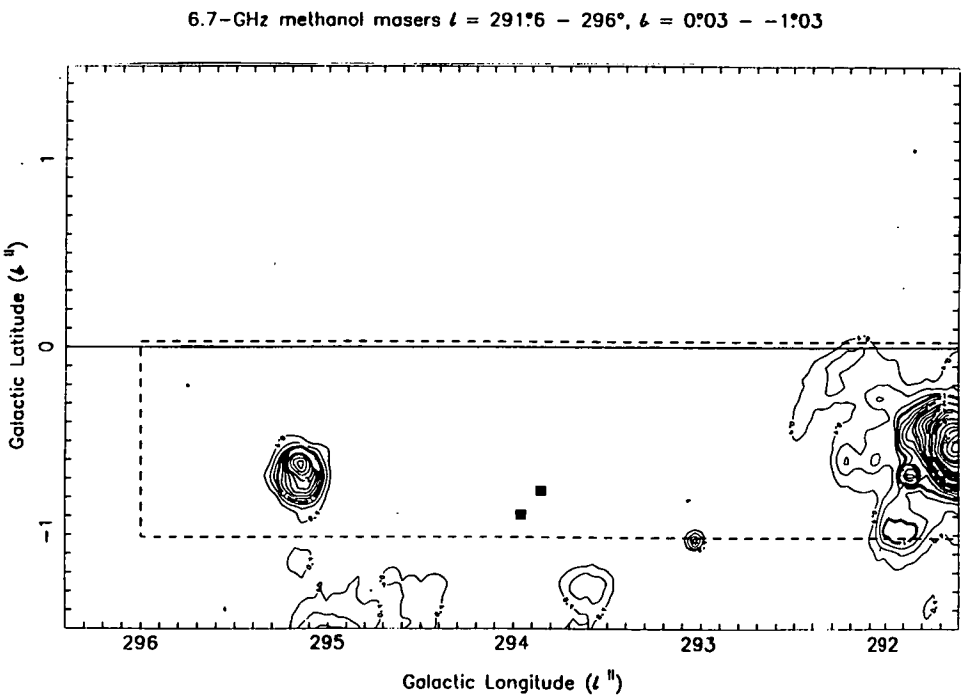

Figure 5.7: 5-GHz continuum emission l = 291°.6 – 296°.4, b = -1°.5 – 1°.5 (Haynes *et al.*, 1978). The positions of the 6.7-GHz CH_3OH masers are marked with filled squares and the dashed line marks the region covered by the Mt Pleasant survey.

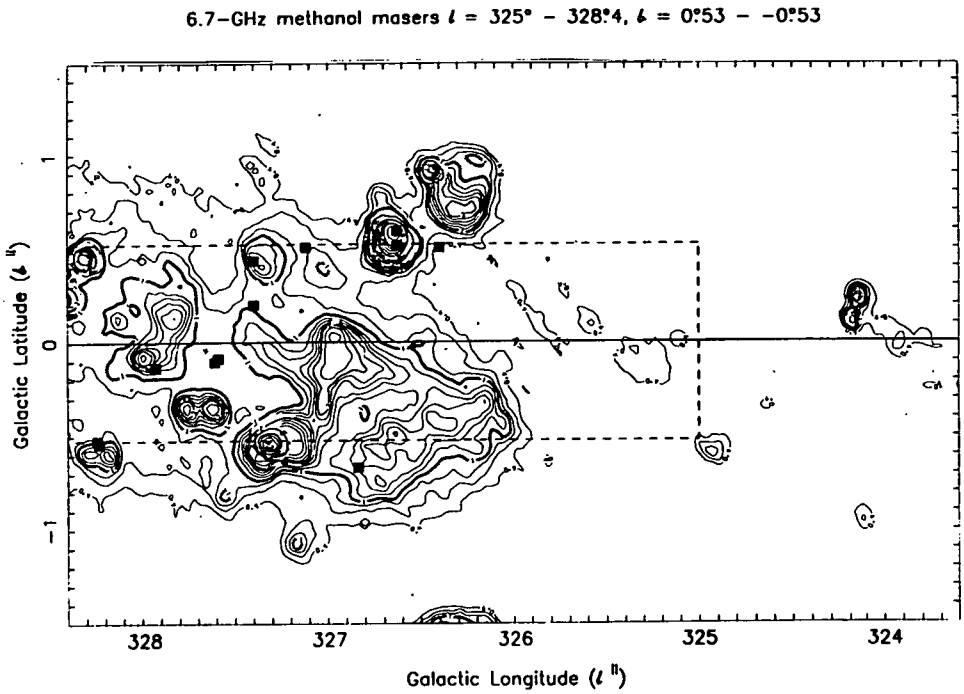

Figure 5.8: 5-GHz continuum emission l = 323°.6 – 328°.4, b = -1°.5 – 1°.5 (Haynes *et al.*, 1978). The positions of the 6.7-GHz CH_3OH masers are marked with filled squares and the dashed line marks the region covered by the Mt Pleasant survey.

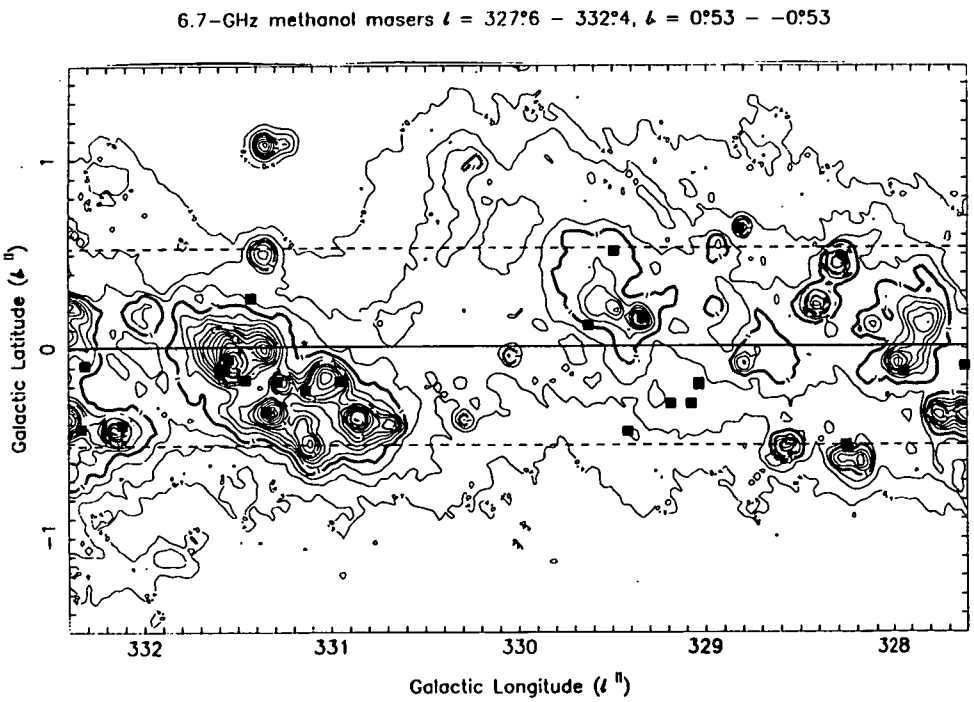

Figure 5.9: 5-GHz continuum emission l = 328°.6 – 332°.4, b = -1°.5 – 1°.5 (Haynes *et al.*, 1978). The positions of the 6.7-GHz CH_3OH masers are marked with filled squares and the dashed line marks the region covered by the Mt Pleasant survey.

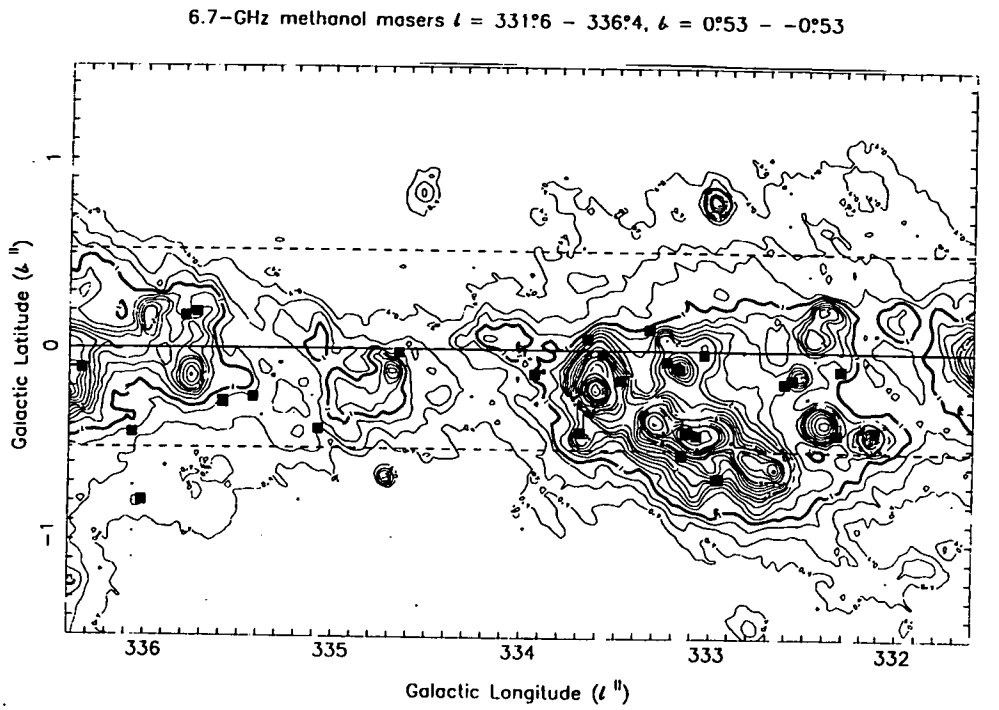

Figure 5.10: 5-GHz continuum emission $l = 331.^{\circ}6 - 336.^{\circ}4$, $b = -1.^{\circ}5 - 1.^{\circ}5$ (Haynes *et al.*, 1978). The positions of the 6.7-GHz CH_3OH masers are marked with filled squares and the dashed line marks the region covered by the Mt Pleasant survey.

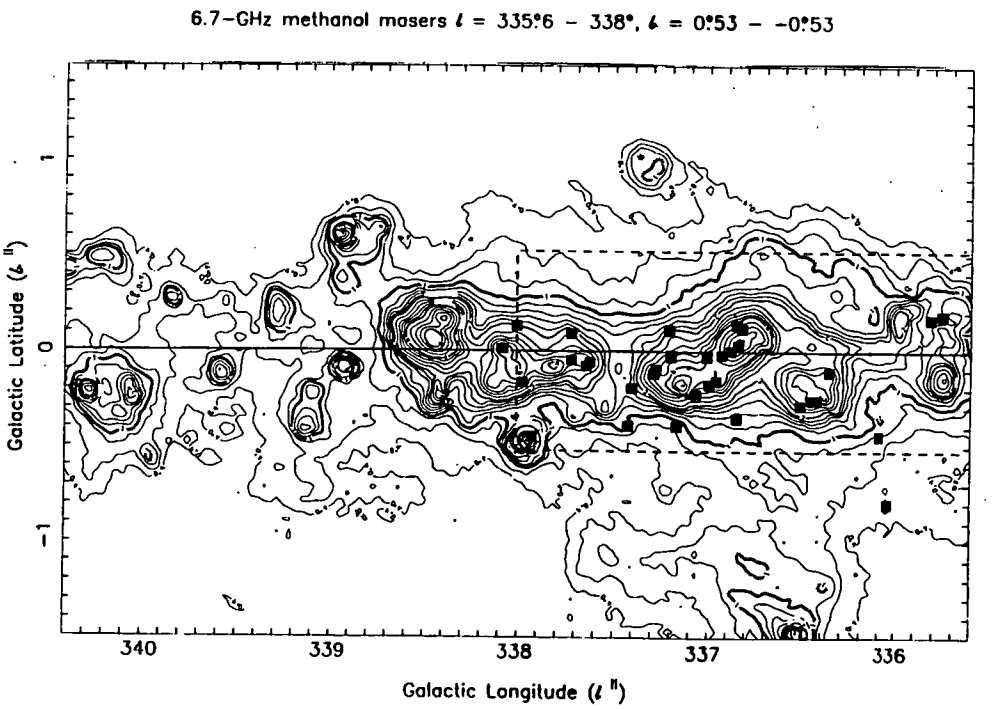

Figure 5.11: 5-GHz continuum emission $l = 335.^{\circ}6 - 340.^{\circ}4$, $b = -1.^{\circ}5 - 1.^{\circ}5$ (Haynes *et al.*, 1978). The positions of the 6.7-GHz CH_3OH masers are marked with filled squares and the dashed line marks the region covered by the Mt Pleasant survey.

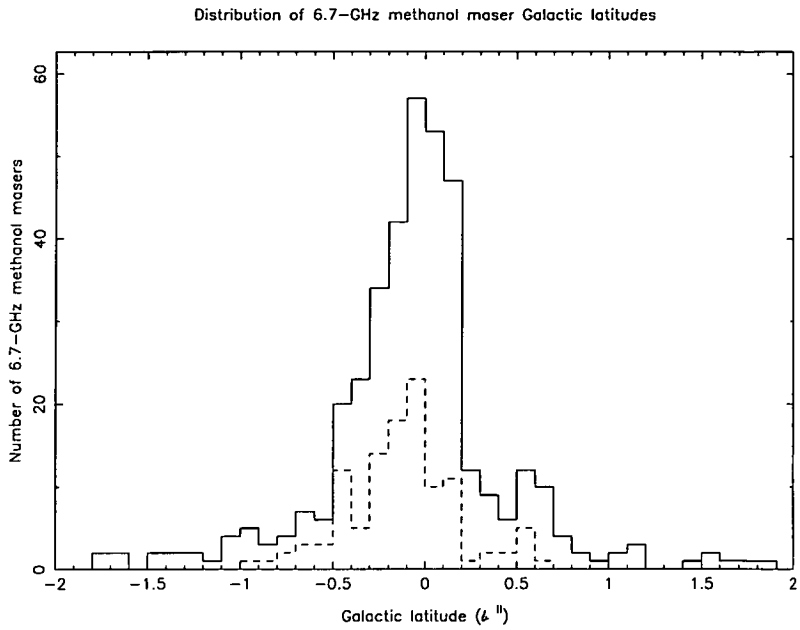

Figure 5.12: The Galactic latitude distribution of 6.7-GHz CH_3OH masers (solid line). The dashed line shows the distribution for 6.7-GHz CH_3OH masers detected in the Mt Pleasant survey.

5.4 Discussion

The Mt Pleasant survey has more than doubled the number of 6.7-GHz CH_3OH masers detected in the region surveyed (see Table 5.1). Excluding the regions I have surveyed there are $\approx$ 280 known 6.7-GHz CH_3OH masers in the Galaxy. If the results of my survey apply to the entire Galactic Plane, then there are at least 650 detectable masers of the 5_1-6_0 A^+ transition of CH_3OH.

I have combined the results from the eight published 6.7-GHz CH_3OH maser surveys, (Caswell, 1996; Caswell *et al.*, 1995c; Menten, 1991a; MacLeod and Gaylard, 1992; MacLeod *et al.*, 1992; MacLeod *et al.*, 1993a; Schutte *et al.*, 1993; van der Walt *et al.*, 1995) with those from my survey in order to examine their distribution within the Galaxy. Fig. 5.12 shows that the Galactic latitude distribution is peaked strongly at the Galactic equator. This is not simply a reflection of the distribution of the objects towards which most of the masers have been detected (OH masers and *IRAS* sources), as a similar plot for my survey regions only, shows the number of masers decreasing rapidly with increasing $|b|$ within the $|b| \lesssim 0.^\circ5$ range covered by this survey. The distribution also shows a distinct asymmetry, with the rate at which the number of masers declines being much smaller for negative latitudes. A possible contributing factor to this is that there appears to be a warp in the Galactic disc around $l \approx 330°$, a region containing many 6.7-GHz CH_3OH masers. The tendency to negative latitudes in that region can clearly be seen in Fig. 5.14.

Fig. 5.13 shows the distribution of 6.7-GHz CH_3OH masers with Galactic longitude. The peak between longitudes -20° and -30° (330° – 340°) corresponds to

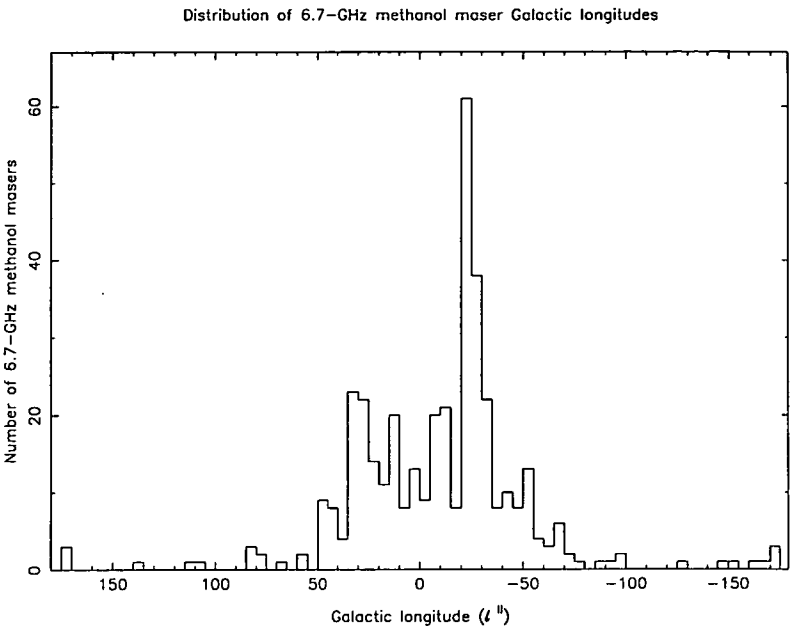

Figure 5.13: The Galactic longitude distribution of 6.7-GHz CH_3OH masers.

the region covered by the Mt Pleasant survey and the ATCA survey of Caswell (1996). Aside from that peak the distribution is relatively flat for $|l| \leq 35°$, suggesting that blind surveys in that region are likely to detect many new 6.7-GHz CH_3OH masers. The distribution of 6.7-GHz CH_3OH masers in the inner region of the Galaxy is perhaps best shown by Fig. 5.14. The dashed boxes show two of the regions covered by the Mt Pleasant survey. There is a high density of known masers on the positive longitude side of both survey regions and it will be interesting to see if a similar number of new masers are detected in these highly populated regions. Fig 5.14 also shows a large number of masers outside the latitude range of the Mt Pleasant survey, particularly at negative latitudes. This suggests that an extension of the latitude range of the survey may discover a reasonable number of new masers.

Previous searches for 6.7-GHz CH_3OH masers have not detected any which are known to be associated with objects other than sites of massive star formation, presumably because of the selection criteria in previous searches. Many of the sources detected in this survey are not associated with *IRAS* or radio continuum sources, and so I have no information on whether these are associated with star formation regions or with some other type of object. There are two possible explanations as to the nature of these 6.7 GHz CH_3OH masers :

1. They are associated with UCHII regions which for some reason have not previously been detected.

2. They are associated with some other class of object.

If the first explanation is correct then it has significant implications for the number of UCHII regions in the Galaxy and their lifetime (see Section 5.4.3). It

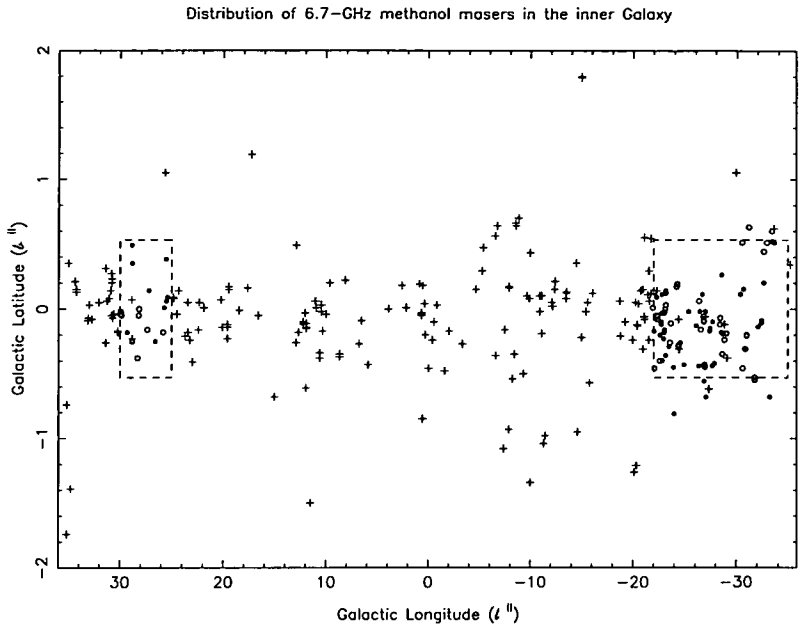

Figure 5.14: The distribution of 6.7-GHz CH_3OH masers in the inner regions of the Galaxy. The crosses, filled and open circles mark the positions of 6.7-GHz CH_3OH masers. The filled circles are 6.7-GHz CH_3OH masers discovered in the Mt Pleasant survey and the open circles the known masers which were detected. The dashed boxes represent two of the regions covered by the Mt Pleasant survey.

also implies that a large percentage of UCHII regions do not have counterparts in the *IRAS* Point-Source Catalog (this is discussed in detail in Section 5.4.1).

The second explanation implies maser emission associated with a class of object which has no known maser emission from any other molecular transition. I used the Simbad database to search for all sources within a 3-arcmin radius of the 6.7-GHz CH_3OH masers detected in this survey, but found no convincing associations with other classes of object. Unfortunately the search for associations was hampered by the relatively poor positional accuracy of the 6.7-GHz CH_3OH masers. If some of the newly detected 6.7-GHz CH_3OH masers are associated with a class of object other than UCHII regions then they might be expected to exhibit different characteristics in some of their observed properties. There are three differences between the UCHII region 6.7-GHz CH_3OH masers and the unassociated masers, no association with *IRAS* sources, no known OH maser emission and they typically have a weaker peak flux density. However, the non-association with an *IRAS* source may be due to confusion of the *IRAS* PSC in the Galactic Plane. Also, there may be OH masers associated with the unassociated 6.7-GHz methanol masers, which were below the detection threshold of the Parkes survey. The generally low peak flux density of the 6.7-GHz CH_3OH masers is also consistent with this argument, as they are typically an order of magnitude stronger than any OH counterparts.

At present the nature of the unassociated 6.7-GHz CH_3OH masers is unclear, but both the possibilities outlined above promise interesting astrophysical returns. The resolution of this question requires further observations toward the

new maser detections in other regions of the electromagnetic spectrum, including high-resolution radio, millimeter and infrared imaging and searches for other maser and thermal transitions.

5.4.1 Associations with *IRAS* sources

5.4.1.1 *IRAS* colours

The ground work for the use of *IRAS* colours to determine likely sites of UCHII regions was performed by Chini *et al.* (1986a; 1986b). They observed the far-infrared spectra of a dozen well known star formation regions and found that they all were very similar in shape. The release of the *IRAS* Point-Source Catalog (1985) provided information in four far-infrared wavebands for a very large number of sources. By examining the *IRAS* colours of known UCHII regions Wood and Churchwell (1989a) and Hughes and MacLeod (1989) independently developed similar colour-based criteria for selecting *IRAS* sources which had a high probability of being UCHII. The selection criteria of Wood and Churchwell and Hughes and MacLeod are discussed in detail in section 5.4.1.3.

5.4.1.2 When is a maser associated with an *IRAS* source?

The question of where to draw the line between an *IRAS* source being associated with a maser and not, is unfortunately rather complex. Although *IRAS*-based selection criteria have successfully been used to detect ultra-compact HII regions and CH_3OH masers, the large beamwidth of *IRAS*, and the high degree of confusion in Galactic fields, means that an *IRAS* beam will typically contain several stars in various stages of formation. This is supported by the fact that at high resolution, many strong 6.7-GHz CH_3OH masers which cover a wide velocity range are found to be two or more sources with separations between a few and a few tens of arcsec (Caswell, 1996; Ellingsen *et al.*, 1996a; Phillips *et al.*, 1996). Each of these 6.7-GHz CH_3OH maser sources is probably associated with a separate UCHII region, but all are covered by one entry in the *IRAS* Point-Source Catalog. Therefore it appears that a more accurate description of the *IRAS*-based selection criteria is that they select active star formation regions containing UCHII regions.

Masers are often detected significantly offset from the positions of the *IRAS* sources, but an association between the two objects is still asserted. A good example of this is the *IRAS* source 14567-5846 toward which OH and 12.2-GHz CH_3OH masers were detected (Cohen *et al.*, 1988a; Kemball *et al.*, 1988). However, the position determined for the masers is consistent with that determined for the OH maser 318.95-0.20 by Caswell & Haynes (1987), which is separated by 2 arcmin from the *IRAS* position. At an assumed distance of 2 kpc, that corresponds to a separation of more than 10 pc. High resolution observations using the ATCA detected radio continuum emission coincident with the *IRAS* position, but the 6.7-GHz CH_3OH masers, like the OH masers are 2 arcmin away (see section 6.3.1). In terms of single dish searches for masers, this "non-association" is not particularly important as a maser is still detected, but it lends further weight to the argument that the *IRAS*-based criteria selected star formation regions, rather than

individual UCHII regions. A more serious problem, however, is the use of doubtful associations to derive far-infrared properties of maser sources and correlations with maser properties. For example WGM suggest that *IRAS* sources separated from 6.7-GHz CH_3OH masers by up to 3.5 arcmin are counterparts, and then use these "associations" to try to constrain far-infrared radiative pumping schemes.

5.4.1.3 Comparison of *IRAS* based search techniques

The rms pointing accuracy of the Mt Pleasant telescope has been measured to be approximately 0.7 arcmin, which is not as good as the positional accuracy of the *IRAS* Point-Source Catalog. Taking this into consideration I decided to call all *IRAS* sources within 1 arcmin of a 6.7-GHz CH_3OH maser "associated" and those with separations between 1 and 2 arcmin "possibly associated". Given the accuracy to which I have determined the positions of the 6.7-GHz CH_3OH masers, a few will undoubtedly be incorrectly categorized, but this is unlikely to have a significant effect on the comparison between the various *IRAS*-based selection criteria.

The Mt Pleasant survey detected 108 6.7-GHz CH_3OH masers, of which only 49 have an *IRAS* source within 1 arcmin. The details of these *IRAS* sources are summarized in Table 5.3. The following discussion is confined to those sources which lie within the spatial boundaries of the survey region. However, I include those sources in this region which have velocities outside the range surveyed. Where I have calculated the fraction of *IRAS* sources with an associated 6.7-GHz CH_3OH maser, that figure applies to searches with a sensitivity limit comparable to this survey and is a lower limit for more sensitive searches.

To assess the various *IRAS*-based selection methods more rigorously, I compared the *IRAS* sources associated with 6.7-GHz CH_3OH masers with all *IRAS* sources contained within the survey region. I detected 98 6.7-GHz CH_3OH masers within the survey region, of which 44 are within 1 arcmin of an *IRAS* source. There are only 42 corresponding *IRAS* sources, as two sources have two centres of maser emission within 1 arcmin of the *IRAS* position. There are a further 21 6.7-GHz CH_3OH masers separated by between 1 and 2 arcmin from an *IRAS* source. Many of these *IRAS* sources have colours typical of ultra-compact HII regions, and a search toward the *IRAS* position with the 7-arcmin beam of the Hobart telescope would have detected a maser source. For the purposes of my analysis I will assume that all maser sources 2 arcmin or more from an *IRAS* source are unassociated. For the ranges listed below, the lower limit has been calculated using only the maser sources within 1 arcmin, and the upper limit with all sources < 2 arcmin from an *IRAS* source. A search of the *IRAS* Point-Source Catalog (1985) found 2195 sources contained in the survey region. If I assume a uniform distribution of *IRAS* sources within the survey region, then there is a 6.7% probability of any 6.7-GHz CH_3OH maser being within 1 arcmin of an *IRAS* source. Thus, for my sample of 98 6.7-GHz CH_3OH masers I would expect ≈ 7 chance associations with *IRAS* sources.

Fig. 5.15 shows a plot of 60/12 μm versus 25/12 μm colours for all 2195 *IRAS* sources in my survey region. Those associated with 6.7-GHz CH_3OH masers are

Table 5.3: *IRAS* sources associated with 6.7-GHz CH_3OH masers. Those which fall outside the completely surveyed region are marked with an asterisk.

Methanol Maser (l,b)	*IRAS* Name	Flux 12 μm (Jy)	25 μm (Jy)	60 μm (Jy)	100 μm (Jy)	$\mathrm{Log_{10}(S_{25}/S_{12})}$	$\mathrm{Log_{10}(S_{60}/S_{12})}$
25.41+0.09	18345-0641	3.5	17.5	109.9	567.2	0.70	1.50
27.36−0.16	18391-0504	97.7	69.8	383.9	1633.0	-0.15	0.59
28.20−0.05	18403-0417	21.8	177.7	1574.0	3937.0	0.91	1.86
28.30−0.38	18416-0420	91.3	821.0	3374.0	4358.0	0.95	1.57
28.83−0.25	18421-0348	5.6	60.8	713.0	1877.0	1.04	2.11
29.94−0.02	18434-0242	217.5	1697.0	7501.0	11670.0	0.89	1.54
29.95−0.02	18434-0242	217.5	1697.0	7501.0	11670.0	0.89	1.54
293.95−0.91	11304-6206	7.9	95.4	594.7	1094.0	1.08	1.88
327.12+0.51	15437-5343	6.0	74.7	987.7	1425.0	1.10	2.22
327.40+0.44	15454-5335	3.9	55.9	1153.0	2697.0	1.15	2.47
327.40+0.20	15464-5348	1.6	9.5	109.3	396.6	0.77	1.83
328.25−0.53*	15541-5349	12.0	110.7	3033.0	6415.0	0.96	2.40
328.81+0.63*	15520-5234	15.5	537.9	10780.0	16380.0	1.54	2.84
329.03−0.21	15566-5304	6.3	4.1	331.8	1652.0	-0.18	1.72
329.07−0.31	15573-5307	3.1	17.0	124.0	1145.0	0.74	1.60
329.33+0.16	15567-5236	195.8	1077.0	7398.0	8360.0	0.74	1.58
329.41−0.46	15596-5301	4.8	51.6	1102.0	2487.0	1.03	2.36
331.28−0.19	16076-5134	36.0	237.3	2823.0	5930.0	0.82	1.89
331.34−0.35	16085-5138	41.3	284.6	2262.0	4841.0	0.84	1.74
331.42+0.26	16062-5108	2.5	2.1	22.3	239.7	-0.07	0.95
331.45−0.18	16084-5127	1.7	9.0	178.7	224.5	0.73	2.03
331.56−0.12	16086-5119	15.1	161.1	1229.0	25800.0	1.03	1.91
332.11−0.42	16124-5110	118.8	290.1	6234.0	8651.0	0.39	1.72
332.31−0.10	16119-5048	10.6	107.5	925.9	2605.0	1.01	1.94
332.95−0.68*	16175-5046	5.5	26.1	539.4	2194.0	0.68	1.99
332.96−0.68*	16175-5045	6.9	30.7	562.1	1820.0	0.65	1.91
333.12−0.43	16172-5028	144.0	1514.0	12380.0	26700.0	1.02	1.93
333.13−0.44	16172-5028	144.0	1514.0	12380.0	26700.0	1.02	1.93
333.16−0.10	16159-5012	4.3	41.3	816.6	3569.0	0.99	2.28
333.33+0.11	16157-4957	4.5	38.8	256.2	3691.0	0.93	1.75
333.47−0.17	16175-5002	10.5	77.0	1135.0	3210.0	0.87	2.04
333.69−0.44	16196-5005	3.4	21.8	305.7	1120.0	0.81	1.96
333.95−0.14	16194-4941	9.2	19.8	207.3	554.8	0.33	1.35
334.65−0.02	16220-4906	3.7	3.0	76.1	304.0	-0.10	1.31
335.59−0.29	16272-4837	5.0	21.9	676.4	1958.0	0.64	2.13
336.02−0.81*	16313-4840	23.9	167.3	1029.0	2219.0	0.85	1.63
336.36−0.14	16297-4757	32.2	206.9	1582.0	3421.0	0.81	1.69
336.43−0.26	16306-4758	15.6	68.0	2288.0	5832.0	0.64	2.17
336.83−0.36	16327-4746	4.1	18.0	128.8	600.7	0.64	1.50
336.99−0.03	16318-4724	5.8	69.7	2007.0	5212.0	1.08	2.54
336.99−0.18	16325-4731	22.8	94.7	1423.0	1571.0	0.62	1.79
337.05−0.23	16329-4730	4.3	10.0	1423.0	9930.0	0.37	2.52
337.15−0.40	16340-4732	1.8	8.5	33.8	438.9	0.68	1.28
337.17−0.04	16326-4718	8.7	38.4	1099.0	4577.0	0.64	2.10
337.39−0.20	16341-4714	6.9	35.1	49.3	942.0	0.71	0.85
337.41−0.40	16351-4722	8.4	133.5	3693.0	8677.0	1.20	2.64
337.61−0.06	16344-4658	7.1	46.7	1130.0	4034.0	0.82	2.20
337.71−0.05	16348-4654	7.4	45.2	843.0	4034.0	0.79	2.06
337.92−0.46	16374-4701	191.9	1768.0	13310.0	24770.0	0.96	1.84

marked with a filled circle. Thirty-three of the sources associated with masers lie in the upper right corner of this colour–colour diagram. Wood and Churchwell (1989a) have shown that there is a high probability that the sources in this area of the colour–colour diagram are UCHII regions. In total there are 267 *IRAS* sources in my sample which satisfy the criteria of $Log_{10}(S_{60}/S_{12}) \geq 1.30$ & $Log_{10}(S_{25}/S_{12}) \geq 0.57$ (the solid lines in Fig. 5.15). I will call these criteria the Wood & Churchwell minus (WC-) criteria (as they are less stringent than the full Wood and Churchwell criteria). For each flux density measurement the *IRAS* catalog contains a quality flag in each wavelength band. Having selected sources according to the WC- criteria, Wood and Churchwell then excluded those for which either the 25- or 60-μm flux density measurement is only an upper limit, as they are most likely to be situated lower and further left in the colour–colour diagram than their current position. I call these criteria the WC criteria.

Assuming that the *IRAS* sources selected using WC- are uniformly distributed throughout the survey region, the probability of detecting a 6.7-GHz CH_3OH maser within 1 arcmin is 0.8%. Thus, for my sample of 98 6.7-GHz CH_3OH masers, I would expect ≈ 1 chance association with an *IRAS* source in the Wood and Churchwell region of the colour–colour diagram. Of the 267 sources which satisfy the WC- criteria, 33 are within 1 arcmin and 42 within 2 arcmin of a 6.7-GHz CH_3OH maser. If I assume that there are no chance associations, then this implies that any search based on these criteria will detect 6.7-GHz CH_3OH masers associated with 12–16% of the selected *IRAS* sources.

If I apply the WC criteria, I am left with 151 sources, 26 of which are within 1 arcmin and 30 within 2 arcmin of a 6.7-GHz CH_3OH maser source. If I again assume no chance associations, this implies that 17–20% of the *IRAS* sources selected using these criteria will have an associated 6.7-GHz CH_3OH maser.

There are two published searches for 6.7-GHz CH_3OH masers toward *IRAS* sources (SWGM,WGM). The first of these by SWGM used selection criteria based on that of Wood and Churchwell (1989a), but with varying lower limits on the 60- and 100-μm flux densities. If I apply their selection criteria to my sample I find 51 sources which satisfy their criteria, 15 of which are within 1 arcmin and 19 within 2 arcmin of a 6.7-GHz CH_3OH maser. Thus, for a sample of *IRAS* sources selected using SWGM's criteria, I would expect 29–37% to have an associated 6.7-GHz CH_3OH maser. The other sources which lie inside the Wood & Churchwell UCHII region of the colour–colour diagram fail one or more of the flux density or flux quality criteria. The distribution of the Galactic latitudes at which SWGM and WGM detected new 6.7-GHz CH_3OH masers is relatively flat for $|b| \lesssim 1.0°$. This implies that *IRAS* colour-based selection criteria may be the most practical for finding sources which are not close to the Galactic Plane.

Hughes and MacLeod (1989) developed an independent method of identifying HII regions on the basis of their *IRAS* colours, which they claim has a confidence level of 89%. Their criteria were that $Log_{10}(S_{25}/S_{12}) \geq 0.40$, $Log_{10}(S_{60}/S_{25}) \geq 0.25$, $S_{100} \geq 80$ Jy and that the flux quality flag for the 25-, 60- and 100-μm bands was not an upper limit. I call these criteria the HM criteria. Of the 2195 *IRAS* sources in the survey region, 137 meet the HM criteria ; 18 of these 137 *IRAS* sources are within 1 arcmin and 23 within 2 arcmin of a 6.7-GHz CH_3OH maser.

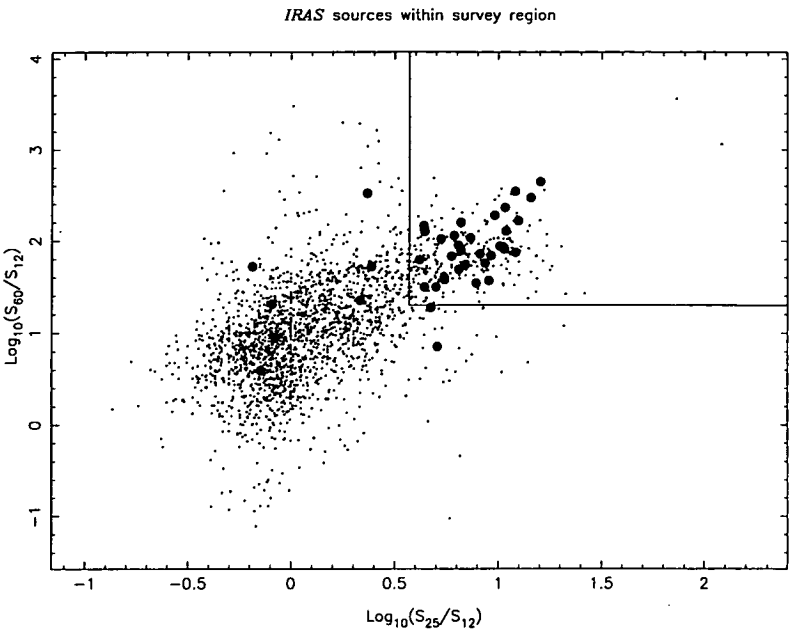

Figure 5.15: Distribution of 60/12 versus 25/12 μm colours for all *IRAS* sources in the region covered by the Mt Pleasant 6.7-GHz CH_3OH maser survey. The sources with a 6.7-GHz CH_3OH maser within 1 arcmin are marked with a filled circle. The box represents the criteria developed by Wood and Churchwell (1989a) to select *IRAS* sources which had a high probability of being UCHII regions.

If I assume that there are no chance associations, this implies that 13–17% of the *IRAS* sources selected using the HM criteria will have an associated 6.7-GHz CH_3OH maser.

1928 *IRAS* sources are outside the UCHII region of the colour-colour diagram. Of these 9 are within 1 arcmin of a 6.7-GHz CH_3OH maser (compared to the 7 or so expected by chance alone). Therefore $< 0.5\%$ of *IRAS* sources in this region of the colour–colour diagram have an associated 6.7-GHz CH_3OH maser.

On the basis of their *IRAS* colours Palla *et al.* (1991) conducted a search for H_2O masers toward a selection of *IRAS* sources, identified as candidate UCHII regions or dense molecular clouds. They separated their detections into two groups, those which satisfied the WC criteria and those which did not. This latter group they labeled "low". Although the 9 *IRAS* sources with associated 6.7-GHz CH_3OH masers which fail the WC criteria occupy a similar region of the colour–colour diagram to the "low" sample of Palla *et al.* (1991), they differ in other ways. In particular, Palla *et al.* found that the masers associated with *IRAS* sources outside the Wood and Churchwell region of the colour–colour diagram were in general weaker than those inside. In contrast, I find that both the median and mean of the peak flux densities is greater for those sources outside the Wood and Churchwell region than those inside. However, the outside sample is small and the mean in particular is dominated by the flux of 329.03-0.21. I have shown above that I expect ≈ 7 chance associations of 6.7-GHz CH_3OH masers with *IRAS* sources within 1 arcmin, and there is a 48% probability of 7 or more chance associations from 98 sources. I therefore consider it likely that these associations are due to

Table 5.4: Distribution of 100-μm flux density for *IRAS* sources in within the survey region which have a moderate or higher flux quality in that *IRAS* waveband.

$Log_{10}(S100_{\mu m})$	Number of *IRAS* sources	Number of 6.7-GHz CH_3OH masers
1.0–1.5	23	0
1.5–2.0	53	0
2.0–2.5	154	1
2.5–3.0	103	2
3.0–3.5	55	9
3.5–4.0	22	10
4.0–4.5	11	4
4.5–5.0	1	0

chance, although further observations are required to confirm this.

Fig. 5.16 and Table 5.4 compare the distribution of 100-μm flux density (excluding those sources which have only an upper limit for the 100-μm flux density) of the *IRAS* sources with associated 6.7-GHz CH_3OH masers, with that of all *IRAS* sources in the region. The probability of maser association clearly increases rapidly with increasing 100-μm flux density. In the survey region 333 *IRAS* sources have a 100-μm flux density of < 1000 Jy, of which 3 are within 1 arcmin and 6 within 2 arcmin of a 6.7-GHz CH_3OH maser. By comparison, of the 89 *IRAS* sources with a 100-μm flux > 1000 Jy, 23 are within 1 arcmin and 29 within 2 arcmin of a 6.7-GHz CH_3OH maser. This implies that the probability of detecting a 6.7-GHz CH_3OH maser associated with an *IRAS* source is $\approx$ 1–2% if the source has a 100-μm flux < 1000 Jy, but 26–33% if the source has a 100-μm flux density $>$ 1000 Jy. There is quite a large degree of overlap between the WC- sample and the sample of sources with a 100-μm flux density > 1000 Jy. Taking the union of the two samples yields 35 *IRAS* sources within 1 arcmin, and 45 within 2 arcmin of a 6.7-GHz CH_3OH maser, from a sample 286 *IRAS* sources. Thus there is a 12–16% probability that an *IRAS* source, selected using these criteria, is associated with a 6.7-GHz CH_3OH maser.

5.4.2 Efficiency of *IRAS*–based searches

Some of the searches towards sources selected from the *IRAS* Point-Source Catalog (1985) detected 6.7-GHz CH_3OH masers associated with a large fraction of those sources. On the other hand, this does not necessarily imply that they detected a large fraction of the maser sources within a given region. This survey represents the first opportunity to examine the overall efficiency of the various *IRAS* search techniques, as I am able to determine the fraction of 6.7-GHz CH_3OH maser sources which would be detected by any particular search method. Of the 98 6.7-GHz CH_3OH masers in the region I have surveyed, 24 have no *IRAS* counterpart within 2 arcmin of the *IRAS* position. I have indicated above that I expect $\approx$ 7 chance positional associations between *IRAS* sources and my sample of 6.7-GHz

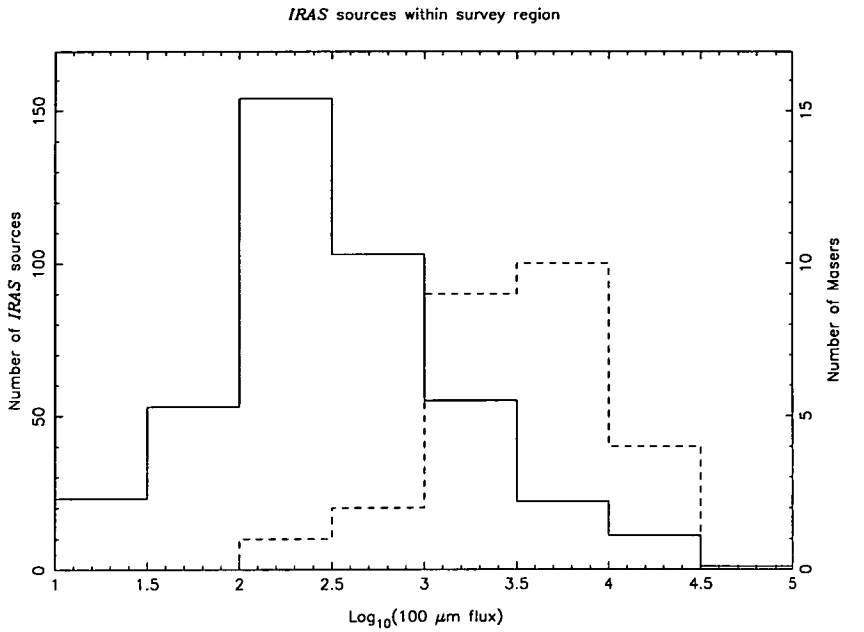

Figure 5.16: The solid line shows the distribution of 100-μm flux for *IRAS* sources in the survey region, with a moderate or higher flux quality. The dashed-line shows the distribution of the sources with 6.7-GHz CH_3OH masers within 1 arcmin, with the vertical scale multiplied by 10.

CH_3OH masers. In general these chance associations cannot be detected by any criteria which exclude most of the *IRAS* sources. This implies that any *IRAS*-based selection criteria will not detect more than about 68% of the CH_3OH masers in any given region. Four of the *IRAS* sources (15566-5304, 16172-5012, 16306-5028 & 16344-4658) are within 2 arcmin of two, and one (18434-0242) is within 2 arcmin of three 6.7-GHz CH_3OH masers. This means that the number of 6.7-GHz masers detected by any given *IRAS* selection criterion which includes any of these sources, will be slightly greater than the number of *IRAS* sources with an associated 6.7-GHz CH_3OH maser.

The WC- criteria detect 35–47 (36–48%) of the 98 6.7-GHz CH_3OH masers in the survey region, whereas the WC criteria detect only 28–34 (28–34%). The SWGM criteria yield the largest fraction of *IRAS* sources with an associated 6.7-GHz CH_3OH maser, but still detect only 17–22 (17–22%) of the maser sources within the region. Interestingly the HM criteria yielded results significantly worse than the WC criteria, detecting less of the 6.7-GHz CH_3OH masers 20–26 (20–27%) and selecting a lower percentage of *IRAS* sources with an associated maser. The two selection criteria cover similar areas of the colour-colour diagram, but the HM criteria were developed using an optically selected sample of HII regions, while the WC criteria were developed using a radio selected sample of HII regions. It is generally accepted that HII regions which are visible at optical wavelengths are at a later evolutionary stage than those which are only visible at radio and FIR wavelengths. This suggests that by the time an HII region becomes optically visible 6.7-GHz CH_3OH maser emission has often ceased. If the selection criterion that the 100-μm flux density of the *IRAS* source should exceed 1000 Jy is adopted then

Table 5.5: A summary of the efficiency of several *IRAS*-based selection criteria. Note : the lower range is for 6.7-GHz CH_3OH masers within 1 arcmin of an *IRAS* source, and the upper for masers less than 2 arcmin from an *IRAS* source.

IRAS selection method	No. of *IRAS* candidates	No. of methanol sources found	Fraction of *IRAS* sources yielding a detection	Fraction of the 41 known masers detected
WC-	267	35–47	12–16%	36–48%
WC	151	28–34	17–20%	28–34%
SWGM	51	17–22	29–37%	17–22%
HM	137	20–26	13–17%	20–27%
$S_{100} \geq 1000$ Jy	89	25–33	26–33%	26–34%
Union of WC- and $S_{100} \geq 1000$ Jy	286	37–51	12–16%	38–52%

25–33 (26–34%) of the 6.7-GHz CH_3OH masers in the region are detected. The final selection criteria I evaluated were the union of the 100-μm and WC- criteria. A search for 6.7-GHz CH_3OH masers towards this sample of *IRAS* sources would detect 37–51 (38–52%) of the masers in the region.

The efficiency of the various *IRAS*-based searching methods, both in terms of the fraction of *IRAS* sources with an associated 6.7-GHz CH_3OH maser and the fraction of masers detected, is summarized in Table 5.5. It is clear that for the various *IRAS* selection criteria there is a compromise between the fraction of *IRAS* sources with associated 6.7-GHz CH_3OH masers and the fraction of the total masers which are detected. Our analysis shows that searching toward *IRAS* sources with a 100-μm flux density greater than 1000 Jy is more efficient than the WC criteria in terms of the fraction of *IRAS* sources associated with 6.7-GHz CH_3OH masers, and detects a similar fraction of 6.7-GHz CH_3OH masers. A possible explanation for this is that because ultra-compact HII regions are some of the brightest objects in the *IRAS* Point-Source Catalog and their flux density peaks near 100 μm, many *IRAS* sources with a large 100-μm flux density are likely to be UCHII regions. The WC criteria are likely to select a larger fraction of all UCHII regions in the Galaxy, as they are based upon spectral properties which do not change with distance. This means that the WC criteria are likely to detect a larger fraction of the 6.7-GHz CH_3OH masers. However, as the survey is flux density limited we are less sensitive to more distant masers and hence may detect only a marginally larger fraction of the CH_3OH masers using the WC criteria than by using the 100-μm criterion.

The comparison of the efficiency of various *IRAS*-based search criteria for 6.7-GHz CH_3OH masers shows that the SWGM criteria are the most efficient in terms of the percentage of the selected *IRAS* sources which have an associated maser. However, the union of the WC- and 100-μm flux density > 1000 Jy detects the greatest percentage of all the 6.7-GHz CH_3OH masers in the region. My analysis shows that most of the *IRAS*-based criteria will fail to detect more than 60% of the 6.7-GHz CH_3OH masers and the best will fail to detect $\approx 50\%$.

5.4.3 Implications of the number of UCHII regions in the Galaxy

This survey has shown that a significant fraction of 6.7-GHz CH_3OH masers cannot be detected using any *IRAS*-based selection criterion. Whether these masers are associated with UCHII regions has yet to be determined. If they are, they may provide a method of estimating the total number of UCHII regions in the Galaxy. Wood and Churchwell (1989a) found 1646 Galactic *IRAS* sources which satisfied the criteria $Log_{10}(S_{60}/S_{12}) \geq 1.30$ & $Log_{10}(S_{25}/S_{12}) \geq 0.57$ and had moderate or better quality flux density measurements at 25 and 60 μm. They argue that the majority of these sources are UCHII regions. Of the 98 6.7-GHz CH_3OH masers in the region I surveyed completely, 34 at most are associated with *IRAS* sources which meet these criteria. If I assume that all 6.7-GHz CH_3OH masers are associated with UCHII regions, then this implies that the number of UCHII regions in the Galaxy is approximately a factor of 3 greater than that estimated by Wood and Churchwell. This suggests that either the current rate of massive star formation within the Galaxy has been significantly underestimated, or the lifetime of the ultra-compact phase of HII regions is longer than previously thought. The currently accepted lifetime of the ultra-compact phase already provides problems for models of the evolution of HII regions (see Section 2.2) and increasing this by a factor of 3 would require further revision of these models.

High-resolution continuum observations have failed to detect radio continuum emission associated with several 6.7-GHz CH_3OH masers (see Section 6.3) which may indicate that some masers are not associated with OB star formation (and hence UCHII regions). Our observations are consistent with an estimate of $\approx$ 5000 UCHII regions in the Galaxy, although the true number may be less, depending on the validity of the assumptions above.

5.4.4 The luminosity function of 6.7-GHz methanol masers

The solid line histogram in Fig. 5.17 shows the distribution of peak flux density of the 92 6.7-GHz CH_3OH masers detected within the fully sampled spatial and velocity range of the Mt Pleasant survey. The dashed-line histogram shows the distribution of peak flux density of those sources known before the Mt Pleasant survey and shows that the majority of the sources detected in the Mt Pleasant survey have a lower peak flux density than those already known. As the masers lie close to the plane of the Galaxy, the distribution is expected to have a slope of -1, corresponding to a two-dimensional isotropic geometric distribution. The sensitivity limit of this survey falls at approximately the mid-point of the first bin of Fig. 5.17 and so only the second and higher bins can be considered in determining the slope of the flux density distribution. The dash-dot line in Fig. 5.17 is the best fit of a line of slope -1 to all bins except the first (the lowest flux density bin). The dotted line is the unconstrained line of best fit to all bins except the first. Fig. 5.17 clearly demonstrates that the peak flux density distribution of 6.7-GHz CH_3OH masers detected in the Mt Pleasant survey has a slope much less than -1. I detected two 6.7-GHz CH_3OH masers with peak flux density in the range

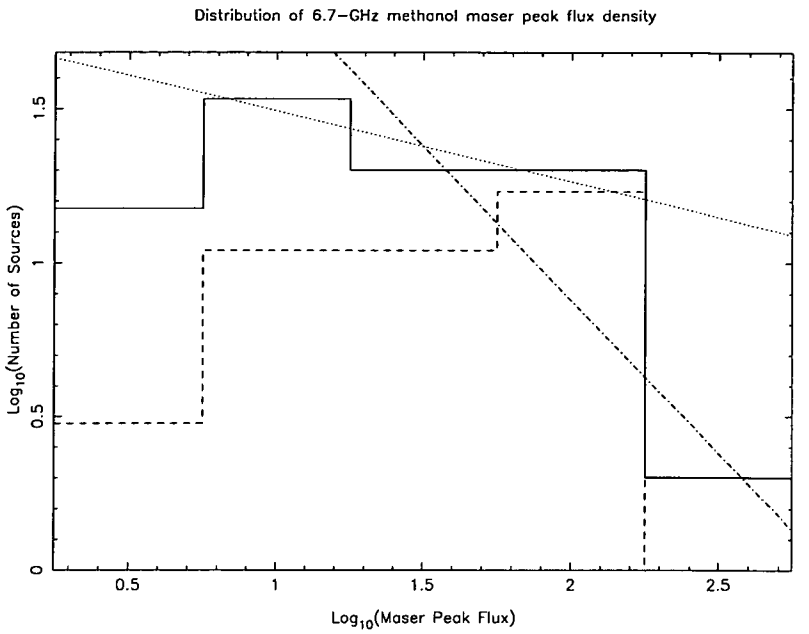

Figure 5.17: The solid line shows the distribution of 6.7-GHz CH_3OH maser peak fluxes for the Mt Pleasant survey. The dashed line shows the distribution for sources known prior to the Mt Pleasant survey. The dash-dot line shows the fit of a line of slope -1 to the four bins of the Mt Pleasant survey data between 0.75 and 2.75 and the dotted line the unconstrained line of best fit to the same data. To ensure that the four highest bins are complete, the histogram has been binned so that lower boundary for the second bin is approximately double the estimated sensitivity limit.

178–562 Jy (the last bin). A distribution with slope -1 predicts that there should be $\approx$ 60 6.7-GHz CH_3OH masers with peak flux density in the range 5.6–18 Jy (the second bin), which is double the number that were detected. Conversely, extrapolating the unconstrained line of best fit from the second bin, implies that I should have detected $\approx$ 6 masers with peak fluxes in the range 18000–56000 Jy!

A slope of -1 for a two-dimensional, isotropic geometric distribution is independent of the underlying luminosity distribution of the sources. One possible reason for the deviation of the distribution from a slope of -1 is that the sample is incomplete, but I do not believe that to be the case (see comments on 291.58-0.43 in Section 5.3.1). I suggest that the most likely reason why the 6.7-GHz CH_3OH maser peak flux density distribution does not have a slope of -1 is that the spatial distribution of the masers is not isotropic. As 6.7-GHz CH_3OH masers appear to be associated with massive star formation they would be expected approximately to follow the spiral arms of the Galaxy in a similar manner to the observed neutral hydrogen and CO distributions. As the Mt Pleasant survey has only covered a relatively small range of Galactic longitudes to date this may cause a clumping of the distribution of observed peak flux density. If this is the case then as the longitude range of the Galaxy which has been surveyed increases the distribution should approach a slope of -1.

In principal one of the interesting statistical distributions that can be derived from a blind search is the luminosity function. However, to calculate luminosity

requires both a flux density and a distance, and the second of these quantities is difficult to determine. Typically distances to masers are determined using models of Galactic rotation, but these "kinematic distances" are ambiguous, yielding two answers.

As in general it is not possible to determine easily which of the distance estimates is correct, this raises the question : is it possible to come up with a meaningful scheme which assigns sources to one or the other distance? This has been examined in detail by Caswell and Haynes (1983b), and I will outline some of the considerations. Typically the far kinematic distances are more than double the near distance so that the volume of sampled space at the far distance is more than four times that at the near distance. However as the flux density of the maser decreases with the square of the distance, similar numbers of masers should be detected at both the near and far kinematic distance. This argument is supported by the fact that assuming all the 6.7-GHz CH_3OH masers detected in the Mt Pleasant survey are at the near kinematic distance, 46% are sufficiently luminous to be detected at the far distance. The distance assignment scheme used by Caswell and Haynes (1983b) was to assume that all sources with peak flux density greater than the median were at the near distance and the others were at the far distance. This scheme will minimize the range of luminosities covered by the distribution, but they claim that it is internally self-consistent. As I was unable to find a satisfactory distance assignment scheme I have produced the luminosity function assuming that all sources are at the near kinematic distance, which is also unlikely to be accurate (see Fig. 5.18). The skewing of the peak to lower luminosities may be due to the underestimation of the luminosity of sources which are really at the far kinematic distance. In order to obtain an accurate estimate of the luminosity distribution of 6.7-GHz CH_3OH masers requires the distance to be determined toward a sample such as that presented here. Perhaps the best way to resolve the kinematic distance ambiguity is by HI absorption against the UCHII region.

5.5 Conclusion

The results of this present work highlight a number of interesting phenomena. They show that many 6.7-GHz CH_3OH masers are not associated with sources in the *IRAS* Point-Source Catalog. This may be because of the large number of sources near the Galactic Plane, which can confuse the *IRAS* flux density measurements and cause some sources to be excluded. Further investigation is required to determine if all the 6.7-GHz CH_3OH masers detected in the Mt Pleasant survey are associated with UCHII regions. If these masers are associated with UCHII regions, this will allow estimates of the number of such objects in the Galaxy (Wood and Churchwell, 1989a) to be improved. In particular the number of UCHII regions is already too high to be accounted for by current star formation models, and this problem will be exacerbated if these masers are all associated with UCHII regions, necessitating a revision of either star formation or UCHII region models. Alternatively, the unassociated 6.7-GHz CH_3OH maser sources may be associated with a

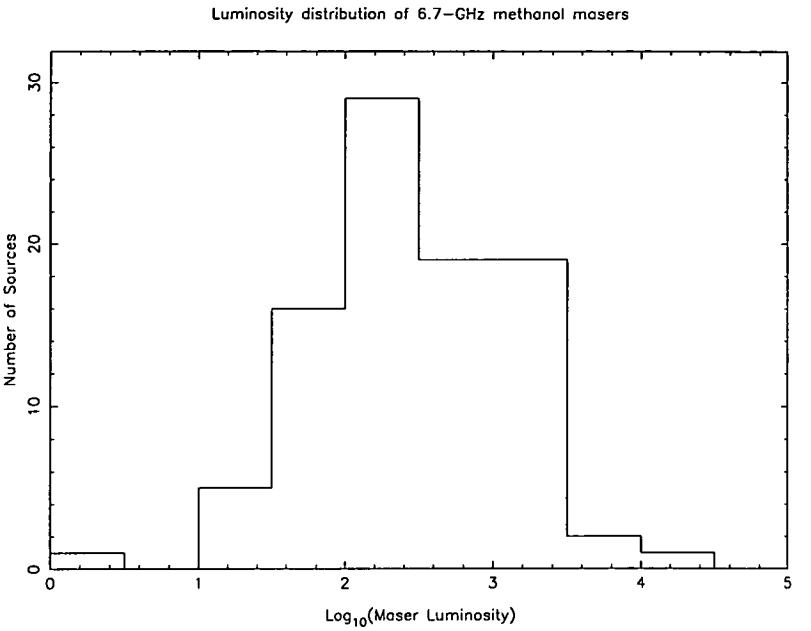

Figure 5.18: The luminosity distribution of the 6.7-GHz CH_3OH masers within the survey region, if they are all assumed to be at the near kinematic distance.

class of object which has not previously been found to exhibit maser emission.

In order to determine the luminosity distribution of the masers, a significant effort is required to resolve the kinematic distance ambiguity that exists for many of the sources. I have also shown that nearly all of the *IRAS*-based searches will detect less than 50% of the 6.7-GHz CH_3OH maser sources.

Chapter 6

The Ultra-compact HII regions associated with 6.7-GHz methanol masers

6.1 Introduction

The 6.7-GHz (5_1-6_0 A^+) transition of CH_3OH produces the second strongest Galactic masers of any known molecule. This makes it ideal for interferometric observations, as the accuracy to which the spatial distribution of the maser spots can be determined is largely dependent on the signal-to-noise ratio of the observation. The first high-resolution spatial images of the 12.2-GHz CH_3OH masers (Norris *et al.*, 1988) showed that, unlike OH or H_2O, the CH_3OH masers often exhibit a simple spatial morphology. Subsequent observations of the 6.7-GHz CH_3OH masers in many of the same sources (Norris *et al.*, 1993) revealed that they also frequently have a curved or linear spatial structure.

Three different models have been suggested to explain the observed curved or linear morphology of the 6.7- and 12.2-GHz CH_3OH masers :

1. They form in the collimated protostellar jets produced by the massive star.
2. They emanate from the shocked gas at the interface between the HII region and the surrounding molecular gas.
3. They originate in the circumstellar disc surrounding the massive star.

The protostellar jet hypothesis seems unlikely because the velocity of the CH_3OH masers is similar to that of the ionized and other molecular gas observed in the same regions. If the 6.7-GHz CH_3OH masers originated in a highly collimated protostellar jet then their velocities would be expected to be much higher than those of the OH maser and recombination lines, as is sometimes seen in H_2O masers, and this is not observed. However, if the protostellar jets are directed approximately perpendicular to the line of sight then the associated CH_3OH masers would be observed to have velocities similar to that of the ionized and molecular gas. Furthermore, they would be expected to point radially away from the centre

of the HII region. Also, the masers are likely to form some distance from the origin of the jet, as the extreme conditions closer to the star would destroy molecular material.

Observations of OH masers have generally found that they lie near the edges of HII regions (Gaume and Mutel, 1987). A common interpretation of this is that the OH masers form in the shocked gas where the expanding HII region meets the molecular cloud. It has been hypothesized that the CH_3OH masers originate in the same shocked gas. This means CH_3OH masers should be found near the edge of HII regions, as is observed for OH masers. Depending upon the orientation of the observer with respect to the shock front, curves or lines of masers may be observed. This model has received support from recent observations by Caswell *et al.* (1995d) who found that the positions of the OH and CH_3OH maser clusters are generally coincident to within 1 arcsec. However, this model does not explain how monotonic velocity gradients form in the CH_3OH masers, or why similar curved and linear morphologies are not commonly observed in OH masers.

The final hypothesis is that the 6.7- and 12.2-GHz CH_3OH masers occur in the circumstellar disc which surrounds massive stars during their formation (Norris *et al.*, 1993; Norris *et al.*, 1996). If these discs are being observed nearly edge-on, then this provides an explanation for the curved and linear structures observed in many CH_3OH masers. One of the predictions of this model is that the masers should show a simple velocity structure, and Norris *et al.* (1996) have presented evidence for this. Another prediction of the circumstellar disc model is that the CH_3OH masers should lie across the centre of the HII region, as that is the approximate position of the massive star.

The three models outlined above each predicts a different location for the 6.7-GHz CH_3OH masers with respect to the HII region. The primary objective of this chapter is to test which of the models is best supported by observations of the relative positions of the masers and ionized gas. In section 6.2, I present details of Australia Telescope Compact Array (ATCA) observations of the 3-cm continuum emission associated with three strong 6.7-GHz methanol masers (G318.95-0.20, G339.88-1.26 and NGC 6334F). In Section 6.3, I present the results of these observations and the relative positions of the associated 6.7-GHz CH_3OH masers. In Section 6.4, I discuss the implications of these observations for models of CH_3OH masers in star formation regions, their association with OH masers and the various hypotheses for the linear spatial morphology of CH_3OH maser emission. The results presented in this chapter have also been published by Ellingsen *et al.* (1996a).

6.2 Observations and data processing

I have used the ATCA to image the continuum emission of the HII regions associated with the 6.7-GHz CH_3OH masers G318.95-0.20, G339.88-1.26 and NGC 6334F (G351.42+0.64). My observations of NGC 6334F include three separate clusters of masers, and so subsequent discussions refer to a total of five clusters of 6.7-GHz methanol masers. The observations were made during 1993 November 7 with the array in the 6A configuration. This has minimum and maximum baseline lengths

Table 6.1: Positions and measured flux at 6.7 and 8.5 GHz, of the secondary calibrators used

Source Name	Right Ascension (J2000)	Declination (J2000)	6.7-GHz Flux Density (Jy)	8.5-GHz Flux Density (Jy)
1414−59	14:17:41.640	-59:50:37.53	1.16	1.08
1740−517	17:44:25.454	-51:44:43.77	3.03	2.51
1744−312	17:43:59.640	-31:07:38.45	0.40	0.40

of 0.33 and 5.9 km respectively. The correlator was configured to record both a 128-MHz band centred at 8.590 GHz, and an 8-MHz band which was alternated between 8.584 and 6.669 GHz. This enabled me to make observations of the 6.7-GHz CH_3OH masers and the H91α recombination line whilst simultaneously imaging the continuum emission. The 8-MHz band was split into 512 channels yielding a velocity resolution of 0.84 km s^{-1} at 6.669 GHz. The HPBW (half-power beam width) of the synthesised beam at 8.590 GHz was approximately 1.2 arcsec.

The three program sources were each observed twelve times for a 16-min period over the 13-h observing session. Each observation of a program source was preceded by a 4-min observation of a calibration source. The observing frequency of the 8-MHz band was changed to the alternate frequency at the end of each observing cycle (an observation of each program and calibration source). As a result, the maser and recombination line observations consist of six 16-min scans, while the continuum observations consist of 12 scans. I have subsequently made further observations of the H91α recombination line toward NGC 6334F and these will be the subject of a future paper.

The data were calibrated and imaged using the AT AIPS (Astronomical Image Processing System), which is based on the NRAO software package of the same name. 1934-638 was used as the primary flux density calibrator, which I assumed to have flux densities of 3.92 Jy and 2.86 Jy at 6.669 GHz and 8.590 GHz respectively. 1414-59, 1740-517 and 1744-312 were used as secondary calibrators and their positions and fluxes, calculated by comparing them with 1934-638 are listed in Table 6.1.

After the initial calibration, the continuum emission for each source was imaged and CLEANed using the AIPS task MX. The spectral resolution of my 6.7-GHz CH_3OH maser observations is four times lower than that of Norris *et al.* (1993). Because of this we did not try to determine the relative positions of the 6.7-GHz methanol masers from these data, but rather used the positions determined by Norris *et al.* . I independently imaged only the reference maser feature.

6.2.1 Phase referencing

In an ideal world an observation of a point source at the phase centre of a synthesis array will have constant amplitude and a constant phase of 0°. In practice however, the amplitude and phase may vary. The culprit is usually the changing atmosphere above the array. Turbulence in the atmosphere changes the path length between the source and the observing antennas and this causes variations in the difference between the predicted and actual arrival time of the wavefronts. The effect of this is to change the observed phase, but if you are observing a point source at the phase

centre then the true phase is known, and the observation is effectively measuring the phase error caused by the atmosphere. Thus occasional observations of a point source at the phase centre of the array can be used to correct the phase errors for observations of more complex sources. This technique is called phase calibration and is familiar to all users of connected element interferometers such as the ATCA or VLA.

In order for phase calibration to work properly the point source (commonly called a phase or secondary calibrator) must be close enough on the sky to the observing source, so that the atmospheric effects for the two sources are essentially the same. Also the interval between observations of the phase calibrator must be significantly less than the interval over which the phase errors change by 2π, otherwise interpolation of the phase between calibrator observations becomes ambiguous ("phase connection" is lost). The maximum distance between the calibrator and program sources and the frequency of phase calibrator observations depends upon a large number of factors including the observing frequency, the size of the array and the weather conditions. These and other considerations are discussed in detail by Beasley and Conway (1995).

A cluster of 6.7-GHz CH_3OH masers typically has a diameter of approximately 1 arcsec, which is roughly the same size as the synthesized beam of the ATCA at 6.7 GHz. This would appear to imply that observations of 6.7-GHz CH_3OH masers with this instrument would not be able to determine the distribution of the maser spots within the cluster. However, by assuming that the masers are point sources, one of the maser spots can be used as a phase calibrator for the rest. This is the perfect case for phase calibration as the phase calibrator is in the same synthesised beam as the program source and is being observed at the same time. This means that the relative positions of the masers can be measured to a small fraction of the synthesised beam and hence the distribution of the maser spots can be determined even though the synthesised beam encompasses the entire cluster.

6.2.2 Measuring the relative position of the masers and the HII region

The observational tests outlined in Section 6.1 require me to determine accurately the relative positions of the 6.7-GHz CH_3OH masers with respect to the HII region. I used three different techniques to determine the offset between the position of the 8.590-GHz continuum peak and the reference feature in the 6.7-GHz CH_3OH maser spectrum. The first and simplest technique was to measure independently the absolute positions of the continuum peak and the reference maser.

The second technique was to phase reference all the channels in the 6.7-GHz CH_3OH maser observations to a channel containing a strong unresolved maser feature (the reference feature). I then formed a continuum image from the channels which did not contain maser emission, and determined the position of the HII region peak. This method works only if the radio continuum emission from the UCHII region is strong, since the bandwidth used for the maser observations is much smaller that that used for the continuum observations. Of the three sources observed, only NGC 6334F had sufficiently strong continuum emission to allow

me to use this technique.

The final technique involved modification of the AIPS task PHSRF to reference the phase of the 8.5-GHz continuum channels to the 6.7-GHz reference feature. If I assume that the same region of the atmosphere causes the phase errors at both 6.7 and 8.5 GHz, then I can correct the 8.5-GHz phase simply by multiplying the 6.7-GHz correction by the ratio of the frequencies. Scaling the phase corrections causes a discontinuity if the reference phase wraps. For these observations I found that after calibration the reference phase did not wrap for many of the baselines. For those where the phase did wrap, it did so only once and I flagged these data before phase referencing the 8.5-GHz data.

To assess the accuracy with which I could measure the offset between a reference maser feature and the 8.5-GHz continuum peak, I calculated the offset for NGC 6334F using each of the above methods. In addition, I calculated the offset for several datasets which had not been fully calibrated, or contained small deliberate errors in the calibration. In all cases the measured offset was very similar, with the rms being 0.2 arcsec. The offsets quoted below are the mean of the offsets calculated from each of the methods outlined above (for G339.88-1.26 only the first and third methods were used). I adopt 0.2 arcsec as a conservative estimate of the standard error.

6.3 Results

Images of the 8.5-GHz radio continuum with the positions of the 6.7-GHz CH_3OH masers marked are shown in Figs 6.1 and 6.2. Five separate sites of 6.7-GHz CH_3OH maser emission were observed in the three sources, but I detected radio continuum emission associated with only two. The observed parameters of the radio continuum emission toward each of the sites of maser emission are summarised in Table 6.2. Two of the sites without continuum emission lie in the NGC 6334 star formation region. The upper limits on the peak flux density I obtained for them (see Table 6.2) are quite large, due to the presence of nearby strong diffuse sources, which severely limited the dynamic range I was able to achieve for images of this region. The resulting upper limits are almost as high as the peak flux measured for G339.88-1.26. The entire NGC 6334 region was imaged with the VLA by Rodríguez *et al.* (1982), but they were able to set only an upper limit of 20 mJy for other compact sources in the region. Gaume & Mutel (1987) also imaged NGC 6334F with the VLA and report no additional compact emission with a 5-σ limit of 6.5 mJy for their 15-GHz image.

6.3.1 G318.95-0.20

I obtained a 5-σ upper limit of 0.82 mJy beam^{-1} for any radio continuum emission from G318.95-0.20. UCHII regions with peak fluxes less than this upper limit have been detected. However, the large-scale, high-resolution studies of UCHII regions which have been made so far (Wood and Churchwell, 1989b; Garay *et al.*, 1993b; Kurtz *et al.*, 1994; Miralles *et al.*, 1994), typically have sensitivity comparable to,

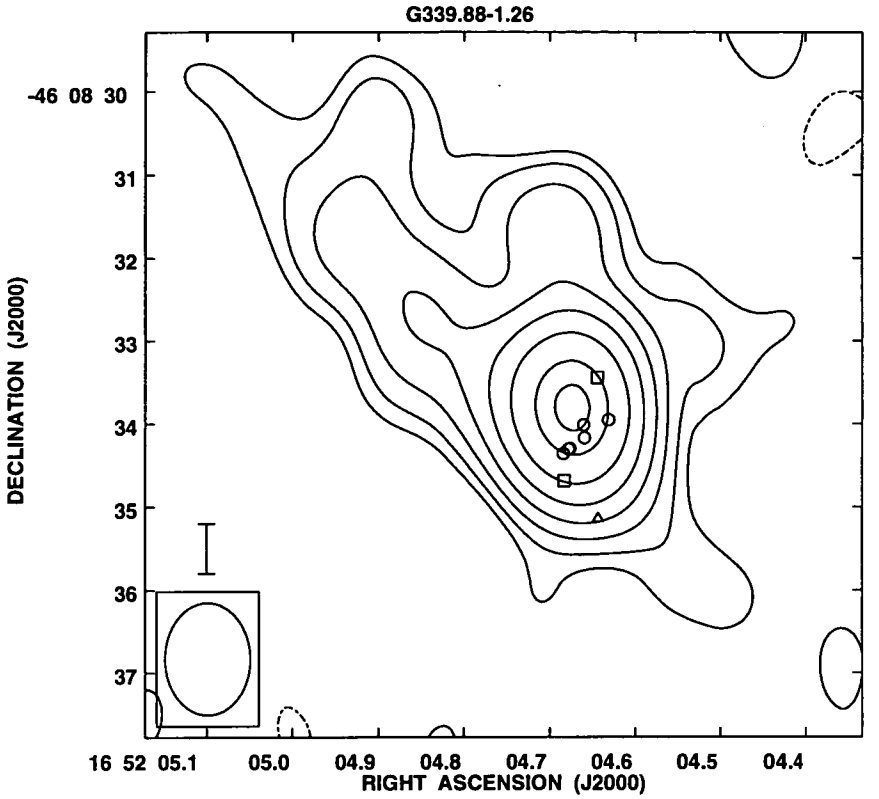

Figure 6.1: Radio continuum image of G339.88-1.26 at 8.59 GHz. The contours are at -1, 1, 2, 4, 8, 16, 32, 64, and 90 per cent of the peak flux (6.14 mJy beam^{-1}). The rms noise level in the image is approximately 0.04 mJy beam^{-1}. The relative positions of the 6.7-GHz CH_3OH masers as measured by Norris *et al.* (1993) are marked as open circles. The position of the OH masers as measured by Caswell *et al.* (1995d) and the H_2O masers as measured by Forster & Caswell (1989) are marked as squares and a triangle respectively. The error bar above the clean beam plot represents the 3-σ error for the relative offset between the CH_3OH masers and the continuum. The error in the relative position of the CH_3OH masers with respect to each other is smaller than the size of the symbols used to plot them. The width of the synthesised beam at the half power points is 1.04 arcsec in Right Ascension and 1.36 arcsec in Declination.

Table 6.2: Positions of observed sites of 6.7-GHz CH_3OH maser emission and some parameters of any associated continuum emission. For the first three sources the positions are those of the reference maser in each source. For NGC 6334F (NW) the position is the centroid of the four maser spots in that region and for G351.54+0.66 the position is that of the -2.5 km s^{-1} feature. The upper limits for sources with no detected continuum emission are 5 times the rms noise level in the final image.

Source Name	Right Ascension (J2000)	Declination (J2000)	8.5-GHz Peak Flux Density (mJy)	8.5-GHz Integrated Flux Density (mJy)	Major Axis (arcsec)	Minor Axis (arcsec)
G318.95−0.20	15:00:55.332	-58:58:42.04	< 0.82			
G339.88−1.26	16:52:01.682	-46:08:34.42	6.14	14.0	6.3	3.4
NGC 6334F (C)	17:20:53.454	-35:47:00.52	585	2780	8.8	6.5
NGC 6334F (NW)	17:20:53.240	-35:46:57.92	< 4.8			
G351.54+0.66	17:20:54.621	-35:45:07.38	< 3.3			

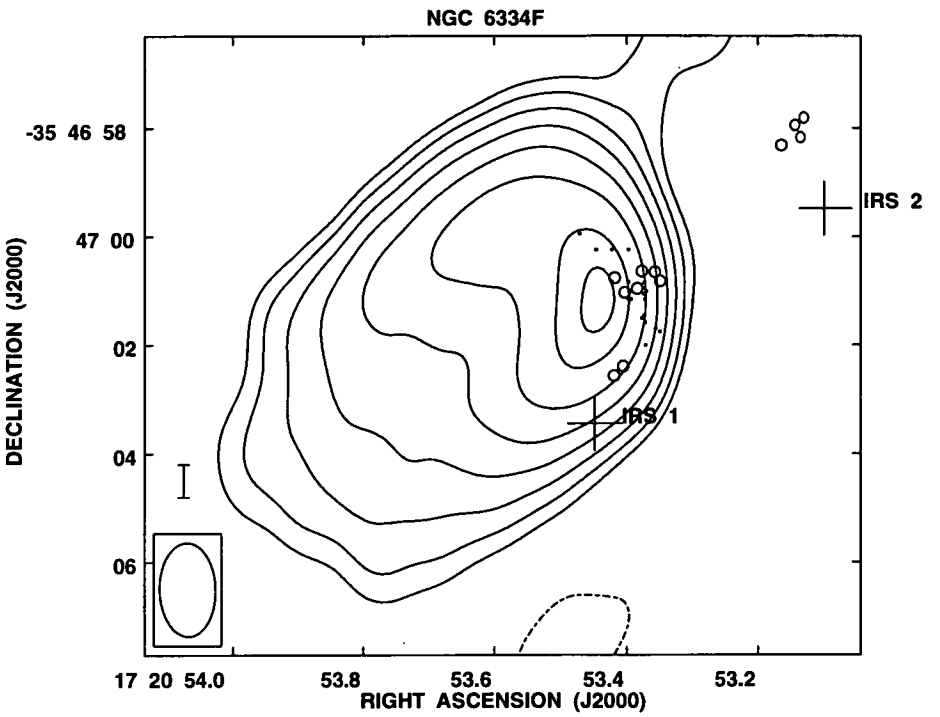

Figure 6.2: Radio continuum image of NGC 6334F at 8.59 GHz. The contours are at -1, 1, 2, 4, 8, 16, 32, 64, and 90 per cent of the peak flux (585 mJy beam^{-1}). The rms noise level in the image is approximately 1.0 mJy beam^{-1}. The open circles show the relative positions of the 6.7-GHz CH_3OH masers (Norris *et al.* 1993), the dots are the positions of the OH masers (Gaume & Mutel 1987) and the crosses mark the positions of two 20-μm infrared sources (Harvey & Gatley 1983). The error bar above the clean beam plot represents the 3-σ error for the relative offset between the CH_3OH masers and the continuum. The error in the relative position of the CH_3OH masers with respect to each other is smaller than the size of the symbols used to plot them. The width of the synthesised beam at the half-power points is 1.04 arcsec in Right Ascension and 1.73 arcsec in Declination.

or worse than this. Thus there is little information on whether UCHII regions with peak fluxes less than 1 mJy are common.

The depth to which I could CLEAN the image toward G318.95-0.20 was limited by the presence of a confusing source with a peak flux density of 29.5 mJy beam^{-1} $\approx$ 160 arcsec west and 34.5 arcsec north of the reference maser position. The confusing source I detected is approximately coincident with the *IRAS* source 14567-5846, which has been identified as an HII region. The radio continuum emission appears to be a cometary HII region with a major axis of $\approx$ 10 arcsec. Two groups have reported maser emission toward 14567-5846 (Cohen *et al.*, 1988a; Kemball *et al.*, 1988). In both cases they measure the position to be consistent with the OH maser position measured by Caswell & Haynes (1987), which, in turn, is coincident with the 6.7-GHz CH_3OH masers discussed here. Therefore, it appears that all the maser emission reported in this region to date is from the same site, which is more than 2 arcmin away from the *IRAS* source 14567-5846.

6.3.2 G339.88-1.26

Our 8.5-GHz image of G339.88-1.26 is shown in Fig. 6.1. This is the first image to be produced of this UCHII region. I measured it to have a peak brightness of 6.1 mJy beam^{-1} at 8.5 GHz, but it was too weak to image from my 6.7-GHz spectral-line observations. The bulk of the continuum emission is unresolved in my 1.2-arcsec synthesised beam, but shows some low-level extension to the north-east, suggesting a possible cometary morphology.

The reference maser (-38.7 km s^{-1}) is the most south-eastern of the spots and is offset from the continuum peak by 0.6$\pm$0.2 arcsec. The offset quoted is the average of those determined using the first and third methods outlined in Section 6.2.2. The CH_3OH masers lie in a line approximately across the centre of the continuum emission, perpendicular to the direction of the extended emission. The positions of two of the OH maser spots have been observed by Caswell *et al.* (1995d), and they straddle the line of 6.7-GHz CH_3OH masers. The position of one of the H_2O masers spots was measured with the VLA by Forster & Caswell (1989). It was the most southerly source in their sample and hence the maser position is less well determined than for the sources further north. The H_2O maser position they quote is approximately 1 arcsec south of the 6.7-GHz CH_3OH masers.

6.3.3 NGC 6334F (G351.42+0.64)

This source was previously imaged at 4.9 and 15 GHz using the VLA (Rodríguez *et al.*, 1982; Gaume and Mutel, 1987). Our 8.5-GHz image, shown in Fig. 6.2, agrees with theirs. Making sensitive high-resolution images of the NGC 6334F region is difficult because of the presence of the sources NGC 6334D and E, two nearby strong, diffuse HII regions. I measure a peak brightness of 585 mJy beam^{-1} for NGC 6334F at 8.5 GHz and 606 mJy beam^{-1} at 6.7 GHz. I also produced an 8.5-GHz image using a restoring beam with the same dimensions as the 6.7-GHz beam and measured the spectral index of the peak to be 0.95 between 6.7 and

8.5 GHz. This implies that the centre of the HII region is still optically thick at 8.5 GHz.

Toward NGC 6334F, three centres of 6.7-GHz CH_3OH maser emission are within the primary beam of the ATCA antennas. I have labelled the three sites NGC 6334F (C) (all those masers which lie in projection against the HII region), NGC 6334F (NW) [the masers to the north-west of NGC 6334F (C)] and G351.54+0.66. G351.54+0.66 is not shown in Fig. 6.2, as it is offset 14.0 arcsec east and 114.2 arcsec north of NGC 6334F (C) (see Table 6.2). The northern clump of masers in NGC 6334F (C) is approximately coincident with the position of the OH masers determined by Gaume & Mutel (1987). No OH masers have been detected at the locations of either NGC 6334F (NW) or G351.54+0.66. The latter is in the same general region as the infrared source NGC 6334I(N), but does not appear to be closely associated with any known radio or infrared sources.

6.4 Discussion

6.4.1 Morphology

Norris *et al.* (1993) observed 15 sites of 6.7-GHz methanol maser emission and found that a large fraction of their sample of 6.7- and 12.2-GHz CH_3OH maser sources have a simple curved or linear spatial distribution. Based on their spatial distribution, Norris *et al.* (1996) divided all 6.7-GHz CH_3OH maser sources into one of two classes: those with a simple linear or curved morphology (e.g. G339.88-1.26), and those with a more complex morphology (e.g. NGC 6334F). I have radio continuum observations associated with only two sites of 6.7-GHz methanol maser emission, one from each class of spatial morphology. No models have been suggested to explain the CH_3OH masers with complex spatial distributions. They may represent a different evolutionary phase of the star formation process, as suggested by Forster & Caswell (1989) for complex OH and H_2O maser distributions. As outlined in Section 6.1, three possibilities have been suggested to explain the curved/linear spatial morphology : shocks fronts, collimated jets, and circumstellar discs (Norris *et al.*, 1993; Norris *et al.*, 1996). If the CH_3OH masers form in the circumstellar discs of young stars, then I would expect to observe them approximately coincident with the continuum peak for the HII region. This is observed in G339.88-1.26 (see section 6.4.3), where the masers lie across the diameter of the HII region. For NGC 6334F (see section 6.4.4) the situation is less clear, with one cluster of 6.7-GHz CH_3OH masers in the same region as the OH maser emission and the other offset from both the OH masers and HII region.

One potential problem with the circumstellar disc model is the question of why are so many edge-on? If all 6.7-GHz CH_3OH masers emanate from circumstellar discs then only a relatively small fraction should appear edge-on, but Norris *et al.* (1993) found 10 of 16 (63%) sources which they observed to have a linear spatial morphology. In addition, the results of the several searches for 6.7-GHz CH_3OH masers (see Chapter 5) suggest that there are at least 650 sources in the Galaxy. If 63% of these are near edge-on, then a large percentage of all Galactic 6.7-GHz CH_3OH masers must be unobservable due to orientation effects. Which would

have significant consequences for the number of UCHII regions in the Galaxy (see Section 5.4.3). Norris *et al.* (1996) have suggested two potential selection effects which may explain why so many of the discs are observed edge-on. The first possible explanation is that in a disc the maximum column density arises in the plane of the disc. The second possible explanation is that as the circumstellar disc bisects the HII region the optical depth is much greater for masers perpendicular to the disc, compared to those in the plane of the disc. All of the 6.7- and 12.2-GHz CH_3OH masers observed by Norris *et al.* (1988; 1993) have large peak flux densities and so they are not a representative sample. Thus, it is possible that while a large number of strong CH_3OH masers are in edge-on discs, many of the weaker masers are in discs which we see at other inclination angles. The question as to what percentage of the CH_3OH masers have a linear spatial morphology is an important test of the circumstellar disc model. This could be resolved by interferometric imaging of a complete sample of 6.7-GHz CH_3OH masers selected from the Mt Pleasant survey. It also may have important implications for the flux density distribution of the masers, similar to those observed for radio-loud quasars (Scheuer and Readhead, 1979).

6.4.2 The energizing star

By making some simplifying assumptions about the nature of the HII regions observed, some of their physical parameters can be estimated (see Table 6.3). I calculated the electron density (n_e), emission measure (EM) and mass of ionized hydrogen (M_{HII}) using the equations of Panagia & Walmsley (1978). These equations assume that the HII region is optically thin, spherically symmetric and has an electron temperature of 10^4 K. In neither case are the HII regions I observe spherically symmetric. Instead, I calculate the linear radius of the HII region using the method outlined in Panagia & Walmsley independently for Right Ascension and Declination and use the geometric mean of the two. I also calculate the excitation parameter (U) using the formula of Schraml & Mezger (1969). Using this I estimate the Lyman continuum photon flux (N_L) and the spectral class of the exciting star (Panagia, 1973). As the excitation parameter depends only upon the flux density and the distance to the source, I was also able to calculate upper limits for the spectral class of the exciting star where I did not detect any continuum emission. For NGC 6334F, the spectral index I calculate for the central peak of the source between 6.7 and 8.5 GHz indicates that it is optically thick at these frequencies. The equations I have used to calculate the HII region parameters assume that they are optically thin. The effect of the violation of this assumption is to reduce my estimate of the ionizing flux of the exciting star, effectively making it a lower limit. So for the HII region NGC6334F, which has a central core that appears to be optically thick from my spectral index calculations, the stellar types I derive are a lower limit. However, the effect is small since Gaume & Mutel (1987) derive similar parameters from observations at 15 GHz where the optical depth effect will be much smaller.

Table 6.3: Derived parameters for HII regions and the exciting stars associated with them.

Source	Distance (kpc)	n_e (cm^{-3})	EM (pc cm^{-6})	M_{HII} ($M_\odot$)	U (pc cm^{-2})	Log N_L (s^{-1})	Spectral Type
G318.95−0.20	2.0				<2.1	<44.73	<B2
G339.88−1.26	3.0	$2.6x10^4$	$5.9x10^7$	0.001	7.2	46.32	B0.5
NGC 6334F-1	1.7	$9.5x10^4$	$9.6x10^7$	0.025	25.7	47.98	O9
NGC 6334F-2	1.7				<3.5	<45.36	<B1
G351.54+0.66	1.7				<3.1	<45.20	<B1

6.4.3 G339.88-1.26

G339.88-1.26 is one of the strongest sources of both 6.7- and 12.2-GHz CH_3OH maser emission. The only published high-resolution infrared observations of the G339.88-1.26 region (Testi *et al.*, 1994) show a strong peak, which appears to be slightly offset from the position I measure for the UCHII region. The CH_3OH maser emission has an approximately linear spatial distribution at both 6.7 and 12.2 GHz (Norris *et al.*, 1988; Norris *et al.*, 1993), and I measure the masers to be offset slightly to the south-west of the peak in the continuum emission, but not significantly so. This is the position predicted for the 6.7-GHz methanol masers if they occur in circumstellar discs.

Unlike the general case observed for OH masers, CH_3OH masers do not lie toward the edge of the HII region (Gaume and Mutel, 1987), which seems to rule out the hypothesis that the masers emanate from shocked gas. However, recent observations by Caswell *et al.* (1995d) have found that CH_3OH and OH maser clusters are typically coincident to within 1 arcsec. Figure 6.1 shows the positions of two OH masers observed by Caswell *et al.* and these roughly straddle the 6.7-GHz CH_3OH masers. Given these two apparently conflicting findings, further observations are required to determine the position of the HII regions with respect to the associated OH and CH_3OH masers.

Conceivably these observations are compatible with the masers lying in a highly collimated outflow, as they are radial to the HII region. However, the distribution of the masers is highly linear and they do not have a wide velocity range as might be expected if they emanated from a high-velocity outflow. Further, a double-sided jet is required, which is almost never seen in stars.

From my radio continuum images I estimate that a B0.5 star is required to produce the observed HII region. However, as the model I used does not take into account the absorption of UV photons by dust, this is a lower limit on the spectral class of the exciting star. Norris *et al.* (1996) used simple modelling to show that the observed spatial and velocity distribution of the masers is consistent with Keplerian motion, but were unable to derive a mass for the star. I find that the position of the masers with respect to the parent HII region also supports the hypothesis that the masers lie in circumstellar discs.

6.4.4 NGC 6334F

The NGC 6334 region is the most active known region of OB star formation in the Galaxy (Harvey and Gatley, 1983). The region has been the subject of several surveys at radio and infrared wavelengths (McBreen *et al.*, 1979; Rodríguez *et al.*,

1982; Loughgran *et al.*, 1986; Straw *et al.*, 1989). These observations show six main sites of radio emission and a similar number of clusters of infrared emission. Unfortunately, the nomenclature of the region is rather confusing. The main site of 6.7-GHz CH_3OH maser emission, called G351.42+0.64 in the CH_3OH maser literature, is associated with the radio source NGC 6334F, which is designated NGC 6334-I at infrared wavelengths.

The NGC 6334F star formation region is often compared to W3(OH). Both these regions show maser emission in many molecular transitions which are rarely detected toward other HII regions. For example, strong maser emission from several class II CH_3OH transitions detected towards only a few sites, and thermal emission from class I transitions, has been detected toward NGC 6334F (Batrla *et al.*, 1987; Haschick *et al.*, 1989; Haschick and Baan, 1989; Menten and Batrla, 1989; Menten, 1991a). This suggests that W3(OH) and NGC 6334F have some special characteristics not generally shared with other massive star-formation regions. Therefore it may not be valid to infer general characteristics of molecular emission, or star formation, from observations of NGC 6334F or W3(OH) alone.

It is well established that 6.7-GHz CH_3OH maser emission is common toward star formation regions which show main-line OH maser emission (Menten, 1991a; MacLeod and Gaylard, 1992; Caswell *et al.*, 1995c). However, recent observations by Ellingsen *et al.* (1996b) have detected many new 6.7-GHz CH_3OH masers in a region of the Galactic Plane previously surveyed for OH maser emission by Caswell, Haynes & Goss (1980). This suggests that in some sources the conditions are favourable for CH_3OH maser emission, but not for OH. Menten *et al.* (1992) found OH masers situated in, or near, all but one of the clumps of CH_3OH maser emission in W3(OH). However, within the clumps there appears to be an anticorrelation between the positions of the OH and CH_3OH masers. For NGC 6334F I find, in agreement with Menten *et al.*, that the OH masers appear to be associated with CH_3OH maser emission. However, unlike the case for W3(OH) there are two clumps of 6.7-GHz CH_3OH maser emission which have no reported OH emission. This, combined with the large scale observations of Ellingsen *et al.* (1996b), suggests that 6.7-GHz CH_3OH masers are more widespread than OH masers in star formation regions.

Infrared observations at a large number of wavelengths by Harvey & Gatley (1983) found the strongest emission in all bands to be coincident with the radio continuum peak (which they designated IRS 1). At 20 and 30 μm the emission is extended to the North-west indicating the presence of a second source (IRS 2) separated from IRS 1 by approximately 6 arcsec. They suggest that IRS 1 and 2 may form a double source. 2.2-μm (K-band) images of the same region by Straw *et al.* (1989) detected a cluster of sources in the general region of NGC 6334F, including a counterpart to IRS 1, but no counterpart to IRS 2.

Observations of CO, NH_3 and recombination lines probe large-scale outflows and the velocity of the ionized gas, and so provide additional information on star formation regions. Two lobes of NH_3 and CO emission have been observed to the north-east and south-west of the radio continuum (Jackson *et al.*, 1988; Bachiller and Cernicharo, 1990). The lobes are approximately perpendicular to the apparent gradient in the continuum emission and both show a velocity gradient.

A rotating molecular disc around IRS 1 (Jackson *et al.*, 1988) and bipolar outflow from IRS 1 (Bachiller and Cernicharo, 1990) have been proposed as explanations for the observed distribution of the molecular gas. The detection of shock-excited H_2 in the general vicinity of NGC 6334F (Straw and Hyland, 1989) and shock-excited NH_3 (3,3) masers at the interface between the molecular gas and ambient medium (Kraemer and Jackson, 1995), support the outflow hypothesis. Recent recombination-line observations also show a velocity gradient in the ionized gas, in approximately the same directions as the molecular gas, but are inconsistent with molecular outflow from IRS 1 (De Pree *et al.*, 1995a). De Pree *et al.* suggest instead that IRS 2 may be the source of the observed molecular outflow

The separation of IRS 1 and 2 is in the same direction, and roughly the same distance, as the two main clusters of 6.7-GHz CH_3OH masers near NGC 6334F which I have labelled NGC 6334F (C) and (NW). Norris *et al.* (1996) have shown that the observed spatial and velocity distribution of the two clusters of CH_3OH masers is consistent with Keplerian motion about two separate stars. If IRS 2 is the source of the molecular outflow then I would expect it to have a circumstellar disc perpendicular to the direction of the outflow. The 6.7-GHz CH_3OH masers NGC 6334F (NW) have a spatial and velocity structure consistent with Keplerian motion and are aligned perpendicular to the molecular outflow. This leads us to speculate that NGC 6334F (NW) may be associated with the infrared source IRS 2. If it can be shown that IRS 2 is coincident with the masers, and that it is the source of the molecular outflow, then this source provides additional evidence for the circumstellar disc model of CH_3OH masers. This requires higher resolution observations in the mid- to far-infrared and of the molecular outflow, particularly at its origin.

In Table 6.3 I present some calculated physical parameters of the HII regions and exciting stars. Our values are all comparable with those calculated by Rodríguez *et al.* (1982) and Gaume & Mutel (1987). From their model of the 6.7-GHz CH_3OH masers, Norris *et al.* (1996) calculate a mass of 70 $M_\odot$ for IRS 1 and 13 $M_\odot$ for IRS 2. These masses are approximate but, encouragingly both are roughly consistent with the spectral types inferred from the radio continuum observations.

6.5 Conclusion

I have detected 8.5-GHz continuum emission toward two of the five sites of 6.7-GHz CH_3OH maser emission detected. For G339.88-1.26 we find the position of the 6.7-GHz CH_3OH masers to be consistent with the hypothesis that these masers occur in circumstellar discs of massive stars. The maser emission toward NGC 6334F has a more complex distribution, with one of the clusters of CH_3OH maser emission being approximately coincident with the OH emission detected by Gaume & Mutel (1987). I also argue that the 6.7-GHz methanol maser cluster I call NGC 6334F (NW) may be in the circumstellar disc of the young stellar object IRS 2 (Harvey and Gatley, 1983).

Chapter 7

VLBI observations of class II methanol masers

7.1 Introduction

Very Long Baseline Interferometry (VLBI) is conceptually very similar to connected element interferometry. However, in a VLBI array antennas are sometimes separated by more than 10000 km, whereas typical connected element interferometers have maximum baseline lengths of a few tens of km or less. Even though VLBI shares much in common with connected element interferometry, there are several important differences :

1. For connected element interferometers correlation is performed in real time, but for VLBI the data is recorded onto tape in an agreed format at each antenna and correlated months, or even years, later.

2. For connected element interferometers the antennas which make up the array are usually very similar, but for VLBI the antennas often have different diameters, receiver types, sensitivity and mounting

3. For connected element interferometers the local oscillator signal and time are distributed to each of the antennas from a central location, but for VLBI they are independent for each station.

4. For connected element interferometers the atmospheric conditions are typically similar over all antennas, but for VLBI the separation between the antennas is such that there is usually no correlation in the atmospheric conditions.

Each of the differences listed above has important consequences for the processing of VLBI data and generally it is more difficult than the processing of data collected with instruments such as the ATCA or VLA. In particular, the first difference means that in general for VLBI experiments it is not known until correlation time whether a given antenna was operating properly. In recent years some of the distinctions between connected element and VLBI arrays have become blurred. MERLIN (Multi-Element Radio-Link Interferometer Network) is

a microwave linked interferometer using different antennas all over Britain, with baseline lengths intermediate between those of traditional connected element and VLBI arrays. The VLBA (Very Long Baseline Array) is a VLBI array of 10 identical antennas located throughout the United States, all of which are operated by 1 institution, NRAO (National Radio Astronomy Observatory).

Despite being relatively difficult to perform and process, VLBI experiments are becoming more common. This is because with the longer baselines available, VLBI can achieve resolutions of the order of 1 mas (milli-arcsecond) or less. This is 100 times better than can be achieved with premier optical instruments such as the *Hubble Space Telescope*. In section 6.2.1 I described how phase referencing can be used to determine the spot distribution of masers. However, the accuracy with which the relative positions of the maser spots can be determined depends primarily on the size of the synthesised beam and the signal to noise ratio of the observations. For 6.7-GHz CH_3OH maser spots relative positional accuracy of between 10–100 mas is achieved with the ATCA (Norris *et al.*, 1993). The VLBI observations described in this chapter have a relative positional accuracy approximately an order of magnitude better. This is because although the signal to noise ratio of the VLBI observations is much worse than for an ATCA observation of the same source, the synthesised beam is $\approx$ 10 mas at 6.7 GHz, as opposed to 1500 mas for the ATCA.

The very precise relative separations which can be measured between individual maser spots means that they are very useful for proper motion experiments. By phase referencing the masers to a background extragalactic source, the proper motion of the object with which the masers are associated can be measured. Such experiments promise to yield information on the proper motion of galaxies within the local group, such as the Magellanic Clouds (see Chapter 3) and M33 (Greenhill *et al.*, 1990). Alternatively by phase referencing to one of the masers the relative proper motion of each of the masers can be determined. This provides 3-dimensional velocity information which can be used to help model the star formation region in which the masers reside. Such a project is currently underway to determine if the proper motion of 6.7- and 12.2-GHz CH_3OH masers which have a curved or linear spatial morphology is consistent with Keplerian motion.

In addition to the greater relative positional accuracy that can be achieved with VLBI observations, they also often find new spots. This is again due to the smaller synthesised beam of VLBI experiments. If there are two or more spots which have very similar velocities within the synthesised beam of a connected element interferometer then only one spot is observed, at a position which depends upon the relative flux density of the individual spots. However, for VLBI observations the size of the synthesised beam is much smaller than the typical separation of the maser spots, and so the position of each of the spots can be determined.

It is well established that for radio sources with very small angular sizes, at low Galactic latitudes, large scale density fluctuations in the interstellar medium (ISM) along the line of sight lead to a number of interesting observational phenomena. These include variations in the flux density and observed position with time, and an increase in the observed size of the source. These effects have been observed for pulsars and some low Galactic latitude extragalactic sources and it

is generally believed that they should affect individual maser spots in a similar manner (Rickett, 1990). There are three major pieces of observational evidence that suggest the masers sizes are broadened by interstellar scattering (ISS). The first is that maser spot sizes are observed to increase generally with distance [e.g. Burke *et al.* (1968) and Hansen *et al.* (1993)]. The second is that the sizes of OH and H_2O masers associated with the same star formation regions scale approximately as $\nu^{-2.2}$ (Gwinn *et al.*, 1988) (which is expected if the sources are scatter-broadened). The third is that van Langevelde *et al.* (1992) observe that the sizes of OH/IR stars increase with decreasing distance from Sgr A*. However, there are other observations which do not support this. Szymczak (1985) compared the observed sizes of OH masers with those predicted from observations of nearby pulsars and found them to be roughly an order of magnitude larger. VLBI observations of 1720-MHz OH masers toward W3(OH) (Masheder *et al.*, 1994) show them to be much smaller than the 1665-MHz OH masers (Reid *et al.*, 1980), but if the 1665-MHz masers are scatter-broadened the 1720-MHz maser should have a similar size.

Thus the question of whether masers are affected by interstellar scattering is currently undecided. Observations of 6.7- and 12.2-GHz CH_3OH masers toward several star formation regions, including NGC 6334F (see Section 7.3.3) have shown that some of the spots are coincident to within $\approx$ 1 mas (Menten *et al.*, 1992). Measuring the spot size of the coincident masers at 6.7 and 12.2 GHz should be a sensitive test of whether the observed spot sizes are intrinsic, or broadened by interstellar scattering. The observations of Menten *et al.* (1992) suggest that they are not, but as they only measured the size of one maser spot in one source, further observations are required to determine if this generally holds. If the masers sizes are broadened by ISS then VLBI observations of the masers may be used to obtain information on the nature of the interstellar medium (ISM) along the line of sight to the masers.

To date there are very few published observations of 6.7- or 12.2-GHz CH_3OH masers which have milliarcsecond resolution (McCutcheon *et al.*, 1988; Menten *et al.*, 1988; Norris *et al.*, 1988; Menten *et al.*, 1992; Norris *et al.*, 1996). The first milliarcsecond resolution observations of 12.2-GHz CH_3OH masers showed that for many of the sources the cross-correlation spectra had significantly lower flux density than the total-power spectra (McCutcheon *et al.*, 1988; Menten *et al.*, 1988). The initial interpretation was that this was probably due to blending of spatially separate features with similar velocities, as observed in OH masers (Reid *et al.*, 1980). This is supported by the observations of Norris *et al.* (1996) who observed flux density in the VLBI images of G309.92+0.48 to be consistent with that in the total-power spectrum, with the exception of one component. However, in contrast, 6.7-GHz VLBI observations of W3(OH) by Menten *et al.* (1992) detected less than half the flux density present in the total-power spectrum.

Table 7.1: The diameter, polarization and system equivalent flux density characteristics at 6.7 and 12.2 GHz for the 6 antennas which participated in the VLBI observations. RCP = Right circular polarization

Antenna	Diameter	6.7-GHz		12.2-GHz	
		Polarization	SEFD	Polarization	T_{sys}
	(m)		(Jy)		(Jy)
Culgoora	22	RCP	1550		
DSS 43	70			Linear	400
Hartebesthoek	26	RCP	1400	RCP	1400
Hobart	26	RCP	1800	RCP	4000
Mopra	22	RCP	1100	Linear	2200
Parkes	64	RCP	100	RCP	140

Table 7.2: The velocity range and resolution of the NRAO MK II correlator at 6.7 and 12.2 GHz. The velocity resolution quoted is for uniform weighting.

Bandwidth	6.7-GHz		12.2-GHz	
	Velocity Range	Velocity Resolution	Velocity Range	Velocity Resolution
(MHz)	(km s^{-1})	(km s^{-1})	(km s^{-1})	(km s^{-1})
0.5	22.5	0.28	12.3	0.15
2.0	90.0	1.12	49.2	0.61

7.2 Observations and data processing

I have used VLBI observations involving five Australian antennas to image the 6.7-GHz CH_3OH masers associated with NGC 6334F and the 12.2-GHz CH_3OH masers associated with G335.79+0.17 and NGC 6334F. These antennas, in conjunction with the Hartebeesthoek antenna in South Africa, were also used to measure the size of the 6.7- and 12.2-GHz CH_3OH maser spots for 8 sources. The properties of each of the antennas is summarized in Table 7.1.

The observations were made during the period 1992 May 29-31, between approximately 7 and 21 h UT on each day. The data were recorded using the MK II VLBI format, with 0.5-MHz bandwidth for the imaging experiments and 2-MHz for the spot size experiment. The data were correlated using the NRAO MK II correlator located in Soccoro, New Mexico. This VLBI correlator, which ceased operation in early 1994, was built in 1971, and its operation when I used it in 1992 was similar to that described by Moran (1976). This correlator had limited spectral capabilities in comparison to more modern correlators. In spectral line mode the NRAO MK II correlator processed one baseline at a time and produced a 96-channel autocorrelation spectrum for each antenna and a 192-channel complex cross-correlation spectrum for each baseline. The resulting velocity range and resolution at 6.7 and 12.2 GHz is summarized in Table 7.2.

After correlation, the data were calibrated and processed using the *AIPS* software package, which is written and distributed by NRAO. A detailed description of the process of reducing VLBI data using *AIPS* is given in Chapter 10 of the *AIPS* Cookbook (1995) and I will only outline that procedure here. The correlated data were loaded into *AIPS* using the special task for loading NRAO MK II VLBI

data (VLBIN). The data were inspected and any bad points flagged. Observations of the compact extragalactic sources 1610-771 and 1921-293 were used to correct the bandpass shape of the spectral line observations using the task BPASS. The task CVEL was used to correct for the changing Doppler shift of the sources, due to the rotation of the Earth. Amplitude calibration was performed using the task ACFIT, which compares a template autocorrelation spectrum (in my case from Parkes) to the autocorrelation spectra from the other antennas, and determines the relative gain with time. Global fitting of the delays and fringe rates for each antenna were calculated using the task FRING. The same task was then used to determine the fringe rate for a strong spectral feature of each of the maser sources.

Of the three imaging experiments, only the 12.2-GHz observations of NGC 6334F contained an unblended spectral feature which was sufficiently strong to use for phase referencing. For the observations of G335.79+0.17, the basic calibration was improved by amplitude and phase self-calibration of the -46.0 km s^{-1} feature (the feature with the peak flux density in the total-power spectrum). This calibration was then applied to all other channels. For the 6.7-GHz observation of NGC 6334F, I tried using both of the previously mentioned techniques, but due to the complexity of the emission neither was able to improved the signal to noise ratio of the images and so no additional calibration was applied. For the three imaging observations, each of the spectral channels containing maser emission was imaged and CLEANed with "natural VLBI" weighting using the task MX. This weighting scheme applies natural weighting to the fourth root of the original weights and was used in order to reduce the difference in weights between baselines.

The position and flux density of each maser spot was determined by fitting a two-dimensional Gaussian to the CLEANed image using the task JMFIT. The formal error estimates returned by non-linear fitting routines such as JMFIT are usually not very accurate. Because they assume that the errors in the input data are uncorrelated, they typically underestimate the size of the error. The best method for obtaining an accurate estimate of the error in routines such as JMFIT is to generate fake data with similar properties to the observed data, and process it in the same manner. The returned values for the parameters can then be compared with those used to generate the model, and so an accurate estimate of the error can be determined. Such a study is beyond the scope of this work, but fortunately one has been undertaken previously by Conway *et al.* (1992). They used JMFIT to find the positions of components in their MKII VLBI images of the nuclei of two radio galaxies. Conway *et al.* found that they were able to determine the relative positions of the major components to between 5–15% of the synthesized beam. While these observations were not of masers and were processed using a different procedure, the positions were determined using JMFIT and so their findings do have some relevance to these observations.

For the measurement of the relative position of individual maser spots, the position of the peak is the most important parameter. There are two factors which limit the accuracy to which the position of the peak can be determined : residual phase errors in the data, and the signal-to-noise ratio of the observation. Which of these is the dominant affect depends very much on the individual observation. The

quality of the phase information in VLBI data is in general much worse than for connected element interferometry, where it can be significantly improved by phase calibration (see Section 6.2.1). However, for maser observations, by referencing the phase of each spectral channel, to one containing a strong unblended, unresolved component the residual phase errors in the data can be significantly reduced.

The formal errors returned by JMFIT for each of the imaging observations were 0.10–0.40 mas and 0.10–0.30 mas for the 6.7- and 12.2-GHz CH_3OH maser images of NGC 6334F respectively and 0.15-0.30 pixels for the 12.2-GHz image of G335.79+0.17. As stated above these values are probably underestimated. Fortunately, I have an independent method of estimating the accuracy to which the positions of the maser spots can be determined (see Section 7.3.3). This estimate agrees with that of Conway *et al.* and I suggest that the accuracy to which the relative positions of the masers have been determined, is better than 20% of the synthesised beam. For the 12.2-GHz observations where self-calibration or phase referencing was performed the accuracy is probably significantly better.

For the maser spot size observations, scalar-averaged cross-correlation spectra were produced for each baseline and each source. From these spectra the flux density of one or more strong spectral features was measured. At 12.2 GHz 2 of the antennas observed right-hand circular polarization (RCP), and the other two observed a linear polarization. For an unpolarized source the cross-correlated amplitude is reduced by $\sqrt{2}$ if one antenna observed RCP and the other linear and a correction for this effect was made.

Cross-correlation spectra can be formed either by coherent (or vector) averaging of the data, or by incoherent (or scalar) averaging of the data. In the former case the spectrum will only contain emission from sources within approximately one synthesized beam of the specified phase centre. This is because for sources away from the phase centre, the phase will vary with time, and so destructive interference will reduce the amplitude to approximately zero. The advantage of coherent averaging is that for spectral channels with no signal the phase will be random, so the noise level for the baseline is very low. For coherent averaging the spectrum is formed by averaging the amplitude for each channel. As the amplitude is an inherently positive quantity the baseline will be offset from zero, by an amount which depends upon the noise level for that baseline. Long integration times reduce the noise level of the baseline, but do not effect the offset from zero. The advantage of coherent averaging is that emission can be detected from anywhere within the primary beam, (provided it is greater than the offset from zero). For the experiment to measure the visibility the observations consisted of only one or two scans per maser source. This is insufficient to image the data, and so I would only be able to obtain a vector average for the spectral feature used for fringe rate calibration. Because of this I chose to use scalar averaged spectra to measure the visibility of the methanol maser spots.

For baselines between the smaller antennas the noise level in each spectral channels was typically quite high, with the observed signal-to-noise ratio occasionally < 2. Because the amplitude of a signal is always positive, for low signal-to-noise observations the amplitudes follow a Rice rather than a Gaussian distribution

(Thompson *et al.*, 1986). The true signal level is related to the mode of the amplitude distribution, but the flux density in each spectral channel represents the mean of the amplitude distribution. For a Gaussian distribution the mode and the mean are the same. However, for a Rice distribution the mean is greater than the mode, hence the observed signal level (Z) is greater than the true signal level (V). The mode of the distribution and hence the true signal level can be calculated from the mean if the noise level (σ) is known. In the absence of signal the amplitude distribution will follow a Rayleigh distribution, which has a mean of $\sqrt{\frac{\pi}{2}}\sigma$. From the scalar cross-correlation spectrum, I was able to use the channels with no emission to calculate the noise level (σ), and the signal level (Z) is simply the flux density of the spectral feature of interest. I then used the method outlined in Section 6.4 of King (1994) to calculate the true signal level (V) from (Z) and (σ).

7.3 Results and Discussion

7.3.1 NGC 6334F

The compact HII region NGC 6334F is one of the best studied sites of massive star formation (see Section 6.4.4) and is associated with strong 6.7- and 12.2-GHz CH_3OH maser emission. The 6.7- and 12.2-GHz VLBI images I obtained are shown on the same scale in Figs. 7.1 and 7.2. The area of each circle representing a maser position is proportional to the flux density of that maser spot. The position, flux density and velocity of each of the maser spots is listed in Tables 7.3 and 7.4. There are three distinct clusters of 6.7-GHz CH_3OH masers which I will refer to as NGC 6334F NW (north west), C (central) and S (south), these are shown in detail in Figs. 7.3, 7.4 and 7.5. At 12.2 GHz only the first two clusters are present (see Figs. 7.6 and 7.7) and in each of these there are only approximately half the number of spots observed at 6.7 GHz.

The 12.2-GHz CH_3OH masers have previously been imaged by Norris *et al.* (1988) using the PTI. The 6.7-GHz CH_3OH masers have also previously been imaged (Norris *et al.*, 1993), and their distribution is shown in Fig. 6.2. The maser distributions I observe agree well with those of Norris *et al.* (1988; 1993), with the exception of the two 6.7-GHz spots they label C & E in the central cluster, which I did not detect. Either these features are variable and no longer detectable, or more likely they result from a blending of several masers in the larger synthesised beam of the ATCA. For the less complicated 12.2-GHz observations the average difference between my VLBI positions and the PTI positions of Norris *et al.* is 3 mas, with the largest offset being only 5 mas. These two sets of observations are separated by four years and one month and this suggests that any proper motion is at a rate of $\lesssim 0.75$ mas per year. Assuming that the distance to NGC 6334F is 1.7 kpc this corresponds to a velocity tangential to the line of sight of $\lesssim 6$ km s^{-1}. If the masers are in edge on circumstellar discs then the expected velocity tangential to the line of sight is less than 1 km s^{-1}, so that this observation does not provide a useful constraint on models of class II CH_3OH masers. In total, Norris *et al.* detected 12 6.7-GHz and 5 12.2-GHz CH_3OH maser

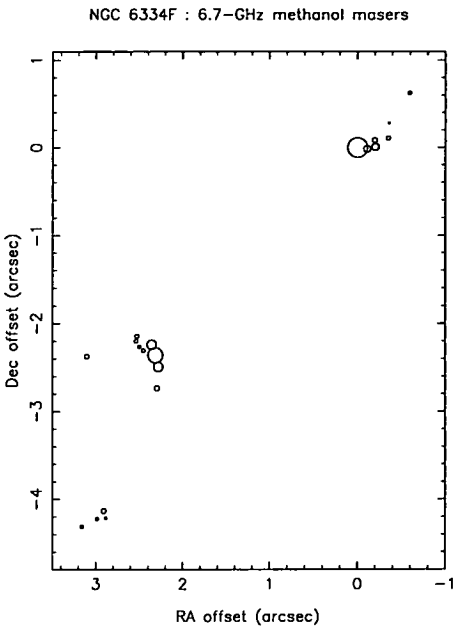

Figure 7.1: The relative positions of the 6.7-GHz CH_3OH masers associated with NGC 6334F. The area of the circle marking the position of each maser spot is proportional to its flux density. The images were made using a 21.4 x 15.5 mas synthesised beam.

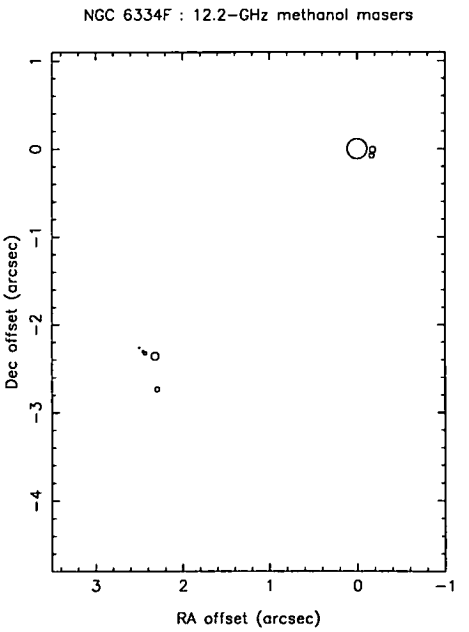

Figure 7.2: The relative positions of the 12.2-GHz CH_3OH masers associated with NGC 6334F. The area of the circle marking the position of each maser spot is proportional to its flux density. The images were made using a 12.3 x 2.5 mas synthesised beam.

Table 7.3: The positions, flux density and velocity of the 6.7-GHz CH_3OH masers associated with NGC 6334F. The positions are relative to RA(J2000)=$17^h20^m53^s.263$, Dec(J2000)=-35°36′58″.16.

Cluster	Right Ascension offset (arcsec)	Declination offset (arcsec)	Flux Density (Jy)	Velocity (km s^{-1})
NW				
	-0.1088	-0.0156	16	-11.3
	0.0000	0.0000	129	-11.1
	-0.2031	0.0075	17	-10.2
	-0.1956	0.0842	8	-9.9
	-0.3603	0.2829	2	-9.5
	-0.3505	0.1081	6	-9.2
	-0.5939	0.6254	4	-7.8
C				
	2.2999	-2.7332	9	-10.6
	2.3168	-2.3573	76	-10.4
	2.3602	-2.2368	30	-10.2
	2.2831	-2.4903	40	-10.2
	2.4548	-2.3049	4	-9.9
	2.5279	-2.1407	5	-9.7
	2.5364	-2.1961	5	-9.5
	2.5009	-2.2602	4	-9.0
	3.1060	-2.3720	7	-8.5
S				
	2.8859	-4.2154	2	-7.6
	2.9093	-4.1319	8	-7.4
	2.9859	-4.2238	4	-6.9
	3.1610	-4.3105	4	-6.7

Table 7.4: The positions, flux density and velocity of the 12.2-GHz CH_3OH masers associated with NGC 6334F. The positions are relative to RA(J2000)=$17^h20^m53^s.263$, Dec(J2000)=-35°36′58.″16.

Cluster	Right Ascension offset (arcsec)	Declination offset (arcsec)	Flux Density (Jy)	Velocity (km s^{-1})
NW				
	-0.1694	-0.0484	2	-11.6
	0.0000	0.0000	174	-11.3
	-0.1658	-0.0771	12	-11.1
	-0.1770	-0.0115	17	-10.1
C				
	2.2943	-2.7346	10	-10.8
	2.3192	-2.3588	27	-10.5
	2.4536	-2.3055	2	-9.8
	2.4299	-2.3245	5	-9.6
	2.4951	-2.2620	1	-8.9

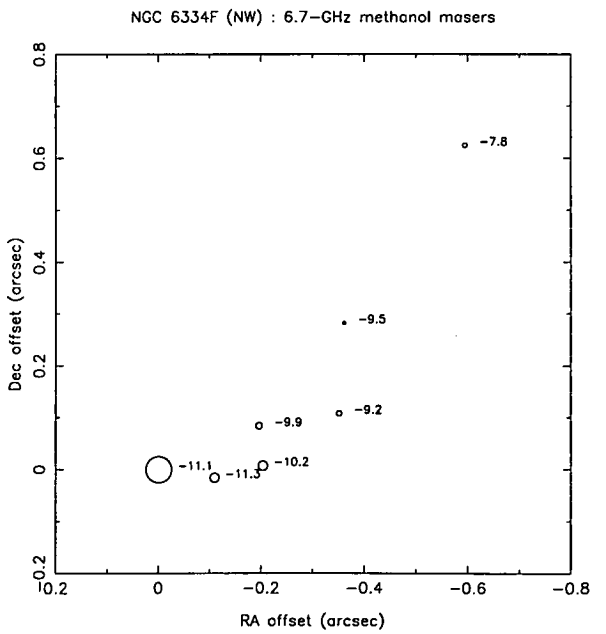

Figure 7.3: The relative positions of the 6.7-GHz CH_3OH masers in the North Western cluster of NGC 6334F. The area of the circle marking the position of each maser spot is proportional to its flux density and each spot is labeled with its LSR velocity in km s^{-1}.

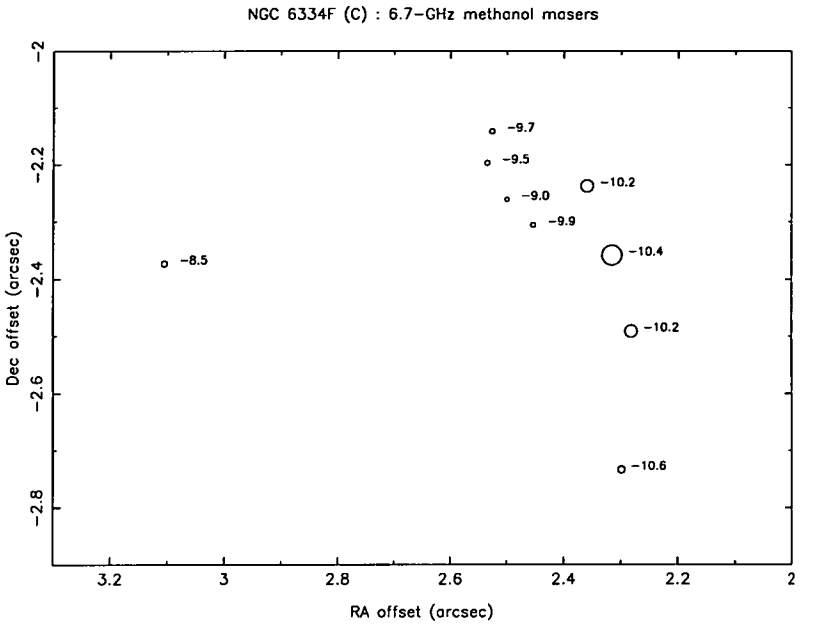

Figure 7.4: The relative positions of the 6.7-GHz CH_3OH masers in the Central cluster of NGC 6334F. The area of the circle marking the position of each maser spot is proportional to its flux density and each spot is labeled with its LSR velocity in km s^{-1}.

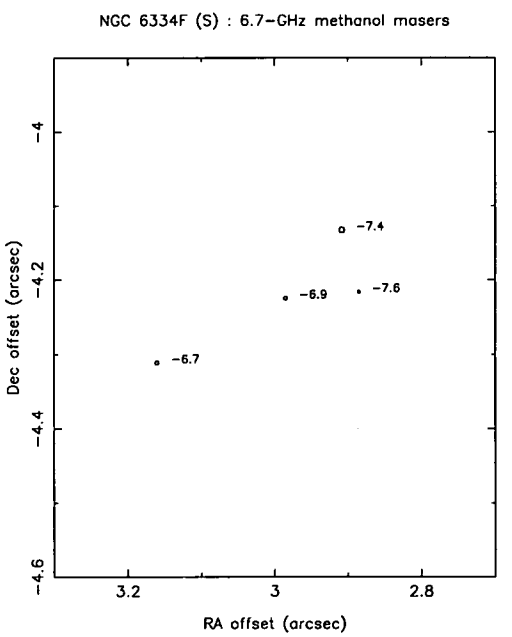

Figure 7.5: The relative positions of the 6.7-GHz CH_3OH masers in the Southern cluster of NGC 6334F. The area of the circle marking the position of each maser spot is proportional to its flux density and each spot is labeled with its LSR velocity in km s^{-1}.

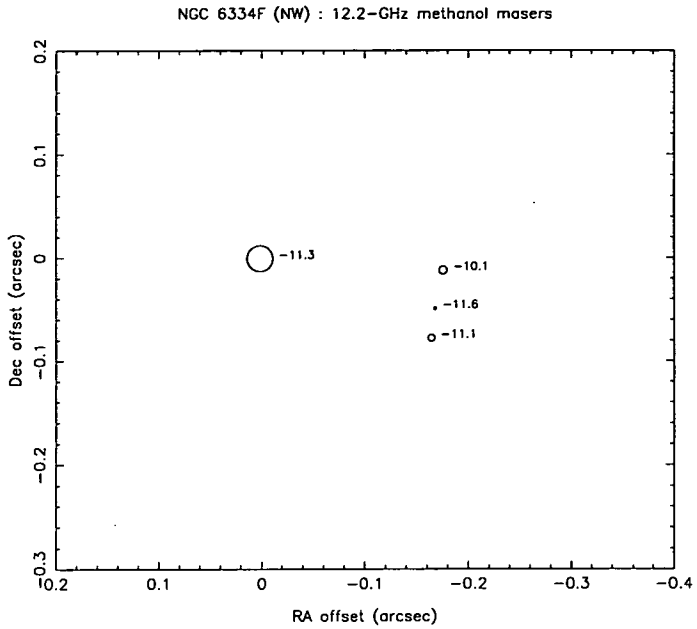

Figure 7.6: The relative positions of the 12.2-GHz CH_3OH masers in the North Western cluster of NGC 6334F. The area of the circle marking the position of each maser spot is proportional to its flux density and each spot is labeled with its LSR velocity in km s^{-1}.

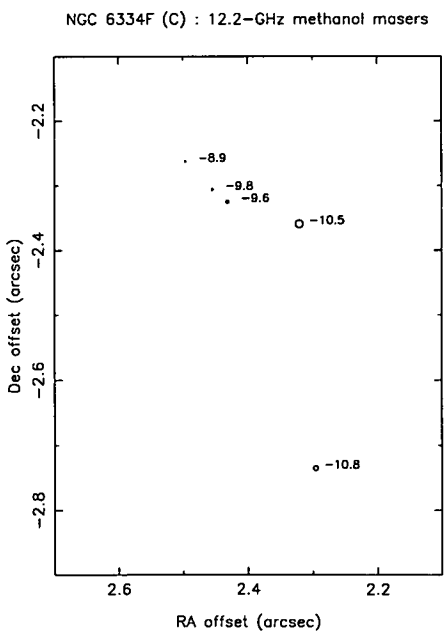

Figure 7.7: The relative positions of the 12.2-GHz CH_3OH masers in the Central cluster of NGC 6334F. The area of the circle marking the position of each maser spot is proportional to its flux density and each spot is labeled with its LSR velocity in km s^{-1}.

spots, while my VLBI observations detected 20 6.7-GHz and 9 12.2-GHz CH_3OH maser spots.

Figure 7.8 shows the total-power spectrum for the 6.7-GHz CH_3OH masers associated with NGC 6334F. The cross-correlation spectrum for one of the long baselines (Parkes-Hobart) is also displayed on the same scale and has much lower amplitude than the total-power spectrum. Similarly, for W3(OH) Menten *et al.* (1992) observed the cross-correlation spectrum of the 6.7-GHz CH_3OH masers on both short and long baselines to have a significantly lower flux density than the total-power spectrum. Figure 7.9 compares the cross-correlation spectrum with the total flux density in each spectral channel imaged. With the exception of the region between -10 – -11 km s^{-1}, the imaged flux density closely matches the cross-correlation spectrum. Figs. 7.10 and 7.11 show similar spectra for the NGC 6334F 12.2-GHz CH_3OH maser emission. The 12.2-GHz observations had a higher spectral resolution in addition with a less complex spatial morphology and exhibit excellent agreement between the cross-correlation spectrum on the Parkes-DSS43 baseline and the imaged flux density in each spectral channel. In combination with the observations of the W3(OH) 6.7- and 12.2-GHz CH_3OH masers (Menten *et al.*, 1988; Menten *et al.*, 1992), these observations suggest that most of the observed differences between the total-power and cross-correlation spectra of class II CH_3OH masers are not due to destructive interference between spatially separate maser spots with similar velocities. This implies that some class II CH_3OH masers must have physical structures which are partially resolved on even the shortest VLBI baselines. This interpretation is supported by my observations of class II CH_3OH maser spot sizes and is discussed further in Section 7.3.4.

Norris *et al.* (1996) have shown that if the masers are located in a near edge-on circumstellar disc then a plot of the major axis offset versus velocity ($\nu - a$) should have points in only two quadrants. Further, if the masers are confined to a small range of radii then the $\nu - a$ plots will form a line, the slope of which can be used to determine an upper limit on the mass of the exciting star. For NGC 6334F, they found that the two major clusters of masers formed two separate lines on a $\nu - a$ diagram and interpreted this as meaning that the two clusters are associated with different stars. My images of NGC 6334F detect approximately twice the number of both 6.7- and 12.2-GHz CH_3OH maser spots observed by Norris *et al.* (1988; 1993). Figs. 7.12–7.14 show the $\nu - a$ diagrams for each of the three clusters of CH_3OH masers associated with NGC 6334F. These plots combine both the 6.7- and 12.2-GHz VLBI observations. Encouragingly, all the newly detected maser spots lie along the same lines in the $\nu - a$ diagrams as those previously detected by Norris *et al.* (1988; 1993).

7.3.2 G335.79+0.17

The peak flux density of G335.79+0.17 at both 6.7- and 12.2-GHz is more than an order of magnitude less than those of NGC 6334F and overall it is quite a different class II CH_3OH maser source. G335.79+0.17 is also one of the few strong CH_3OH maser sources with a 12.2-GHz peak flux density comparable to that at 6.7-GHz. 8.6-GHz radio continuum observations by Phillips *et al.* (1996) failed to

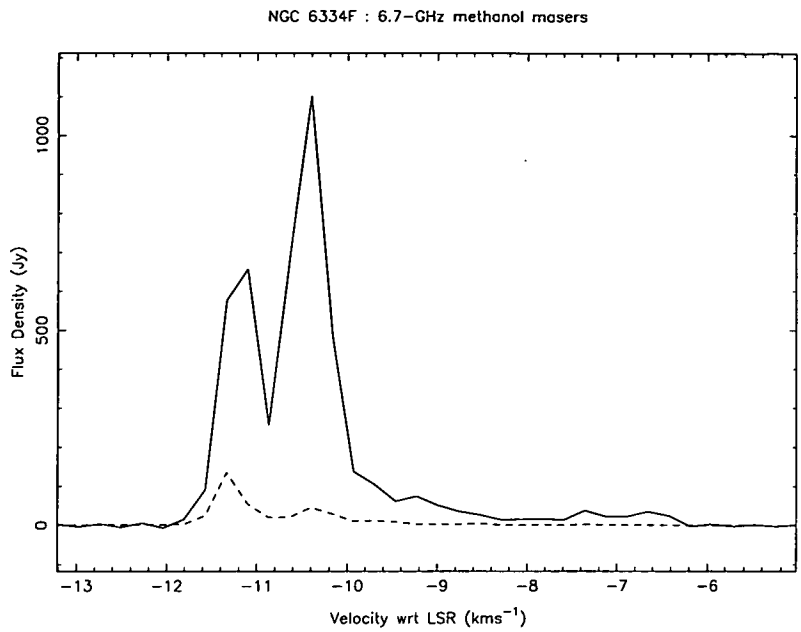

Figure 7.8: The solid line is the total-power spectrum of the NGC 6334F 6.7-GHz CH_3OH masers, observed with the Parkes antenna. The dashed line is a scalar averaged cross-power spectrum for the Parkes-Hobart baseline. Neither spectra have been Hanning smoothed, yielding a velocity resolution of 0.28 km s^{-1}.

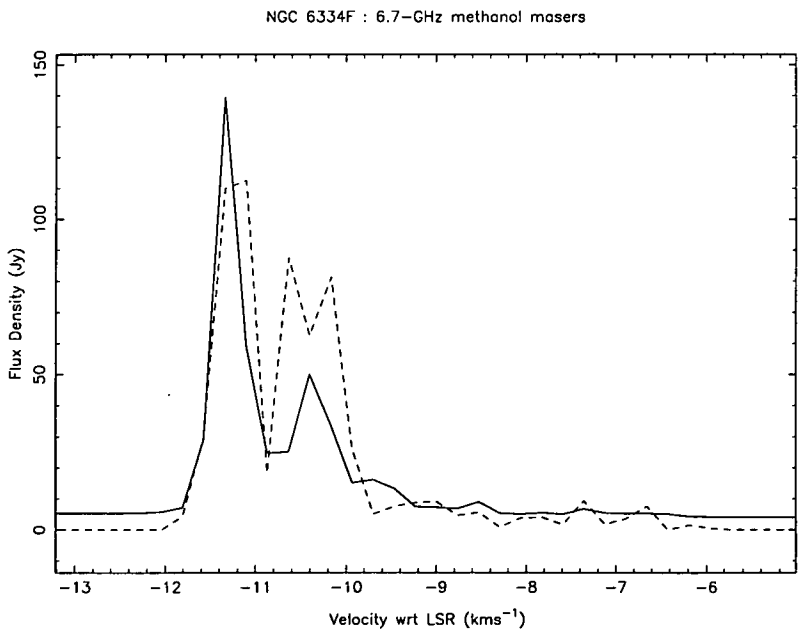

Figure 7.9: The solid line is a scalar averaged cross-power spectrum of the NGC 6334F 6.7-GHz CH_3OH masers for the Parkes-Hobart baseline. The dashed line is the spectrum of the total flux density in each imaged channel. The amplitude of the -10.4 km s^{-1} peak in the cross-correlation spectrum is probably reduced by the interference of the maser spots at -10.2 km s^{-1} and -10.6 km s^{-1}. However in general the observed flux density in the images is consistent with the cross-correlation spectrum.

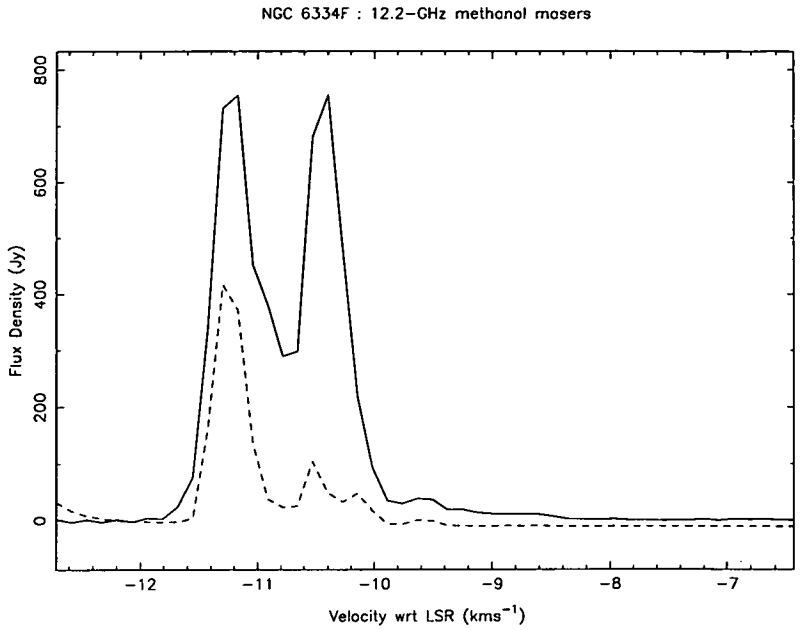

Figure 7.10: The solid line is the total-power spectrum of the NGC 6334F 12.2-GHz CH_3OH masers, observed with the Parkes antenna. The dashed line is a scalar averaged cross-power spectrum for the Parkes-DSS43 baseline. Neither spectra have been Hanning smoothed, yielding a velocity resolution of 0.15 km s^{-1}.

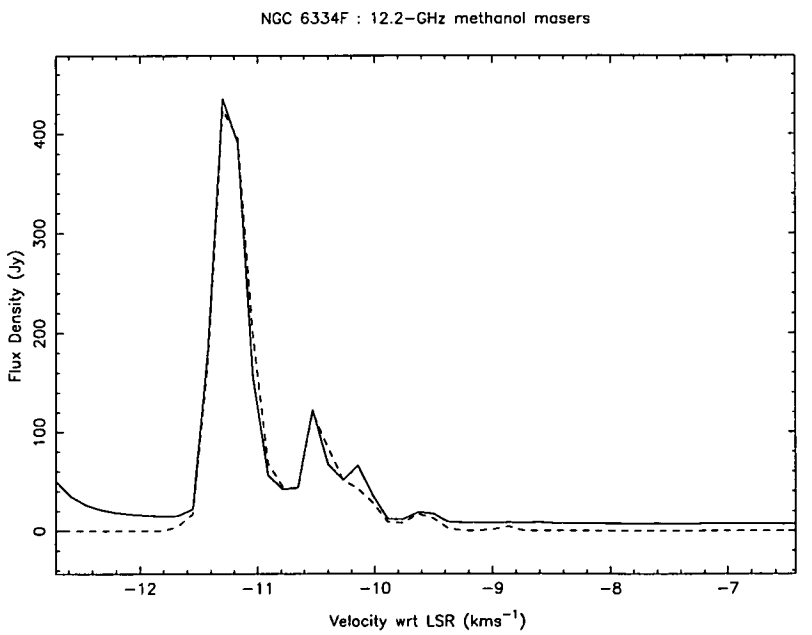

Figure 7.11: The solid line is a scalar averaged cross-power spectrum of the NGC 6334F 12.2-GHz CH_3OH masers for the Parkes-DSS43 baseline. The dashed line is the spectrum of the total flux density in each imaged channel. The very close agreement between these two spectra suggests that the observed differences between the total-power and cross-correlation spectra are not due to interference, but rather large scale structures in the CH_3OH maser emission

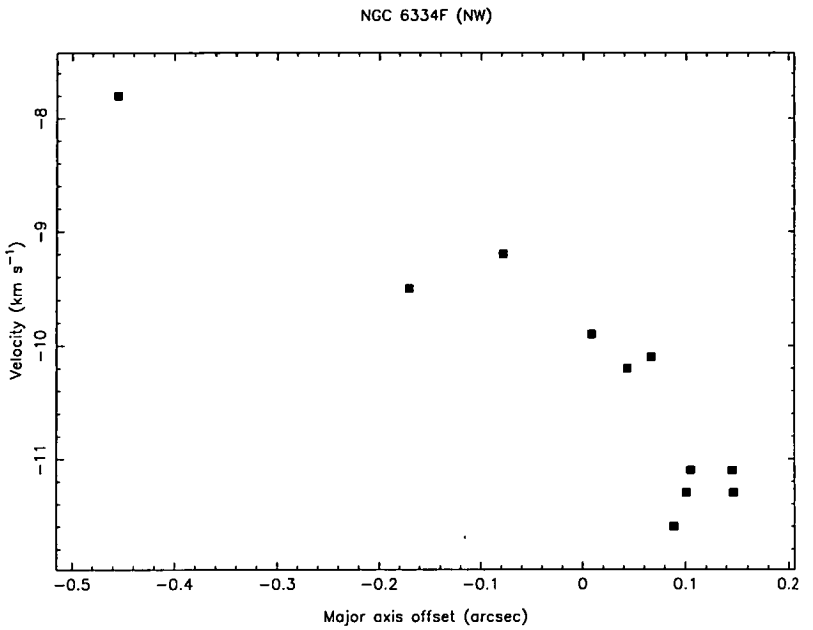

Figure 7.12: Major axis offset versus velocity diagram combining the 6.7- and 12.2-GHz CH_3OH masers from NGC 6334F (NW).

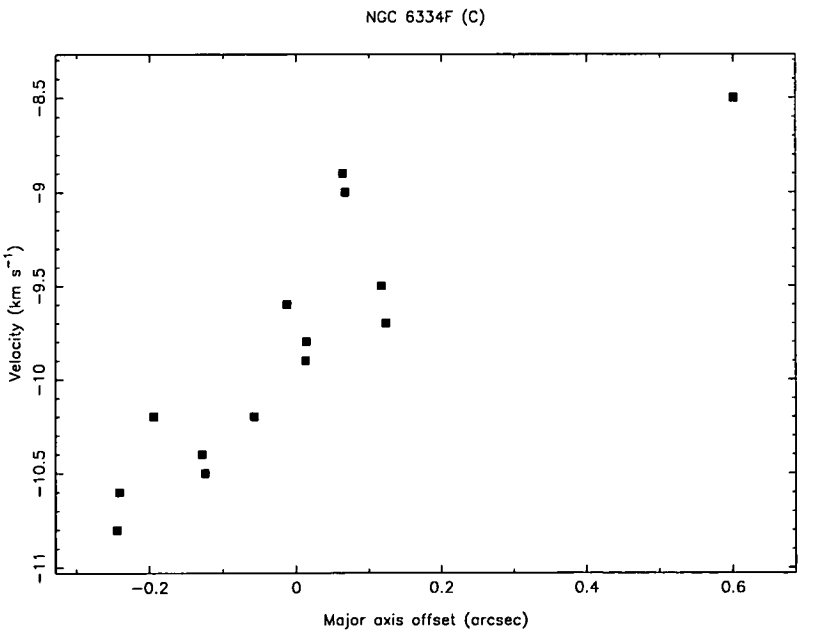

Figure 7.13: Major axis offset versus velocity diagram combining the 6.7- and 12.2-GHz CH_3OH masers from NGC 6334F (C).

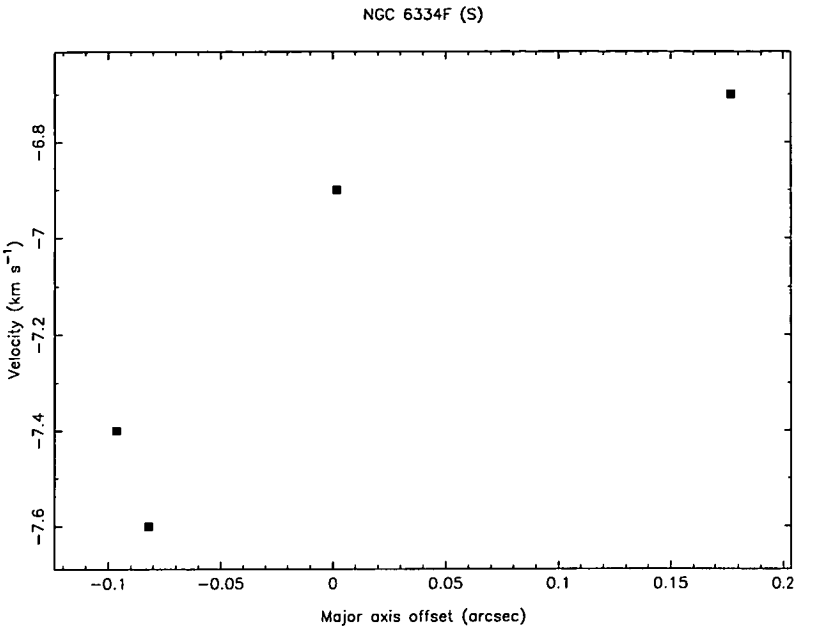

Figure 7.14: Major axis offset versus velocity diagram combining the 6.7- and 12.2-GHz CH_3OH masers from NGC 6334F (S).

detected any emission stronger than 0.3 mJy beam^{-1} associated with the CH_3OH masers. Figs. 7.15 and 7.16 shows the distribution of 12.2-GHz CH_3OH masers associated with G335.79+0.17. The total spatial extent of the 12.2-GHz CH_3OH maser emission is 550 mas in Right Ascension and 300 mas in Declination, but the majority of the emission emanates from a region which is only 110 by 100 mas. Table 7.5 lists the position, flux density and velocity of each of the 12.2-GHz CH_3OH maser spots.

Figure 7.17 compares the total-power spectrum of the 12.2-GHz CH_3OH masers associated with G335.79+0.17 with the cross-correlation spectrum for the Parkes-DSS43 baseline. The cross-correlation spectrum is similar to that observed by McCutcheon *et al.* (1988) on the same baseline. Figure 7.18 shows that some, but not all, of the reduction in amplitude of the cross-correlation spectrum is due to destructive interference between spatially separated components with similar velocities. The offset in the baseline of the cross-correlation spectrum is due to noise bias (see Section 7.2).

G335.79+0.17 is another strong class II CH_3OH maser which shows a roughly linear spatial morphology. However, examination of Fig 7.16 shows that the change in velocity is not monotonic. Fig 7.19 shows that the maser spots clearly lie in only two quadrants of the major axis velocity diagram, which is consistent with the masers originating in a circumstellar disc. In general class II CH_3OH masers do not show a double or triple peaked spectrum as is observed for the H_2O masers associated with NGC 4258 (Miyoshi *et al.*, 1995). For G335.79+0.17 there are two masers offset from the majority of the emission in both position and velocity. This may indicate that we are detecting maser emission from the two tangential regions of the disc, but not the central region.

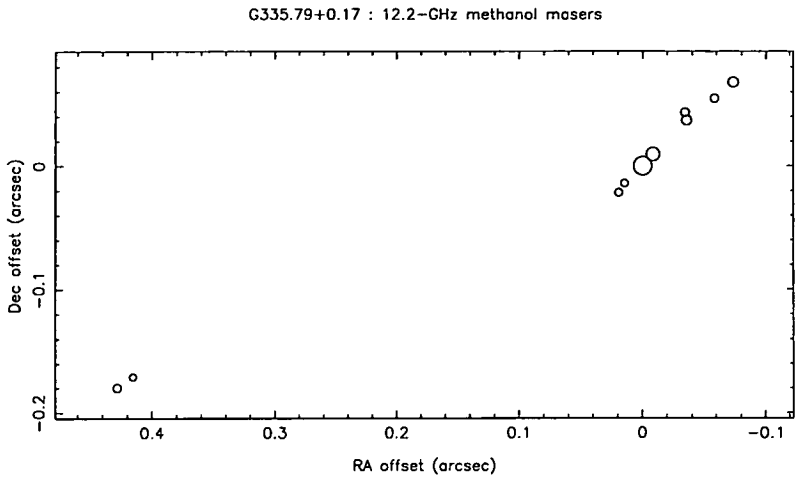

Figure 7.15: The relative positions of the 12.2-GHz CH_3OH masers associated with G335.79+0.17. The area of the circle marking the position of each maser spot is proportional to its flux density. The images were made using a 9.1 x 4.5 mas synthesised beam.

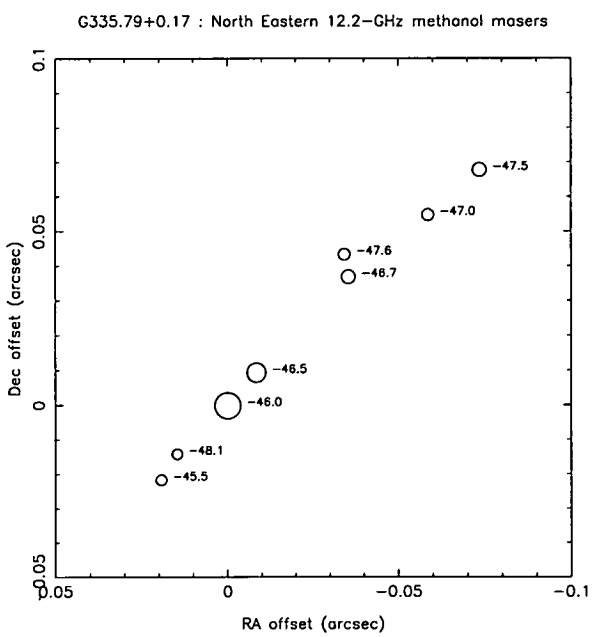

Figure 7.16: The relative positions of the North Western 12.2-GHz CH_3OH masers in G335.79+0.17. The area of the circle marking the position of each maser spot is proportional to its flux density and each spot is labeled with its LSR velocity in km s^{-1}.

Table 7.5: The positions, flux density and velocity of the 12.2-GHz CH_3OH masers associated with G335.79+0.17. The positions are relative to RA(J2000)=$16^h29^m47^s.330$, Dec(J2000)=-48°15′52″.42.

Right Ascension offset (arcsec)	Declination offset (arcsec)	Flux Density (Jy)	Velocity (km s^{-1})
0.0194	-0.0215	2.0	-45.5
0.0000	0.0000	12.7	-46.0
-0.0084	0.0095	6.5	-46.5
-0.0354	0.0370	3.3	-46.7
-0.0585	0.0549	2.4	-47.0
-0.0734	0.0679	3.4	-47.5
-0.0342	0.0435	2.4	-47.6
0.0148	-0.0140	1.9	-48.1
0.4281	-0.1796	2.4	-49.8
0.4155	-0.1707	1.7	-50.0

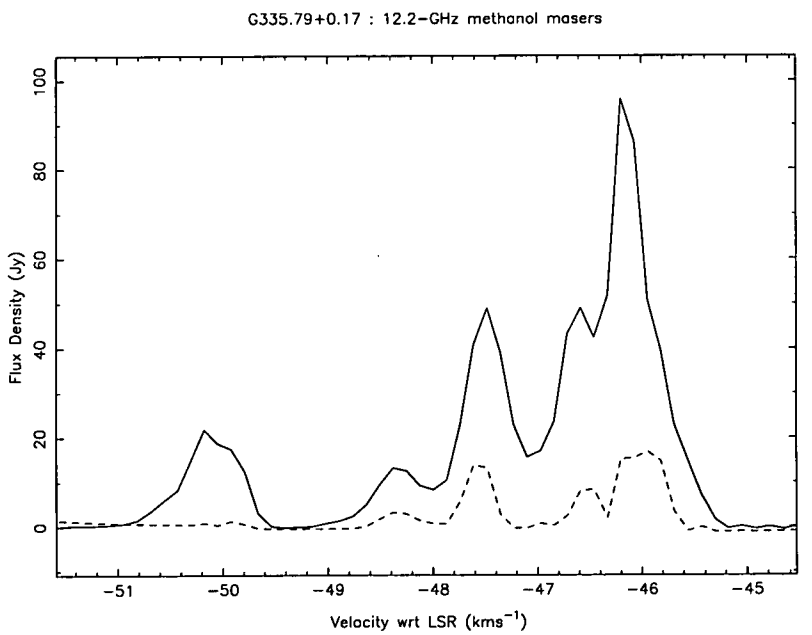

Figure 7.17: The solid line is the total-power spectrum of the 12.2-GHz CH_3OH maser G335.79+0.17, observed with the Parkes antenna. The dashed line is a scalar averaged cross-power spectrum for the Parkes-DSS43 baseline. Both spectra are uniformly weighted and have a velocity resolution of 0.15 km s^{-1}.

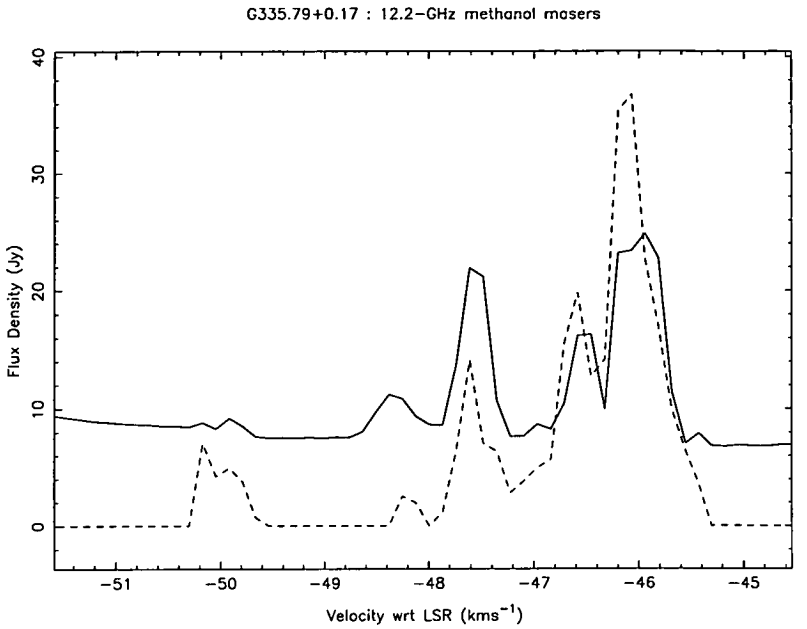

Figure 7.18: The solid line is a scalar averaged cross-power spectrum of the 12.2-GHz CH_3OH maser G335.79+0.17 for the Parkes-DSS43 baseline. The dashed line is the spectrum of the total flux density in each imaged channel. For a number of the channels the imaged flux density exceeds that of the cross-correlation spectrum, but it is still significantly less than the flux density for the total-power spectrum. The offset in the baseline of the cross-correlation spectrum is caused by noise bias (see Section 7.2).

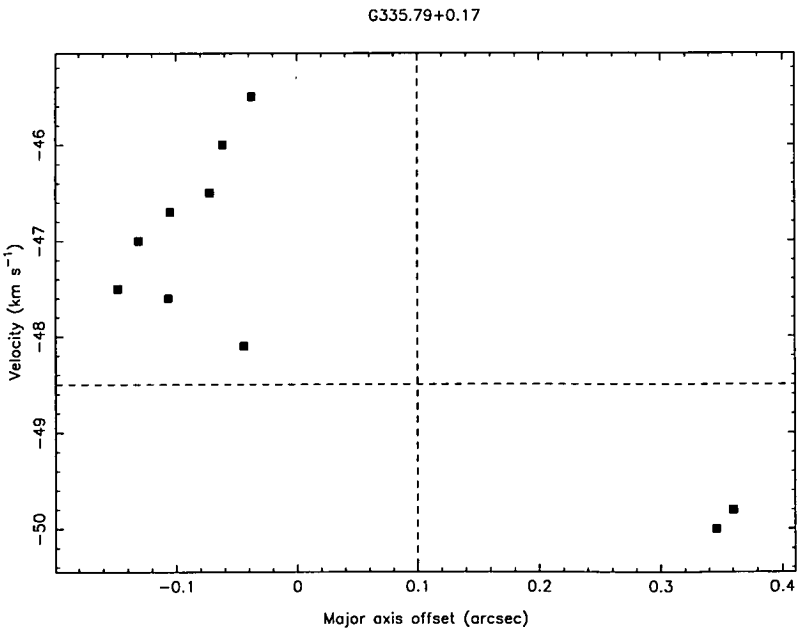

Figure 7.19: Major axis offset versus velocity diagram for G335.79+0.17 12.2-GHz CH_3OH masers).

7.3.3 Comparison of 6.7- and 12.2-GHz maser positions

The spectral morphology of 6.7- and 12.2-GHz CH_3OH masers is often observed to be quite similar (Menten, 1991a; Caswell *et al.*, 1995c). If many of the individual maser spots at 6.7 and 12.2 GHz have the same line of sight velocities, then it seems logical to assume that they arise from the same general area of the star formation region. Observations by Menten *et al.* (1992) and Norris *et al.* (1993) found the positions of some 6.7- and 12.2-GHz CH_3OH masers to be coincident to within the positional errors of their observations. As has been noted by Menten *et al.*, this provides a stringent constraint on any pumping mechanism, as any scheme which produces 6.7-GHz CH_3OH masers must also be able to produce 12.2-GHz CH_3OH masers and *vice versa.*

Figs. 7.1 and 7.2 show the 6.7- and 12.2-GHz CH_3OH maser emission associated with the HII region NGC 6334F. Comparison of these two images shows that the 12.2-GHz masers are also observed in two of the three clusters which show 6.7-GHz CH_3OH maser emission, but close coincidence of individual spots is not obvious. However, a detailed examination shows that 5 of the nine 12.2-GHz CH_3OH maser spots are coincident (to within $\approx$ 4 mas) with a 6.7-GHz CH_3OH maser spot which has the same velocity (see Table 7.3.3). Figure 7.20 shows four of the five maser spots which are coincident for the two transitions. The rms difference between the positions of the five masers at 6.7 and 12.2 GHz is 3.7 mas, which is comparable to the relative positional accuracy. Thus it appears that the emission from the two transitions is truly coincident. This is supported by the observations of Menten *et al.* (1992) which had greater resolution and found positional coincidence to within 1–2 mas. Further supporting evidence is that the rms difference between the 6.7- and 12.2-GHz positions I observed is dominated by the Right Ascension offset (3.6 mas as opposed to 0.7 mas for the Declination offset) and the beam shape of these observations was significantly elongated in Right Ascension.

If I assume that the five maser spots are coincident, then the observed difference in the positions at the two frequencies, will depend upon the accuracy to which the relative positions of the maser spots have been estimated by the processing technique outlined in Section 7.2. As the 6.7-GHz observation did not use phase referencing and had a larger synthesized beam, it would be expected to have greater errors in the relative positions of the masers than the 12.2-GHz observation. If it is assumed that the difference in the positions of the coincident spots is due purely to the errors in relative positions of the masers at 6.7-GHz then this implies errors of 17% and 5% of the synthesized beam for the Right Ascension and Declination components respectively. This is similar to the range determined by Conway *et al.* (1992) (see Section 7.2).

Unfortunately there are no published 6.7-GHz CH_3OH maser observations of G335.79+0.17 which have resolution comparable to my 12.2-GHz CH_3OH maser observations. Phillips *et al.* (1996) have used the ATCA to image the 6.7-GHz CH_3OH masers and they observe the spatial morphology to be similar to that which I observe at 12.2 GHz. However, as for the 12.2-GHz masers, most of the strong 6.7-GHz CH_3OH maser emission arises from a very compact region. For this compact region, the blending of features is severe with the large synthesized

Table 7.6: Table of coincident 6.7- and 12.2-GHz CH_3OH masers for NGC 6334F.

6.7-GHz CH_3OH masers				12.2-GHz CH_3OH masers				Difference	
Velocity LSR (km s^{-1})	RA offset (arcsec)	Dec offset (arcsec)	Flux Density (Jy)	Velocity LSR (km s^{-1})	RA offset (arcsec)	Dec offset (arcsec)	Flux Density (Jy)	RA offset (arcsec)	Dec offset (arcsec)
-11.1	0.0000	0.0000	129	-11.3	0.0000	0.0000	246	0.0000	0.0000
-10.6	2.2999	-2.7332	9	-10.8	2.2943	-2.7346	14	0.0056	0.0014
-10.4	2.3168	-2.3573	76	-10.5	2.3192	-2.3588	38	-0.0024	0.0015
-9.9	2.4548	-2.3049	4	-9.8	2.4536	-2.3055	3	0.0012	0.0006
-9.0	2.5009	-2.2602	4	-8.9	2.4951	-2.2620	1	0.0058	0.0018

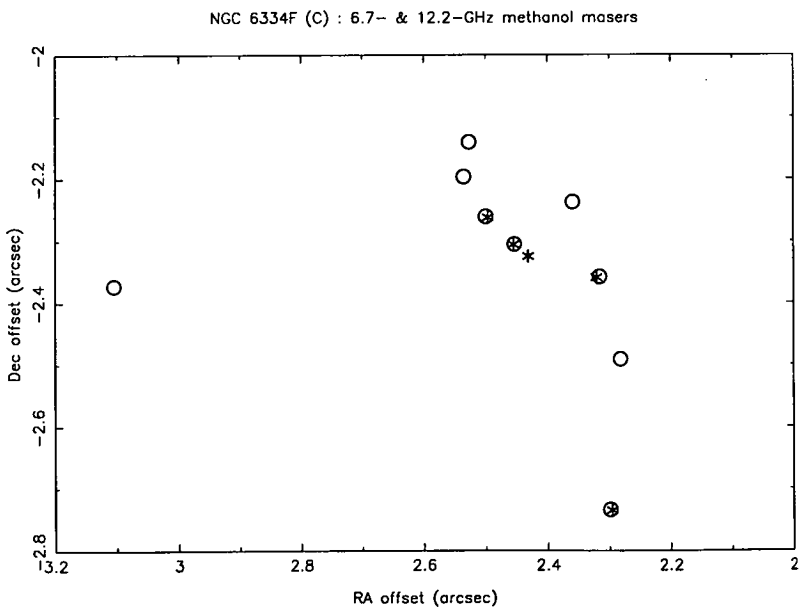

Figure 7.20: The relative positions of the 6.7-GHz CH_3OH masers associated with NGC 6334F (C) are marked by open circles and the 12.2-GHz CH_3OH masers are marked by stars.

beam of the ATCA and makes any detailed comparison of the positions of the 6.7- and 12.2-GHz CH_3OH masers impossible.

7.3.4 The size of 6.7- and 12.2-GHz CH_3OH masers

Figs. 7.8, 7.10 & 7.17 show that for the imaging observations the amplitude of the cross-correlation spectra for both short and long baselines is significantly reduced compared to the total-power spectra. This is consistent with other milliarcsecond resolution observations of class II methanol masers (McCutcheon *et al.*, 1988; Menten *et al.*, 1988; Menten *et al.*, 1992). Figs. 7.21 and 7.22 show plots of visibility versus baseline for one or more spectral channels from each of the eight 6.7-GHz and six 12.2-GHz CH_3OH masers observed. For the 12.2-GHz observations, some of the antennas used linearly polarized feeds, while the others used right circularly polarized feeds (see Table 7.1). As previously stated, for baselines using different feed types on the two antennas the correlated amplitude is reduced by a factor of $\sqrt{2}$, and the data displayed in Figure 7.22 has been corrected to account for this. Due to antenna motor problems I was only able to observe five of the eight 6.7-GHz and two of the six 12.2-GHz CH_3OH masers on baselines including Hartebeesthoek. None of the CH_3OH maser sources at either frequency was detected on baselines including Hartebeesthoek, but the source 1921-293 was. This implies that the spot sizes of the CH_3OH masers are greater than the minimum fringe spacing for the Parkes-Hartebeesthoek baseline, which is $\approx$ 0.1 mas at 6.7 GHz and $\approx$ 0.06 mas at 12.2 GHz.

The visibility-versus-baseline plots in Figs 7.21 and 7.22 can be classified into three categories. The first category contains those for which the short baselines show an increasing visibility with increasing baseline length, the best example of this is Figure 7.21(a). The second category contains those which have relatively constant visibility for all the observed baseline, for example Figure 7.21(b). The third contains those which have a constant or slightly decreasing visibility on the short baselines and constant visibility but lesser visibility on the longer baselines, for example Figure 7.21(i). The visibilities of maser spots are usually modelled as either point sources, which have constant visibility with baseline, or scatter-broadened point sources for which the visibility versus baseline has a Gaussian profile. Clearly the visibility versus baseline plots I have observed for 6.7- and 12.2-GHz CH_3OH masers conform to neither of these models. Where possible I have fitted a Gaussian profile to the visibilities, but this is merely an aid to estimating the size of some of the structure present in the maser spots rather than a serious attempt to model the visibilities.

7.3.4.1 Calibration of the visibility data

The observed variation of visibility with baseline for the 6.7- and 12.2-GHz CH_3OH maser spots is quite different from that of other types of masers [see for example van Langevelde (1992)] and for this reason calibration errors must be considered as a potential explanation. There are four pieces of evidence that suggest that the basic calibration of the data is correct :

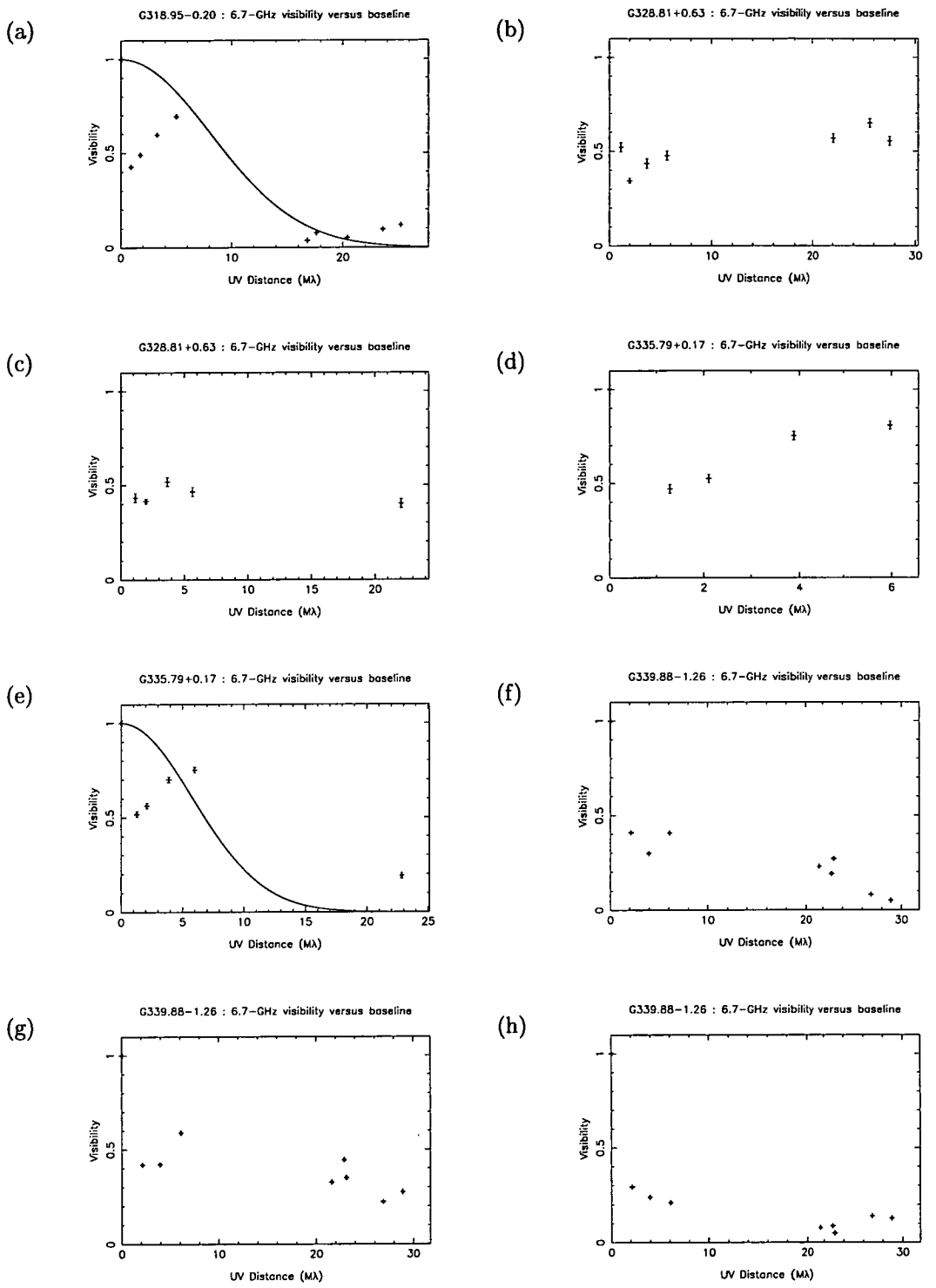

Figure 7.21: Visibility versus baseline for 6.7-GHz CH_3OH masers. The observations were made with a velocity resolution of 1.12 km s^{-1}.

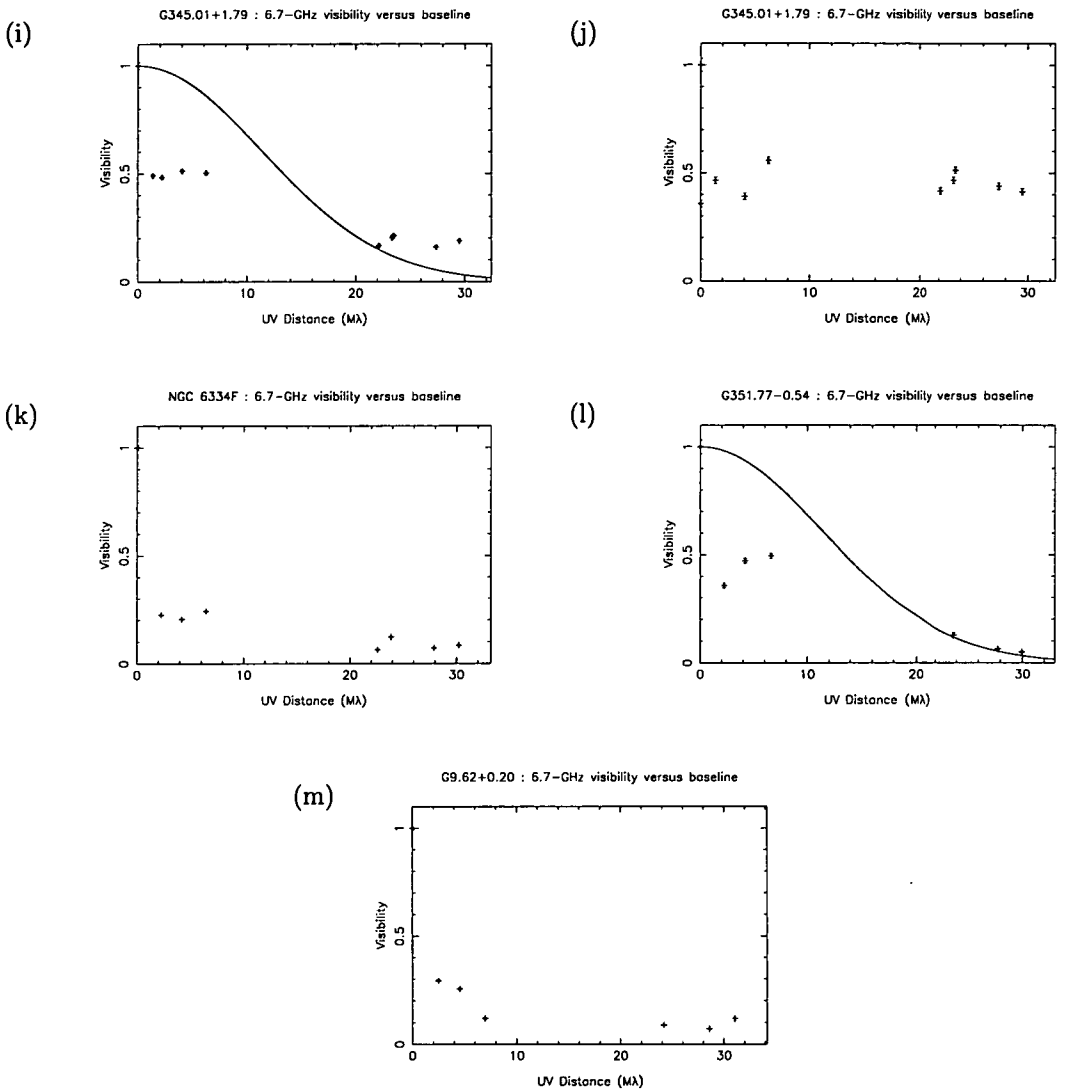

Figure 7.21: *continued...*

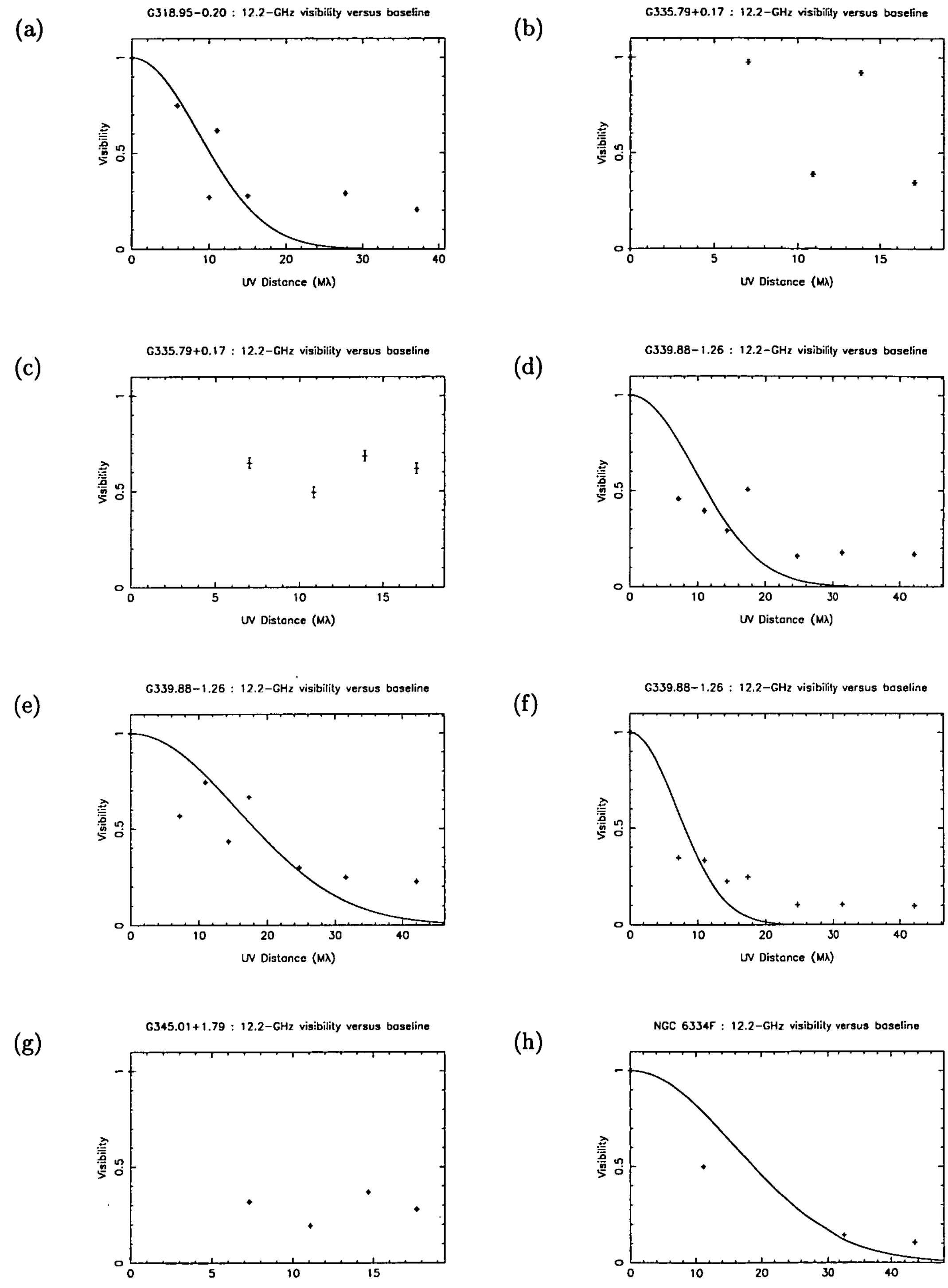

Figure 7.22: Visibility versus baseline for 12.2-GHz CH_3OH masers. The observations were made with a velocity resolution of 0.61 km s^{-1}.

(i)

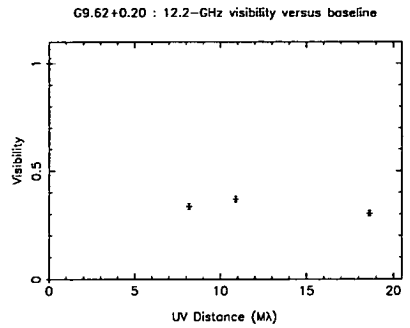

Figure 7.22: *continued...*

1. For each of the sources I have examined the total-power spectrum for each antenna and they have essentially the same peak flux density. This is not the case prior to amplitude calibration and indicates that the relative gains of each antenna have been correctly calculated by ACFIT.

2. The imaging data agrees very well with previous high resolution observations, and is internally self consistent (some of the 6.7- and 12.2-GHz maser spots for NGC 6334F are coincident to within the errors). This shows that the procedure used to calibrate the imaging data (which is the same as that used to calibrate the visibility data) has worked correctly.

3. Other milliarcsecond resolution observations of class II CH_3OH masers have shown the cross-correlation spectra on short baselines to have significantly less flux than the total-power spectra (McCutcheon *et al.*, 1988; Menten *et al.*, 1988; Menten *et al.*, 1992). The 12.2-GHz observations of G309.92+0.48 by Norris *et al.* (1996) are the only exception, as in general the total flux in their images agreed well with the total-power spectrum, but one feature appears largely resolved on all baselines.

4. Fig 7.23 compares the visibility data from Fig 7.22(h) with the imaging data from Fig 7.25(e). While the agreement between the two sets of points is far from perfect, it is quite good for two of the three UV distances for which a comparison is possible. The differences may be due to a greater blending of features in the visibility data, or because the velocity of the spectral channels for the two observations was slightly different.

I conclude from the evidence above that the observed variation of visibility with baseline is probably not an artifact of the calibration procedures, but that it cannot be completely ruled out. Further observations, preferably with greater spectral resolution, some shorter baselines and a larger number of antennas are required to confirm these observations. For the purposes of the present discussion I will assume that the visibility observations are correct. However, a significant reduction in the cross-correlation spectrum for short baselines compared to the total-power

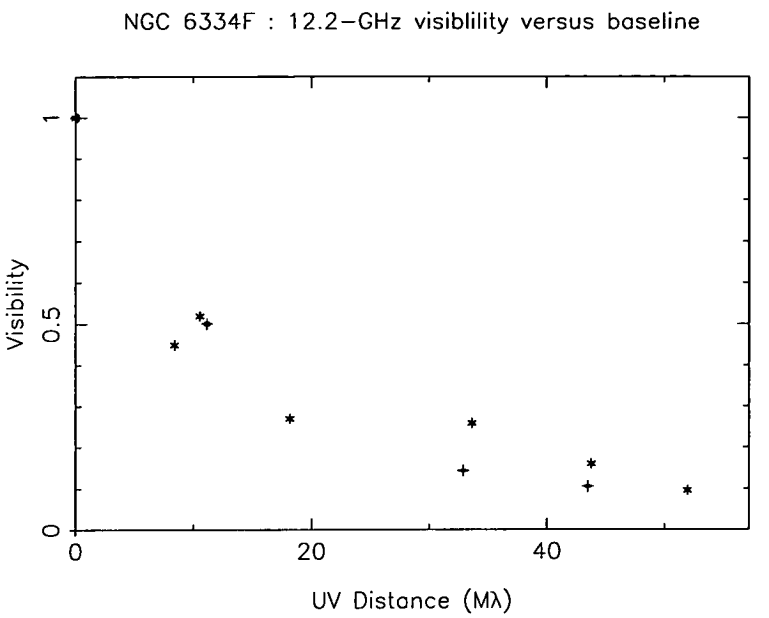

Figure 7.23: Visibility versus baseline for the 12.2-GHz CH_3OH masers associated with NGC 6334F. The crosses are data from the visibility experiment and the stars are from the imaging experiment.

spectrum has been observed by independent investigators and is almost certainly a real effect.

7.3.4.2 Interpretation

If the unexpected variation of visibility with baseline is not due to calibration errors, then what is the cause? Some of the unusual behavior for short baselines is almost certainly due to blending of features within a spectral channel. The limited number of spectral channels available in the NRAO MKII correlator and the need to cover a wide velocity range means that the velocity resolution, particularly at 6.7-GHz, is very coarse. If blending of features is the cause of the increasing visibility with increasing baseline observed in several of the 6.7-GHz sources then it should be reduced, in visibility-versus-baseline plots from the higher spectral resolution imaging observations. However, it can still occur when two maser features have an overlapping velocity range. In order to check this I have produced visibility versus baseline plots for several of the strongest features from each of the imaging experiments (see Figs. 7.24 & 7.25). Particularly at 12.2-GHz where the velocity resolution is greatest, increasing visibility with increasing baseline length seems to be absent.

While in general the visibility versus baseline data is rather difficult to interpret, the plots from the 12.2-GHz imaging data, in particular, suggest a core-halo model, as the visibility drops rapidly on the short baselines, but then remains relatively constant on the longer baselines. Where a fit of a Gaussian profile has been possible I use the FWHM of this Gaussian as an crude estimate of the scale of the halo. An upper limit on the size of the core can be obtained from the maximum

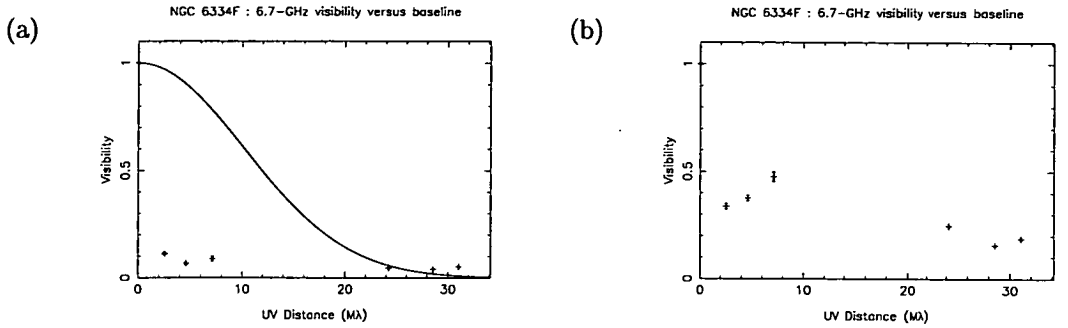

Figure 7.24: Visibility versus baseline for 6.7-GHz CH_3OH masers observed during imaging experiments. These observations were made with a velocity resolution of 0.28 km s^{-1}.

baseline length displayed in the plots and a lower limit by assuming that all the masers are resolved on baselines to Hartebeesthoek. This information is summarized in Tables 7.7 & 7.8 which show that the most compact structure present in 6.7- and 12.2-GHz methanol masers has a linear size of between a few, and ten or so astronomical units. The linear sizes are similar for both the 6.7- and 12.2-GHz CH_3OH masers, which implies that they are not being broadened by interstellar scattering. The rough estimates for the linear size of the halo component are typically of the order of a few tens of astronomical units, which suggests that in the gas from which the 6.7- and 12.2-GHz CH_3OH masers originate there are large regions which must be much less turbulent than expected, and this may present problems for the circumstellar disc model. An alternative explanation is that the masers are scattered. Although this appears to contradict my earlier statement, the constraints on the maser sizes at the two frequencies are not very tight. In addition, while OH masers do not emanate from the same positions as CH_3OH masers (Menten *et al.*, 1992), they are closely associated (Caswell *et al.*, 1995d). This raises the question : why don't we see a similar phenomenon in OH masers associated with star formation regions?

7.4 Conclusions

I have made milliarcsecond resolution images of the 6.7- and 12.2-GHz CH_3OH maser emission associated with the well known star formation region NGC 6334F. The images agree well with previous lower resolution observations, but detect approximately double the number of spots seen in the earlier work. Comparison of the relative positions of the 6.7- and 12.2-GHz maser spots shows that 5 of them are coincident to within the positional accuracy of these observations ($\approx$ 4 mas). Menten *et al.* (1992) observed similar positional coincidence for W3(OH) and in each case the flux density of the 6.7-GHz maser spot was greater than that of the 12.2-GHz CH_3OH maser spot. This is not the case for NGC 6334F, for which several of the coincident maser spots have a larger 12.2-GHz flux density than that at 6.7-GHz. Also I detected several 12.2-GHz CH_3OH maser spots with

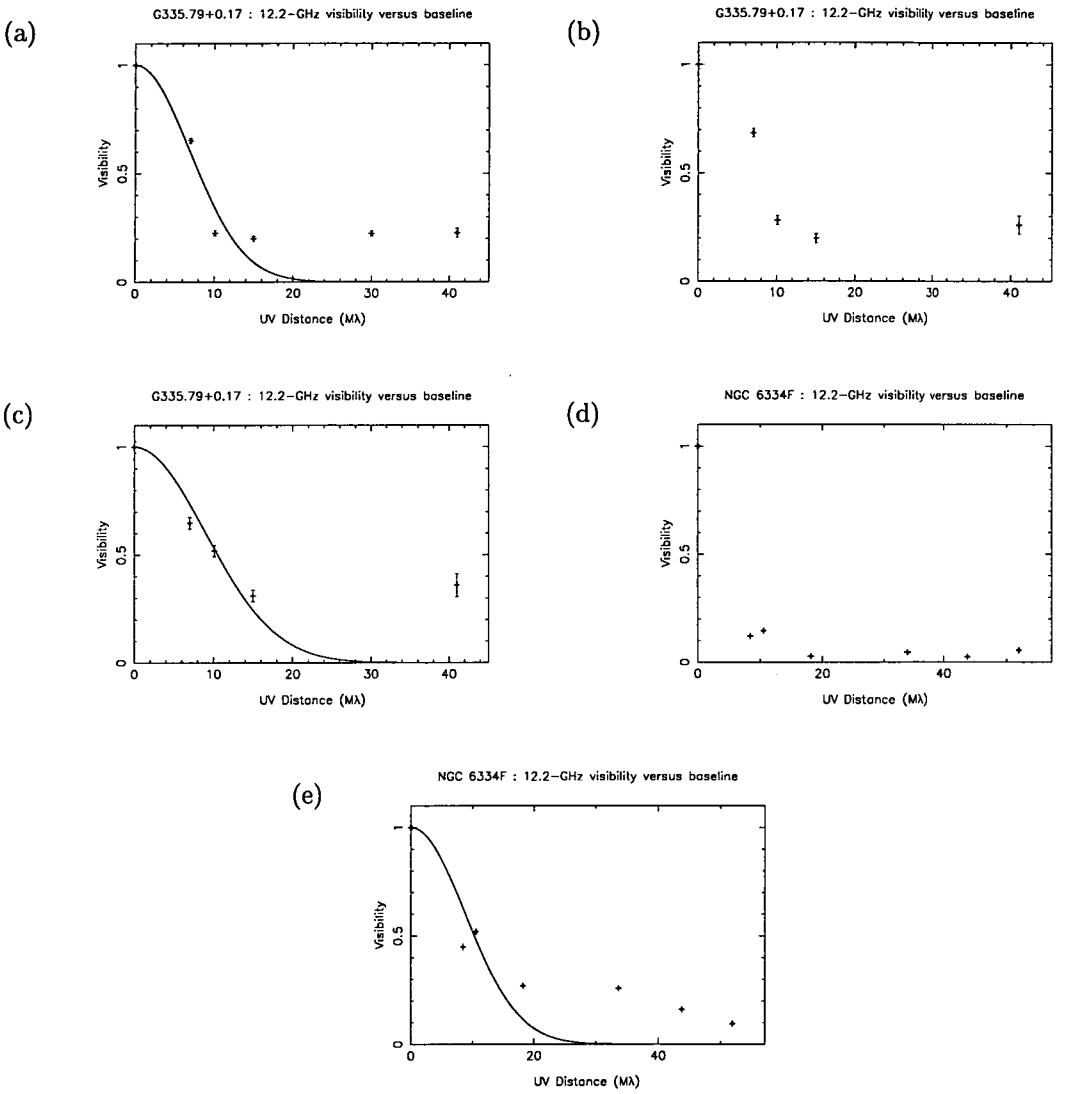

Figure 7.25: Visibility versus baseline for 12.2-GHz CH_3OH masers observed during imaging experiments. These observations were made with a velocity resolution of 0.15 km s^{-1}.

Table 7.7: A summary of the 6.7-GHz CH_3OH maser spot size results. * = Visibility information obtained from imaging experiment.

Source Name	Distance (kpc)	Velocity (km s^{-1})	Fig. #	θ_{halo} (mas)	θ_{core} (mas)	R_{halo} (AU)	R_{core} (AU)
G318.95-0.20	2.0	-34.7	7.21(a)	1.09	$0.10 < \theta_{core} < 0.80$	21.8	$1.92 < R_{core} < 16.4$
G328.81+0.63	3.1	-44.9	7.21(b)		$0.10 < \theta_{core} < 0.75$		$2.97 < R_{core} < 23.3$
G328.81+0.63	3.1	-46.7	7.21(c)		$0.10 < \theta_{core} < 0.93$		$2.97 < R_{core} < 28.9$
G335.79+0.17	3.3	-46.6	7.21(d)		$0.10 < \theta_{core} < 4.12$		$3.17 < R_{core} < 136.0$
G335.79+0.17	3.3	-48.5	7.21(e)	1.52	$0.10 < \theta_{core} < 0.90$	50.0	$3.17 < R_{core} < 29.9$
G339.88-1.26	3.0	-35.0	7.21(f)		$0.10 < \theta_{core} < 0.71$		$2.88 < R_{core} < 21.4$
G339.88-1.26	3.0	-36.9	7.21(g)		$0.10 < \theta_{core} < 0.71$		$2.88 < R_{core} < 21.4$
G339.88-1.26	3.0	-37.8	7.21(h)		$0.10 < \theta_{core} < 0.71$		$2.88 < R_{core} < 21.4$
G345.01+1.79	2.3	-17.9	7.21(i)	0.77	$0.10 < \theta_{core} < 0.70$	17.8	$2.20 < R_{core} < 16.1$
G345.01+1.79	2.3	-22.6	7.21(j)		$0.10 < \theta_{core} < 0.70$		$2.20 < R_{core} < 16.1$
NGC 6334F	1.7	-11.4	7.21(k)		$0.10 < \theta_{core} < 0.68$		$1.63 < R_{core} < 11.6$
NGC 6334F*	1.7	-10.4	7.24(a)	0.58	$0.10 < \theta_{core} < 0.67$	9.8	$1.63 < R_{core} < 11.3$
NGC 6334F*	1.7	-11.3	7.24(b)		$0.10 < \theta_{core} < 0.67$		$1.63 < R_{core} < 11.3$
G351.77-0.54	2.2	1.0	7.21(l)		$0.10 < \theta_{core} < 0.69$		$2.11 < R_{core} < 15.1$
G9.62+0.20	2.0	1.3	7.21(n)	0.76	$0.10 < \theta_{core} < 0.66$	15.3	$1.92 < R_{core} < 13.3$

Table 7.8: A summary of the 12.2-GHz CH_3OH maser spot size results. * = Visibility information obtained from imaging experiment.

Source Name	Distance (kpc)	Velocity (km s^{-1})	Fig. #	θ_{halo} (mas)	θ_{core} (mas)	R_{halo} (AU)	R_{core} (AU)
G318.95-0.20	2.0	-34.5	7.22(a)	1.02	$0.06 < \theta_{core} < 0.56$	20.4	$1.17 < R_{core} < 11.1$
G335.79+0.17	3.3	-46.2	7.22(b)		$0.06 < \theta_{core} < 1.21$		$1.92 < R_{core} < 40.0$
G335.79+0.17	3.3	-47.2	7.22(c)		$0.06 < \theta_{core} < 1.21$		$1.92 < R_{core} < 40.0$
G335.79+0.17*	3.3	-46.2	7.25(a)	1.27	$0.06 < \theta_{core} < 0.50$	42.0	$1.92 < R_{core} < 16.6$
G335.79+0.17*	3.3	-46.6	7.25(b)		$0.06 < \theta_{core} < 0.50$		$1.92 < R_{core} < 16.6$
G335.79+0.17*	3.3	-47.5	7.25(c)	0.98	$0.06 < \theta_{core} < 0.50$	32.3	$1.92 < R_{core} < 16.6$
G339.88-1.26	3.0	-34.1	7.22(d)	0.57	$0.06 < \theta_{core} < 0.49$	17.0	$1.74 < R_{core} < 14.7$
G339.88-1.26	3.0	-35.1	7.22(e)	0.92	$0.06 < \theta_{core} < 0.49$	27.5	$1.74 < R_{core} < 14.7$
G339.88-1.26	3.0	-38.7	7.22(f)	0.79	$0.06 < \theta_{core} < 0.49$	38.3	$1.74 < R_{core} < 14.7$
G345.01+1.79	2.3	-22.0	7.22(g)		$0.06 < \theta_{core} < 1.61$		$1.34 < R_{core} < 26.8$
NGC 6334F	1.7	-10.9	7.22(h)	0.55	$0.06 < \theta_{core} < 0.47$	9.3	$0.99 < R_{core} < 8.0$
NGC 6334F*	1.7	-10.5	7.25(d)		$0.06 < \theta_{core} < 0.40$		$0.99 < R_{core} < 6.8$
NGC 6334F*	1.7	-11.3	7.25(e)	1.00	$0.06 < \theta_{core} < 0.40$	17.0	$0.99 < R_{core} < 6.8$
G9.62+0.20	2.0	1.3	7.22(i)		$0.06 < \theta_{core} < 1.11$		$1.16 < R_{core} < 22.2$

no coincident 6.7-GHz emission. This implies that although the 6.7-GHz CH_3OH masers usually have a greater flux density than their 12.2-GHz counterparts there exist regions within the gas cloud where the conditions are more favourable for 12.2- than 6.7-GHz CH_3OH maser emission. Further milliarcsecond resolution observations of both 6.7- and 12.2-GHz CH_3OH masers are required to determine the distribution of 6.7:12.2-GHz CH_3OH flux density ratios. If conditions which give rise to the various observed ratios can be determined then VLBI images of class II CH_3OH masers will allow the physical conditions of the star formation region to be probed with unprecedented resolution.

I have also carried out an experiment to measure the size of the 6.7- and 12.2-GHz CH_3OH maser spots. Surprisingly they both appear to have large scale structure, which is not observed for other maser species. The presence of large scale structure implies that the turbulence in the gas producing the CH_3OH masers must be much lower than expected, or that there is a large scattering disc. The CH_3OH masers also have smaller scale structure which has a linear size somewhere in the range of a few to ten or so astronomical units. The linear sizes of the 6.7- and 12.2-GHz masers are similar, which may indicate that they are not significantly broadened by interstellar scattering. Although these findings are in general agreement with other milliarcsecond resolution observations of class II CH_3OH masers (McCutcheon *et al.*, 1988; Menten *et al.*, 1988; Menten *et al.*, 1992), further work with higher spectral resolution and better UV coverage are required to confirm these observations. At 12.2 GHz, the VLBA is an ideal instrument for this type of observation and at 6.7 GHz the high spectral resolution of the Australian ad hoc VLBI network, using the S2 recording format, should enable a more accurate determination of the variation in visibility with baseline.

Chapter 8

Conclusions and further work

This thesis has presented new findings relating to three different aspects of the study of class II CH_3OH masers in star formation regions, and a preliminary search for extragalactic maser emission from the 6.7-GHz 5_1-6_0 A^+ transition of CH_3OH. The results presented include the first complete, large scale untargeted survey for any masing transition of CH_3OH. Very few similar searches have been performed for any species of maser. Observations of class II CH_3OH masers and their environments have been made at three different resolutions, using individual radiotelescopes, connected element interferometers and very long baseline interferometers.

8.1 Extragalactic CH_3OH masers

Two searches for 6.7-GHz CH_3OH masers toward a total of 115 star formation regions in the Magellanic clouds have resulted in 3 detections (Ellingsen *et al.*, 1994b; Beasley *et al.*, 1996). The second of these searches was toward *IRAS* sources which satisfy the criteria outlined by Wood and Churchwell (1989a) and detected 2 masers from 75 sources searched. Similar Galactic searches typically detected CH_3OH maser emission toward 13–17% of the *IRAS* sources searched. However, when the relative sensitivity of the two searches is taken into consideration their appears to be little difference between the detection rates in the two samples. Searches for OH and H_2O masers in the Magellanic clouds have also been relatively unsuccessful and lower metallicity has been suggested as a possible cause. It is unclear from these observations whether the Magellanic Clouds are deficient in CH_3OH masers compared with the Galaxy, but an increase in the sensitivity of the *IRAS* based search by a factor of 2 or more would allow a more meaningful comparison with Galactic searches towards the sources selected using the same criteria.

A search for 6.7-GHz CH_3OH maser emission toward 10 extragalactic sources failed to detect emission or absorption toward any of them (Ellingsen *et al.*, 1994a). Of the sources searched, 8 of the 10 exhibit OH or H_2O maser emission. These observations show that if luminous extragalactic 6.7-GHz CH_3OH masers exist, they are not associated with either OH or H_2O megamaser emission.

8.2 A search for 6.7-GHz CH_3OH masers

A two year search for 6.7-GHz CH_3OH masers toward several regions of the Galactic Plane has detected 108 sources (Ellingsen *et al.*, 1996b). Of the 108 6.7-GHz CH_3OH masers detected, 57 (53%) were discovered by this survey and this percentage of new detections is relatively constant for all regions searched. Extrapolating this result to the entire Galaxy implies that there are more than 650 detectable 6.7-GHz CH_3OH masers in the Galaxy. Despite the large number of new masers detected, there appears to be an underabundance of weak masers, which may be due to the anisotropic distribution of masers within the regions of the Galaxy searched thus far.

By examining the infra-red colours of a sample of radio-selected UCHII regions, Wood and Churchwell (1989a) developed criteria for selecting *IRAS* source which are likely to be UCHII regions. Using these criteria they estimated that there are $\approx$ 1700 UCHII regions in the Galaxy. From a sample of 98 6.7-GHz CH_3OH masers detected in the Mt Pleasant survey, at most 34 are associated with *IRAS* sources which meet the Wood and Churchwell UCHII region criteria. Assuming that all 6.7-GHz CH_3OH masers are associated with UCHII regions, then the number of UCHII regions in the Galaxy is $>$ 5000. Therefore either the Galactic rate of massive star formation has been significantly underestimated, or the lifetime of UCHII regions is longer than present estimates, or 6.7-GHz CH_3OH masers are associated with another class of object as well as UCHII regions.

In recent years searches for masers toward *IRAS* sources selected on the basis of their colours have been very popular. I have used the results of the Mt Pleasant survey to compare the efficiency of a number of *IRAS*-based search criteria in terms of the percentage of *IRAS* sources selected which have associated maser emission, and the percentage of the total masers in the region detected by the search. The comparison shows that 32% of the masers are not associated with *IRAS* sources and that none of the commonly used *IRAS*-based search techniques detect more than 50% of the CH_3OH masers.

8.3 The UCHII regions associated with class II CH_3OH masers

The ATCA has been used to search for 8.5-GHz radio continuum emission toward three sites of strong 6.7-GHz CH_3OH maser emission (Ellingsen *et al.*, 1996a). At high resolution the three sites contain a total of five clusters of 6.7-GHz CH_3OH maser emission, only two of which have associated radio continuum. For G339.88-1.26 the 6.7-GHz CH_3OH masers lie across the diameter of the UCHII region, which supports the hypothesis that they form in the circumstellar disc. There are two main clusters of 6.7-GHz CH_3OH maser emission associated with the compact HII region NGC 6334F, which appear to be coincident within the errors with the two strongest FIR sources in the region. There is no radio continuum emission associated with the weaker of these two FIR sources, which may indicate that the object is pre-main sequence, or is ZAMS but has not yet developed a detectable

UCHII region.

8.4 Milli-arcsecond resolution observations of class II CH_3OH masers

VLBI images have been made of the 6.7- and 12.2-GHz CH_3OH masers associated with NGC 6334F and of the 12.2-GHz CH_3OH masers associated with G335.79+0.17 have been made. The class II CH_3OH masers associated with NGC 6334 have previously been imaged at lower resolution. The VLBI images revealed approximately double the number of maser spots detected in the previous observations, but the new spots do not deviate significantly from the structures observed in the lower resolution images. This supports the findings of Norris *et al.* (1996) that lower resolution synthesis images accurately portray the general morphology of the masers. Comparison of the 6.7- and 12.2-GHz CH_3OH maser positions for NGC 6334F shows that 5 of the 9 12.2-GHz maser spots are coincident with a 6.7-GHz maser spot to within the positional accuracy of the observations ($\approx$ 4 mas). Unlike the case for W3(OH) (Menten *et al.*, 1992) the 12.2-GHz CH_3OH masers are in some cases stronger than the associated 6.7-GHz masers. This suggests that the physical conditions within each cluster of masers varies significantly

For each of the imaging observations the cross-correlation spectrum, even for the shortest baselines has a significantly lower flux density than the total-power spectrum. Further, the total imaged flux density agrees well with the cross-correlation spectrum, which suggests that the difference between cross-correlation and total-power spectrum cannot be explained solely in terms of destructive interference between separated maser spots with similar velocities. The same phenomena has been observed by Menten *et al.* (1988; 1992) in 6.7- and 12.2-GHz VLBI imaging of W3(OH). These findings are in agreement with the experiment performed to try and measure the size of the 6.7- and 12.2-GHz CH_3OH maser spots. The results of this experiment are quite difficult to interpret due to the poor spectral resolution of the observations, but they suggest that the masers contain structure on two scales. The majority of the emission seems to be associated with structure which has a scale $\gtrsim$ 10 AU, with between 10–50% of the emission contained in a core with dimensions between a few and ten astronomical units. The linear sizes of both the large and small scale components for 6.7- and 12.2-GHz CH_3OH masers appear to be similar, which may indicate that they are not broadened by interstellar scattering.

8.5 Further work

This thesis has presented several new and interesting findings regarding class II CH_3OH masers, but it has also raised a number of interesting questions which are worthy of further investigation. These include :

- Are all class II CH_3OH masers associated with UCHII regions? If not, what other types of objects are they associated with?
- Are there OH, H_2O and other class II CH_3OH masers associated with the newly detected 6.7-GHz CH_3OH masers?
- What is the luminosity distribution of 6.7-GHz CH_3OH masers and why are there less weak masers than expected?
- Where in star formation regions do the 6.7-GHz CH_3OH masers occur? The observations presented in this thesis suggest that some are projected across the centre of HII regions, consistent with the circumstellar disc hypothesis, but the observations of Caswell *et al.* (1995d) find them to be coincident with OH masers, which are typically near the edges of HII regions.
- What is the nature of the association between 6.7- and 12.2-GHz masers, what percentage of masers spots show emission from both transitions and what is the distribution of the flux density ratios? Are other class II CH_3OH transitions also coincident with the 6.7- and 12.2-GHz maser spots?
- What is the structure of the 6.7- and 12.2-GHz CH_3OH masers spots, do they really contain structure on the scale of 10's of AU?

All together the questions raised above represent many years of work, but all promise to answer yield important information about the nature of class II CH_3OH masers or massive star formation regions. While sharing some similarities with other strong maser transitions (particularly ground state OH), class II CH_3OH masers also have some unique properties which will make them very useful tools for the study of star formation.

References

Anderson, N. and Genzel, R.: 1993, in A. W. Clegg and G. E. Nedoluha (eds.), *Astrophysical Masers*, pp 97–107, Springer-Verlag, Heidelberg, Germany

Baan, W. A.: 1985, *Nat.* **315**, 26–31

Baan, W. A., Güsten, R., and Haschick, A. D.: 1986, *ApJ* **305**, 830–836

Baan, W. A., Henkel, C., Schilke, P., Mauersberger, R., and Güsten: 1990, *ApJ* **353**, 132–139

Baan, W. A., Wood, P. A. A., and Haschick, A. D.: 1982, *Astrophys. J., Lett.* **260**, L49–L52

Baart, E. E. and Cohen, R. J.: 1985, *MNRAS* **213**, 641–655

Bachiller, R. and Cernicharo, J.: 1990, *A&A* **239**, 276–286

Ball, J. A., Gottlieb, C. A., Lilley, A. E., and Radford, H. E.: 1970, *ApJ* **162**, L203–L210

Barrett, A. H., Ho, P., and Martin, R. N.: 1975, *ApJ* **198**, L119–L122

Barrett, A. H., Schwartz, P. R., and Waters, J. W.: 1971, *ApJ* **168**, L101–L106

Batchelor, R. A., Caswell, J. L., Goss, W. M., Haynes, R. F., Knowles, S. H., and Wellington, K. J.: 1980, *Aust. J. Phys.* **33**, 139–157

Batrla, W., Matthews, H. E., Menten, L. M., and Walmsley, C. M.: 1987, *Nat.* **326**, 49–51

Batrla, W. and Menten, K. M.: 1988, *ApJ* **329**, L117–L120

Beasley, A. J. and Conway, J. E.: 1995, in J. A. Zensus, P. J. Diamond, and P. J. Napier (eds.), *VLBI and the VLBA*, pp 319–334, Astronomical Society of the Pacific, San Fransisco

Beasley, A. J., Ellingsen, S. P., Claussen, M. J., and Wilcots, E.: 1996, *ApJ,* in press

Berulis, I. I. and Ershov, A. A.: 1983, *Sov. Astron. Lett.* **9**, 341–344

Bloemhof, E. E., Reid, M. J., and Moran, J. M.: 1992, *ApJ* **397**, 500–519

Bodenheimer, P., Tenorio-Tagle, G., and Yorke, H. W.: 1979, *ApJ* **233**, 85–96

Bottinelli, L., Gougeuenheim, L., Le Squeren, L., Martin, J. M., and Paturel, G.: 1987, *IAU Circ. 4379*

Braatz, J. A., Wilson, A. S., and Henkel, C.: 1994, *ApJ* **437**, L99–L102

Braz, M. A. and Sivagnanam, P.: 1987, *A&A* **181**, 19–24

Breckenridge, S. M. and Kukolich, S. G.: 1995, *ApJ* **438**, 504–505

Burke, B. F., Moran, J. M., Barett, A. H., Rydbeck, O., Hansson, B., Rodgers, A. E. E., Ball, J. A., and Cudaback, D. D.: 1968, *AJ* **73**, S27(A)

Caswell, J. L.: 1995, *MNRAS* **272**, L31–L34

Caswell, J. L.: 1996, *MNRAS,* in press

Caswell, J. L., Batchelor, R. A., Forster, J. R., and Wellington, K. J.: 1983, *Aust.*

J. Phys. **36**, 401–415
Caswell, J. L., Batchelor, R. A., Forster, J. R., and Wellington, K. J.: 1989, *Aust. J. Phys.* **42**, 331–344
Caswell, J. L., Gardner, F. F., Norris, R. P., Wellington, K. J., McCutcheon, W. H., and Peng, R. S.: 1993, *MNRAS* **260**, 425–436
Caswell, J. L. and Haynes, R. F.: 1981, *MNRAS* **194**, 33p–35p
Caswell, J. L. and Haynes, R. F.: 1983a, *Aust. J. Phys.* **36**, 417–442
Caswell, J. L. and Haynes, R. F.: 1983b, *Aust. J. Phys.* **36**, 361–399
Caswell, J. L. and Haynes, R. F.: 1987, *Aust. J. Phys.* **40**, 215–238
Caswell, J. L., Haynes, R. F., and Goss, W. M.: 1980, *Aust. J. Phys.* **33**, 639–669
Caswell, J. L. and Vaile, R. A.: 1995, *MNRAS* **273**, 328–346
Caswell, J. L., Vaile, R. A., and Ellingsen, S. P.: 1995a, *Publ. Astron. Soc. Aust.* **12(1)**, 37–54
Caswell, J. L., Vaile, R. A., Ellingsen, S. P., and Norris, R. P.: 1995b, *MNRAS* **274**, 1126–1152
Caswell, J. L., Vaile, R. A., Ellingsen, S. P., Whiteoak, J. B., and Norris, R. P.: 1995c, *MNRAS* **272**, 96–138
Caswell, J. L., Vaile, R. A., and Forster, J. R.: 1995d, *MNRAS,* in press
Cesaroni, R., Palagi, F., Felli, M., Catarzi, M., Commoretto, G., Di Franco, S., Giovanardi, C., and Palla, F.: 1988, *A&AS* **76**, 445–458
Charnley, S. B., Kress, M. E., Tielens, A. G. G. M., and Millar, T. J.: 1995, *ApJ* **448**, 232
Cheung, A. C., Rank, D. M., Townes, C. H., Thornton, D. D., and Welch, W. J.: 1969, *Nat.* **221**, 626–628
Chini, R., Kreysa, E., Mezger, P. G., and Gemünd, H. P.: 1986a, *A&A* **154**, L8–L11
Chini, R., Krügel, E., and Kreysa, E.: 1986b, *A&A* **167**, 314–324
Churchwell, E.: 1990, *A&A Rev* **2**, 79–123
Churchwell, E., Witzel, A., Huchtmeier, W., Pauliny-Toth, I., Roland, J., and Sieber, W.: 1977, *A&A* **54**, 969–971
Claussen, M. J., Heiligman, G. M., and Lo, K. Y.: 1984, *Nat.* **310**, 298–300
Claussen, M. J. and Lo, K. Y.: 1986, *ApJ* **308**, 592–559
Cohen, R. J., Baart, E. E., and Jonas, J. L.: 1988a, *MNRAS* **231**, 205–227
Cohen, R. S., Dame, T. M., Garay, G., Montani, J., Rubio, M., and Thaddeus, P.: 1988b, *ApJ* **331**, L95–L99
Conway, J. E., Pearson, T. J., Readhead, A. C. S., Unwin, S. C., Xu, W., and Mutel, R. L.: 1992, *ApJ* **396**, 62–79
Cragg, D. M., Johns, K. P., Godfrey, P. D., and Brown, R. D.: 1992, *MNRAS* **259**, 203–208
Davies, R. D., Elliot, K. H., and Meaburn, J.: 1976, *Mem. R. astr. Soc.* **81**, 89–128
De Pree, C. G., Rodríguez, L. F., Dickel, H. R., and Goss, W. M.: 1995a, *ApJ* **447**, 220
De Pree, C. G., Rodríguez, L. F., and Goss, W. M.: 1995b, *Revista Mexicana de Astronomía y Astrofísica,* in press
Deguchi, S.: 1994, *ApJ* **420**, 551–557

dos Santos, P. M. and Lépine, J. R. D.: 1979, *Nat.* **278**, 34–35
Elitzur, M.: 1992, *Astronomical Masers*, Vol. 170 of *Current research*, Kluwer Academic Publishers, Dordrecht
Ellingsen, S. P., Norris, R. P., and McCulloch, P. M.: 1996a, *MNRAS,* in press
Ellingsen, S. P., Norris, R. P., Whiteoak, J. B., Vaile, R. A., McCulloch, P. M., and Price, M. G.: 1994a, *MNRAS* **267**, 510–512
Ellingsen, S. P., von Bibra, M. L., McCulloch, P. M., Norris, R. P., Deshpande, A. A., and Phillips, C. J.: 1996b, *MNRAS,* in press
Ellingsen, S. P., Whiteoak, J. B., Norris, R. P., Caswell, J. L., and Vaile, R. A.: 1994b, *MNRAS* **269**, 1019–1024
Forster, J. R. and Caswell, J. L.: 1989, *A&A* **213**, 339–350
Gaines, L., Casleton, K. H., and Kukolich, S. G.: 1974, *ApJ* **191**, L99–L100
Garay, G., Moran, J. M., and Rodríguez, L. F.: 1993a, *ApJ* **413**, 582–592
Garay, G., Rodríguez, L. F., Moran, J. M., and Churchwell, E.: 1993b, *ApJ* **418**, 368–385
Gardner, F. F. and Whiteoak, J. B.: 1982, *MNRAS* **201**, 13p–15p
Gardner, F. F. and Whiteoak, J. B.: 1984, *MNRAS* **210**, 23–41
Gaume, R. A. and Mutel, R. L.: 1987, *ApJS* **65**, 193–253
Gaylard, M. J. and MacLeod, G. C.: 1993, *MNRAS* **262**, 43–48
Genzel, R., Downes, D., Moran, J. M., Johnston, K. J., Spencer, J. H., Matveyenko, L. I., Kogan, L. R., and Kostenko, V I Ronnang, B.: 1981, *ApJ* **247**, 1039–1051
Goss, W. M., Haynes, R. F., Knowles, S. H., Batchelor, R. A., and Wellington, K. J.: 1977, *MNRAS* **180**, 51p–56p
Greenhill, L. J., Jiang, D. R., Moran, J. M., Reid, M. J., Lo, K. Y., and Claussen, M. J.: 1995, *ApJ* **440**, 619–627
Greenhill, L. J., Moran, J. M., Reid, M. J., Gwinn, C. R., Menten, K. M., Eckart, A., and Hirabayshi, H.: 1990, *ApJ* **364**, 513–526
Gwinn, C. R., Moran, J. M., Reid, M. J., and Schneps, M. H.: 1988, *ApJ* **330**, 817
Habing, H. J. and Israel, F. P.: 1979, *Ann. Rev. Astron. Astrophys.* **17**, 345–385
Hansen, J., Booth, R. S., Dennison, B., and Diamond, P. J.: 1993, in A. W. Clegg and G. E. Nedoluha (eds.), *Astrophysical Masers*, pp 255–258, Springer-Verlag, Heidelberg, Germany
Harvey, P. M. and Gatley, I.: 1983, *ApJ* **269**, 613–624
Haschick, A. D. and Baan, W. A.: 1989, *ApJ* **339**, 949–955
Haschick, A. D., Baan, W. A., and Menten, K. M.: 1989, *ApJ* **346**, 330–335
Haynes, R. F. and Caswell, J. L.: 1981, *MNRAS* **197**, 23p–25p
Haynes, R. F., Caswell, J. L., and Simons, L. W. J.: 1978, *Aust. J. Phys. Astrophys. Suppl.* **45**, 1–87
Heinze, K. G.: 1956, *ApJS* **2**, 315
Henkel, C., Baan, W. A., and Mauersberger, R.: 1991, *A&A Rev* **3(1)**, 47–90
Henkel, C., Güsten, R., Downes, D., Thum, C., Wilson, T. L., and Biermann, P.: 1984, *A&A* **141**, L1–L3
Henkel, C., Jacq, T., Mauersberger, R., Menten, K. M., and Steppe, H.: 1987, *A&A* **188**, L1–L4

Herbst, E.: 1991, in A. D. Haschick and P. T. P. Ho (eds.), *"Skylines", Proceedings of the Third Haystack Observatory Meeting*, pp 313–322, Astronomical Society of the Pacific, San Fransisco

Hollenbach, D., Johnstone, D., Lizano, S., and Shu, F.: 1994, *ApJ* **428**, 654–669

Hughes, V. A. and MacLeod, G. C.: 1989, *AJ* **97**, 786–800

Hüttemeister, S., Wilson, T. L., Henkel, C., and Mauersberger, R.: 1993, *A&A* **276**, 445–462

IRAS: 1985, IRAS *Point Source Catalog*, *IRAS* Science Working Group, U.S, Government Printing Office, Washington D.C.

Jackson, J. M., Ho, P. T., and Haschick, A. D.: 1988, *ApJ* **333**, L73–L77

Kaufmann, P., Gammon, R. H., Ibanez, A. L., Lepine, J. R. D., Marques dos Santos, P., Paes de Barros, M. H., Scalise Jr, E., Schaal, R. E., Zisk, S. H., Carter, J. C., Meeks, M. L., and Sobolewski, J. M.: 1976, *Nat.* **260**, 306–307

Kazès, I., Proust, D., Mirabel, L. F., Combes, F., Balkowski, C., and Martin, J. M.: 1990, *A&A* **237**, L1–L4

Kemball, A. J., Gaylard, M. J., and Nocolson, G. D.: 1988, *ApJ* **331**, L37–L40

King, E. A.: 1994, *Ph.D. Thesis*, University of Tasmania, Hobart

Koo, B., Williams, D. R. W., Heiles, C., and Backer, D. C.: 1988, *ApJ* **326**, 931–940

Kraemer, K. E. and Jackson, J. M.: 1995, *ApJ* **439**, L9–L12

Kurtz, S., Churchwell, E., and Wood, D. O. S.: 1994, *ApJS* **91**, 659–712

Lees, R. M.: 1973, *ApJ* **184**, 763–771

Lépine, J. R. D. and dos Santos, P. M.: 1977, *Nat.* **270**, 501

Lonsdale, C. J., Diamond, P. J., Smith, H. E., and Lonsdale, C. J.: 1994, *Nat.* **370**, 117–120

Loughgran, L., McBreen, B., Fazio, G. C., Rengarajan, T. N., Maxson, C. W., Serio, S., Sciortino, S., and Ray, T. P.: 1986, *ApJ* **303**, 629–637

Mac Low, M. M., van Buren, D., Wood, D. O. S., and Churchwell, E.: 1991, *ApJ* **369**, 395–409

MacLeod, G. C. and Gaylard, M. J.: 1992, *MNRAS* **256**, 519–527

MacLeod, G. C., Gaylard, M. J., and Kemball, A. J.: 1993a, *MNRAS* **262**, 343–349

MacLeod, G. C., Gaylard, M. J., and Nicolson, G. D.: 1992, *MNRAS* **254**, 1p–6p

MacLeod, G. C., Gaylard, M. J., Scalise Jr, E., and Hughes, V. A.: 1993b, in A. W. Clegg and G. E. Nedoluha (eds.), *Astrophysical Masers*, pp 116–119, Springer-Verlag, Heidelberg, Germany

Makishima, K., Fujimoto, R., Ishisaki, Y., Kii, T., Lowenstein, M., Mushotzky, R., Serlemitsos, P., Sonobe, T., Tashiro, M., and Yaqoor, T.: 1994, *Publ. Astron. Soc. Japan* **46**, L77–L80

Manchester, R. N., Robinson, B. J., and Goss, W. M.: 1970, *Aust. J. Phys.* **23**, 751

Maoz, E.: 1995, *ApJ* **447**, L91

Masheder, M. R. W., Cohen, R. J., Caswell, J. L., Walker, R. N., and Shepherd, M.: 1993, in A. W. Clegg and G. E. Nedoluha (eds.), *Astrophysical Masers*, pp 133–136, Springer-Verlag, Heidelberg, Germany

Masheder, M. R. W., Field, D., Gray, M. D., Migenes, V., Cohen, R. J., and

Booth, R. S.: 1994, *A&A* **281**, 871–881
McBreen, B., Fazio, G. G., Stier, M., and Wright, E. L.: 1979, *ApJ* **232**, L183–L187
McCutcheon, W. H., Wellington, K. J., Norris, R. P., Caswell, J. L., Kesteven, M. J., Reynolds, J. E., and Peng, R. S.: 1988, *ApJ* **333**, L79–L82
McGee, R. X., Brooks, J. W., and Batchelor, R. A.: 1972, *Aust. J. Phys.* **25**, 581–597
McGee, R. X., Newton, L. M., and Butler, P. W.: 1976, *Aust. J. Phys.* **29**, 329–341
Menten, K. M.: 1991a, *ApJ* **380**, L75–L78
Menten, K. M.: 1991b, in A. D. Haschick and P. T. P. Ho (eds.), *"Skylines", Proceedings of the Third Haystack Observatory Meeting*, pp 119–136, Astronomical Society of the Pacific, San Fransisco
Menten, K. M.: 1993, in A. W. Clegg and G. E. Nedoluha (eds.), *Astrophysical Masers*, pp 199–202, Springer-Verlag, Heidelberg, Germany
Menten, K. M. and Batrla, W.: 1989, *ApJ* **341**, 839–846
Menten, K. M., Reid, M. J., Moran, J. M., Wilson, T. L., Johnston, K. J., and Batrla, W.: 1988, *ApJ* **333**, L83–L86
Menten, K. M., Reid, M. J., Pratap, P., Moran, J. M., and Wilson, T. L.: 1992, *ApJ* **401**, L39–L42
Menten, K. M., Walmsley, C. M., Henkel, C., Wilson, T. L., Snyder, L. E., and Hollis, J. M.: 1986, *A&A* **169**, 271–280
Miralles, M. P., Rodríguez, L. F., and Scalise, E.: 1994, *ApJS* **1994**, 173–188
Miyoshi, M., Moran, J., Herrnstein, J., Greenhill, L., Nakai, N., Diamond, P., and Inoue, M.: 1995, *Nat.* **373**, 127–129
Moran, J. M.: 1976, in M. Meeks (ed.), *Methods of Experimental Physics Vol 12C*, pp 174–197, Academic Press, New York
Morimoto, M., Ohishi, M., and Kanzawa, T.: 1985, *ApJ* **288**, L11–L15
Nakai, N., Inoue, M., and Miyoshi, M.: 1993, *Nat.* **361**, 45–47
Nakano, M. and Yoshida, S.: 1986, *Publ. Astron. Soc. Japan* **38**, 531–545
Norris, R. P.: 1985, *MNRAS* **216**, 701–711
Norris, R. P.: 1988, *MNRAS* **230**, 345–351
Norris, R. P. and Booth, R. S.: 1981, *MNRAS* **195**, 213–226
Norris, R. P., Byleveld, S. E., Diamond, P. J., Ellingsen, S. P., Kesteven, M. J., McCulloch, P. M., Reynolds, J. E., Tzioumis, A. K., Takahashi, Y., Troup, E. R., and Wellington, K. J.: 1996, *ApJ,* submitted
Norris, R. P., Caswell, J. L., Gardner, F. F., and Wellington, K. J.: 1987, *ApJ* **321**, L159–L162
Norris, R. P., Gardner, F. F., Whiteoak, J. B., Allen, D. A., and Roche, P. F.: 1989, *MNRAS* **237**, 673–681
Norris, R. P., McCutcheon, W. H., Caswell, J. L., Wellington, K. J., Reynolds, J. E., Peng, R. S., and Kesteven, M. J.: 1988, *Nat.* **335**, 149–150
Norris, R. P., Whiteoak, J. B., Caswell, J. L., Wieringa, M. H., and Gough, R. G.: 1993, *ApJ* **412**, 222–232
NRAO: 1995, *AIPS Cookbook*, NRAO, Socorro, NM
Palla, F., Brand, J., Cesaroni, R., Comoretto, G., and Felli, M.: 1991, *A&A* **246**,

249–263
Panagia, N.: 1973, *AJ* **78(9)**, 929–934
Panagia, N. and Walmsley, C. M.: 1978, *A&A* **70**, 411–414
Peng, R. S. and Whiteoak, J. B.: 1992, *MNRAS* **254**, 301–305
Peng, R. S. and Whiteoak, J. B.: 1993, *MNRAS* **260**, 529–536
Phillips, C. J., Norris, R. P., Ellingsen, S. P., and McCulloch, P. M.: 1996, *MNRAS,* in preparation
Plambeck, R. L. and Menten, K. M.: 1990, *ApJ* **364**, 555–560
Reid, M. J., Haschick, A. D., Burke, B. F., Moran, J. M., Johnston, K. J., and Swenson Jr, G. W.: 1980, *ApJ* **239**, 89–111
Reid, M. J. and Moran, J. M.: 1981, *Ann. Rev. Astron. Astrophys.* **19**, 231–276
Rickett, B. J.: 1990, *Ann. Rev. Astron. Astrophys.* **28**, 561–605
Rodríguez, L. F., Cantó, J., and Moran, J. M.: 1982, *ApJ* **255**, 103–110
Rohlfs, K.: 1986, *Tools of Radio astronomy,* Astronomy and Astrophysics library, Springer-Verlag, Berlin
Scalise Jr, E. and Braz, M. A.: 1982, *AJ* **87**, 528–531
Scheuer, P. A. G. and Readhead, A. C. S.: 1979, *Nat.* **277**, 182–185
Schraml, J. and Mezger, P. G.: 1969, *ApJ* **156**, 269–301
Schutte, A. J., van der Walt, D. J., Gaylard, M. J., and MacLeod, G. C.: 1993, *MNRAS* **261**, 783–794
Sinclair, M. W., Carrad, G. J., Caswell, J. L., Norris, R. P., and Whiteoak, J. B.: 1992, *MNRAS* **256**, 33p–34p
Slysh, V. I., Kalenskii, S. V., and Val'tts, I. E.: 1993, *ApJ* **413**, L133–L135
Slysh, V. I., Kalenskii, S. V., Val'tts, I. E., and Otrupcek, R.: 1994, *MNRAS* **268**, 464–474
Smette, A. and Kuijken, K.: 1995, *Nat.* **375**, 286
Smits, D. P.: 1994, *MNRAS* **269**, 11p–16p
Sobolev, A. M. and Deguchi, S.: 1994, *A&A* **291**, 569–576
Solomon, P. M. and Sage, L. J.: 1988, *ApJ* **334**, 613–625
Staveley-Smith, L., Norris, R. P., Chapman, J. M., Allen, D. A., Whiteoak, J. B., and Roy, A. L.: 1992, *MNRAS* **258**, 725–737
Straw, S. M. and Hyland, A. R.: 1989, *ApJ* **340**, 318–343
Straw, S. M., Hyland, A. R., and McGregor, P. J.: 1989, *ApJS* **69**, 99–140
Strel'nitskii, V. S. and Syunayev, R. A.: 1973, *Sov. Astron. - AJ* **16**, 579–584
Szymczak, M.: 1985, *Acta Astronomica* **35(3–4)**, 305–312
Tenorio-Tagle, G.: 1979, *A&A* **71**, 59–65
Tenorio-Tagle, G., Yorke, H. W., and Bodenheimer, P.: 1979, *A&A* **80**, 110–118
Testi, L., Felli, M., Persi, P., and Roth, M.: 1994, *A&A* **288**, 634–646
Thompson, A. R., Moran, J. M., and Swenson, G. W.: 1986, *Interferometry and Synthesis in Radio Astronomy,* Wiley Interscience, New York
Tielens, A. G. G. M. and Haden, W.: 1982, *A&A* **114**, 245–260
Val'tts, I. E., Dzura, A. M., Kalenskii, S. V., Slysh, V. I., Booth, R. S., and Winnberg, A.: 1995, *A&A* **294**, 825–830
Van Buren, D., Mac Low, M. M., Wood, D. O. S., and Churchwell, E.: 1990, *ApJ* **353**, 570–578
van der Walt, D. J., Gaylard, M. J., and MacLeod, G. C.: 1995, *A&AS* **110**,

81–98
van Langevelde, H. J., Frail, D. A., Cordes, J. M., and Diamond, P. J.: 1992, *ApJ* **396**, 686–695
Walker, R. C., Matsakis, D. N., and Garcia-Barreto, J. A.: 1982, *ApJ* **255**, 128–142
Watson, W. D. and Wallin, B. K.: 1994, *ApJ* **432**, L35–L38
Weaver, H., Williams, D. R. W., Dieter, N. H., and Lum, W. T.: 1965, *Nat.* **208**, 29–31
Weinreb, S.: 1963, *A digital spectral analysis technique and its application to radio astronomy*, Technical Report 412, MIT
Weliachew, L.: 1971, *ApJ* **167**, L47–L52
Whiteoak, J. B. and Gardner, F. F.: 1973, *Astrophys. Lett.* **15**, 211–215
Whiteoak, J. B. and Gardner, F. F.: 1976, *MNRAS* **174**, 51p–52p
Whiteoak, J. B. and Gardner, F. F.: 1986, *MNRAS* **222**, 513–523
Whiteoak, J. B., Gardner, F. F., and Höglund, B.: 1980, *MNRAS* **190**, 17p–22p
Whiteoak, J. B., Wellington, K. J., Jauncey, D. L., Gardner, F. F., Forster, J. R., Caswell, J. L., and Batchelor, R. A.: 1983, *MNRAS* **205**, 275–279
Wilson, T. L., Walmsley, C. M., Menten, K. M., and Hermsen, W.: 1985, *A&A* **147**, L19–L22
Wilson, T. L., Walmsley, C. M., Snyder, L. E., and Jewell, P. R.: 1984, *A&A* **134**, L7–L10
Wilson, W. J. and Barrett, A. H.: 1968, *Science* **161**, 778–779
Wood, D. O. S. and Churchwell, E.: 1989a, *ApJ* **340**, 265–272
Wood, D. O. S. and Churchwell, E.: 1989b, *ApJS* **69**, 831–895
Wynn-Williams, C. G., Becklin, E. E., and Neugebauer, G.: 1972, *MNRAS* **160**, 1–14
Yorke, H. W., Bodenhiemer, P., and Tenorio-Tagle, G.: 1982, *A&A* **108**, 25–41
Yorke, H. W., Tenorio-Tagle, G., and Bodenheimer, P.: 1983, *A&A* **127**, 313–319
Zuckerman, B., Lilley, A. E., and Penfield, H.: 1965, *Nat.* **208**, 441–443